UNIVERSITÄT ZU LÜBECK

From the Lübeck Institute of Experimental Dermatology
of the University of Lübeck
Director: Prof. Dr. med Ralf Ludwig

Identification and Characterization of Type VII Collagen-Targeting Autoantibodies in Experimental Epidermolysis Bullosa Acquisita

Dissertation for Fulfillment of Requirements for the
Doctoral Degree of the University of Lübeck

From the Department of Natural Sciences

Submitted by

Leon Felipe Schmidt-Jiménez
From Engelskirchen, Germany

Lübeck June 2025

First referee: PD. Dr. rer. physiol. Katja Bieber

Second referee: Prof. Dr. rer. nat. Rudolf Manz

Date of oral examination: 10th of October 2025

Approved for printing: Lübeck 13th of October 2025

"I can live with doubt and uncertainty and not knowing.
I think it's much more interesting to live not knowing
than to have answers which might be wrong."

– Richard Feynman (1918–1988)
From a BBC Horizon interview, 1981

Abstract

Autoantibodies (Aab) are a major cause of autoimmune diseases. Understanding the generation and molecular properties of Aab is pivotal to understanding Aab-mediated autoimmunity. Epidermolysis bullosa acquisita (EBA) is a severe Aab-mediated autoimmune blistering disease (AIBD) characterized by Aab targeting type VII collagen (COLVII) at the dermal-epidermal junction (DEJ) in the skin. In EBA, Aab deposition at the DEJ leads to subsequent inflammation through effector functions mediated by the Aab constant region. Despite significant advances in understanding downstream pathomechanisms after Aab binding, the etiology of Aab—their clonal origins, genetic constraints, and subclass contributions determining pathogenicity remain poorly characterized. Monoclonal Aabs capable of inducing disease in murine models have not been identified, limiting mechanistic insights into Aab-mediated tissue damage. This study employed phage display coupled with next-generation sequencing (NGS) to isolate and characterize monoclonal antibodies (mAbs) targeting murine COLVII (mCOLVII). This represents the first comprehensive genetic-level analysis of the murine B cell receptor repertoire in EBA research, revealing germinal center-driven affinity maturation of autoreactive clones. Using two immune-libraries from lymphoid tissues of an mCOLVII-immunized mouse, four dominant variable heavy chain (V^H) clonotypes with restricted genetic diversity were identified, suggesting constraints in the autoreactive B cell response. B cell receptor repertoire sequencing (BCR-seq) revealed tissue-specific isotype distribution and expansion patterns, while tracking clonotypes to originating tissues. BCR-seq uncovered an unexpected predominance of IgG1 in highly mutated clones in the draining lymph nodes (dLN), potentially challenging the current understanding of subclass roles in EBA pathogenesis. Selected clones were expressed in the complement-activating IgG2b format, demonstrating antigen specificity and constant region functionality *in vitro*. Additional mCOLVII-targeting clones were acquired from fellow researchers and likewise expressed and characterized. *In vivo* validation of six phage display-derived clones and two acquired clones revealed DEJ binding of all and complement C_3 deposition for the latter; however, these molecular events proved insufficient for clinical disease manifestation, indicating additional requirements for pathogenic Aab beyond target recognition and complement activation. These findings suggest that synergistic epitope targeting, enhanced Fc-mediated effector functions or multiple subclasses may be required for clinical disease induction.

This study provides critical insights into anti-mCOLVII Aab genetics and functionality, establishing foundations for understanding Aab pathogenicity determinants in EBA while providing valuable tools for understanding tissue-specific Aab mechanisms.

Zusammenfassung

Autoantikörper (AAk) sind eine Hauptursachen für Autoimmunerkrankungen. Das Verständnis der Entstehung und molekularen Eigenschaften von AAk ist entscheidend für das Verständnis von AAk-vermittelten Autoimmunität. Epidermolysis bullosa acquisita (EBA) ist eine schwere AAk-vermittelte autoimmune blasenbildende Erkrankung (AIBD), in der Akk Typ-VII-Kollagen (COLVII) an der dermal-epidermalen Junktionszone (DEJ) in der Haut binden. Bei der EBA führt die AAk-Ablagerung an der DEJ zu nachfolgenden Entzündungen, vermittelt durch die Effektordomäne der Akk. Trotz bedeutender Fortschritte im Verständnis der nachgeschalteten Pathomechanismen, bleibt die Ätiologie der AAk – deren Klonalität, Genetik und für die Pathogenität essentiellen Subklassenkomposition nur unzureichend charakterisiert. Monoklonale AAk, die in der Lage sind, die Enzündungsprozesse der EBA in Mausmodellen zu induzieren, wurden bisher nicht identifiziert und stellen eine bedeutende Lücke in der Chrakterisierung der Erkrankung dar. Diese Studie nutzte Phage-Display in Kombination mit Next-Generation-Sequenzierung (NGS), um monoklonale Maus Akk zu isolieren die gegen murines COLVII (mCOLVII) gerichtet sind um diese nachfolgend genetisch sowie funktional zu charakterisieren. Unter Verwendung von zwei Immunbanken, generiert aus lymphatischen Geweben einer mCOLVII-immunisierten Maus, wurden vier dominante variable Schwerketten (V^H)-Klonotypen mit eingeschränkter genetischer Vielfalt identifiziert, was auf Einschränkungen in der autoreaktiven B-Zell-Antwort hindeutete. B-Zell-Rezeptor-Repertoire-Sequenzierung (BCR-seq) zeigte gewebespezifische Isotypverteilungen und Expansionsmuster, und erlaubte die Klonotypen in die Ursprungsgeweben zurück zu verfolgen. Durch BCR-seq wurde eine unerwartete Dominanz von IgG1 in hochmutierten Klonen identifiziert, welche das aktuelle Verständnis der Rollen von Antikörper Subklassen in der Pathogenese der EBA in Frage stellt. Ausgewählte Klone wurden im komplementaktivierenden IgG2b-Format exprimiert und Antigenspezifität sowie Funktionalität wurden *in vitro* nachgewiesen. Weitere mCOLVII-targetierende Klone wurden von Kooperationspartner erworben und analog exprimiert und charakterisiert. Die *in-vivo*-Validierung von sechs mittels Phage-Display identifizierten Klonen und zwei erworbener Klone zeigte DEJ-Bindung für alle und Komplementfaktor C_3-Ablagerung für letztere; Bindung und Komplementaktivierung erwiesen sich jedoch als unzureichend für die klinische Krankheitsmanifestation, was auf zusätzliche Anforderungen für pathogene AAk jenseits der Zielerkennung und Komplementaktivierung hinweist. Diese Arbeit liefert wichtige Einblicke in die Genetik und Funktionalität von anti-mCOLVII AAk und schafft damit Grundlagen für das Verständnis der AAk-Pathogenitätsdeterminanten in der EBA, und liefert zusätzlich wertvolle Werkzeuge für das Verständnis gewebespezifischer AAk-Mechanismen.

Contents

Chapter 1

Introduction

1.1 Immunology: An Introduction to Concepts, Terms and Definitions

The immune system is commonly divided between the innate and adaptive response [1]. While this paradigm, remains a foundational framework, calls for a more holistic view on immunity, given emerging evidence of cross regulation of both branches, were already postulated more than three decades ago [2, 3]. Despite its limitations, this dichotomy offers a useful conceptual framework for introducing and discussing fundamental immunological principles.

1.1.1 Innate and Adaptive Branches of Immunity: A Classical Distinction

The innate branch of immunity is characterized by rapid responses to damage-associated molecular patterns (DAMPs) [4] and pathogen-associated molecular patterns (PAMPs) [5]. This response relies on the recognition of evolutionary conserved structures, by appropriate pattern recognition receptors and molecules [2, 6]. It is limited in its extent of flexibility regarding the resulting overall response, which can in essence be described by the following terminology in a more or less fixed order: Recognition, Alert, Kill, Clear [2]. It is important to denote, that the innate branch of immunity comprises both a cellular and molecular armory, which is not only involved in pathogen clearance but also mediates inflammatory processes, tissue homeostasis and intensive cross-talk with the second- the adaptive branch of immunity [7].

The adaptive branch of immunity provides, as indicated by the terminology, an adaptive, thus highly flexible means to react to the environment. Adaptivity relies on

the adaptome [8], which in the context of adaptive immunity is constituted by the potential genetic diversity of two distinct types of adaptive immune receptor molecule classes, recognizing antigen and generated through somatic gene recombination [9, 10]. These include (1) antigen-peptide-recognition surface receptors, able to recognize peptide-antigen exclusively in the context of major histocompatibility complex (MHC) molecules, and (2) antigen binding receptors, binding directly to native antigen structures, independent of biochemical origin [11, 12]. The term antigen in turn is defined as any molecule or molecular structure that can be specifically recognized by one of these two receptor classes [7, 13].

1.1.2 The Adaptome and Adaptive Immune Receptor Repertoires

Peptide-recognition receptors or TCRs are exclusively expressed by and on the outer membrane surface of T-cells, whereas antigen binding receptors are exclusively expressed by B-cells, and thus termed BCR [11, 14]. BCRs can be membrane bound or secreted [15]. The secreted form of the BCR is termed antibody, with the entirety of antibodies being considered the humoral adaptive immune response [7]. BCRs and antibodies while technically describing the very same molecules, belong to the broader class of immunoglobulins (Ig) [16]. Together, T and B cells and their respective receptors constitute the foundation of adaptive immunity. Upon cognate antigen recognition, this allows for an antigen-specific, so-called acquired immune response and generation of long-lasting immunological memory of this particular response [10].

The diversity of the Adaptome relies on a closely supervised cascade of mechanisms, of which combinatorial genetic diversity, also termed gene recombination, is both the foundation and key evolutionary feature to introduce near limitless diversity [17]. Both TCRs and BCRs are encoded by a set of germline variable (V), diversity (D) and junction (J) (V(D)J) genes which upon recombination result in the expression of a distinct (functional) receptor per individual cell [18, 19]. Mature B cells may further undergo additional diversification by somatic hypermutation (SHM) post-gene rearrangement [20]. The entirety of expressed TCRs and BCRs at one moment is considered the adaptive immune receptor repertoire of one individual [21].

1.2 Antibody Structure, Genetic Diversification, and B Cell Development: Molecular Foundations of Humoral Adaptive Immunity

Antibodies are functionally divided into two regions, the antigen-binding fragment variable (Fv) and the effector-mediating fragment crystallizable (Fc) [22]. The structure of any given antibody is defined by two identical heavy (H) and light (L) chains. Antibodies are thus bivalent molecules, comprising two identical binding sites constituted by the combination of the variable portions of heavy (V^H) and light (V^L) chains [19]. Each Fv domain is independently defined by their individual recombination of V(D)J genes, while the constant regions are encoded by a set of germline constant region genes. For the heavy chains in mice, these include eight contiguous genes on chromosome 12, resulting in the expression of five isotypes: IgM, IgD, IgG, IgA, and IgE, which can be coupled to the same Fv, thereby mediating different effector functions without changing the recognized antigen [7, 23]. IgG is further subdivided into (in mice strain-dependent) subclasses: IgG1, IgG2a/c, IgG2b, and IgG3, enhancing the diversity of effector functions, which also influence autoimmunity, as demonstrated in both murine and human (IgG 1-4) studies [24–30]. IgG2a and IgG2c represent strain specific allotypes of the same constant region [31, 32]. The change of one isotype to another is termed class switching. This process is irreversible due to the nature of deletional recombination during class switching. Genes preceding the targeted isotype are physically deleted; thus, the order of class switching is fixed by the chromosomal arrangement of constant genes [23].

The constant heavy (CH) chains for any isotype are divided into domains, which will be further explained using the example of IgG, the most abundant isotype in mice and men, and the most prevalent isotype in autoimmune disease [35]. CH1 is directly attached to the N-terminal V^H and connected to the C-terminal CH2 and CH3 via a flexible linker region, termed hinge. The functional significance of the hinge region is highlighted by subclass variations: murine IgG2b features a hinge with four inter-heavy chain disulfides, enabling moderate flexibility, while IgG2a/c exhibit a shorter hinge with two disulfides, resulting in increased flexibility compared to IgG2b [34, 36, 37]. A similar phenomenon of varying flexibility is observed when comparing human IgG subclasses [38]. Along with the hinge-region disulfides between heavy chains, the complete IgG molecule is stabilized by disulfide bonds connecting the constant light (CL) domain of each light chain to the CH1 domain of its paired heavy chain, with no variations in this bond between isotype subclasses [34]. Constant region glycosylation

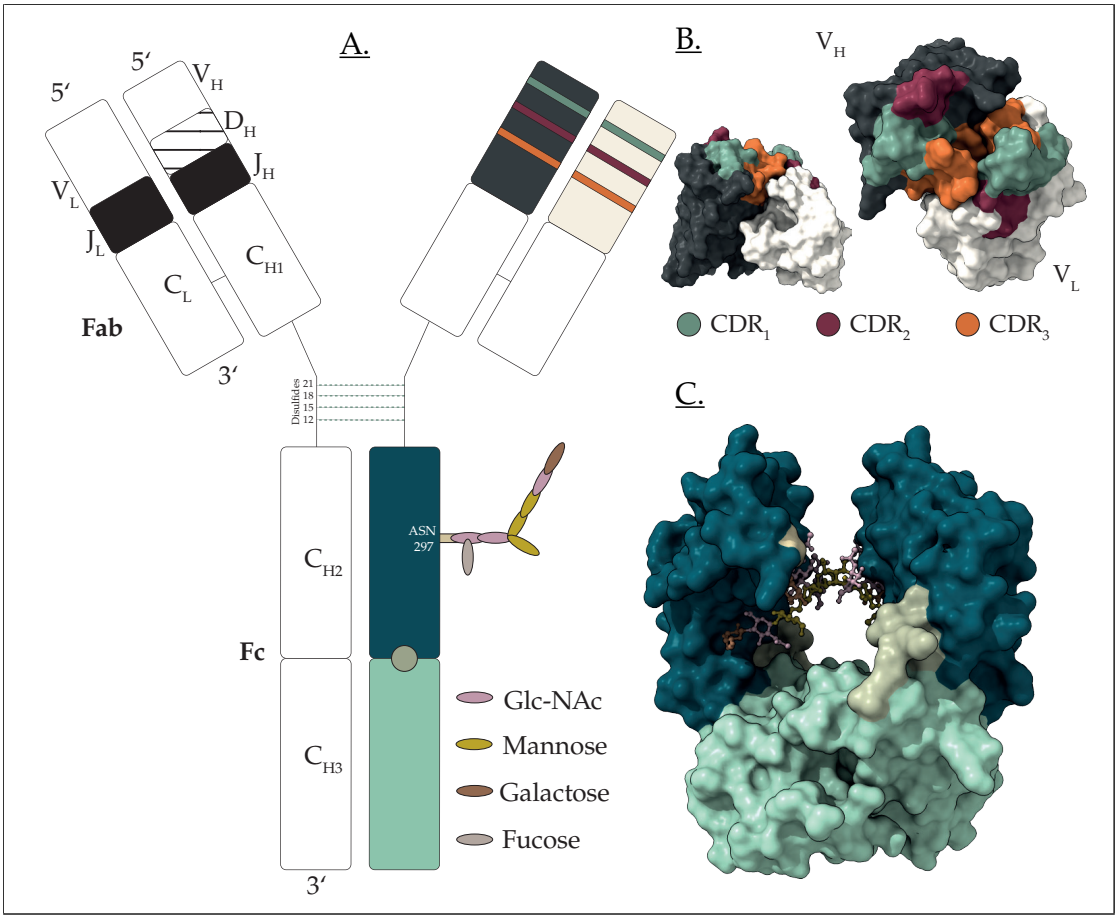

Figure 1.1: Two and three dimensional model of an IgG2b molecule. (A) Two dimensional schematic depiction of IgG2b. Chain composition, fragment names and directionality is shown on the left. Functional regions, such as CDR localization and glycosylation sites are shown on the right. (B) Alpha-fold derived three-dimensional structure of the variable region, V^H [charcoal], V^L [off-white], CDR_1 [green], CDR_2 [red], CDR_3 [orange]. (C) Crystall structure of IgG2b CH2-CH3, including glycosylation, derived and modified from PDB 2RGS [33]. Sugar group coloring corresponds to A. A was adapted from [7, 22, 34].

patterns critically modulate downstream effector functions [39–41].

The antigen-binding site within the Fv is termed the paratope, which is complementary to the epitope on the antigen. The paratope is formed by three loops originating from the nine β-strands of each Fv (V^H and V^L). These structural loops, termed complementarity-determining regions (CDRs), interact with the epitope primarily via hydrogen bonds, electrostatic interactions, and van der Waals forces mediated by charged amino acids (AA) within the CDRs. The paratope-epitope interaction is non-covalent, and the CDRs determine the binding affinity between antibody and antigen. The third CDR of V^H (CDR3) is widely regarded as the most critical region, contributing significantly to antibody binding and exhibiting the highest variability within the Fv. This variability originates from V(D)J gene recombination and SHM during V^H generation [7].

The mouse C57BL/6 genome, including the immunoglobulin gene loci (IG), has traditionally been characterized intensively; thus, this strain serves as an example for the description of IG genetics. However, importantly, laboratory mouse strains significantly vary in their number of IG gene segments and exhibit low overlap between strains [42]. The C57BL/6 genome comprises approximately 228 functional IG genes per haploid genome, distributed across three major IG loci. The heavy chain locus (*IGH*) is located on chromosome 12, whereas the kappa (*IGK*) and lambda (*IGL*) light chain loci are located on chromosomes 6 and 16, respectively [34]. V^H is generated by combinatorial joining of 102 V, 9 D, and 4 J gene segments. Of note, IGHD2-5*01 and IGHD2-6*01 are identical. The IGK locus represents approximately 95% of the germline light chains and contains 91 V and 4 J segments, whereas IGL features 3 V and 3 J gene segments [43–45].

B cell development from bone marrow stem cells initiates in pro-B cells with random D-J joining (V^H). Successful V-D-J V^H recombination transitions cells to the pre-B cell stage, where light chain (V-J) rearrangement occurs. Immature B cells express surface IgM, while mature naïve B cells co-express IgD via alternative RNA splicing of the derived mRNA [7, 22].

Gene recombination is guided by recombination signal sequences (RSS) flanking V, D, and J segments. Lymphoid-specific RAG-1/RAG-2 recombinases recognize RSS and mediate cleavage, while terminal deoxynucleotidyl transferase adds non-templated (N) nucleotides. Junctional diversity arises from exonuclease trimming, palindromic (P) and N additions, and imprecise joining, further increasing repertoire diversity [7, 19, 34].

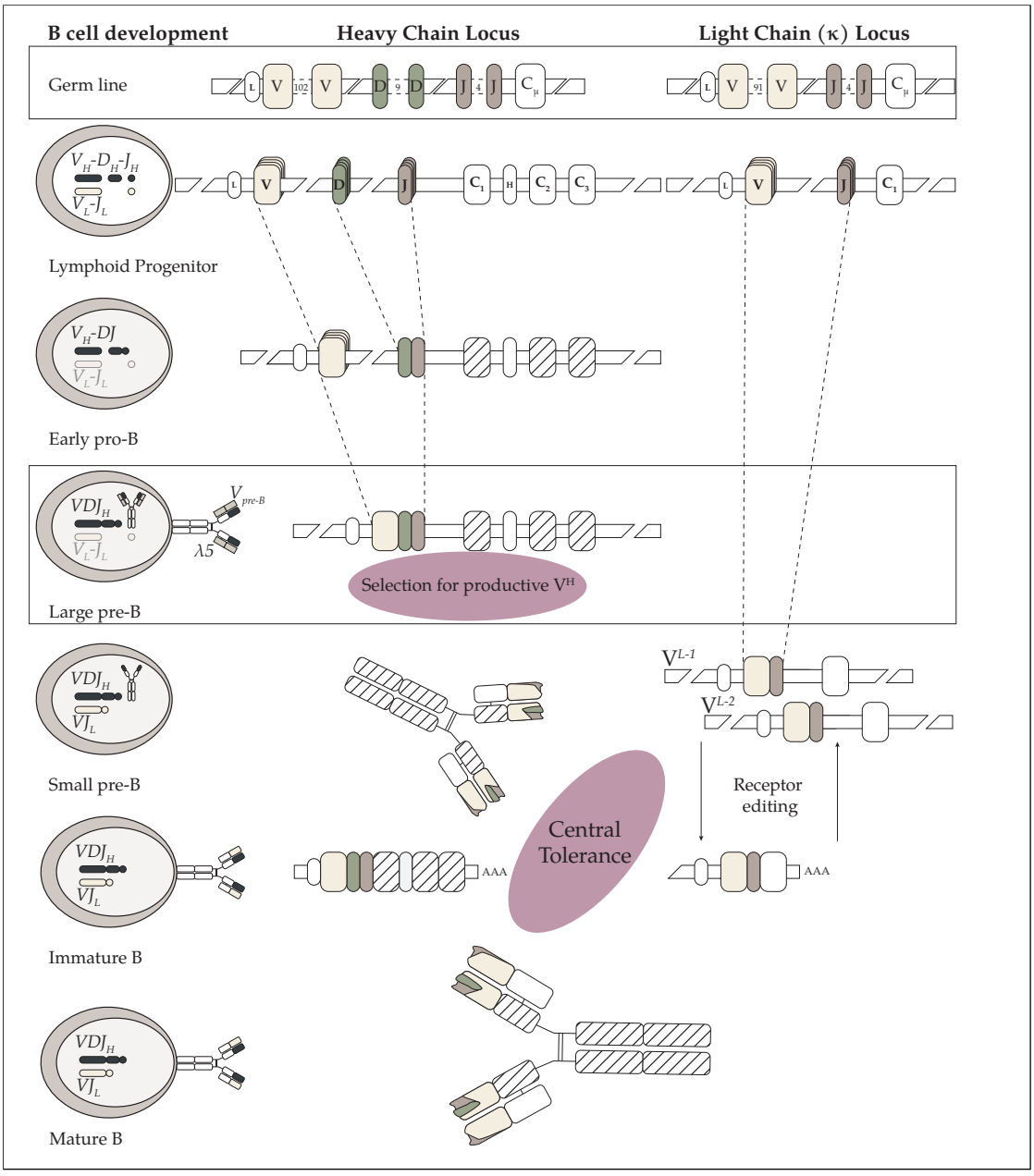
B cell development
Heavy Chain Locus
Light Chain (κ) Locus
Germ line
Lymphoid Progenitor
Early pro-B
Large pre-B
Selection for productive V^H
Small pre-B
Central Tolerance
Receptor editing
Immature B
Mature B

Figure 1.2: B cell development and stages of V(D)J gene rearrangement. B cell development initiates in the bone marrow from germline cells committed to the common lymphoid progenitor lineage. D-J rearrangement marks B lineage commitment, with DJ-rearranged cells classified as early pro-B cells. V-DJ joining and expression of the pre-B cell receptor (pre-BCR)—composed of μ heavy chain (V^H) paired with a surrogate light chain (VpreB and λ5)—enables selection of productively rearranged V^H in large pre-B cells [19]. From this stage onward, B cell survival depends on pre-BCR/BCR signaling. Small pre-B cells undergo V^L (light chain) V-J rearrangement, with immature B cells expressing a fully assembled BCR (IgM). Central tolerance mechanisms—including receptor editing (initiated at the pro-B/pre-B transition) and clonal deletion—act primarily at the immature B cell stage [46]. Mature B cells egress from the bone marrow to secondary lymphoid organs, where peripheral tolerance occurs [7].

Together, V(D)J recombination and joining of V^H and V^L results in combinatorial repertoire diversity of approximately 1.4×10^6 different antibodies, further enhanced by junctional diversity, which has been estimated to raise diversity up to theoretically 10^{10}–10^{11} unique Igs [34]. The subsequent process of SHM during the germinal center (GC) reaction, occurring upon antigen encounter, further diversifies and refines the antigen-binding affinity of BCRs in GC-participating B cells. While combinatorial diversity generates initial repertoire breadth, SHM provides antigen-driven refinement. Of note, while (conventional) B cells of adaptive immunity rely on the herein described processes, natural IgM producing B1 cells of innate immunity, incorporate (biased) VDJ gene recombination, but do not mirror the development, function and phenotype of conventional B cells [47].

While the mechanisms of diversity generation are shared between mice and humans, the human repertoire heavily relies on junctional diversity (especially N nucleotide addition) and SHM to achieve a broad repertoire, whereas the murine repertoire diversity is generated by increased germline diversity [42]. Compared to the theoretically estimated diversity of human Igs (2×10^{12}), the murine repertoire is further skewed by observed preferential V/J usage and the aforementioned fewer N nucleotide additions [42].

1.2.1 Crosstalk and Clonality

Apart from the (partially) shared genetic recombination mechanisms during development, T and B cells engage in a close relationship during antigen driven selection in the secondary lymphoid organs (SLO). Antigen is delivered to SLOs via different routes. While dendritic cells (DC) acquire antigen in the periphery and egress to SLOs, priming T cells by MHC class II receptor molecule (MHCII) associated peptide-antigen presentation, native antigen can passively drain to SLOs through the lymphatic system and is

presented by subcapsular sinus macrophages to B cells for antigen recognition. After initial antigen recognition a majority of B cells depends on the stimulation by T cells to gain the ability to proliferate and expand [48]. These B cells are considered T-dependent B cells. A cognate B cell will be stimulated by a T cell when both cells recognize the same antigen. Upon recognition of native (peptide-derived) antigen, a given B cell will internalize and digest the antigen-BCR complex. The resulting peptides are presented on MHCII on the B cell surface for T cell recognition [7]. TCRs can only recognize peptide antigens, exclusively in the context of MHC receptors [11]. Given a TCR matches one of the peptides presented by the B cell, it will provide so-termed "help" to the B cell for further maturation and proliferation. T cell help is not a singular process and indeed has bi-directional implications, underlining the interdependence of T - B interaction [48, 49]. A B cell stimulated in this manner will give rise to a clonal lineage of B cells, with all progeny initially expressing the same V(D)J rearrangement as the ancestral cell [20, 50]. This emphasizes the role of clonality. While SHM may further alter the exact specificity of each cell's receptor individually by introducing point mutations during GC reactions, the gene usage for this clonal line is fixed, and can thus be traced back to the common ancestor of the clone [21, 50].

1.3 Autoreactivity vs Autoimmunity: A Fine Line

While the introduction of diverse repertoires, limited only by the biological maintenance capacity of the host, provides an enormous evolutionary benefit for pathogen clearance, it concurrently poses an equally significant risk of self-recognition and subsequent self-damage by the immune system to the host itself. To avoid strong self-reactivity, the adaptive repertoire is tightly controlled by tolerance mechanisms during B and T cell generation and maturation [51]. Similar to the previously described dualisms of innate and adaptive immunity, and TCR- and BCR-mediated adaptive responses, tolerance in the context of the BCR is conventionally divided into two branches. Building on the clonal selection hypothesis [52], the clonal deletion concept was established, whereby cells expressing highly autoreactive BCRs are deleted during B cell development in the bone marrow [53]. This central, or negative, selection is complemented by peripheral tolerance mechanisms in secondary lymphoid tissues, including anergy [54], clonal deletion, and inhibition via sialic acid-binding immunoglobulin-like lectin receptors [55]. Peripheral tolerance ensures the means for the BCR repertoire to react to pathogen-derived antigens similar to self-antigens and, due to its reversibility and immunological role, is not an absolute barrier. The susceptibility of B cells to peripheral tolerance depends on their

developmental stage and the molecular presentation of antigen, with multimeric or membrane-bound antigens promoting deletion and soluble antigens favoring tolerance induction [46]. In addition to clonal deletion, central tolerance includes receptor editing, which allows rescue from clonal deletion of highly autoreactive B cells in the bone marrow by alteration of the BCR. The process is therefore also termed receptor selection, emphasizing the change within the receptor and differentiating it from classical clonal selection. Receptor editing is primarily directed by the replacement of L chains within the BCR during B cell maturation. B cells harbor the genetic potential to simultaneously express two different heavy and two (IGK) or four (IGL) different light chains (mouse). Allelic exclusion during V(D)J rearrangement, ensures the expression of a single heavy-light chain pairing, which is closely regulated by feedback signaling of the BCR. The expression of a singular functional heavy chain at the pro-B cell stage is a prerequisite for developmental progression to the pre-B cell stage, thereby preventing further genetic heavy chain activity [56]. Rearrangement of V^L and assembly with V^H enables primary expression of the BCR and subsequent receptor-antigen interaction. Positive selection, indicating productive BCR expression, will cease further V(D)J activity. Failed, weak, or BCR signaling upon self-antigen encounter during positive selection may result in secondary V^L rearrangement and thus receptor editing. T and B cells harboring receptors that recognize self-antigen are termed autoreactive. Autoreactivity itself is a naturally occurring phenomenon, arising as a byproduct of immune repertoire diversification. Persisting autoreactive cells—retained via anergy or escaping tolerance mechanisms—may, when triggered become pathogenic if they initiate, participate in, or drive reactions, resulting in self damage or inflammation. Autoreactive, self-damage-inflicting cells are termed autoimmune effector cells. Expansion and subsequent progressive damage, whether directly inflicted or initiated by these cells, resuling in pathological conditions are classified as autoimmune diseases.

1.3.1 T and B cell Collaboration in Autoimmunity

The traditional dichotomy of separating between primarily T and B cell mediated autoimmune diseases is challenged by the more recent understanding of the interconnectivity of these cell types in autoimmunity [48, 57]. As previously discussed, the majority of B cells is dependent on T cell interaction, for proliferation, which has been shown also in the context of autoimmunity [58]. T cells in turn are dependent on MHCII-associated presentation of antigen, which B cells are capable of performing [48]. This dualism of partial to total dependency illustrates the complex interconnectivity between T and B

cells. Nonetheless, the mechanistic breadth (antibodies, cytokines, antigen production) in and the manifestation of autoimmune diseases, associated with B cells is more prevalent than exclusively T cell mediated damage and disease [59–61]. This is underlined by findings, that despite the absence of disease associated antibodies, patient conditions improved, when treated with B cell depleting therapeutic antibodies [59, 62]. Similar to non-autoreactive B cells, autoreactive B cells secrete their cognate BCR in soluble form, then termed autoantibody (Aab), into the circulation.
Antibodies constitute approximately 20% of total protein in normal human serum and are distributed systemically by diffusion and active, receptor-mediated transport to tissues and extra body fluids [22, 38, 63]. A "classical" antibody-antigen reaction is defined by the specific binding of an antibody, mediated by its Fv domains, to antigen. The binding of antibodies to antigen will elicit direct or indirect effects [7]. Antibodies are therefore commonly attributed with neutralizing or non-neutralizing effects [64]. Neutralizing antibodies elicit an immediate effect on antigen by sole binding to an epitope, which in turn causes a loss of functionality of the antigen, due to the antibody effectively neutralizing or blocking its biological functional domain. Non-neutralizing antibodies bind epitopes of antigen not directly involved in antigen effector function [7]. Antibody-bound antigens together form immune complexes (IC). Upon IC formation, the Fc domain of antibodies, not involved in antigen binding, becomes accessible for recognition and binding by other factors of both adaptive and innate immunity. A downstream signaling cascade of events is initiated, which is summarized in the term antibody effector function. One of two major events is the activation of the complement system, a pivotal system of the innate branch of immunity, which is able to opsonize antigen, lyse pathogens, and recruit immune cells of both branches [7, 38, 65, 66]. Another is the enhanced recognition by Fc receptors. Fc receptors are a branch of the family of Ig receptors, present on almost all immune cells and pivotally involved in eliciting and regulating immune responses [67–69].

1.4 Autoantibody-Mediated Autoimmunity

Contrary to the differentiation of neutralizing and non-neutralizing antibodies, in infectious contexts, the concept can not be directly translated to autoimmunity. In autoimmunity, antibodies are instead classified by "pathogenicity", defined by their capacity to cause sustained self-damage regardless of the mode of action. Pathogenicity may arise through several mechanisms: (1) direct antibody-antigen interactions such as antigen internalization or receptor (over) activation with downstream pathological effects upon

binding or (2) Fc-mediated effector functions such as complement activation and Fcγ receptor engagement [70]. Detailed characterization of the self-antigen including epitope specificity, binding affinity, and structural context provides critical insights into the mode of pathogenicity.

Aab may give rise to a certain type of autoimmune disease, so-termed autoantibody-mediated autoimmune diseases, which cumulatively affect about 2.5–6% of the population [61, 71]. Interrestingly 23.6% of disease-free individuals harbor Aab, suggesting subclinical autoimmunity [72]. While Aab-driven diseases may affect a multitude of tissues within the body [73], structures of the skin are targeted in multiple Aab-driven diseases [74]. Of these, the spectrum of autoimmune blistering diseases (AIBDs) is well characterized. Aabs in AIBDs target various structural components of the dermal-epidermal junction (DEJ) zone, an extracellular matrix pivotal for skin integrity, or neighbouring keratinocyte-associated adhesion proteins [75, 76]. AIBDs are further subdivided into pemphigus and pemphigoid diseases (PD), of which the latter are of particular interest due to the inflammatory nature of the disease-causing Aabs themselves [77]. Again, PDs constitute several diseases, which are differentiated by the Aab-targeted structures [76]. Despite the higher prevalence of bullous pemphigoid (BP), epidermolysis bullosa acquisita (EBA) is of particular interest for this study, due to the availability of robust murine model systems [78] which allowed to explore the underlying pathomechanism [79–81].

EBA, though rare in humans (0.08-0.05 cases per million worldwide, 2.8 cases per million in Germany) [82], is mechanistically well-characterized in mice and men, featuring an autoreactive T-dependent B-cell response mainly directed against the first non-collagenous (NC)-1) domain of collagen type VII (COLVII) [83, 84]. BP the prototypic PD, has a much higher prevalence (13–42 cases per million) [76]. In patients, Aab are primarily directed against subdomains within NC-1, one of which is the second von Willebrand factor A-like domain 2 (vWFA2), which shares high structural homology with the human von Willebrand factor A (vWFA) domain [85–87]. Aab in EBA are mainly of the IgG subclass, with a variant of disease, termed linear IgA disease-like variant of EBA exhibiting IgA Aabs [88]. EBA can be further divided into an inflammatory variant, which will be the focus of this study and a non-inflammatory, mechanobullous variant, which presents with COLVII-targeting IgG Aab, but no inflammatory penotype [79].

1.5 From Autoantibodies to Autoantigen: Milestones in EBA Research

The thorough characterization of the mechanisms involved in EBA pathology relies on both human and murine studies. Early research employed patient-derived materials, such as serum and skin, to explore the etiology of the disease [89–91]. The development of several mouse models has allowed for detailed characterization of all disease stages [79, 80, 92, 93].

1.5.1 Discovery and Characterization of EBA Autoantibodies

The identification of Aab as a disease-causing agent preceded the identification of the actual autoantigen in EBA. While early studies in the 1960s suggested a defect in fiber expression that resulted in the clinically apparent loss of DEJ integrity [94], it became clear by the 1970s that tissue-bound IgG antibodies were present, along with deposited complement factor 3 (C_3) in patients' skin biopsies [95, 96]. The early identification of tissue-deposited complement already hinted towards the underlying pathophysiology of the disease, although this was not explicitly concluded at the time. Collagen type VII was first described in 1983, following tissue homogenate analysis, and was further characterized structurally in the following years. By 1985, the first monoclonal antibody (mAb) (clone H3a) targeting the still unknown antigen was found, which localized similarly to patient-derived serum at the DEJ in the skin [97]. Within the same year, the expression of the target antigen was detected in keratinocytes [89]. One major early functional study revealed differences in the immune-activating capacities of Aab ICs in EBA between patients. The activation of complement and subsequent attraction of leukocytes provided a first insight into the pathogenic mechanisms [98, 99]. By 1987, another mAb, clone LH7.2, was described, which was explicitly determined to be directed against collagen type VII [100]. In 1988, Woodley and colleagues identified the globular carboxyl terminus of type VII procollagen as the antigen in EBA by mapping of patient IgG and mAb H3a [91]. To further investigate the pathogenicity of Aab in EBA, Shigemoto *et al.* injected patient IgG into both adult and neonatal mice, which, despite binding *in vivo*, did not elicit pathogenicity [101]. This was a particularly interesting finding, underlining that Aab binding does not necessarily correlate with disease. However, it has to be taken into account that mice and humans, though harboring similar to equivalent mechanisms of immunity, are still different, especially in terms of expressed Fc receptors and functional interaction [102, 103]. Further even within different mouse strains there is

a proven difference in the extend susceptibility to blister induction [104]. Thus Shigemoto *et al's.* failure to induce blisters likely stemmed from incompatibility between human IgG and murine Fcγ receptors or choice of mouse strain, as shown in later studies.
The following decade provided deeper insight into the structural nature of collagen type VII (COLVII), its natural interaction partners within the skin, and the localization of Aab binding [83, 105–107]. By today, we know that COLVII is a major component of anchoring fibrils within the DEJ, critical for skin integrity [105, 106].

1.5.2 Collagen Type VII: Structural and Functional Insights into the EBA Autoantigen

Anchoring fibrils of the DEJ or basement membrane, essentially provide the extracellular connection of cells of the dermis and epidermis. COLVII as its major component therefore interacts with other protein members of the DEJ, providing a framework for the formation of the anchoring fibrils [108]. Structurally, (pro)COLVII (350 kDa) harbors three main domains: a large 145 kDa N-terminal NC-1 domain, connected to a central 145 kDa collagenous domain by a cysteine rich region, and a C-terminal 34 kDa NC-2 domain [109]. The central collagenous domain is further interrupted by short NC regions, the longest termed hinge region [110]. COLVII assembles into a homotrimer of three alpha-chains in which the collagenous regions form a triple helical structure, which is stabilized by Gly-X-Y repeats centrally and the cysteine regions of each strand. Upon secretion, two triple helical monomers then form antiparallel dimers, which in turn are stabilized by disulfide bonds between the NC2 regions [86, 111, 112]. The NC-1 domain contains subdomains with homology to adhesion proteins, including nine fibronectin type III-like (FNIII) domains and two vWFA-like domains: one at its N-terminus (vWFA1) and one at its C-terminus (vWFA2) [110]. The N-terminal vWFA1 domain was previously termed cartilage-matrix-like protein. The vWFA2 subdomain shares 60–70% homology with the A domain of von Willebrand factor and mediates interactions with type I collagen (COLI), laminin-332 (L332), and β1 integrins [86, 87, 107]. Fibronectin binds to residues 615–1161 within the collagenous domain, further stabilizing extracellular matrix (ECM) interactions [113]. Epitope mapping of patient Aab to fragments of human COLVII revealed that a majority target multiple regions within the FNIII stretch of NC-1, as well as the vWFA2 subdomain [83, 85, 114]. Similarly, previously described monoclonal antibodies H3a [97] and L3D [115] targeted FNIII 2–4 and FNIII 8–9, respectively [85], emphasizing the multiplicity of antigenic regions within COLVII.

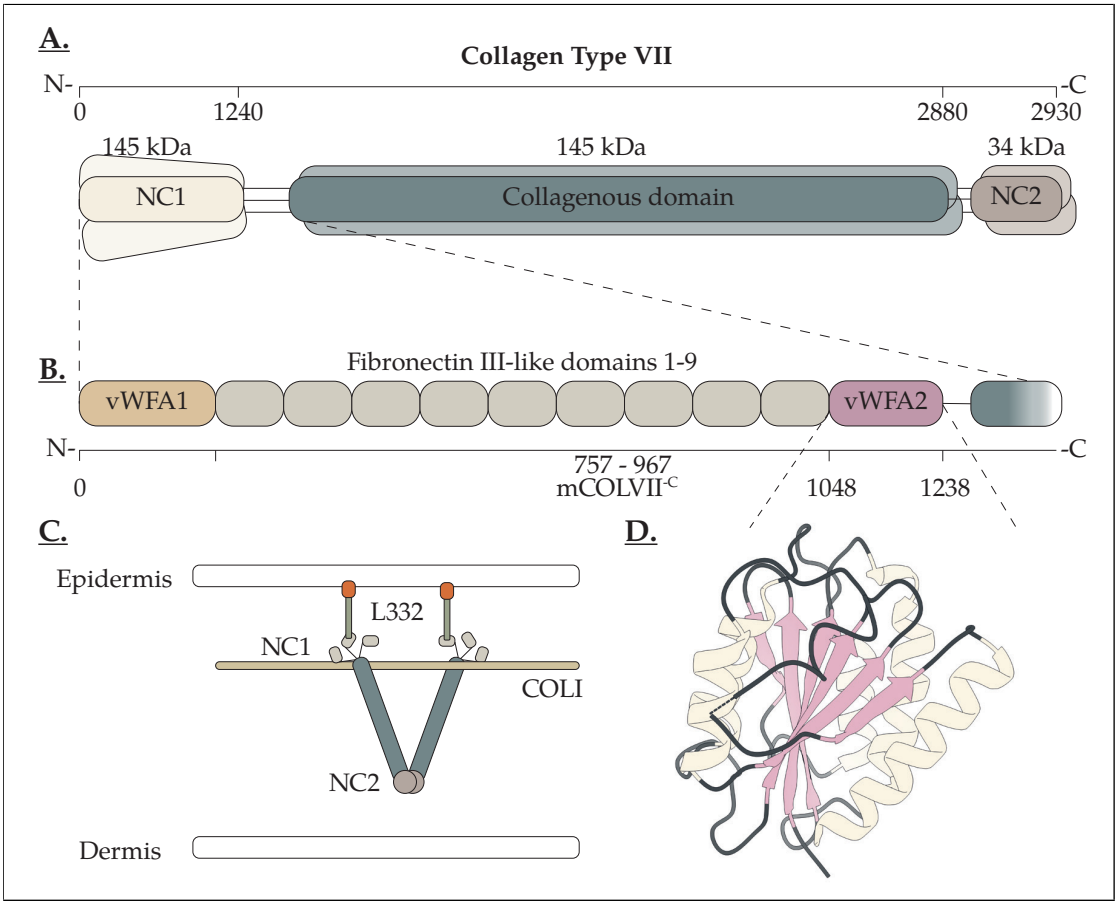

Figure 1.3: Collagen Type VII a triple helical anchoring fibrill. (A.) Schematic structural organization of collagen type VII (COLVII) alpha chain; modified from [87]. (B.) Schematic structural organization of NC-1 including major domains and the artifical fragment mCOLVII^{-C}, used for the first immunization-induced murine model of EBA [93]; modified from [110]. (C.) COLVII within the DEJ architecture; modified from [112]. (D.) Structural organization within the vWFA2 domain; obtained and modified from PDB 6S4C [87] Abbreviations: Non-collagenous (NC), von Willebrand factor A like domain (vWFA) 1 and 2, laminin 332 (L332), collagen I (COLI).

1.5.3 Establishing Pathogenicity: Animal Models and Mechanistic Proof

The era of the 2000s provided a massive gain in knowledge about the pathomechanisms of EBA. The finding that patient-derived Aabs could induce dermal-epidermal separation *ex vivo* by stimulating neutrophil activation via Fcγ receptors revealed one of the processes now known to be pivotal for tissue damage in EBA [116]. The first successful xenogeneic transfer of murine COLVII-reactive IgG fundamentally proved that pathogenicity in EBA relies on Aab recognition of COLVII [92]. The concept of complement-driven tissue destruction was further supported by the protection observed in complement component 5 (C5)-deficient mice. The IgG used in this study was derived from rabbits immunized with mCOLVII-C, an artificial fragment spanning residues 757–967 within the FNIII-like domains of NC-1 [92].

Building on this first antibody transfer model, an immunization-induced disease model was developed by immunizing mice of different strains with mCOLVII^{-C} in adjuvant [93]. This study suggested that disease in mice depends on the induction of IgG2b, a murine IgG subclass effective in fixing and activating complement, thereby enabling tissue deposition. It also revealed strain-specific susceptibility disparities: despite comparable Aab levels, strains like SKH-1 and C57BL/6 were resistant to disease induction, implicating MHC-II-dependent genetic factors [93].

Further validation came from antibody transfer studies demonstrating that NC-1-purified patient IgG could induce blistering in mice [117]. Complement dependency was elucidated further using knockout strains, demonstrating involvement of both the classical (CP) and alternative (AP) pathways in EBA pathogenesis [118]. The AP is genuinely known for its amplification of CP-driven inflammation [66]. Fcγ receptor dependency was confirmed by transferring chicken IgY, lacking FcγR binding in mammals, into mice, proving that pathology requires Fc-mediated engagement of humoral and cellular immunity [119]. The neonatal Fc receptor (FcRn) was shown to recycle Aab, thereby explaining Aab persistence in EBA patients [120].

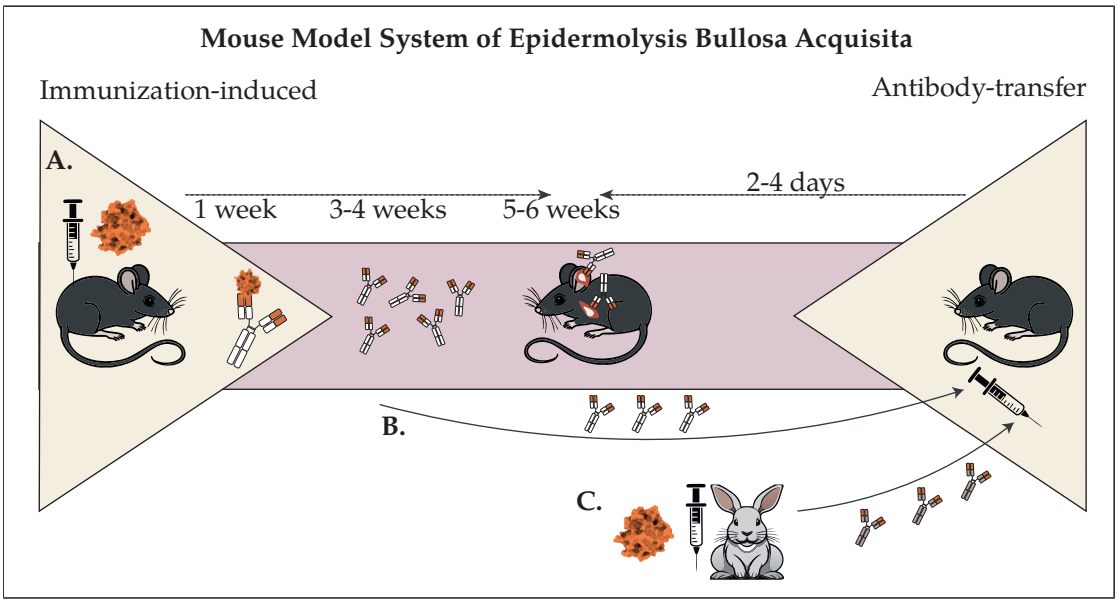

Figure 1.4: The mouse model system of EBA. (A.) The immunization-induced model of EBA relies on the immunization of susceptible mice with immunodominant fragments (mCOLVII^{-C} [93] mCOLVII^{vWFA2} [121]) of mCOLVII. The model allows to study all disease stages from early development of autoreactive T and B cells, the progression to an autoimmune condition and finally autoimmune disease. IgG Aab are first detectable 1 week post immunization (p.I), peaking around 3-4 weeks p.I.. Macroscopic signs of disease on the body surface are observed 5-6 weeks p.I. and are continous with healing of previous blisters and lesions, while new ones are formed acjecent or at different locations of the skin. (B.) Transfer of Aab into healthy recipient mice, leads to cinical blistering 2-4 days post injection (p.I) which is discontinuous after stopping Aab administration. (C.) Immunization of rabbits and transfer of total immune IgG into recipient mice leads to a comparable phenotype than B. Antibody tansfer models allow to exclusively observed the effector phase of disease, where Aab mediate tissue destruction [80, 122].

1.5.4 Pathogenicity Dissected

In the following decade the existing murine models were used and refined to explore the underlying pathomechanisms in EBA. Epitope specificity studies revealed that patient-derived sera cross-react with recombinant fragments of NC-1 mapping to similar hot-spots consistent with earlier human studies [85, 123]. These fragments were used to immunize rabbits, with subsequent transfer of IgG into mice or immunize mice directly. Both experimental lines demonstrated fragement-dependent variability of disease manifestation. Antibody transfer further showed fragment-specific localization of disease in mice. The capacity of neutrophil recruitment *in vivo*, as well as dermal-epidermal separation *in vitro*, was also fragment-dependent, suggesting epitope-dependent cooperativity of Aab in Fc-mediated interactions.

Active immunization of mice confirmed that IgG1 and IgG2b titers correlated with disease activity *in vivo* (immunization-induced model); however, fragment 5 (AA 1108–1323), partially covering the vWFA2 domain, failed to elicit disease *in vivo* [124]. The dominance of complement-fixing IgG subclasses in mice was mirrored by monoclonal anti-hCOLVII antibodies, demonstrating that only complement-fixing subclasses were able to induce dermal-epidermal separation in the presence of monocytes *ex vivo* [125].

Two studies further dissected the murine Aab response, employing 20 overlapping peptides of mCOLVII^{-C} [126, 127]. Despite discrepancies, the latter study demonstrated that pathogenicity is associated with an Aab response against several specific regions within the antigen. Later work, with patient sera, human fragments of NC-1, and COLVII-humanized mice, demonstrated that (1) human Aabs, similar to murine Aabs, target multiple epitopes across NC-1 and that (2) these Aab exhibit cross-reactivity between FNIII epitopes, likely reflecting high similarity between the regions, thereby explaining the wide targeting range of Aab in EBA [128].

Sitaru *et al.* (2010) further demonstrated that the transfer of autoreactive T cells into immunization-induced, disease-resistant SJL$^{nu/nu}$ mice results in the generation of specific IgG1, IgG2a, and IgG2b, showing that (1) T cells are required for autoreactive B cell proliferation and (2) that the resulting Aab response results in IgG1, IgG2a, and IgG2b expression [126]. A landmark paper by Ludwig *et al.* consequently proved the MHC-II association with disease susceptibility in mice, by immunizing distinct laboratory strains with mCOLVII^{-C}. Though all immunized strains developed Aab, disease-susceptible mice harboring the MHC-II H2s haplotype, presented with IgG and C_3 deposition at the DEJ, and preferably developed IgG2a and IgG2b Aabs, which were associated with preferential binding to the aforementioned specific peptide fragments of the antigen [127]. The

MHC-II and T cell association is of utmost importance, as it highlights the close relationship of T and B cells in generating specific Aabs which give rise to the pathophysiology of EBA.
The T cell side was further explored by Hammers *et al.*, showing that EBA is dominated by a T helper cell 1 (Th1)response in the draining lymph nodes (dLN), which is closely associated with an IgG2 dominated response. Circulating titers of Aab are not mediators of disease, but tissue-bound IgG, where IgG2b and IgG1 peak in early phases (21 days post-injection (p.i.)), whereas IgG2c peaks at later phases (42 days p.i.), providing insight in Aab dynamics and origin in EBA. Further, the elevated expression of FcγRIV on leukocytes in disease-susceptible mice hinted towards the involvement of this particular Fcγ receptor in mediating tissue destruction upon Aab binding [129].
The production of Aab in EBA by plasma cells in the dLN was further explored by Tiburzy *et al.* It was shown that, unlike the known production of Ab by short-lived plasma cells in secondary lymphoid tissues and long-lived plasma cells in the spleen and bone marrow [130], Aabs in murine models of EBA are produced by a model-specific intermediate phenotype of short/long-lived plasma cells in the dLN. In contrast to the Aab-producing plasma cells, specific CD4 T cells were not restricted to the lymph nodes, suggesting a sustained survival of specific plasma cells, even in the absence of elevated T cell help. Further, the study revealed a strong adaptive reactivity to the artificial GST-tag of mCOLVII-C, highlighting the need for an optimized immunization protocol that minimizes off-target responses [131]. The immunization-induced model of EBA was therefore refined by immunization with the vWFA2 domain of mCOLVII, which is purified using a cleaved intein tag [110]. Aab targeting of the vWFA2 domain by patient-derived sera had already been shown in early studies [85], and the IgG subclass distribution in this refined model proved to be similarly dominated by IgG1, IgG2a, and IgG2b antibodies, which, upon transfer to healthy mice, were able to induce disease [121]. On the side of the antibody transfer-induced model, it was found that differences between mouse strains—unlike the susceptibility in the immunization-induced EBA model [127]—are not attributed to major MHCII, but rather to distinct genes, one of which, retinoid-related orphan receptor alpha, was shown to be involved in neutrophil function [104].
Other studies further explored Aab clearance [132], the role of glycosylation [133, 134], and downstream Fcγ interaction [135] in EBA. Cumulatively, the previously discussed FcγRIV expression on neutrophils was proven essential for tissue destruction, while IgG1 galactosylation and overall cleavage of glycosylation contributed to or abolished the reduction of tissue destruction. One study further elucidated the extend of Aab transfer-induced disease and found differences between mouse strains, which was unlike the

susceptibility in immunization-induced EBA [127] not attributed to MHCII but distinct genes, one of which (ROR$alpha) was shown to be involved in neutrophil function [104]. The following decade saw a great number of studies focusing on the underlying molecular mechanisms of tissue destruction, involved cell populations, tracking of pathway activation, and means to disrupt tissue destruction by targeting downstream effector pathways in EBA [71, 79, 136]. Of these, Clauder *et al.* addressed MHC-II-dependent changes in the resulting Aabs. By comparing the Aab response in susceptible congenic C57BL/6 mice, carrying the MHC-II H2s haplotype, to wild type (WT) C57BL/6J (H2b) mice, the study demonstrated differential N-glycosylation patterns, which translated into an increased Fcγ activation capacity of IgG1 from susceptible mice. While Aab levels were in general significantly lower in non-susceptible mice, IgG1 was found to be the most frequent IgG subclass in this study, in contrast to the previously described studies, where a shift in the IgG1 to IgG2a/b ratio was attributed with pathogenicity. Importantly, the assessment of regulatory T-cell (T-reg) frequencies in the dLN, previously shown to modulate local tissue destruction [137], showed no difference between susceptible and non-susceptible mice; however, T-regs from susceptible mice exhibited reduced capacity to suppress T-effector cells *in vitro* [138]. Recently, a monoclonal mCOLVII^{vWFA2}-targeting antibody (H510), derived from T-reg-deficient scurfy mice, exhibited the potential of *in vivo* split formation in neonatal mice, importantly without inflammatory involvement [139].

A. Proposed pathomechanisms in EBA

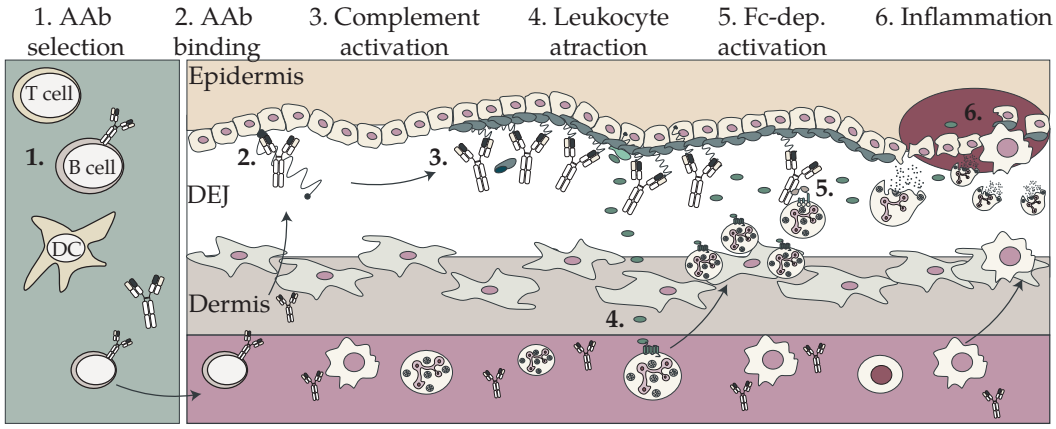

B. Fc-dependent effector mechanisms

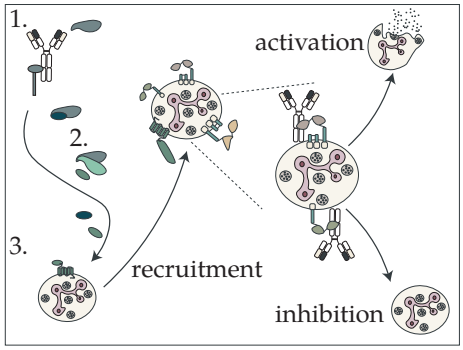

C. Murine Fc receptor activation profile

	FcγRI	FcγRIIB	FcγRIII	FcγRIV	FcRn
IgG1	-	++	++	-	+++
IgG2a/c	+++	++	++	+++	+++
IgG2b	++	++	++	+++	+++
IgG3	+/-	-	-	-	+++

Figure 1.5: Current understanding of EBA pathophysiology A. Proposed Pathomechanism in EBA: 1. Autoantibodies (Aab) arise in the draining lymph nodes (dLN); T cells (T cell help) and dendritic cells (DC) (antigen presentation) are of pivotal importance for the selection process of Aab [121]. 2. B cell plasmablasts may leave the dLN (proposed) and secrete Aab into the circulation, which rapidly, [140] bind to their respective target. 3. Binding of Aab mediates Fc-dependent activation (classical pathway (CP)) of the complement system, further perpetuated by the alternative, Fc-independent pathway [93]. 4. Activation of the complement cascade leads to proteolytic generation of C_{3a} and C_{5a}, of which the latter is the more potent chemotactic factor for neutrophils expressing C5a receptors (C5aR), leading to neutrophil extravasation from the circulation and infiltration of the skin, [141–143]. 5. Neutrophils are locally activated by Aab-activating-Fcγ interaction and cytokine environment, [79]. FcγRIV has been shown to be the most relevant activating receptor in the murine model system of EBA. [135] 6. Neutrophil degranulation, upon activation, leads to initial tissue damage and recruitment of further leukocytes, resulting in perpetuated tissue inflammation. B. Fc-dependent effector mechanism: 1. CP activation is mediated by C_{1q}-Fc binding and activation of the C_1 complex, 2. leading to downstream proteolytic activation of C_3 and C_5, 3. in turn recruiting neutrophils. Fc receptors can mediate activating effects, leading to neutrophil degranulation, or inhibitory effects, depending on Aab class. C. The mode of action is defined by the affinity of IgG subclasses to the different types of murine Fc receptors. Green: activating receptors, red: inhibitory receptors, - no affinity, +/- low affinity, ++ intermediate affinity, +++ high affinity. Figure modified from [68, 79, 80, 143].

1.6 Generation of Monoclonal Antibodies

Previous studies in the field of EBA have generated mAbs using hybridoma technology [97, 139]. The fusion of mature, antigen-experienced, donor-derived B cells with myeloma cells, first introduced by Köhler and Milstein in 1975, enables the generation of immortalized cell lines that produce mAbs [144]. To obtain antigen-experienced B cells, animals are typically immunized with a target antigen, and B cells from secondary lymphoid tissue (such as the spleen or dLN) are harvested for the fusion process. The mAbs produced by individual hybridoma lines are then screened for reactivity to the target antigen to isolate those expressing the desired specificity. While hybridoma technology remains valuable for mAb discovery and isolation, it presents several technical and biological limitations.

As discussed in Section 1.2, the antibody repertoire-and thus the diversity of mature B cells-is vast. However, the success of the fusion process between donor and myeloma cells is limited by several factors, such as the fusion strategy, often resulting in low fusion efficiency [145]. Despite advances that have improved fusion yields [146], these improvements necessitate the maintenance and screening of all resulting cell lines. Fur-

thermore, some hybridoma cell lines are intrinsically low antibody producers and may completely lose expression upon prolonged culture [147], resulting in the loss of both the cell line and the corresponding mAb. Efforts to preserve hybridoma clones also highlight genetic limitations: hybridoma lines, despite their intended monoclonality, can exhibit heterogeneity and express more than one mAb. Aberrant heavy and light chain gene expression-arising from the myeloma line, from the fusion of more than two cells, or from the second allele of the fusion partner, can result in ambiguous amplicons when cloning mAb sequences from hybridomas [148, 149].

Consequently, the hybridoma approach is less suited to comprehensive exploration of mAbs within immune repertoires. Display techniques, such as phage display, enable extensive screening of BCR repertoires by linking the genetic and structural information of antibody variable regions for subsequent expression and selection [150]. Phage display is based on the pioneering work of George P. Smith, who demonstrated the display of peptide fragments on the surface of filamentous phages [151]. This approach was subsequently adapted by Gregory P. Winter to generate and display antibody fragments, allowing for selection against specific antigens and isolation of antigen-specific antibody fragments [152]. Both Smith and Winter were awarded the Nobel Prize in Chemistry in 2018 for these discoveries. The application of phage display in antibody discovery has greatly facilitated the exploration of antibody repertoires and enabled the rapid isolation of multiple mAbs with diverse binding properties [153]. All display techniques are fundamentally based on the original concept of phage display and rely on the reliable cloning of functional IG genes into suitable expression and selection systems, thereby coupling genetic information to polypeptide structure for recombinant expression and selection [147, 149, 150].

Phage display relies on antibody libraries that incorporate IG gene diversity. These libraries can be synthetic (allowing selection against a broad variety of target antigens), naïve (derived from human donors), or immune (constructed from antigen-experienced lymphoid tissues of immunized animals) [150, 154, 155]. To generate naïve or immune antibody libraries, messenger ribonucleic acid (mRNA) encoding rearranged V^H and V^L chains is isolated, amplified, and molecularly cloned with the introduction of a linker region to join the chains [147, 152]. The resulting single-chain fragment variable (scFv) constructs exhibit binding properties similar to the corresponding full-length antibodies [156]. Of note, chain pairing in scFv generation is undirected, thereby possibly generating scFv's, non existing in the donor tissue.

The scFvs are genetically fused to the coat protein (e.g., M13 pIII) of bacteriophages via a phagemid vector, enabling co-expression of scFv-coat protein fusion proteins on

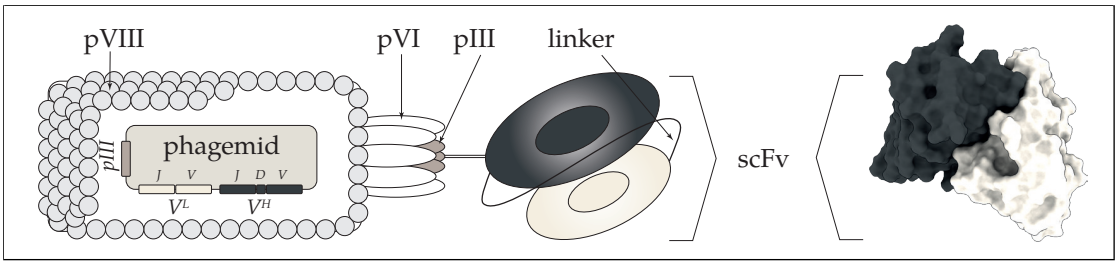

Figure 1.6: Structural composition of a single-chain fragment variable (scFv)-coupled phage Wild filamentous M13-bacteriophages are single stranded DNA viruses, constituted by five different coat proteins (pIII, pVI, pVIII, pVII, pIX). (Left) In phage display, the introduced phagemid encodes pIII fused to a scFv, resulting in the presentation of the scFv on the phage surface. (Right) Alpha fold modelled scFv (without linker region); the linker connects both variable chains and is located between V^H and V^L (loop in schematic depiction, left).

fully assembled phage particles [157]. To produce scFv-displaying phages, bacteria harboring the replication-deficient phagemid are infected with helper phages, leading to scFv-phage production [158]. These scFv-phages display the scFv on their surface while encapsulating the phagemid vector containing the paired V^H and V^L sequences. Through a process termed panning [159], scFv-phages are selected against the antigen of interest, bound phages are eluted, and the enriched pool is used to reinfect bacteria for library propagation. Multiple panning rounds enable *in vitro* affinity selection of scFvs, partially mimicking the affinity maturation of B cells during GC reactions. The V^H and V^L sequences of binding scFv-phages can be recovered and sequenced, allowing for analysis of clonality and recombinant expression in various formats (e.g., scFv, full-length IgG - independent of species) [147].

1.6.1 Mouse Immune Libraries for the Generation of ScFv Fragments Targeting mCOLVII

Recombinant antibodies can be derived from immune libraries generated from immunized animals [125, 160, 161]. Immune libraries are highly biased toward the antigen used for immunization, increasing the probability of isolating antigen-specific antibodies. Smaller library sizes (5×10^5 to 1×10^6 independent clones) are sufficient for isolating high-affinity binders in immune libraries due to the preceeding *in vivo* preselection [160]. However, laboratory mouse strains exhibit a less diverse BCR repertoire compared to wild mice due to limited antigen exposure in controlled housing conditions [7]. As discussed

in Section 1.3, autoantigen immunogenicity is tightly regulated by self-tolerance. In the immunization-induced EBA model, this tolerance is breached using antigen-adjuvant emulsions in susceptible mice [121], increasing the likelihood of isolating autoreactive (and potentially pathogenic) antibodies.

To isolate mCOLVII^{vWFA2}-specific mAbs, two scFv antibody immune libraries for phage display selection were generated from the spleen (S) and dLN (LN) of a B6.SJL-H2^{s} C3/1CyJ mouse, immunized with recombinant mCOLVII^{vWFA2} [121, 162] using a two-step cloning strategy as described in [162–164] and depicted in Fig. 1.7 A. Several mice were immunized and assessed weekly for their disease-affected body surface area (procedure described in detail in Subsection 3.1.5), to verify disease onset and progression of EBA. After euthanization at different timepoints, secondary lymphoid tissues most possibly harboring mCOLVII^{vWFA2}-specific B cell clones [131] were sampled with following phenol-chloroform ribonucleic acid (RNA) extraction. Samples of one mouse, euthanized at week 8 post immunization (p.I.), were chosen for library preparation, after assessment of mCOLVII^{vWFA2}-specific serum IgG, the capacity of serum IgG to bind to healthy murine skin sections, and RNA integrity analysis (Fig. 1.7 C-E). First-strand copy deoxyribonucleic acid (cDNA) synthesis was performed for both samples and V^{H} and V^{L} chains amplified by multiplex gradient polymerase chain reaction (PCR), using a set of degenerated primers to account for amplicon diversity (Fig. 1.7 F, G) [149]. Using a two-step cloning strategy, heavy and light chain sublibraries were generated separately in cloning vector pUC19-MSC2017 (2.7) (Fig. 1.7 H). ScFv immune libraries were assembled in pUC19-MSC2017, using the Sfi multiple cloning site (MSC), and cloned into pJB12 (2.7) phagemid for phage display selection (Fig. 1.7 I). Both libraries exhibited a potential diversity of 2.325×10^{7} (S) to 3×10^{7} (LN) clones as determined by colony forming units (CFU) and insert controls after library assembly in phagemids [162].

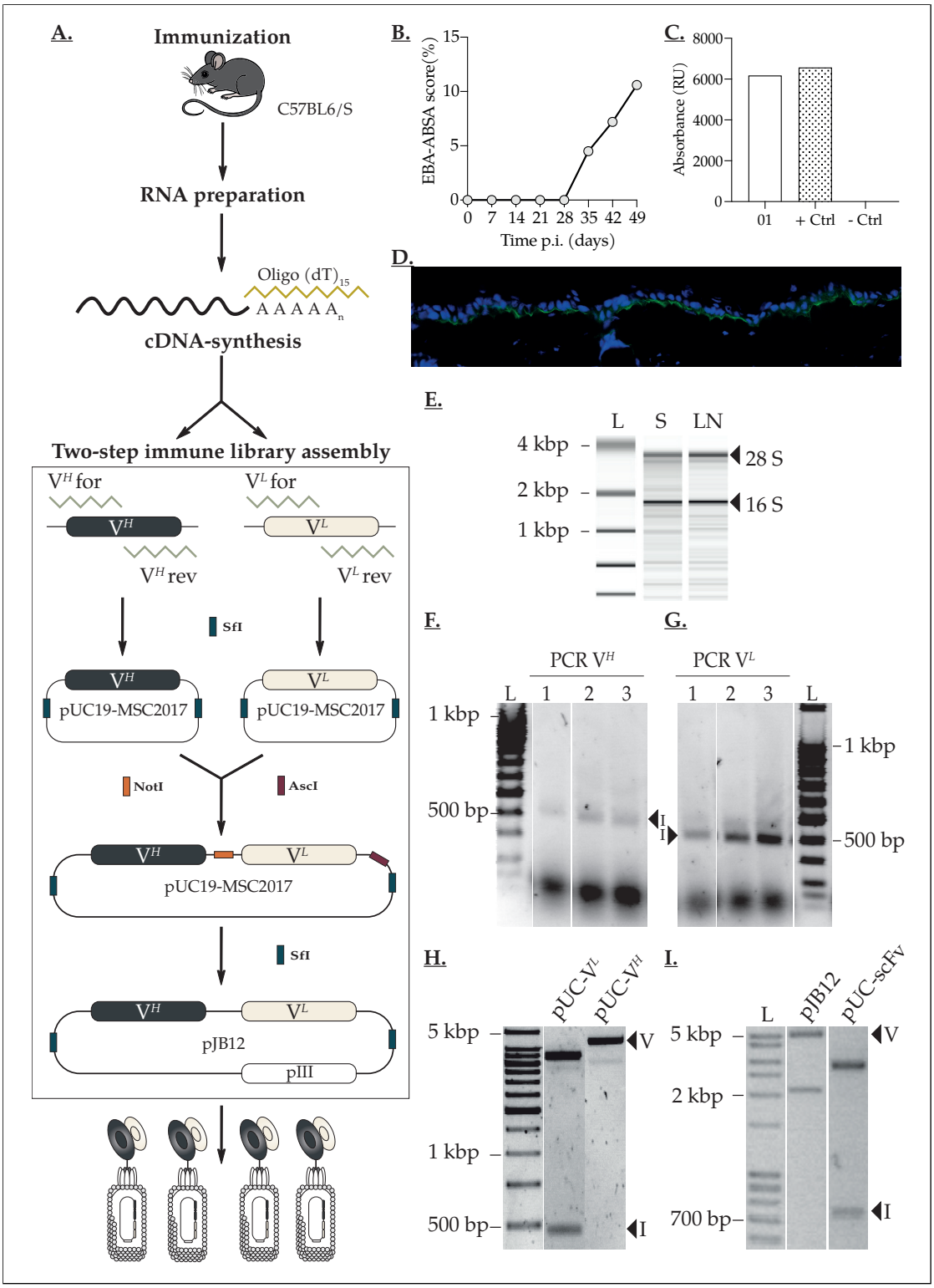
A.
Immunization
C57BL6/S
RNA preparation
Oligo (dT)15
A A A A A An
cDNA-synthesis
Two-step immune library assembly
VH for
VL for
VH
VL
VH rev
VL rev
SfiI
pUC19-MSC2017
NotI
AscI
pJB12
pIII
B.
EBA-ABSA score (%)
Time p.i. (days)
C.
Absorbance (RU)
01
+ Ctrl
- Ctrl
D.
E.
L
S
LN
4 kbp
2 kbp
1 kbp
28 S
16 S
F.
PCR VH
G.
PCR VL
500 bp
H.
pUC-VL
pUC-VH
5 kbp
I.
pJB12
pUC-scFv
700 bp

Figure 1.7: Generation of two antibody immune libraries for phage display selection of mCOLVII^{vWFA2}-specific antibody clones. Schematic workflow of the process of immune library construction: (A) A B6.SJL-H2s C3/1CyJ mouse was immunized with recombinant mCOLVII^{vWFA2}. (B) Active disease progression was determined by assessment of affected body surface area in %. (C) Specific serum IgG was detected in an antigen-specific ELISA, using a pool of sera from immunized mice as positive control (+Ctrl) and serum pool from non-immunized mice as negative control (-Ctrl). (D) Linear binding of serum IgG to full-length protein at the DEJ was verified by indirect IF on healthy murine skin (anti-IgG-FITC (green), DAPI (blue)). (E) Spleen (S) and draining lymph nodes (LN) were sampled, and RNA extracted by phenol-chloroform extraction. RNA quality was assessed using capillary electrophoresis, followed by calculation of the RNA integrity number (RIN) using the 28S to 16S ratio of ribosomal RNA, with both samples exhibiting intact RNA (F,G). V^H and V^L chains were amplified from copy DNA (cDNA) using multiplex gradient polymerase chain reaction (PCR) with a set of degenerated primers. Gel electrophoresis revealed amplicon bands (I) at all respective annealing temperatures (1-3: 45°C, 50°C, 55°C), indicating successful amplification of both targets. PCR negative controls without reverse transcriptase and reactions without template confirmed no contamination with foreign DNA or genomic material (data not shown). (H) Using a two-step cloning strategy, gel-purified V^H and V^L amplicons (I) were cloned into pUC19-MSC2017 (V) using the SfiI multiple cloning site (MSC), and approximately 400 basepair (bp) -sized V^L fragments (I) were cloned into linearized pUC-V^H (V) using NotI-HF and AscI-HF, generating scFvs. (I) Phagemid pJB12 (V) and pUC-scFv (I) were digested with SfiI prior to ligation of the scFv insert into pJB12.

1.6.2 Next-Generation Sequencing in the Context of Antibody Immune Libraries and Repertoires

Coupling phage display with high-throughput next-generation sequencing (NGS) of immune libraries is a powerful tool to trace enriched antibody clonotypes across the panning procedure. The combined use of NGS and phage display was first described by Ravn *et al.* in 2010, who observed parallel enrichment of specific CDR3 sequences and antigen-binding antibodies during panning [165]. Ever since, This strategy has been applied to various antibody libraries (synthetic, naïve, immune), which have been analyzed using NGS platforms to characterize changes in antigen-binding sequence composition during iterative panning [166]. By sequencing V^H or paired V^H and V^L regions, CDR3s are determined which enables systematic tracking of clonal dynamics, identification of rare high-affinity clones, and elimination of nonspecific binders early in the selection process [161, 163, 164].

1.7 Aim of The Study

The following study was conducted to generate and thoroughly characterize mAbs in the context of (murine) EBA. Despite an advanced understanding of the downstream pathomechanisms mediated by Aab in EBA, the clonality of Aab remains unadressed. Along the same line mAbs capable of inducing inflammatory EBA upon transfer are still missing The generation of disease-causing recombinant Aab would strengthen the validity of antibody transfer models of EBA by fully murinizing the model and providing extended control over the system. Effector functions could be further explored in detail by subclass switching and Fc engineering of such pathogenic mAbs. Additionally, knowledge of Aab clonality in EBA would deepen our current understanding of the processes that distinguish pathogenic from non-pathogenic Aab in (murine) EBA.

Chapter 2

Material

The following section lists the materials used in this study. If applicable manufacturer names are abbreviated in the table descriptions to ensure stable formatting of the respective tables. In Section 2.10 buffers and solutions are provided with corresponding protocols (Protoc.) from the material chapter to allow for direct identification. Standard unit, experimental practice, as well as established laboratory practice abbreviations (chemicals and methods), are listed in Tab. S7, S6 and S8 and are therefore not further introduced.

2.1 Mouse Strains

Table 2.1: Mouse strains used in this study. The table details strain names, genetic backgrounds, and relevant references.

Strain	**Background**	**Reference**
000664	C57Bl/6J	RRID:IMSR_JAX:000664
000966	B6.SJL-H2s C3/1CyJ	RRID:IMSR_JAX:000966

2.2 Bacteria and Cell Strains

Table 2.2: Commercially obtained bacteria and cell strains used for molecular cloning and protein expression. Manufacturers (Mfr.) are abbreviated as indicated: AG (Agilent Technologies), NB (New England Biolabs), ME (Merck), TF (Thermo Fisher Scientific). Headquarters locations (City, State - County (Ctry.)) are provided for each manufacturer.

Species	Strain	Mfr.	City, State	Ctry.
Escherichia coli	XL-1 Blue	AG	Santa Clara, CA	USA
Escherichia coli	ER 2566	NB	Ipswich, MA	USA
Escherichia coli	NovaBlue	ME	Darmstadt	DE
Escherichia coli	TG-1	AG	Santa Clara, CA	USA
Chinese Hamster(Ovary)	CHO-S	TF	Waltham, MA	USA

2.3 Antibodies

Table 2.3: Commercially or in-house obtained antibodies used in this study. Antibodies were sourced from various suppliers, including Jackson ImmunoResearch (JIR), HycultBiotech (HB), BD Biosciences (BD), Creative BioMart (CB), Biolegend (BL), Cappel (CP), and Cedarlane (CL). Keyhole Limpet Hemocyanin (KLH), In-house (IH). A complete list of antibodies, their properties (host-/target species, conjugate, clonality and format), and source is provided.

Target	Species		Conjugate	Clone	Format	Source
	Host	Anti				
Biotin	*S. avidinii*	–	HRP	–	streptavidin	JIR
C_3	chicken	human	biotin	Poly	IgY	CL
C_3	goat	mouse	FITC	Poly	IgG	CP
C_3	rat	mouse	–	11H9	IgG2a	HB
HER2	rat	human	–	4D5	scFv	IH
IgG (H+L)	donkey	mouse	FITC	Poly	F(ab')2	JIR
IgG (H+L)	goat	mouse	HRP	Poly	IgG	JIR
IgG (H+L)	goat	rat	AF 694	Poly	IgG	JIR
IgG2b	goat	mouse	–	Poly	IgG	Bethyl
IgG2b (H)	goat	mouse	HRP	Poly	IgG	Bethyl
KLH	mouse	*Megathura crenulata*	–	MG2b-57	IgG2b, κ	BL
KLH	rat	*Megathura crenulata*	–	RTK2758	IgG2a, κ	BL
N.A.	mouse	N.A.	-	MOPC-173	IgG2a, κ	BL
Ly6C	rat	mouse	FITC	AL-21	IgM, κ	BD
Ly6G	rat	mouse	PE-Cy^7	1A8	IgG2a, κ	BD
M13	mouse	M13 bacteriophage	HRP	–	IgG1	CB
$mCOLVII^{-C}$	rabbit	mouse	–	Poly	IgG	[93]
$mCOLVII^{vWFA2}$	rabbit	mouse	–	Poly	IgG	[167]

2.3.1 Obtained mCOLVII Targeting Antibody Clones

Apart from the mCOLVII-targeting clones generated in this study, additional antibody clone DNA sequences were obtained from collaboration partners. Prof. Dr. Ralf J. Ludwig and Dr. Annika Kasprick from the Lübeck Institute of Experimental Dermatology, University of Lübeck, Germany, provided mCOLVII^{vWFA2}-targeting clone 16A1C8 (further referred to as clone C7). The clone was generated using hybridoma technology with lymph nodes from SJL/J mice (strain 000686). Two clones targeting mCOLVII^{-C} (C8, C9) were acquired from PD Dr. Andreas Recke from the *Klinik für Dermatologie, Allergologie und Venerologie* (*Hautklinik*), University Medical Center Schleswig-Holstein, Lübeck, Germany. These clones originated from a different phage display approach using spleens from mCOLVII^{-C} immunized SJL/J mice (strain 000686) for immune library preparation. Clone H510 (C10), which has been published by Vicari *et al.* [139], was obtained from Prof. Dr. Eva Hadaschik and Dr. Elisabeth Vicari at the Department of Dermatology, Heidelberg University Hospital, Germany. H510 was generated from B6.Cg-Foxp3^{sf}/J (scurfy) mice using hybridoma technology. A detailed description of the methodology can be obtained from Haeberle *et al.* [168].

Table 2.4: Antibodies targeting mCOLVII, generated or used in this study. Internal IDs were assigned for all clones and are used to refer to full-length IgG. Abbreviations: Leon F. Schmidt-Jiménez (L.F.S.J), Ralf J. Ludwig (R.J.L), Anika Kasprick (A.K), Andreas Recke (A.R), Elisabeth Vicari (E.V), Eva Hadaschik (E.H).

Internal ID	Clone	Target	Tissue Origin	Source
1	S4	*mCOLVII^{vWFA2}*	spleen	L.F.S.J
2	S8	*mCOLVII^{vWFA2}*	spleen	L.F.S.J
3	S11	*mCOLVII^{vWFA2}*	spleen	L.F.S.J
4	S16	*mCOLVII^{vWFA2}*	spleen	L.F.S.J
5	L16	*mCOLVII^{vWFA2}*	lymph nodes	L.F.S.J
6	L20	*mCOLVII^{vWFA2}*	lymph nodes	L.F.S.J
7	16A1C8	*mCOLVII^{vWFA2}*	lymph nodes	R.J.L, A.K.
8	B8	*mCOLVII^{-C}*	spleen	A.R.
9	C10	*mCOLVII^{-C}*	spleen	A.R.
10	H510	*mCOLVII^{vWFA2}*	spleen / lymph node pool	E.V., E.H.

2.4 Primer

The following table indicates the DNA sequences of the primers used for Sanger sequencencing of V^L and V^H 2.5 and NGS of V^H 2.5. Costum designed primer sequences for V^H-C^H RNA-sequencing lie with iRepertoire, Inc. and were not provided by the company.

Table 2.5: Sequencing primers used for NGS and Sanger analysis. The table lists the sequencing primers used for both next-generation sequencing (NGS) and Sanger analysis. The NGS primers include forward and reverse sequences, with placeholders for adapter and index sequences required for library preparation.

Primer	**Sequence (5'–3')**
NGS *for*	Adapter-Index-Adapter-CGGCAGCCGCTGGATTGTTATTAC
NGS *rev*	Adapter-Index-Adapter-CGAGGAAACGGTGACCGTGGT
	Adapter-Index-Adapter-CGAGGAGACTGTGAGAGTGGT
	Adapter-Index-Adapter-CGCAGAGACAGTGACCAGAGT
	Adapter-Index-Adapter-CGAGGAGACGGTGACTGAGGT
Sanger V^H	CGTATGTTGTGTGGAATTGTGAGCGG
Sanger V^L	CATAGCCCCCTTATTAGCGTTTGCC

2.5 Reagents

The following section contains complete, alphabetically structured tables of all reagents used in this study.

Table 2.6: Reagents used in this study, including their empirical formulas (if available), and their manufacturers (Mfr.), inlcuding headquarte locations - City, State and country (Ctry.). Abbreviations: SA (Sigma-Aldrich), CR (Carl Roth), ME (Merck), TF (Thermo Fisher Scientific), RO (F. Hoffmann-La Roche), BR (BioRad), LO (Lonza), FK (Fresenius Kabi), VE (Vetoquinol), SB (SouthernBiotech), WA (WAK-Chemie Medical), NEB (New England Biolabs), RA (Ratiopharm), BI (Biochrom), CL (ClearH2O), MP (MP Biomedicals), MI (Miltenyi Biotec), GS (GenScript) JI (Jackson ImmunoResearch), QI (QIAGEN), TG (Th. Geyer), SE (SERVA Electrophoresis), PR (Progen Biotechnik), CY (Cytiva), SF (Sakura Finetek Japan Co., Ltd.), TI (TiterMax USA), BL (BioLegend), BG (BioScience GmbH), NB (Novateinbio), IL (Illumina), MC (MaxCyte), NT (Nanotemper), MN (Macherey Nagel), NBio (NovaTein Biosciences), GE (Genaxxon BioScience), ROC (F. Hoffmann-La Roche), BD (BD Biosciences).

Reagent	**Empirical Formula**	**Mfr.**	**Location**	
			City, State	**Ctry.**
(±)-Ketamine hydrochloride	$C_{13}H_{16}ClNO \cdot HCl$	SA	Darmstadt	DE
100 bp DNA ladder	-	TF	Waltham, MA	USA
1-propanol	$CH_3CH_2CH_2OH$	CR	Karlsruhe	DE
250 bp DNA ladder	-	TF	Waltham, MA	USA
2-propanol	$(CH_3)_2CHOH$	CR	Karlsruhe	DE
β-mercaptoethanol	C_2H_6OS	SA	Darmstadt	DE
2xYT agar	-	CR	Karlsruhe	DE
2xYT medium	-	CR	Karlsruhe	DE
MOPS	$C_7H_{15}NO_4S$	CR	Karlsruhe	DE
Bromophenol blue	$C_{19}H_{10}Br_4O_5S$	CR	Karlsruhe	DE
DAPI	$C_{16}H_{15}N_5$	TF	Waltham, MA	USA
Luminol	$C_8H_7N_3O_2$	SA	Darmstadt	DE
ABTS™ tablets	$C_{18}H_{18}N_4O_6S_4$	RO	Basel	CH
Acetone ≥99.5%	C_3H_6O	CR	Karlsruhe	DE
Acetic acid	$C_2H_4O_2$	CR	Karlsruhe	DE
Methanol	CH_3OH	CR	Karlsruhe	DE
Affi-Gel® 10 Active Ester Agarose	-	BR	Hercules, CA	USA

Continued on next page...

Reagent	Empirical Formula	Mfr.	Location	
			City	Ctry.
Agarose	$C_{24}H_{38}O_{19}$	LO	Basel	CH
Agarose Ultra Pure	$C_{24}H_{38}O_{19}$	LO	Basel	CH
Ammonium thiocyanate ≥99%, p.a., ACS, ISO	NH_4SCN	CR	Karlsruhe	DE
Ampicillin	$C_{16}H_{19}N_3O_4S$	CR	Karlsruhe	DE
Ampuwa (H_2O)	H_2O	FK	Bad Homburg	DE
Antisedan	$C_{14}H_{16}N_2HCl$	VE	Magny-Vernois	FR
Calcium chloride	$CaCl_2$	ME	Darmstadt	DE
Carbenicillin	$C_{17}H_{18}N_2O_6S$	CR	Karlsruhe	DE
Chloramphenicol	$C_{11}H_{12}Cl_2N_2O_5$	CR	Karlsruhe	DE
Collagenase from *Clostridium histolyticum* Type VI	-	SA	Darmstadt	DE
Coomassie Brilliant Blue R-250	$C_{45}H_{44}N_3NaO_7S_2$	BR	Hercules, CA	USA
cOmplete™ protease inhibitor cocktail, EDTA free	-	ME	Darmstadt	DE
DAPI Fluoromount-G®	-	SB	Birmingham, AL	USA
Difco(TM) TC Yeastolate	-	TF	Waltham, MA	USA
Dimethyl sulfoxide (DMSO)	C_2H_6OS	WA	Starnberg	DE
Domitor	$C_{13}H_{16}CN_2HCl$	VE	Magny-Vernois	FR
Ethanol	C_2H_5OH	CR	Karlsruhe	DE
Ethidium bromide	$C_{21}H_{20}BrN_3$	CR	Karlsruhe	DE
EDTA ≥99%	$C_{10}H_{14}N_2Na_2O_8 \cdot 2H_2O$	CR	Karlsruhe	DE
BSA biotin free	-	CR	Karlsruhe	DE
FCS	-	TF	Waltham, MA	USA
Gel Loading Dye, Purple (6X)	-	NEB	Ipswich, MA	USA
Glucose	$C_6H_{12}O_6$	CR	Karlsruhe	DE
Glycerol	$C_3H_8O_3$	CR	Karlsruhe	DE
Glycine	$C_2H_5NO_2$	CR	Karlsruhe	DE
Heparin-Sodium-2500	-	RA	Ulm	DE

Continued on next page...

Reagent	Empirical Formula	Mfr.	Location	
			City	Ctry.
HEPES	-	BI	Cambridge	UK
HT-Supplement (100x)	-	TF	Waltham, MA	USA
Hydrogel®	-	CL	Westbrook, ME	USA
IPTG	$C_9H_{18}O_5S$	CR	Karlsruhe	DE
Kanamycin A	-	CR	Karlsruhe	DE
LB Medium	-	MP	Irvine, CA	USA
L-Glutamine Penicillin Streptomycin	-	SA	Darmstadt	DE
Magnesium chloride	$MgCl_2$	CR	Karlsruhe	DE
Magnesium chloride hexahydrate	$MgCl_2 \cdot 6H_2O$	CR	Karlsruhe	DE
Mowiol	$(\text{-}CH_2CHOH\text{-})_n$	CR	Karlsruhe	DE
Nuclease-free H_2O	-	QI	Venlo	NL
Penicillin sodium salt	-	SA	Darmstadt	DE
Pluronic® F-68	-	ME	Darmstadt	DE
Polyethylene glycol 20000	$HO(C_2H_4O)_nH$	SE	Heidelberg	DE
Polyethylene glycol 6000	$HO(C_2H_4O)_nH$	CR	Karlsruhe	DE
Polymorphprep	-	PR	Heidelberg	DE
Polysorbate 20 (Tween® 20)	$C_{58}H_{114}O_{26}$	CR	Karlsruhe	DE
Propidium iodide	$C_{27}H_{34}I_2N_4$	MI	Bergisch Gladbach	DE
Protein G Sepharose 4 Fast Flow resin	-	CY	Marlborough, MA	USA
Protein G Resin		GS	Nanjing	CHN
RNase Away	-	CR	Karlsruhe	DE
RNase-free H_2O	-	QI	Venlo	NL
ROTI® Histofix (4% formaldehyde, phosphate buffered)	-	CR	Karlsruhe	DE

Continued on next page...

Reagent	Empirical Formula	Mfr.	Location	
			City	Ctry.
ROTI® Mount FluorCare DAPI	-	CR	Karlsruhe	DE
Sodium azide	NaN_3	ME	Darmstadt	DE
Sodium bicarbonate	$NaHCO_3$	ME	Darmstadt	DE
Sodium carbonate	Na_2CO_3	ME	Darmstadt	DE
Sodium dodecyl sulfate	$C_{12}H_{25}NaO_4S$	ME	Darmstadt	DE
Sodium hydroxide solution 2 mol/L - 2 N	NaOH	CR	Karlsruhe	DE
Sodium phosphate monobasic monohydrate	$NaH_2PO_4 \cdot H_2O$	ME	Darmstadt	DE
Sodium acetate	$C_2H_3NaO_2$	TF	Waltham, MA	USA
Sodium butyrate	$C_4H_7NaO_2$	ME	Darmstadt	DE
Sodium chloride	NaCl	CR	Karlsruhe	DE
Streptomycin	$C_{21}H_{39}N_7O_{12}$	SA	Darmstadt	DE
Sulfuric acid 25%	H_2SO_4	ME	Darmstadt	DE
Tetracycline	$C_{22}H_{24}N_2O_8$	CR	Karlsruhe	DE
Tissue-Tek® O.C.T. Compound	-	SF	Tokyo	JP
Titermax® Classic	-	TI	Norcross, GA	USA
TRIS	$C_4H_{11}NO_3$	ME	Darmstadt	DE
Trizol	-	TF	Waltham, MA	USA
Trypan blue	-	SA	Darmstadt	DE
Tryptone / peptone from casein	-	CR	Karlsruhe	DE
Xylazine	$C_{12}H_{16}N_2S$	SA	Darmstadt	DE
Yeast extract	-	CR	Karlsruhe	DE

2.5.1 Biologics

Biologics refers to reagents that are of biological origin, such as plasmids, antisera and recombinant protein, which are listed and described in the following tables.

Table 2.7: Plasmids used in, or used for the generation of pivotal proteins for this study. The table indicates the respective plasmid, relevant properties, references (if applicable) and designated application. Abbreviations: TF (ThermoFisher Scientific), MCS (Multiple Cloning Site).

Plasmid	Properties	Reference	Application
pcDNA3.1(+)	Mammalian Expression Vector	TF, V790-20	mIgG2b expression
pGEX-6P-1	GST-Tagged Protein Expression	Sitaru *et al.* [93]	mCOLVII^{-C} expression
pJB12	Phagemid Vector	Krebber *et al.* [149]	Immune library selection
pTWIN1	Intein-Tagged Protein Expression	Leineweber *et al.* [110]	mCOLVII^{vWFA2} expression
pUC19-MSC2017	pUC19 with Sfi MCS	Krohn *et al.* [164]	Immune library assembly

Table 2.8: Biologics used in experimental procedures. The table lists recombinant (recomb.) proteins, enzymes, and sera utilized in this study together with their respective manufacturer (Mfr.) and their headquarter locations (City, State - Country). Abbreviations: SA (Sigma-Aldrich), TF (ThermoFisher Scientific), JIR (Jackson ImmunoResearch), NEB (New England Biolabs), IH (In-House).

Item	Type	Mfr.	Location	
			City, State	Country
DNAse	enzyme	SA	Darmstadt	DE
GST	recomb. protein	IH	Lübeck	DE
Helper phage	M13KO7	TF	Waltham, MA	USA
mCOLVII-antisera	serum	IH	Lübeck	DE
mCOLVII^{-C}	recomb. protein	in-house	Lübeck	DE
mCOLVII^{vWFA2}	recomb. protein	IH	Lübeck	DE
normal donkey serum	serum	JIR	West Grove, PA	USA
normal goat serum	serum	JIR	West Grove, PA	USA
normal human serum	serum	IH	Lübeck	DE

Continued on next page...

Item	Type	Mfr.	Location	
			City, State	Country
normal murine serum	serum	IH	Lübeck	DE
SfII	enzyme	NEB	Ipswich, MA	USA

2.5.2 Commercial Kits and Buffers

Table 2.9: Commercial kits and buffers used in this study. The table lists all buffers and kits, including their manufacturers (Mfr.), and locations - City, State and country (Ctry.). Abbreviations: SA (Sigma-Aldrich), NEB (New England Biolabs), TF (Thermo Fisher Scientific), MB (Miltenyi Biotec), QI (Qiagen), MN (Macherey Nagel), TG (Th. Geyer), BL (BioLegend), IL (Illumina), FK (Fresenius Kabi), GE (Genaxxon BioScience), PR (Promega), MC (MaxCyte), BD (BD Biosciences), ROC (F. Hoffmann-La Roche), BG (BioScience GmbH), NB (Novateinbio), NT (Nanotemper).

Buffer / Kit	Mfr.	Location	
		City	Ctry.
10 x CutSmart	NEB	Ipswich, MA	USA
TMB one solution	PR	Madison, WI	USA
ABTS buffer (x10)	ROC	Basel	CH
BD CompBeads Anti-Rat and Anti-Hamster Ig κ /Negative Control Compensation Particles Set	BD	Franklin Lakes, NJ	USA
CaptureSelect LC-kappa (mur) Affinity Matrix	TF	Waltham, MA	USA
CD CHO-Medium	TF	Waltham, MA	USA
CD OptiCHO-Medium	TF	Waltham, MA	USA
CHO CD EfficientFeed	TF	Waltham, MA	USA
D-PBS w.o. Ca^{2+}, Mg^{2+}	TF	Waltham, MA	USA
EPB-1	MC	Gaithersburg, MD	USA

Continued on next page...

Table 2.9 – Continued from previous page

Buffer / Kit	Mfr.	Location	
		City, State	Ctry.
Gelatin Veronal Buffer With Mg & Ca (GVB++)	NB	Woburn, MA	USA
GlutaMAX Supplement	TF	Waltham, MA	USA
L-Glutamin Penicillin Strept.	SA	Darmstadt	DE
MACSQuant running buffer	MB	Bergisch-Gladbach	DE
MiSeq Reagents Kit 2	IL	San Diego, CA	USA
MiSeq Reagents Kits 3	IL	San Diego, CA	USA
NaCl 0.9%	FK	Bad Homburg	DE
Neutrophil Isolation Kit, mouse	MB	Bergisch-Gladbach	DE
NucleoBond PC 2000 EF	MN	Düren	DE
NucleoBond Xtra Maxi Kit	MN	Düren	DE
NucleoSpin Plasmid kit	MN	Düren	DE
PH-Buffer Solutions pH 4, 7, 10	TG	Renningen	DE
Protein Labeling Kit RED-NHS 2nd Generation	NT	Munich	DE
QIAquick Gel Extraction Kit	QI	Venlo	NL
RPMI	SA	Darmstadt	DE
RPMI-1640 w/o phenolred w/o glucose	BG	Ulm	DE
Super Optimal Broth (SOC)-Medium	TF	Waltham, MA	USA
Zombie NIR Fixable Viability Kit	BL	San Diego, CA	USA

2.5.3 Buffers and Solutions

Table 2.10: Buffers and solutions used in this study. The table lists all buffers and solutions, their composition, pH (if applicable), and application. If not otherwise indicated, given percentages are defined as weight per volume (w/v).

Buffer / Medium	Composition	pH	Application
1 M $MgCl_2$	50.83 g in 250 ml ddH_2O	–	3.2.1
10xMOPS	0.4 M MOPS, 0.1 M NaOAc, 0.01M EDTA in ddH_2O	7	3.2.1
1M Sodiumbutyrate	110.9 g/L sodiumbutyrate in ddH_2O	–	3.5.2
1xPBS	1.8g NaH_2PO_4 x H_2O, 8g NaCl	7.4	General
2xYT-Agar-plates	3.1 % (w/v) 2xYT, 1.8 % (w/v) agar	–	3.2
2xYT-Medium	3.1 % (w/v) 2xYT	7.0 ± 0.2	3.2
2xYT-Top-Agar	2xYT Medium, 8 g/L 2xYT agar, 5 mM $MgCl_2$	–	3.2.1
50xTAE	0.2 M TRIS, 50mM EDTA	7.4	3.2
ABTS-substrate	5 mL 10xABTS-buffer, 45 mL ddH_2O, 1 ABTS-tablett	–	3.2.5
Anesthesia stock	2 mL ketamine stock, 2.65 mL Medetomidin, 11 mL 0.9% NaCl	–	3.1
B1 buffer	20 mM HEPES, 500 mM NaCl, 1mM EDTA	7	3.2.2
Bicarbonate buffer	0.05 M Na_2CO_3, 0.05 M $NaHCO_3$	9.6	3.6.1
Binding buffer	20 mM Na_2HPO_4, 150 mM NaCl	-	3.1.4
Binding buffer	0.05M Na_2CO_3, 0.05M $NaHCO_3$	9.6	3.6.4
Blocking buffer	1% (w/v) BSA in 1xPBS	7.4	3.6.1
Blocking buffer	2% (w/v) BSA in PBS	–	3.2.5
Blocking buffer	4% (w/v) BSA in 1x PBS	7.4	3.6.2, 3.6.2
Blocking buffer	5% (v/v) milk powder in 1xPBS	7.4	3.6.1
Blocking Buffer	0.05% (v/v)Tween20, 1% (w/v) BSA in 1xPBS	7.4	3.6.4

Continued on next page...

Buffer / Medium	Composition	pH	Application
CD Opti CHO-Production-Medium	CD OptiCHO^{TM}-Medium, 1% (v/v) Pluronic® F-68, 1% (v/v) GlutaMAX^{TM} Supplement, 1% (v/v) HT-Supplement (100x)	–	3.5.2
CHO-Growth -Medium	CD CHO-Medium, 1% GlutaMAX^{TM} Supplement, 1% HAT-Supplement (100x)	–	3.5.2
Chloramphenicol	30 mg/ml in EtOH	–	3.2
CL medium	RPMI-1640 w/o phenolred, w. L-glutamine, 25mM HEPES, 2% glucose, 1% FCS	7.2	3.6.4
Coating buffer	0.1 M $NaHCO_3$	8.8	3.6.1
Coomassie Brilliant Blue	2.5 mg/mL (0.25% w/v) in 50% methanol, 10% acetic acid, 40% water	–	3.5.3
EDTA in PBS	10 mM EDTA in 1x PBS	7.4	3.6.4
Elution buffer	0.1 M glycine	3	3.5.3
Elution buffer	0.2 M glycine	2.8	3.1.4
FACS buffer	0.5% (w/v)BSA in 1xPBS	7.2	3.6.4
Feed Stock	28 mL 0.5% Yeastolate solution, 140 mL CHO CD EfficientFeed^{TM}, 7 mL GlutaMAX^{TM} Supplement, 24.8 mL Glucose (450 g/L)	–	3.5.2
FLUSH buffer	1% (v/v) BSA in 1xPBS	7.2	3.6.4
Freezing Medium	20% (v/v) glycerol in 2xYT-medium	–	3.2
Glucose	20% (w/v) in ddH_2O	–	3.2
Glycerol	10% in ddH_2O	–	3.2
IPTG	1M in ddH_2O	–	3.2
Kanamycin A	50mg/ml in ddH_2O	–	3.2
Ketamine stock solution	100 mg/mL in 0.9% NaCl	–	3.1
LB medium	1 μg/mL carbenicillin in LB medium	–	3.2.2
MACS Buffer	0.5% (w/v) BSA, 2mM EDTA in 1xPBS	7.2	3.6.4
NaAzide	2% (w/v) NaN_3 in D-PBS	–	3.2

Continued on next page...

Buffer / Medium	Composition	pH	Application
Neutralization	1 M TRIS	8	3.5.3
Neutralization	1 M TRIS	9	3.1.4
PBS-T	0.1% (v/v) Tween20 in 1xPBS	7.4	3.6.1
PEG/NaCl solution	20% (w/v) PEG-6000, 2.5 M NaCl	–	3.2
Sample buffer	0.05% (v/v) Tween20, 0.1% (w/v) BSA in 1xPBS	7.4	3.6.1
SB-medium	30 g/L tryptone, 20 g/L yeast-extract, 10 g/L MOPS in ddH_2O	7	3.2
SDS-PAGE Running Buffer	25 mM TRIS, 0.1% (m/v) SDS, 200 mM glycine		3.5.3
Staining Buffer	2% goat serum (v/v) in 1x PBS	7.4	3.6.2
Staining Buffer	2% (w/v) BSA in 1xPBS	–	3.6.2
Tetracycline	5 mg/ml in EtOH	–	3.2
TRIS / HCL	1M TRIS	8	3.5.3
Trypsin	50 mM TRIS, 1mM $CaCl_2$, 10 mg/mL trypsin	–	3.2.3
Washing buffer	0.1% (w/v) BSA in PBS	–	3.2.5
Washing buffer	0.1% (v/v) Triton-X-100 in 850 nM NaCl	–	3.1.4
Washing buffer	0.05% (v/v)Tween20 in 1xPBS	7.4	3.6.4
Working buffer 01	1% (w/v) milk powder, 0.1% (v/v) Tween20 in 1xPBS	7.4	3.6.1
Working buffer 02	0.5% (w/v) BSA, 0.1% (v/v) Tween20 in 1xPBS	7.4	3.6.1
x5 loading buffer non-reducing	312.5 mM TRIS, 10 % (w/v) SDS, 25 % (v/v) Glycerin, 0.5 % (m/v) bromphenol blue	6.8	3.5.3
x5 loading buffer reducing	312.5 mM TRIS, 10 % (w/v) SDS, 25 % (v/v) Glycerin, 0.5 % (m/v) bromphenol blue, 10% (v/v) β-mercaptoethanol	–	3.5.3
Yeastolate (0.5%) stock solution	167 g/L Difco^{TM} TC Yeastolate	–	3.5.2

2.6 Laboratory Equipment

2.6.1 Devices

Table 2.11: Equipment used in this thesis, including their manufacturers (Mfr.), and locations - City, state and country (Ctry.). Abbreviations: TF (Thermo Fisher Scientific), BR (BioRad), MI (Miltenyi Biotec), CY (Cytiva), LE (Leica Biosystems), EP (Eppendorf SE), SA (Sartorius), ME (Merck KGaA), NU (Nuaire Ltd.), AS (Antylia Scientific), VWR (VWR International), AH (Andreas Hettich GmbH & Co.), ZT (Zebra Technologies Corporation), LLG (Lab Logistics Group GmbH), HL (Hirschmann Laborgeräte GmbH), CN (Consort nv.), MC (MaxCyte, Inc.), KC (Keyence Corporation), HLGL (Herolab GmbH Laborgeräte), BG (BINDER GmbH), IKA (IKA-Werke GmbH & Co.), GI (Grant Instruments Ltd.), TG (Tecan Group Ltd.), HI (HANNA instruments, INC.), XI (Xylem Inc.), HE (Heidolph Instruments GmbH), CR (Carl Roth GmbH), PR (Promega Corporation), FST (Fine Science Tools Group), DB (DITABIS AG), DWK (DWK Life Sciences GmbH), HS (Heathrow Scientific LLC.), GFL (GFL Gesellschaft für Labortechnik mbH), JU (JULABO GmbH), KS (Kern & Sohn GmbH), SY (Systec GmbH), BRAND (BRAND), PG (Precisa Gravimetrics AG), AG (Agilent).

Device	Model	Mfr.	City, State	Ctry.
Analytical scale	ABT-5NM	KS	Balingen-Frommern	DE
Autoclave	VX-150	SY	Linden	DE
Benchtop shaking incubator	CERTOMAT® BS-1	SA	Göttingen	DE
Biological safety cabinet	HERAsafe HS	TF	Waltham, MA	USA
Biological safety cabinet	NU-440-401E	NU	Plymouth, MN	USA
Block heater	Stuart Block Heater BB130D	AS	Vernon Hills, IL	USA
Centrifuge	5417R	EP	Hamburg	DE
Centrifuge	5810R	EP	Hamburg	DE
Centrifuge	Fresco™ 21	TF	Waltham, MA	USA
Centrifuge	Galaxy Mini	VWR	Radnor, PA	USA
Centrifuge	Heraeus Biofuge Pico	TF	Waltham, MA	USA

Continued on next page...

Device	Model	Mfr.	City, State	Ctry.
Centrifuge	Megafuge 1.0R	TF	Waltham, MA	USA
Centrifuge	Rotina 380 R	AH	Tuttlingen	DE
Chromatography system	ÄKTA pure	CY	Marlborough, MA	USA
CO_2 incubator	Hera Cell 240	TF	Waltham, MA	USA
Cytometer	MACSQuant Analyzer 10	MI	Bergisch Gladbach	DE
Desktop printer	ZD420 4-inch	ZT	Lincolnshire, IL	USA
Electronic pipett filler	LLG-Pipettierhilfe easy	LLG	Meckenheim	DE
Electric pipette filler	Pipetus®	HL	Eberstadt	DE
Electrophoresis power supply	E143	CN	Turnhout	BE
Electrophoresis system	BioAnalyzer2100	AG	Santa Clara, CA	USA
Electrophoresis system	Mini-PROTEAN® Tetra	BR	Hercules, CA	USA
Electroporation system	STX	MC	Gaithersburg, MD	USA
Electroporator	MicroPulser™	BR	Hercules, CA	USA
Fluorescence microscope	BZ-9000E	KC	Osaka	JP
Fluorescence microscope	BZ-X810	KC	Osaka	JP
Fraction collector	F9-C	CY	Marlborough, MA	USA
Gel electrophoresis chamber	Wide Mini-Sub Cell GT	BR	Hercules, CA	USA
Gel observation chamber	E.A.S.Y. 440K	HLGL	Wiesloch	DE
Heating / magnetic stirrer	Rotilabo® MH15	CR	Karlsruhe	DE
Incubator	BD23	BG	Tuttlingen	DE

Continued on next page...

Device	Model	Mfr.	City, State	Ctry.
Incubator	Heraeus Function Line B12	TF	Waltham, MA	USA
Magnetic stirrer	RCT basic	IKA	Staufen	DE
Microplate orbital shaker	PMS-1000i	GI	Royston	GB
Microplate reader	GloMax® Discover	PR	Mannheim	DE
Microplate reader	GloMax® Explorer	PR	Mannheim	DE
Microplate reader	Spectra Rainbow	TG	Männedorf	CH
Microtome	CM1900 Cryostat	LE	Wetzlar	DE
Microtome	CM3050 S Cryostat	LE	Wetzlar	DE
Multichannel pipette	Multichannel pipette (200 µl)	BRAND	Wertheim	DE
Multipipette	Multipette® M4	EP	Hamburg	DE
NanoDrop™One	Spectralphotometer	TF	Waltham, MA	USA
pH/ORP meter	HI2215	HI	Woonsocket, RI	USA
pH meter	inoLab® pH7110	XI	Washington	USA
Pipette	10 µl, 100 µl, 200 µl, 1000 µl	BRAND	Wertheim	DE
Pipette	10 µl, 100 µl, 200 µl, 1000 µl	EP	Hamburg	DE
Platform shaker	Duomax 1030	HE	Schwabach	DE
Rotator	Stuart SRT1	AS	Vernon Hills, IL	USA
Scale	EMB 2000-2	KS	Balingen-Frommern	DE
Scale	Precisa XB 2200 C	PG	Dietikon	CH
Separator	MidiMACS™	MI	Bergisch Gladbach	DE
Separator	QuadroMACS™	MI	Bergisch Gladbach	DE
Shaking incubator	CERTOMAT® BS-T	SA	Göttingen	DE
Surgical instruments	Scissors, forceps	FST	Heidelberg	DE
Thermocycler	PTC-200	BR	Hercules, CA	USA
Thermomixer	MHR 13	DB	Pforzheim	DE

Continued on next page...

Device	Model	Mfr.	City, State	Ctry.
Thermomixer	Thermomixer comfort	EP	Hamburg	DE
Tissue homogenizer	Dounce-homogenizer	DWK	Wertheim	DE
Transilluminator	Safe Imager 2.0 Blue-Light	TF	Waltham, MA	USA
UV/VIS spectrophotometer	BioPhotometer 6131	EP	Hamburg	DE
Vortex	HS120212	HS	Vernon Hills, IL	USA
Water bath	GFL 1004	GFL	Burgwedel	DE
Water bath	Julabo 13	JU	Seelbach	DE
Water purification system	Arium® Pro Ultrapure Water Systems	SA	Göttingen	DE
Water purification system	Milli-Q® EQ 7000	ME	Darmstadt	DE

2.6.2 Consumables

Table 2.12: Consumablest used in this study, including their manufacturers (Mfr.), and locations - City, state and country (Ctry.).) and location. Abbreviations: CR (Carl Roth GmbH + Co. KG), BD (Becton, Dickinson and Company), SAK (Sarstedt AG & Co. KG), BB (B. Braun SE), MI (Miltenyi Biotec B.V. & Co. KG), ME (Merck KGaA), TF (Thermo Fisher Scientific), BL (BioLegend, Inc.), EP (Eppendorf SE), EH (Erpedal Holdings Ltd.), MC (MaxCyte, Inc.), CY (Cytiva), SF (Sakura Finetek Japan Co., Ltd.), SR (Feather Safety Razor Co., Ltd.), GE (Greiner Bio-One International GmbH), BI (Beaphar), GL (Glaswarenfabrik Karl Hecht GmbH & Co. KG), SP (Spectra/Por), CO (Corning), FI (Filpro).

Description	Model	Mfr.	City, State	Ctry.
Affinity matrix	Chitin resin	NEB	Ipswich, MA	USA
Baffled flasks	ROTILABO® 0.5 L 1L 2L	CR	Karlsruhe	DE

Continued on next page...

Description	Model	Mfr.	City, State	Ctry.
Cannula	Sterican® 0.45 x 25 mm 26G x 1	BB	Melsungen	DE
Cannula	Microlance® 3 30G x 1/2, 0.3x13mm	BD	Franklin Lakes, NJ	USA
Cell culture flask	T-75, PS	SAK	Nümbrecht	DE
Cell separation column	LS columns	MI	Bergisch Gladbach	DE
Cell separation column	MS columns	MI	Bergisch Gladbach	DE
Cell strainer	70 µm	SAK	Nümbrecht	DE
Centrifugal Concentrators	Amicon-Ultra Centricons 30 kDa MWCO (15 mL)	ME	Darmstadt	DE
Centrifugal Concentrators	Vivaspin™ 6mL	ME	Göttingen	DE
Centrifuge tubes	Nalgene® PPCO 250 mL	TF	Waltham, MA	USA
Chromatography column	PolyPrep Chromatography Columns	BR	Hercules, CA	USA
Chromatography column	Econo-Column Chromatography Column	BR	Hercules, CA	USA
Combitips advanced	2.5 mL, 50 mL	EP	Hamburg	DE
Cover glasses	Menzel Nr.1, 24x60mm	EH	Kalamazoo, MI	USA
Cuvette	Eppendorf UVettes, 0.1 cm gap	EP	Hamburg	DE
Cuvette	OC-400 RUO™	MC	Gaithersburg, MD	USA
Cuvette	UV cuvette, 2mL	SA	Nümbrecht	DE
Dialysis membrane	Membrane-Cel™ 44 mm	CR	Karlsruhe	DE
Enteral/Feeder flask	DUDRAN® 100 mL, 250 mL	CR	Karlsruhe	DE
Falcons	15mL, 50mL	SAK	Nümbrecht	DE

Continued on next page...

Description	Model	Mfr.	City, State	Ctry.
Filters	Acrodisc Syringe Filter 0.22 Supor Membrane	CY	Marlborough, MA	USA
Glass bottles	50 mL, 100 mL, 500 mL, 1L, 2L	CR	Karlsruhe	DE
Hydrophobic Pen	Advanced PAP Pen	ME	Darmstadt	DE
Microplate	96 well, F-bottom, high-binding, lumitrac	GE	Kremsmünster	AUT
Microplate	Nunc® MaxiSorp®, flat-bottom, 96 well	BL	San Diego, CA	USA
Microscope slides	Superfrost® Plus-adhesion microscope slides, White Tab	EH	Kalamazoo, MI	USA
Needle	Beaphar U-needle and Nasensalbe	BI	Leverkusen	DE
Pasteur pipet	150 77120, 230mm	GL	Wertheim	DE
Petri dish	90 mm, 20 mm	SAK	Nümbrecht	DE
Petri dish	150 x 20 mm	SAK	Nümbrecht	DE
Pipette tips	10 µL, 20 µL, 200 µL, 1000 µL	SAK	Nümbrecht	DE
Pipette tubes (caplock)	1.5mL, 5mL, 2mL, 5mL	SAK	Nümbrecht	DE
Plastic tubes (screw lock)	1.5 mL	SAK	Nümbrecht	DE
Plastic tubes (snap lock)	1.5 mL, 2 mL	SAK	Nümbrecht	DE
Scalpel	No. 11, 15cm, 17cm	SR	Osaka	JPN
Self-adhesive film	4-15% Mini-PROTEAN™ TGX™	BR	Hercules, CA	USA
Self-adhesive film	PCR film, free from DNAse/RNAse	SAK	Nümbrecht	DE
Self-aspirating pipette	50mL, 25mL	SAK	Nümbrecht	DE

Continued on next page...

Description	Model	Mfr.	City, State	Ctry.
Serum tube	Microvette® 500 EDTA K3E	SAK	Nümbrecht	DE
Spatula	S-Monovette® /Hubna, 1.6x13mm	SAK	Nümbrecht	DE
Spatula	Drigalski spatula	SAK	Nümbrecht	DE
Syringe	Omnifix® 1mL, w. cannula (0.30 x 12mm)	BB	Melsungen	DE
Syringe	Luer Slip® 1mL w.o. needle	BD	Franklin Lakes, NJ	USA
Syringe	Omnifix® 10mL, 20mL	BB	Melsungen	DE
Tissue tube®	Falcon® 12x75mm tube with cell strainer snap cap	CO	Corning, NY	USA
Cryomold®				
Tissue-tek®	15x15x5mm	SF	Torrance, CA	USA
Cryomold®				
Tubing	Spectra/Por Dialysis Membrane, MWCO: 3.5 kD	SP	Rancho Dominguez, CA	USA
Vacuum filtration unit	Filpro® VCU 500, 50 mL, PES, 0.45 µm	FI	Karlsruhe	DE

2.7 Software

Table 2.13: Software used in this study. The table lists all software applications, their versions, and developers used throughout this research.

Software	Version	Developer
SabPred	ABody-Builder2 [169]	Oxford Protein Informtaics Group [170]
Adobe Illustrator	29.2.1	Adobe Inc.
Adobe Lightroom Classic	14.2	Adobe Inc.
E.A.S.Y. Win	32	Herolab GmbH Laborgeräte
FlowJo™	10.10.0	Becton, Dickinson and Company (2023)
GraphPad Prism	10.4.1	GraphPad Software, Inc.
iControl™	V1.12	Tecan Group Ltd.
ImageJ	1.54p	Wayne Rasband, NIH
IMGT V-Quest	3.6.4	[171], [172]
Jamovi	2.5	The Jamovi Project (2024)
MEGA12	12.0.8	[173]
Microsoft Office	365 Business	Microsoft Corporation
Perplexity AI	Pro	Perplexity Labs, Inc.
R	4.3.3	R Core Team
RStudio	2024.12.1+563	Posit PBC
SnapGene	8.0.1	Dotmatics
TeXstudio	4.8.5	Benito van der Zander [174]
TeX Live	2024	TeX Users Group, Sebastian Rahtz
UNICORN	–	Cytiva
Zotero	6.0.36	Digital Scholar

Chapter 3

Methods

The following chapter describes the applied methods and protocols. Cross-references to Chapter 2 are provided, especially for the used buffers, which are linked to their corresponding protocol 2.10. Brief introductions to the described methods are provided if deemed essential to follow the procedure.

3.1 Animal Experiments

3.1.1 Ethical Approval

All animals were bred and maintained by the Joint Animal Facility (Gemeinsame Tierhaltung, GTH) of the University of Lübeck (UzL) in compliance with institutional guidelines for animal experiments. Both the Institutional Animal Care and Use Office (Tierschutz UzL) and the "Ministerium für Energiewende, Landwirtschaft, Umwelt, Natur und Digitalisierung" of the state Schleswig-Holstein approved all animal experiments. Detailed information on the animal proposals "5.1_2023-07-17_Bieber" and "5.1 (69-12/23)_Ludwig" can be obtained upon request S6.

3.1.2 Anesthesia Protocol

Anesthetic stocks and injection stocks were prepared and maintained under sterile conditions. $1\,\mathrm{mg\,mL^{-1}}$ ketamine stocks were prepared using (±)-ketamine hydrochloride and 0.9% NaCl solution (Tab 2.9 and stored at $-80\,^{\circ}\mathrm{C}$. Medetomidine stocks were acquired at a concentration of $1\,\mathrm{mg\,mL^{-1}}$ and stored at room temperature (RT). Per gram of body weight, $0.075\,\mathrm{mg}$ of ketamine and $0.001\,\mathrm{mg}$ of medetomidine were administered. The injection stock was formulated as described in (Tab. 2.10. Anesthesia was administered

via intraperitoneal (i.p.) injection (100 µL/ 20 20 g mouse), using Omnican®-F 1 mL syringes with 0.30 x 12 mm cannula. For reversal of anesthesia, 0.005 mg g^{-1} atipamezole hydrochloride (Antisedan) was injected i.p., 30 min after the initial anesthesia administration. Following antagonist administration, the eyes of the mice were treated with Bepanthen® eye and nose ointment to prevent excessive drying, and the animals were placed under red light for 30 min to prevent hypothermia during the recovery phase. Anesthesia was administered according to 5.1 (69-12/23)_Ludwig.

3.1.3 The Immunization-Induced EBA Mouse Model

In the immunization-induced model of EBA, several fragments of the NC-1 domain of mCOLVII have been used, to elicit an autoinflammatory immune response (Section 1.5.3) [93, 121]. Immunization with mCOLVII^{vWFA2} is the most recent and commonly used procedure. The established protocol for this and other experimental EBA model systems is described in detail in Kasprick *at al.* [167]. Disease susceptibility in the immunization-induced mouse model of EBA is linked to the MHC haplotype H2s [127]. B6.SJL-H2s C3/1CyJ (C57BL/6S) mice were obtained from JAX (Tab. 2.1). These mice, carrying the susceptible H2s haplotype, were used for the immunization-induced EBA mouse model at a minimum age of 8 weeks, as previously described in [167]. The immunization-induced EBA mouse model was used to obtain spleen and dLN for immune library generation in previous work [162], and is therefore not further described in this study.

3.1.4 Autoantibody-Transfer-Induced EBA Mouse Models

The transfer of disease-causing, pathogenic antibodies was first used to prove the causality of Aab in the pathogenicity of EBA [92]. The transfer of mCOLVII-targeting antibodies allows for rapid observation of the effector phase of the disease including the involved pathways, cells, and molecules [80]. Different routes of Aab injection are described in the literature, thereby generating models of different duration and severity. For the local Aab-transfer model IgG is injected into the base of one ear to evaluate antibody pathogenicity. Mice are anesthetized for the injection and subsequent scoring of affected areas of the ear. The experiment is terminated after four days. Disease manifestation is genuinely limited to the ears in this model system [175]. I.p. or subcutaneous (neck) injection of Aab results in widespread and more severe disease, compared to the local model, due to its systemic manifestation and extended duration. Antibody is injected at two day intervals, with total injections depending on the concentration, route [80],

and nature [117] of the injected antibody fraction. Disease manifestation is observed after approximately four days; the duration varies between experiments and is typically twelve to sixteen days [80, 176].

Generation of recombinant protein for immunization

Recombinant mCOLVII^{-C}-GST (AA757 to 967 x GST) was generated as described in [93]. Briefly, *E. coli* NovaBlue transformed with mCOLVII^{-C}-GST encoding pGEX-6P-1 vector were cultivated, protein expression induced, and cells lysed by sonication. The protein was purified by glutathione-affinity chromatography, concentrated, and quality-controlled by SDS-PAGE and *in vivo* batch testing for pathogenicity. The protein was stored at $-80\,°C$ at $2\,mg\,mL^{-1}$ in PBS, pH 7.2. Recombinant mCOLVII^{vWFA2} (AA1048 – 1238) was generated as described in [167]. *E. coli* ER2566 transformed with mCOLVII^{vWFA2}-bearing pTWIN1 plasmid were cultivated, protein expression induced, and cells lysed by sonication. The protein was purified using the Intein Mediated Purification with an Affinity Chitin-binding Tag-Two Intein (IMPACT™-TWIN) system as described in [110]. This system uses an intein-flanked chitin-binding domain (CBD) that binds to chitin beads and is subsequently cleaved by pH change. The eluted protein was concentrated, quality-controlled by SDS-PAGE and *in vivo* batch testing for pathogenicity, and stored at $-80\,°C$ at $2\,mg\,mL^{-1}$ in PBS, pH 7.2.
Production, affinity chromatography, and quality control, including batch testing, were performed by Dr. Natalie Gross and laboratory technicians Claudia Kauderer and Alexandra Wobig.

Generation, isolation and purification of total and mCOLVII targeting rabbit IgG

Eurogentec was provided with recombinant mCOLVII^{-C} or mCOLVII^{vWFA2} (paragraph 3.1.4) to immunize New Zealand White (NZW) rabbits. $250\,\mu g$ of antigen was administered subcutaneously (s.c.) in complete Freund's adjuvant. Immunization was boosted at $14\,d$ intervals three times with an equivalent dose of antigen in incomplete Freund's adjuvant. Serum was drawn at three week intervals starting two months after the first immunization. Collected serum was shipped to the laboratories of the Lübeck Institute of Experimental Dermatology for antibody purification. IgG was purified as originally described in Sitaru *et al.* [92]; a detailed description can be obtained from Kasprick *et al.* [167]. In brief, total rabbit IgG (rIgG) was purified from immune serum using protein G affinity chromatography. The columns were equilibrated by incubation with 10 mL of binding buffer and 10 mL of protein G resin, followed by washing with 100

mL of binding buffer. Sera were diluted in 1× PBS and incubated for 1 h at 4 °C, with orbital shaking on the column, allowing for IgG-matrix binding. The flow-through was discarded and the column washed with washing buffer (see 2.5.3) until optical density measurement at 280 nm (OD_{280}) reached ≤ 0.5. IgG was eluted by an acidic change of pH, using 0.1 mol L^{-1} glycine elution buffer and fractions collected in tubes containing 3 mL of neutralization buffer. Elution was continued until OD_{280} reached 0.1, indicating the elution of the majority of protein. Fractions were pooled, pH equilibrated to 7.2 using neutralization buffer, and incubated for 2 h in polyethylene glycol (20.000) for purification of protein and to concentrate IgG content, using a dialysis membrane (Membra-Cel™). Finally, IgG was concentrated using 30 kDa centricons (Tab. 2.12) centrifuged at 1500 g at 4 °C and resuspended in PBS. Concentrations were determined by OD_{280} measurement. To access specific mCOLVII or mCOLVIIvWFA2-targeting IgG, the purified total IgG fraction was further purified using columns loaded with antigen-coupled Affi-Gel 10 active ester agarose. In brief, 5 mg mL^{-1} antigen was incubated with Affi-Gel 10 for 1 h at RT in MOPS buffer (see 2.5.3) for antigen coupling on the loaded column, followed by a 1 h RT incubation of a 1:20 dilution of MOPS in ethanolamine. The matrix was washed with 1× PBS, loaded with total IgG fraction, and incubated for 1 h at 4 °C gently shaking on a rocking platform for antibody-antigen binding. The column was washed with 1× PBS, followed by washing buffer. Washing was stopped once the OD_{280} in eluent reached 0.01. Specific IgG was eluted and prepared analogously to the total IgG fraction. Specific IgG was filtered to achieve sterility and adjusted to a concentration of 2 mg mL^{-1} and stored at −20 °C. Affinity chromatography and purification were performed by laboratory technicians Claudia Kauderer and Alexandra Wobig. Dr. Natalie Gross performed the batch testing of IgG prior to *in vivo* experiments.

3.1.5 Scoring of EBA Skin Inflammation

To assess the macroscopic extent of EBA in mice, an established scoring system was applied, in which the percentage of affected body surface area is calculated and translated into a global body surface area score [80, 167]. The mice were anesthetized as described in Subsection 3.1.2, and each body section was scored individually for the percentage extent of skin lesions, blistering, scabbing, and hair loss. The body section scores were multiplied by a fixed scaling factor, considering the relative size of the respective body section in relation to the total body. The scaling factors are indicated in Fig. 3.1. The resulting sum of the scaled individual percentages yielded the global EBA score per mouse. The scoring was performed in accordance with the individual ethical approval

for the respective experiment.

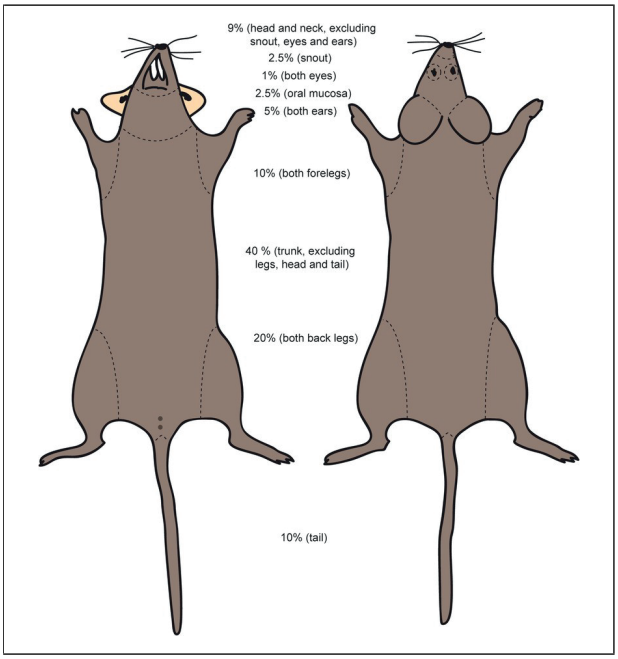

Figure 3.1: Scoring scheme for the assessment or murine EBA. Anesthetized mice are scored for their disease affected body surfacen area. Each body section was scored individually. Global score was calculated by factoring in the scaling factors (middle) of the respective body sections. Figure modified from [167].

3.1.6 Pathogenicity Testing

To evaluate the pathogenic potential of the anti-mCOLVII IgG2b antibody clones *in vivo*, all tested clones were injected into C57BL/6J WT mice, in accordance with 5.1 (69-12/23)_Ludwig (Subsection 3.1.1). Initial testing followed a two-step trial regimen, in which the antibodies were initially tested by local injection into the base of the right ear. This procedure was chosen due to its minimal stress infliction on the animals, followed by systemic i.p. injections into the same mice four days after the start of the local injections. For the local injections, the animals received subcutaneous injections of $50\,\mu L$ of the respective antibody clones into the base of the right ear for three consecutive days (days 0, 1 and 2). IgG dosage administration followed an escalative scheme: on day 0, $50\,\mu g$ of antibody was injected, while on the subsequent two days, $100\,\mu g$ was injected, totaling $250\,\mu g$ of injected antibody per animal. Animals were examined daily for clinical signs of EBA according to [167] until day 4 p.i. The termination criterion in this phase was an induced affected ear surface area of $30\,\%$ per mouse. Mice reaching this criterion by day 4 p.i. received no further antibody injections. The experimental group would be concluded if three out of five mice reached the termination criterion at day 4. Animals not reaching the termination criterion by day 4 progressed to receiving i.p. injections at

two day intervals until day 16 p.i. of local model initiation. Administered dosages were increased in concentration: 250 µg on days 4 and 6, and 500 µg on days 8, 10, 12, and 14, totaling 2.75 mg of injected antibody per mouse. The termination criterion for this phase was 2 % to 5 % affected body surface area. Mice were euthanized on day 16, and serum and skin samples were collected post-mortem.

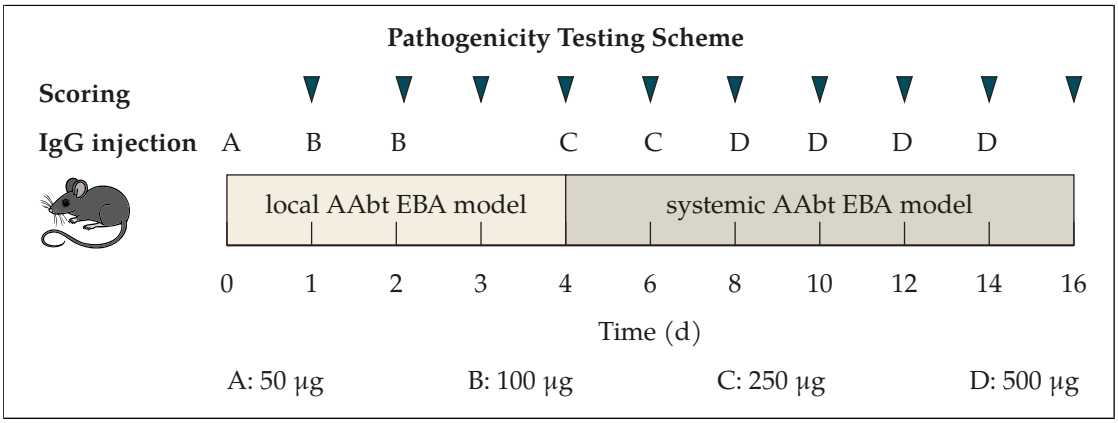

Figure 3.2: Injection and scoring procedure for the combined model of antibody-transfer for pathogenicity testing. Different antibody doses (A, B, C, D) were injected on different days (d) and mice scored for disease affected body surface area (indicated by triangles). On d0 50 µg (A) of antibody were injected locally into the base of the right ear, followed by injection of 100 µg (B) of antibody on d1 and 2 for the local autoantibody-transfer EBA model (local AAbt EBA model). On d4 250 µg (C) of antibody were injected intraperitoneal (i.p.), followed by a two day rythm of i.p. injections with 250 µg (d6) or 500 µg (d8, d10, d12) of antibody for the systemic autoantibody-transfer model.

3.1.7 Mouse Dissection and Tissue Sampling

Sampling of blood

The mice were anesthetized by i.p. injection, as described in Protoc. 3.1.2. Mice were immediately sacrificed by cervical dislocation after blood sampling. For retroorbital blood collection, an EDTA-coated glass cannula was used to penetrate the retrobulbar plexus. Blood was sampled into EDTA serum tubes and placed on ice for 20 min. For heart puncture, 1 mL syringes were used with 26G cannulas. Both the syringe and cannula were coated with heparin to prevent clotting during the drawing procedure. Depending on the intended use, the blood was transferred into either low-binding 1.5 mL tubes without any anticoagulant or into EDTA serum tubes and placed on ice for 20 min.

For serum preparation, the samples were centrifuged at 2000 g for 10 min at 4 °C, and the serum (supernatant) was aliquoted into new tubes, snap-frozen in liquid nitrogen, and stored at −80 °C. For complement-competent serum preparations, samples were centrifuged at 600 g for 10 min at 4 °C, and serum samples from 3 to 5 animals were pooled before proceeding to the previously described storage procedure.

Sampling of skin

The mice were euthanized by cervical dislocation, and ear tissue samples were obtained by separating the ears at the base from the skull. The ears were bisected vertically, and one half of each of the right (E_R) and left ear (E_L) was immersed in 4 % formaldehyde and stored for histological processing at RT. The remaining halves of E_R and E_L were snap-frozen in liquid nitrogen and stored at −80 °C. 4 µm sections were prepared from frozen tissues by student assistent Bejtije Naumann for subsequent tissue stainings.

3.2 Phage Display

Antibody display and selection strategies represent powerful tools for isolating highly specific, high-affinity antibody fragments from antibody libraries. For phage display library construction (Fig. 1.7), RNA from murine S and LN was reverse-transcribed to cDNA [177]. V-D-J diversity was assessed via multiplex gradient PCR using a set of degenerated primers, adapted from Krebber*et al.* [149, 162]. Sub-libraries for V^H and V^L domains were assembled in *E. coli* XL1-Blue using pUC19-MSC2017 (Tab. 2.7). V^L domains were subsequently cloned into V^H-containing pUC19-MSC2017, followed by scFv insertion into phagemid pJB12 (Tab. 2.7), which encodes the M13 phage pIII surface protein. The resulting two libraries (S, LN) contained scFv-pIII constructs that, upon helper phage infection, produce phages, displaying monoclonal scFv fragments while encapsulating the encoding phagemid.

3.2.1 Generation of M13KO7 Helper Phages

Helper phages encode all structural proteins (Fig. 1.6) which are crucially needed for phage assembly and are not encoded on the phagemid vector, thereby restricting phage propagation in the absence of helper phage.

Generation of Electro Competent *E. coli* XL1-Blue / TG-1

Commercially obtained *E. coli* XL1-Blue or TG-1 cells were serially diluted (1×10^{-2}, 1×10^{-3}, 1×10^{-4}) in SOC medium, and $50\,\mu L$ of each dilution was plated on 2xYT agar containing $40\,\mu g\,mL^{-1}$ tetracycline. A single colony was used to inoculate $20\,mL$ of SB medium supplemented with $40\,\mu g\,mL^{-1}$ tetracycline overnight (o/n) at $37\,°C$ while shaking. $500\,mL$ of SB medium was supplemented with glucose and $MgCl_2$ to final concentrations of $0.387\,\%$ (w/v) and $9.66\,mM$, respectively and incocculated with $2.5\,mL$ of the o/n culture. This culture was incubated at $37\,°C$, monitoring OD_{600} until it reached 0.7–0.8 (approximately (approx.) 4 h). The culture was cooled in an ice-water bath for $15\,min$. All subsequent steps were performed at $4\,°C$. The cooled culture was divided into $50\,mL$ falcon tubes and centrifuged at $4000\,rpm$ for $20\,min$ at $4\,°C$. Each pellet underwent two washing cycles of resuspension in $25\,mL$ of ice-cold 10% glycerol and centrifugation under the previously described conditions. The washed pellets were combined and resuspended in $12.5\,mL$ ice-cold 10% glycerol, then centrifuged at $3500\,rpm$ for $15\,min$ at $4\,°C$. After careful supernatant removal, the final pellet was resuspended in its residual liquid (approximately $2\,mL$ to $2.5\,mL$). Aliquots of $50\,\mu L$ were prepared and flash-frozen in liquid nitrogen before storage at $-80\,°C$. To assess cell transformation capacity, $1\,\mu L$ of pUC19 plasmid ($0.01\,pg\,\mu L^{-1}$) was used for electroporation. A 1:10 dilution series in SOC medium was plated on 2xYT agar supplemented with $100\,\mu g\,mL^{-1}$ ampicillin. The expected transformation efficiency was 2×10^9 CFU/μg of DNA.

Helper phage propagation plaque assay

To ensure clonal purity and phage functionality, a plaque assay was used to generate a fresh helper phage stock from one single phage induced plaque, thereby reducing genetic heterogeneity and contamination risk for further phage related working procedures.
$30\,\mu L$ of *E. coli* TG-1 were incubated in $20\,mL$ of 2xYT medium containing $10\,\mu g\,mL^{-1}$ tetracycline at $37\,°C$ until the OD_{600} reached >0.5 (logarithmic growth phase). $5\,mM$ $MgCl_2$ containing 2xYT top agar was prepared and $3\,mL$ were equilibrated at $50\,°C$ in sterile FACS tubes for phage dilution. M13KO7 phage stock was serially diluted 1/100 in 2xYT medium. For each phage dilution, $100\,\mu L$ of the prepared bacteria were mixed with $10\,\mu L$ of the phage dilution and incubated at $37\,°C$ for $10\,min$. The bacteria-phage mixture was then added to the equilibrated top agar, briefly shaken, and poured onto pre-warmed and dry 2xYT agar plates ($5\,mM$ $MgCl_2$). After solidification at RT for approx. $5\,min$, the plates were incubated at $37\,°C$.

Helper phage precipitation

10 µL of frozen *E. coli* TG-1 phage-competent stock was added to 25 mL SB medium and incubated to early mid-log phase determined by OD_{600} monitoring. A single M13KO7 plaque was picked from stock plates, added to 5 mL cultured TG-1 and incubated for 2 h at 37 °C while shaking to enable phage infection. The infected pre-culture was split, transferred to 250 mL SB medium in baffled flasks and incubated for 1.5 h at 37 °C for bacterial growth. Kanamycin was added to a final concentration of 50 µg mL^{-1}, followed by orbital shaking at 30 °C for selection of phage-infected bacteria. After incubation, 120 mL culture was centrifuged at 3830 g for 20 min at 4 °C. 100 mL supernatant was mixed with 25 mL PEG/NaCl and incubated on ice for 1 h. Following centrifugation at 12 400 g for 20 min at 4 °C, and the removal of supernatant, phage pellets were air-dried for 5 min to 10 min, and combined by resuspension in 2 mL to 4 mL 1xPBS. Aliquots of phage preparation (1.5 mL screw-cap tubes) were heated at 65 °C for 5 min, then centrifuged at 25 000 g (10 min, RT) and phage containing supernatant transfered to new tube. The solution was equilibrated to a final concentration of 0.02% (w/v) NaN_3 before storage at 4 °C.

3.2.2 Phage-Immune Library Propagation

To select for antigen-specific scFv during the panning procedure, the two immune libraries (Fig. 1.7), bearing the scFv-encoding phagemids, were expanded to reflect all scFv originally cloned into the library. Supplementation of the bacteria with IPTG induces the production of scFv due to the interaction of IPTG with the lac repressor, thereby inducing a conformational change in the latter and enabling gene expression of the lac operon-controlled inserted genes. Subsequently, the scFv-expressing bacteria are infected with the M13KO7 helper phage. The phage infects bacteria by initially binding to the F pili on the bacterial surface; therefore, the initial presence of tetracycline in the growth medium is crucial, since the F-plasmid encoding for the F pili carries the tet resistance gene.

500 mL of SB medium supplemented with 1 % (w/v) glucose, 30 µg mL^{-1} chloramphenicol, and 10 µg mL^{-1} tetracycline was inoculated with a 1 mL aliquot of immune library (S or LN) culture (starting $OD_{600} < 0.1$) and grown at 37 °C until OD_{600} reached 0.5 to 1. Following, 50 mL of the expanded immune library culture were adjusted to a final concentration of 0.5 mM IPTG in a pre-warmed (37 °C) reaction tube. The culture was then infected with the M13KO7 helper phage at a multiplicity of infection (MOI) of 20. An

OD_{600} of 1 is equivalent to approx. 1×10^9 CFU/mL, therefore, the appropriate volume of M13KO7 stock was added for each immune library preparation. The infected culture was incubated for 30 min without shaking at 37 °C. Next, two 250 mL preparations of SB medium supplemented with 1 % (w/v) glucose, 0.5 mM IPTG, and 30 µg mL^{-1} chloramphenicol stock were prepared; each was added with half of the infected immune library and distributed into two 2 L baffled flasks, which were then shaken for 1.5 h at 37 °C. The cultures were adjusted to a final concentration of 25 µg mL^{-1} kanamycin and incubated for a minimum of 16 h at 30 °C while shaking. The cultures were then divided into 125 mL aliquots and centrifuged for bacterial removal for 20 min at 4 °C and 3830 g. The supernatant was mixed with 25 mL of PEG/NaCl solution in a new vessel and incubated on ice for 30 min for phage precipitation. The mixture was centrifuged for 20 min at 12 400 g at 4 °C; the supernatant was discarded, and the resulting colorless pellet was air-dried for 5–10 min, followed by removal of residual liquid. The phage pellets per immune library were resuspended in 2–4 mL of sterile PBS, pooled, and transferred to an appropriate tube. The resuspended phage solution was centrifuged for 10 min at RT and 25 000 g to remove residual bacterial carry-over. The supernatant was transferred to a new vessel, and a sample was taken for phage titer determination. 10 µL of a 2 % (w/v) NaN_3 solution was added per mL of phage solution before storing the samples at 4 °C.

Phage Titer Determination

The phage titer was determined by accessing the CFU of infected *E. coli* XL1-Blue by serial dilution.
30 µL aliquots of *E. coli* XL1-Blue cells were thawed on ice and inoculated into 40 mL of 2xYT medium containing 10 µg mL^{-1} tetracycline at 37 °C while shaking. The optical density at 600 nm (OD_{600}) was monitored until it exceeded 0.5, corresponding to approximately 1×10^8 CFU/mL. Subsequently, previously prepared phage preparations 3.2.2 were serially diluted in $\log_{10}$ (from 1×10^2 to 1×10^8) in 2xYT medium.100 µL of the bacterial culture was infected with 10 µL of the phage dilutions and incubated for 30 min at 37 °C without shaking. Following this incubation, 50 µL of the phage-infected bacterial suspension was plated on 2xYT agar containing 1 % (w/v) glucose, 30 µg mL^{-1} chloramphenicol, and 10 µg mL^{-1} tetracycline, and incubated o/n at 37 °C. Single colonies on several plates were counted the following day, and colony-forming units (CFU) were calculated as the mean value of individual plate CFU.

Generation of ER2566 lysate for phage display depletion

Two aliquots of 20 µL *E. coli* ER2566 from a frozen glycerol stock were each transferred to separate conical flasks containing 250 mL of 2 × YT medium. Both flasks were incubated OV at 37 °C, with shaking. The cells were centrifuged at 3500 g for 12 min at 4 °C, to pellet and isolate the bacteria from the culture. The bacterial cell pellets were resuspended and combined in B1 buffer, followed by centrifugation as previously described. The resulting pellet was weighed, and 2 g of bacterial pellet were resuspended in 50 mL of B1 buffer containing 1 unit of cOmplete™ EDTA-free protease inhibitor. The cells were lysed by sonication on ice for 4 × 50 s (seven cycles at 100% power). The lysate was centrifuged at 612 g for 40 min at 4 °C. The supernatant was transferred to a conical tube and filtered sequentially using 0.45 µm and 0.2 µm syringe filters. The filtered supernatant was then stored at −80 °C for future use.

3.2.3 Phage Display Selection of Immune Libraries

Antibody selection in phage display is termed panning [159]. For the panning procedure, antigen is immobilized or coated on high absorbent immunotubes, representing the most common procedure [178], [147, Chapter 9].

Immuno tubes were coated with 150 µg of recombinant mCOLVII^{vWFA2} (Protoc. 3.1.4) in 1× PBS and added with NaN_3 to a final concentration of 0.02 % (w/v). Additional immuno tubes were coated with *E. coli* ER2566 lysate supernatant (Protoc. 3.2.2) diluted 1:100 in 1× PBS and equally adjusted with NaN_3 to a final concentration of 0.02 % (w/v). The final volume in all tubes was 1.5 mL. All tubes were incubated o/n at 4 °C. Coating solution was removed completely from coated immuno tubes which were subsequently blocked with 3 mL of sterile 1 % skim-milk in 1× PBS blocking solution. *E. coli* ER2566 lysate supernatant coating solution was saved and stored for liquid phase depletion. Blocking solution was removed from *E. coli* ER2566 lysate supernatant coated tube and 1 mL of titered phages (Protoc. 3.2.2) and 250 µL of fresh blocking solution were added and incubated for 30 min at RT on a rocking plate for solid phase depletion. The depletion procedure was repeated twice, by transferring the 1.25 mL of phage / blocking solution mix to additional *E. coli* ER2566 lysate supernatant coated tubes. Blocking solution was removed from mCOLVII^{vWFA2}-coated tubes and the phage / blocking solution mix transferred to this tube and incubated for 2 h at RT on a rocking plate for phage binding. 30 µL of *E. coli* XL1-Blue were incubated in 20 mL of 2× YT medium containing 10 µg mL^{-1} tetracycline at 37 °C until the OD_{600} reached >0.5 while still situated in the

logarithmic growth phase. Phage solution was removed and immuno tubes washed ten times with 3 mL of cold, sterile 1× PBS. For phage elution, trypsin was diluted 1/10 in 1× PBS and 1 mL of this 1 mg mL^{-1} trypsin-PBS solution were incubated in immuno tube with bound phages for 10 min. The viral envelope proteins are stable under these conditions and not excessively cleaved by trypsin [147][Chapter 10]. Phage eluent was inoculated with 10 mL of *E. coli* XL1-Blue for 30 min at 37 °C in a water bath for infection. Suspension was spun down for 10 min at 1900 g 4 °C, supernatant discarded and pellet resuspended in 2 mL of 2× YT medium. Phage-infected bacteria were plated on 10 15 cm 2× YT-agar-plates, supplemented with 30 µL mL^{-1} chloramphenicol and 10 µg mL^{-1} tetracycline and incubated 20 h at 37 °C. In addition, a serial dilution of infected bacteria was prepared and plated on 2× YT-agar-plates, containing the aforementioned supplements, to determine the CFU and thus recovery rate and enrichment after panning. All plates were thoroughly washed with 2× YT medium, using a spatula, to detach all grown colonies. One third of the resulting bacterial solution was used to prepare phagemid (plasmid) DNA, using Macherey-Nagel's NucleoBond Xtra Maxi Kit, for subsequent NGS of the immune library (Subsection 3.4.2). Residual sample volume was centrifuged for 20 min at 1900 g. The supernatant was discarded, pellet resuspended in freezing medium, snap-frozen in liquid nitrogen and subsequently stored at −80 °C for further pannings.

3.2.4 Propagation of Single Colonies

To characterize the binding of monoclonal scFv-phages, single bacterial colonies, harboring monoclonal phage were propagated from (1) existing *E. coli* XL1-Blue culture, (2) fresh inocculated culture from single colony or (3) newly transformed *E. coli* XL1-Blue. 25 mL of SB medium (containing 1 % (w/v) glucose, 30 µL mL^{-1} chloramphenicol, and 10 µL mL^{-1} tetracycline) was inoculated with (1), (2) or (3) ($OD_{600} < 0.1$) and incubated at 37 °C until the OD_{600} reached 0.6-0.8. IPTG was added to 10 mL of the culture to a final concentration of 0.5 mM. The culture was then infected with M13KO7 at a MOI of 20. The infected culture was incubated for 30 min at 37 °C without shaking and then transferred to 100 mL of SB medium (supplemented with 1 % (w/v) glucose, 0.5 mM IPTG, and 30 µL mL^{-1} chloramphenicol) in a 2 L baffled flask and shaken for 1.5 h at 37 °C. Kanamycin was added to a final concentration of 25 µL mL^{-1}, followed by shaking for an additional 16 h at 30 °C. Aliquots of 110 mL were centrifuged (20 min, 4 °C, 3830 g) to pellet the bacteria. 100 mL of supernatant were mixed thoroughly with 25 mL PEG/NaCl and incubated on ice for 30 min. The mixture was centrifuged for 20 min at 25 000 g at

4 °C; the supernatant was discarded, and residual liquid was removed. The resulting pellet was air-dried for 5–10 min, followed by careful removal of residual. The pellet was resuspended in 0.5 mL of sterile PBS, and centrifuged for 10 min (RT, 25 000 g) to remove residual bacterial carryover. The supernatant was transferred to a new tube for phage titration (plaque forming units PFU/mL). 10 µL of a 2 % NaN_3 solution were added per mL of phage solution before storing the samples at 4 °C.

Propagation of single colonie without phage precipitation

3 mL of 2xYT medium (containing 1 % (w/v) glucose, 30 µL mL^{-1} chloramphenicol, and 10 µg mL^{-1} tetracycline) were inoculated with a picked single colony and incubated o/n at 37 °C. 4 mL of 2xYT medium (with the aforementioned supplements) were inoculated with an appropriate volume of the o/n culture to ensure an OD_{600} of 0.1. The culture was incubated shaking at 37 °C until an OD_{600} of approximately 0.5 was reached. Subsequently, bacteria were infected with 500 µL of M13KO7 diluted to 4×10^{10} pfu in 500 µL and mixed. The culture was incubated at 37 °C for 30 min without shaking, followed by an additional 30 min with shaking. The preparations were centrifuged at 4 °C for 10 min at 1377 g, and the supernatant was discarded. The pellet was resuspended in 4 mL of 2xYT medium (containing 1 % (w/v) glucose, 30 µL mL^{-1} chloramphenicol, 0.5 mM IPTG, and 25 µg mL^{-1} kanamycin) and incubated shaking at 30 °C o/n. The following day, the infected bacterial culture was centrifuged for 20 min at 25 000 g at 4 °C. The phage-containing supernatant was transferred to a new tube and stored at 4 °C.

3.2.5 Phage ELISA

Wells were coated with 10 µg well^{-1} of recombinant mCOLVII^{vWFA2} (*E.coli*) or mCOLVII^{vWFA2}-fusion-protein (CHO), or *E. coli* ER2566 lysate supernatant (Protoc. 3.2.2) diluted 1:4 in PBS at 4 °C o/n without shaking. All wells were washed three times with 200 µL of washing buffer and blocked with 200 µL of blocking buffer for 1 h at 37 °C. After blocking, the buffer was discarded, and the wells were incubated with 100 µL of phage supernatant (Protoc. 3.2.4), titered phage (Protoc. 3.2.2), control phage (Tab 2.3), or 2xYT medium for 1 h at RT. The titered phage and control phage were equalized concerning their CFU before application, if applicable. Phage preparations were discarded, and the plate was washed by incubation with blocking buffer for 1 h at 37 °C. The anti-M13 x HRP mIgG2b detection antibody was diluted 1:2000 in blocking buffer, and 100 µL was applied to the plate for 1 h at RT. The detection antibody was discarded, and the plate was washed with 200 µL of blocking buffer, followed by two washes with

1 ×PBS. ABTS substrate was prepared by dissolving one ABTS unit (tablet) in 45 mL of ddH□O and 5 mL of x10 ABTS buffer. Finally, 100 µL of ABTS buffer was applied per well, and the OD_{405} was measured at 5 min intervals after the start of reaction.

3.3 Molecular Biology

3.3.1 RNA: Preparation and Quality Control

The RNA isolation, quality control and processing for immune library generation has been described in detail in Schmidt-Jiménez 2020 [162]. The procedures are briefly described, due to the usage of the RNA for V_H and V_L RNA-receptor-sequencing in this study.

RNA extraction was performed using Guanidinium thiocyanate-phenol-chloroform precipitation. Snap-frozen tissues (S, LN) were homogenized on ice with 1 mL of 4 °C cooled TRIzol reagent per 50 mg tissue until the solution was turbid and homogeneous using a douncer. 1 mL aliquots were transferred to 1.5 mL tubes and incubated for 5 min at RT. Phase separation was initiated by adding 200 µL chloroform to each 1 mL TRIzol homogenate, mixing by inversion, and incubating for 3 min at RT. Samples were centrifuged at 12 000 g, 4 °C for 15 min, and the upper aqueous phase was transferred to a new tube. For RNA isolation, 500 µL 1-propanol was added to the aqueous phase from 1 mL TRIzol homogenate and incubated for 10 min at RT. Samples were centrifuged at 12 000 g, 4 °C for 15 min. The supernatant was carefully removed and each pellet was washed with 1 mL of 75% ethanol and centrifuged at 7500 g, 4 °C for 5 min. The supernatant was thoroughly removed, and pellets were air-dried at RT for 5–10 min until clear. Pellets were resuspended in 20–50 µL RNase-free water, incubated at 55 °C for 15 min, and pooled for respective samples. The RNA was aliquoted for quantity and quality analysis and subsequently stored at −80 °C. RNA integrity and concentration was assessed by capillary electrophoresis utilizing an Agilent Bioanalyzer with the RNA Nano-Kit according to the manufacturer's protocol.

3.3.2 DNA: Isolation, Preparation and Quality Control

Plasmid DNA was isolated from bacteria to test for correct insert containment and subsequent sequencing. Insert size was determined by gel electrophoresis with prior restriction digestion. Sanger sequencing was performed to obtain scFv DNA sequences from single colonies; next-generation V^H sequencing was performed to assess library diversity.

Plasmid DNA purification

Plasmid DNA was isolated using the NucleoSpin® Plasmid Mini kit for plasmid DNA from Macherey-Nagel according to the manufacturer's manual [179]. In brief, transformed and cultivated bacteria were lysed using alkaline lysis buffer; the lysate was neutralized, and plasmid DNA was bound to a silica membrane. Contaminants were washed away, and pure plasmid DNA was eluted in a low-salt buffer.

Endotoxin-free plasmid DNA purification

Extraction of plasmid DNA from 3.5.1 was performed using the Macherey-Nagel NucleoBond PC 2000 EF Mega Kit for endotoxin-free plasmid DNA according to the manufacturer's manual without deviations [180].

DNA restriction digestion

SfiI is a multi-site restriction enzyme that can cleave double-stranded DNA at multiple specific recognition sites. This multi-site cleavage enables the site-specific design of restriction sites, facilitating targeted manipulations in genetic engineering. Sfi I cleaves after indicated initiation sequence at the base pairs highlighted by bold font.
5'GGCCNNN **N** **N** GGCC3'
3'CCGG**NN**NNNCCGG5'
The master mix, as indicated in Table 3.1, was scaled individually and added to 0.2 mL reaction tubes. For each sample, 1 µL (10 U) of SfiI was added, including a negative control that did not contain the enzyme; the respective volume was filled with H_2O. The samples were incubated at 50°C o/n in a thermocycler. Finally, five µL of each sample were run on an analytical agarose gel as described in Section 3.3.2.

Table 3.1: Sfi I digestion master mix

Reagent	**Volume / sample**	**$C_{(final)}$**
Vector	n µl (1 µg)	33 ng / µl
10x CutSmart	5 µl	1x CutSmart
Sfi I	1 µl	10 U
Nuclease-free H_2O	add to 49 µl	

DNA gel electrophoresis

Gel electrophoresis enables the separation of charged biomolecules through migration in an electric field. Nucleic acids, characterized by their constant mass-to-charge ratio from the phosphate backbone, migrate through the agarose matrix at rates inversely proportional to their size and dependent on the applied electric field strength and gel concentration [177, Chapter 5.2].
For DNA fragment analysis, $1.5\,\%$ agarose gels were prepared by heat-dissolving $2.25\,\mathrm{g}$ of molecular biology-grade agarose in $150\,\mathrm{mL}$ of $1\times$ TAE buffer, followed by transfer to gel chambers for polymerization. Restriction-digested DNA samples mixed with loading dye were loaded alongside DNA size markers and run at $200\,\mathrm{V}$ for approximately $30\,\mathrm{min}$ or until the bromophenol blue tracking dye had migrated approx. $7\,\mathrm{cm}$ of the chamber. Following electrophoresis, gels were stained in ethidium bromide solution ($0.5\,\mu\mathrm{g\,mL^{-1}}$) for $20\,\mathrm{min}$ and visualized under ultraviolet (UV) illumination using a Herolab E.A.S.Y 440K documentation system with E.A.S.Y Win32 acquisition software.

3.4 Sequencing

3.4.1 V^H and V^L Sanger Sequencing

Sanger sequencing [181] was performed at the Institute of Clinical Molecular Biology (IKMB) of the *Christian-Albrechts-Universität zu Kiel*. $300\,\mathrm{ng}$ of isolated scFv plasmid DNA (Protoc. 3.3.2) was amplified in two sequencing reactions using 5′ V^H- and 3′ V^L(Tab. 2.5) primer at a final concentration of $4.8\,\mu\mathrm{M}$. Chromatograms were analyzed for nucleotide integrity by Dr. Steffen Krohn, and V^H and V^Lsequences were converted to FASTQ format. Gene usage and resulting V(D)J clonotypes were annotated using The International ImMunoGene Tics Information System®(IMGT) V-QUEST tool.

V-D-J alignment and annotation

IMGT/V-QUEST is a standardized analysis tool for IG and T cell receptor (TR) nucleotide sequences [171]. The algorithm performs successive global alignments of input sequences against IMGT reference directory sets to identify V, D, and J genes/alleles [182]. It delimits framework (FR-IMGT) and complementarity-determining regions (CDR-IMGT) using the IMGT unique numbering system, detects somatic mutations, and provides translated junction analysis through integrated IMGT/JunctionAnalysis [172]. The output includes alignments, nucleotide/AA sequences, and 2D Collier de

Perles representations of variable regions. Gene usage and resulting V(D)J clonotypes were annotated using IMGT/V-QUEST.

Determination of Philogeny

To compare the Sanger-derived sequences a multi-alignment was performed at the codon level using ClustalW with the software MEGA12 (Tab. 2.13) for V^H and V^L separately. Using the MaximumLikelihood method [183] and Tamura-Nei model [184] of nucleotide substitutions, phylogenetic trees of V^H and V^L were inferred based on the multi-alignment data. Initial trees were constructed using the Neighbor-Joining (NJ) method, which estimates evolutionary distances to infer tree topology, and BioNJ, an improved version of NJ that minimizes variance in distance estimation. These initial trees were optimized by the program, using nearest-neighbor in terchange, a heuristic method that refines branch arrangements to maximize the likelihoodof the observed sequence data under the Tamura-Nei model.

3.4.2 Next-Generation-Sequencing of V^H in Immune Libraries

Immune library sequencing was performed using the Illumina MiSeq system in collaboration with the *Sektion für Hämatologische Spezialdiagnostik* at the University-Medical-Center Schleswig-Holstein, Campus Kiel. Due to a read length limitation of 500 bp to 600 bp of the MiSeq plattfrom, wich is exceeded by the typical scFv lengths of 700 bp to 800 bp, libary sequencing was restricted to the V^H region. Vector DNA prepared from bacteria (Protoc. 3.3.2) was amplified by PCR adding required adapters and indices to the V^Hregions. The forward primer binds 5′ of the V^Hon the phagemid-vector, while reverse primers consist of a mixture targeting different V^HJ-genes (Tab 2.5). Depending on required sequencing throughput, either reagent Kit v2 or v3 was used according to manufacturer protocols 2.9. V^H sequence data were converted to FASTQ format and analyzed using the ARResT/Interrogate platform maintained and analysis performed by the *Sektion für Hämatologische Spezialdiagnostik* [185]. For each V^H sequence, the platform annotated V, D, and J gene segments, junction regions where all three genes converge, and resulting CDR3 sequences. This analysis enabled clonotype identification (smiliar to IMGT analysis), where each unique V/D/J combination with distinct junction sequences represents a B-cell clone. By quantifying V^H reads per clonotype, the frequencies of Sanger derived V^H clonotypes within the immune libraries were calculated. Dr. Steffen Krohn performed initial analysis on the provided ARResT annotated data, which were refined by the author for figure preparation.

3.4.3 B-cell Receptor Repertoire Sequencing and Analysis

BCR sequencing (BCR-seq) was performed by iRepertoire, Inc. (Huntsville, AL) using the RNA previously used for S and LN library preparation. The workflow performed and provided by iRepertoire, Inc. is described in the following paragraphs.

Library preparation and sequencing

Custom primers targeting mouse IgH, Igκ, and Igλ chains were designed to distinguish IGH isotypes and subclasses using dimer-avoided multiplex PCR. Primer validation details (e.g., efficiency across V-gene families) were not provided. Libraries were sequenced on an Illumina NextSeq 1000/2000 system (2×150 bp paired-end configuration), with 8bp sample barcodes and 10bp Unique Molecular Identifiers (UMIs) added to track individual RNA molecules.

Data processing pipeline

Paired-end reads were stitched using NGmerge v0.3 and demultiplexed by barcode. UMIs enabled removal of PCR duplicates, though the minimum threshold of 1 read/UMI precluded sequencing error correction. Constant regions were identified via Smith-Waterman alignment, followed by primer trimming and chain separation. IgBlast v1.18.0 annotated sequences against IMGT reference databases (release 202430-2). A final Hamming distance (HD) filter (≤1 mismatch in CDR2-FR4 regions) reduced residual PCR/sequencing errors.

Repertoire analysis

SHM with normalization (SHM1) was calculated as the percentage of nucleotide mismatches relative to IMGT V references from CDR2 to FR4, stratified by isotype [186]. Class-switch recombination analysis followed Bashford-Rogers' method, quantifying CDR3 peptides shared between isotypes (IgM/IgD combined; IgE excluded due to low tissue abundance) [186]. Diversity metrics included Shannon entropy, Simpson index, and d50 (percentage of clones constituting 50% of UMIs) [187]. Bootstrapping normalized UMI counts across samples [188]. Gene usage distributions for V/J genes and isotypes were calculated with two approaches: expression-weighted (UMI counts) or clone-normalized (unique sequences). BCR treemaps displayed clone size (proportional to UMI counts) and CDR3 peptide identity.

Sharing analysis R^2_{outer}

To access the sharing between samples different metrics of diversity and clonality were calculated [189]. The R^2 (coefficient of determination) was calculated to assess reproducibility of technical replicates. The herein described R^2_{outer} is a stringent metric that quantifies the statistical correlation between CDR3 abundance distributions by incorporating all unique CDR3 sequences from both samples, assigning zero values to non-shared clonotypes to provide a comprehensive assessment of repertoire similarity.

$$R^2_{\text{outer}} = \left(\frac{\sum_{i=1}^{n}(A_i - \overline{A})(B_i - \overline{B})}{\sqrt{\sum_{i=1}^{n}(A_i - \overline{A})^2}\sqrt{\sum_{i=1}^{n}(B_i - \overline{B})^2}} \right)^2$$

Where A_i and B_i are the counts of the i-th unique CDR3 in sample A and B (0 if absent), n is the total number of unique CDR3s across both samples, and $\overline{X}$ and $\overline{Y}$ are the mean CDR3 counts in sample A and B, respectively.

Sharing analysis: uCDR3

The uCDR3 sharing was calculated to quantify the proportion of unique CDR3 sequences from one sample that are shared with another sample, providing a measure of repertoire overlap at the sequence diversity level. This metric represents the fraction of unique CDR3s in the reference sample that are also present in the comparison sample, regardless of their relative abundances.

$$\text{uCDR3} = \frac{|U_A \cap U_B|}{|U_A|}$$

U_A represents the uCDR3 in sample A, U_B represents the uCDR3 in sample B, $|U_A \cap U_B|$ represents the number of uCDR3 shared between sample A and sample B, and $|U_A|$ represents the total number of uCDR3 sequences in sample A.

Sharing analysis: expression

The chain expression sharing was calculated to quantify the shared abundance of CDR3s between sample pairs, providing insight into clonal expansion dynamics. This metric represents the proportion of reads in sample A that correspond to CDR3 sequences shared with sample B, normalized by the total read count of sample A.

$$\text{Expression} = \frac{\sum_{i \in S} N_{i,A}}{N_{\text{total},A}}$$

S represents the set of CDR3 sequences shared between sample A and sample B, $N_{i,A}$ represents the number of reads for the i-th shared CDR3 in sample A, and $N_{total,A}$ represents the total number of reads in sample A.

Sharing analysis: Sørensen

The Sørensen-Dice (Sørensen) index was calculated to quantify the similarity between CDR3 repertoires based on the presence or absence of unique sequences, providing a measure of repertoire overlap that emphasizes shared diversity. This coefficient represents the proportion of shared unique CDR3 sequences relative to the average repertoire size of both samples.

$$\text{Sørensen} = \frac{2(\text{uCDR3 in sample A} \cap \text{uCDR3 in sample B})}{\text{uCDR3 in sample A} + \text{uCDR3 in sample B}}$$

The numerator represents twice the number of unique CDR3s shared between samples A and B, and the denominator represents the sum of total unique CDR3s in both samples. The Sørensen index ranges from 0 (no shared sequences) to 1 (identical repertoires), with values closer to 1 indicating higher similarity between the compared CDR3 repertoires.

Sharing analysis: Morisita-Horn

The Morisita-Horn index was calculated to assess the similarity between CDR3 repertoires while accounting for both sequence diversity and abundance patterns. This metric quantifies the overlap between samples by considering the relative frequencies of shared CDR3 sequences, providing a comprehensive measure of repertoire similarity that is sensitive to clonal expansion dynamics.

$$\text{Morisita-Horn} = \frac{2\sum_{i=1}^{n} f_{i,A} \cdot f_{i,B}}{\sum_{i=1}^{n} f_{i,A}^2 + \sum_{i=1}^{n} f_{i,B}^2}$$

$f_{i,A}$ represents the relative frequency of the i-th unique CDR3 in sample A, $f_{i,B}$ represents the relative frequency of the i-th unique CDR3 in sample B, n represents the total number of unique CDR3s across both samples, and MH represents the Morisita-Horn similarity index value. The Morisita-Horn index ranges from 0 (no overlap) to 1 (perfect overlap), where higher values indicate greater similarity in both the identity and abundance patterns of CDR3s between samples. This abundance-weighted approach provides biologically relevant information about clonal expansion and repertoire dynamics beyond sequence sharing.

3.5 Recombinant Antibody Expression

Known V^H and V^L DNA sequence allow for recombinant antibody and antibody-derivate expression in pro- or eukaryotic systems. The choice of host species and the respective expression system has a pivotal influence on antibody properties [190]. The majority of an recombinant Ig molecule can be actively influenced by the choice of (primarily) heavy and light chain portion, however the species background of the V^H and V^L regions remains of crucial immunogenic importance when intended for *in vivo* application [191]. Post-translational modifications such as glycosylation crucially impact antibody effector functions [192]. Prokaryotes lack the ability to introduce glycosylation, alienating bacteria-derived recombinant antibodies when introduced to eukaryotic species. In addition, the prokaryotic protein production machinery is not suited to produce full-length antibodies, leading to incomplete production, assembly, and the need for antibody extraction from inclusion bodies (gram-negative bacteria) due to a lack of secretion, thus resulting in low yields [193]. All commonly used eukaryotic cell lines for recombinant protein expression introduce species-specific glycosylation patterns and equally vary in properties such as transfection efficacy, viability, and protein expression [194]. This variability, even within mammalian expression systems, emphasizes the importance of choice for recombinant antibody expression. For the previously described reasons, the majority of commercially available antibodies and nearly all therapeutic monoclonal antibodies are expressed in stable mammalian cell lines, with chinese hamster ovary cells (CHO) among the most frequent in use [147, Chapter 33] [195]. Transient gene expression cell lines are favored for small-scale production of candidate antibodies in pre-clinical research due to rapid screening advantages, cost-efficacy for low-amount production procedures, and recent advances in transfection efficacy and yield, even in small-scale production [196]. For the production of the herein described antibodies, a transient transfection of CHO cells was chosen.

3.5.1 Re-Transformation of Electrocompetent *E. coli* for Plasmid Production

Electrocompetent *E. coli* XL1-Blue cells were thawed on ice, and $50\,\mu L$ were transferred to a pre-cooled tube and incubated with $20\,ng$ of plasmid DNA. The cell-plasmid mixture was transferred to a pre-cooled $0.1\,cm$ electroporation cuvette and transformed using a voltage of $1.8\,kV$ in an electroporator. The cuvette was immediately rinsed with $1\,mL$ of SOC medium (Tab. 2.9). A 1:10 dilution ($1\,\mu L$ bacteria + $10\,\mu L$ SOC medium) of transformed bacteria was cultivated o/n on 2×YT agar plates with $0.1\,mg\,mL^{-1}$ ampicillin

at 37 °C. The following day, single colonies were picked and expanded in 3 mL of 2×YT medium supplemented with 0.1 mg mL^{-1} ampicillin, o/n at 37 °C. An aliquot of this pre-culture was inoculated into 500 mL of 2×YT medium the following day for large-scale plasmid production and purification. Plasmid purification was performed as described in Protoc. 3.3.2.

3.5.2 CHO Cultivation and MaxCyte Transfection

CHO-S cells were briefly thawed in a water bath and added to 10 mL of pre-warmed (37 °C) CHO medium (Tab. 2.9) in a 50 mL falcon tube. Cells were centrifuged for 5 min at 850 g, resuspended in 5 mL of CHO medium, and transferred to a 250 mL Erlenmeyer flask containing 100 mL of CHO medium. The cells were incubated at 37 °C, 6% CO_2 with horizontal shaking. With an approximate doubling time of 24 h, cells were split three times per week and cultivated until an adequate number for the respective transfection was reached. Cells were adjusted to 2×10^6 cells/mL one day prior to transfection, allowing them to reach the desired density of 4×10^6 cells/mL for transfection o/n. Approximately 8×10^8 cells were transfected per construct. The cells were distributed into 50 mL falcons, centrifuged for 5 min at 544 g at RT, and the supernatant decanted. Cell pellets were detached in residual medium by gentle scratching and each preparation washed with 5 mL of MaxCyte electroporation buffer (Tab. 2.9) by brief vortexing. Following centrifugation with previously described settings, the supernatant was carefully removed, cells detached by scratching, and each cell pellet resuspended in 400 µL of MaxCyte electroporation buffer. The previously isolated plasmid DNA was thawed on ice, and a master mix for the respective transfection was generated using the following formula:

$$\frac{0.15\,\mu g\,\mu L^{-1}}{C_{DNA}} \times 400\,\mu L \times N_{samples} \tag{3.1}$$

Per transfection, 120 µg of plasmid DNA was used, resulting in a final DNA concentration of 0.3 µg µL^{-1} (60 µg V^H + 60 µg V_L) in 400 µL. Equal amounts of V^H and V^L DNA were added to each preparation. 400 µL of the reaction mix was transferred to an OC-400 electroporation chamber and transfected using the MaxCyte electroporator with the CHO-S protein expression protocol. Transfected cells were collected in a 6-well plate and incubated at 37 °C, 5% CO_2 for 30 min. Subsequently, the cells were transferred to 150 mL of CD OptiCHO medium (2.9) and incubated at 37 °C, 6% CO_2 o/n for recovery and viability maintenance. After assessing viability the following day, 1 µL mL^{-1} of 1 M Na-butyrate was added to stimulate antibody overexpression [197]. The culture was then incubated at 32 °C, 5% CO_2 with horizontal shaking for 11 to 14 days. Feeder

stock was added on days 4 and 8 (15 mL and 16 mL, respectively). Cells were pelleted by centrifugation twice at 4000 rpm for 15 min at 4 °C. The supernatant was sterile filtered using 0.2 µm pore size filters and stored at 4 °C for a maximum of 1 week until purification.

3.5.3 Protein Purification and Quality Assessment

The cell culture supernatant was mixed with 1 mL of Capture Select Beads (CH1-XL; Kappa-specific) and incubated o/n at 4 °C. The mixture was centrifuged at 850 g for 10 min at 4 °C. The supernatant was stored at 4 °C for further purification. The beads were resuspended in 3 mL cold 1× PBS and applied to a PolyPrep chromatography column, followed by two 10 mL PBS washes. Elution was performed using 1 mL 0.1 M Glycine-HCl buffer (pH 3.0) per fraction, collecting eluates in tubes containing 200 µL 1 M Tris-HCl buffer (pH 8.0). The protein solution (eluate) was pooled and transferred into dialysis membrane tubing and immersed in 2 L of sterile 1× PBS at 4 °C o/n. PBS was changed twice in 24-hour intervals following the initial dialysis step.
Fractions were dialyzed against 2 L cold 1× PBS at 4 °C o/n. Dialysis was repeated twice. For additional purification, beads were washed with PBS and incubated o/n at 4 °C with previously stored supernatant. After dialysis, the purified proteins were collected and transferred to Vivaspin® 6 mL centrifugal concentrators and filtered under sterile conditions using an Acrodisc® syringe filter (0.22 μm membrane, low-protein-binding,). Antibody concentrations were determined using a NanoDrop spectrophotometer, followed by SDS-PAGE to evaluate purity and molecular weight.
For SDS-PAGE (reducing and non-reducing), 2 μL of respective samples were prepared for gel-loading by adding 4 μL of 5× loading buffer and 14 μL of 1× PBS. Loading mix was then heated to 95 °C for 10 min to break non-covalent binding, followed by centrifugation at 13,000 rpm for 2 min. For reducing conditions, samples were loaded on 12% SDS-polyacrylamide gels, while non-reducing conditions were analyzed on 6% gels. Rituximab standards were included on each gel to generate calibration curves for quantitative analysis. Electrophoresis was conducted at 125 V for 75 min (1 h 15 min). Gels were stained o/n with Coomassie Brilliant Blue R-250 under gentle agitation, followed by destaining in distilled water to remove excess dye. To remove unwanted polypeptide fragments detected during SDS-PAGE, size-exclusion chromatography was conducted using the ÅKTA pure 25 system according to the manufacturer's instructions.
All antibody expression related procedures were for the majority conducted by Thomas Theocharis from the Division of Antibody-Based Immunotherapy, Department of Hema-

tology and Oncology, University Hospital Schleswig-Holstein, Kiel, Germany, lead by Prof. Dr. Peipp.

3.6 Immunoassays and Stainings

3.6.1 Enzyme-linked Immunosorbent Assay

Enzyme-linked immunosorbent assays (ELISA) are colorimetric assays that allow the detection and quantification of target proteins, by using antibody enzyme conjugates. Horseradish peroxidase (HRP) is a commonly used conjugate, driving a redox reaction by hydrolyzing H_2O_2 in the substrate, which then oxidizes TMB to TMB^+, resulting in a color change of the substrate. The reaction is stopped by a drastic change of pH, typically by addition of acid, such as H_2SO_4, which inhibits HRP activity and thus substrate conversion. The absorbance of the final solution is measured at 450 nm, with a reference measurement at 570 nm [198].

Anti-mCOLVII ELISA

96 well plates were coated with $0.0035\,\mu g$ antigen (mCOLVII^{vWFA2}, mCOLVII^{-C}, GST) in bicarbonate buffer (Tab. 2.10) and incubated o/n at $4\,°C$ on a shaker (200 rpm) to enable antigen binding. The plate was washed four times with $200\,\mu L$ of PBS-T (Tab. 2.10) to remove unbound antigen. Wells were then blocked with $150\,\mu L$ of blocking buffer (Tab. 2.10) and incubated for $1\,h$ at $37\,°C$ to cover residual free binding positions. After removal of the blocking buffer, $50\,\mu L$ of diluted sera or monoclonal antibody in dilution buffer (Tab. 2.10) were applied and incubated for $1\,h$ at $37\,°C$. The plate was washed four times with $200\,\mu L$ of PBS-T. Subsequently, $50\,\mu L$ of anti-mIgG /mIgG2b HRP conjugated detection antibody, diluted 1:10,000 in dilution buffer, were applied and incubated for $1\,h$ at RT on an orbital shaker (200 rpm). After another four washes with $200\,\mu L$ of PBS-T, $50\,\mu L$ of TMB substrate were added and incubated in the dark. The reaction was stopped by adding $50\,\mu L$ of H_2SO_4. Absorption was measured at 450 nm - 560 nm using an ELISA reader (GlowMax).

Anti-mCOLVII avidity ELISA

Antibody avidity is defined as the functional affinity of a given antibody. The avidity is determined by the combined antibody-antigen interactions, thus incorporating the valency of the antibody molecule, the affinity of individual binding sites, and the three-dimensional structure of the antibody-antigen complex. In contrast, antibody

affinity is determined by the monovalent binding and thus interaction of one paratope with a single epitope on the antigen [199]. Determination of antibody avidity allows for comparison between different antibody clones targeting the same antigen, providing insight into their overall binding strength to the respective target. To evaluate antibody avidity increasing concentrations of chaotropic substances are used in an ELISA assay, breaking covalent and non-covalent antibody-antigen interactions. The avidity is determined by calculating the avidity index, reflecting the maximum binding of a given antibody in relation to the binding in presence of the chaotropic substance [200].

The following protocol essential follows the procedure of 3.6.1 with an additional incubation with NH_4SCN to break antigen-antibody interaction [201]. 96 well plates were coated with $0.0035\,\mu g$ of antigen (mCOLVII^{vWFA2}, mCOLVII^{-C}) in bicarbonate buffer and incubated o/n at $4\,°C$ on a shaker (200 rpm). The plate was washed four times with $200\,\mu L$ of PBS-T. Wells were then blocked with $150\,\mu L$ of blocking buffer and incubated for $1\,h$ at $37\,°C$. After removing the blocking buffer, $50\,\mu L$ of diluted sera in dilution buffer were applied and incubated for $1\,h$ at $37\,°C$. The plate was washed four times with $200\,\mu L$ of PBS-T. Subsequently, $50\,\mu L$ of respective 1-10 molar NH_4SCN (2.10)were applied for $20\,min$ at RT to concentration-dependently disrupt antibody binding. After another four washes with PBS-T, $50\,\mu L$ of anti-mIgG /mIgG2b HRP conjugated detection antibody, diluted 1:10,000 in dilution buffer, were applied and incubated for $1\,h$ at RT on an orbital shaker (200 rpm). Following four more washes, $50\,\mu L$ of TMB substrate were added and incubated in the dark. The reaction was stopped by adding $50\,\mu L$ of H_2SO_4. Absorption was measured at 450 nm - 560 nm using an ELISA reader.
Avidity Index was calculated as follows: Mean absorbance of coating (baseline) was substracted from all measured values, top correct for baseline signal. Mean absorbance of non-treated wells(0 M NH_4SCN) was used to calculate the avidity index for each clone, by the following formular: (X / Mean OD-450-560nm$_{0\,M}$)*100. Avidity indices were normalized per plate (min–max), to compare clones within each plate, and different experiments with each other.

Anti-h/m C_3 ELISA

All applied volumes in the following protocol were fixed to $100\,\mu L$. Wells were coated with 1 500 diluted (from $1\,mg\,mL^{-1}$ stock) rat-anti-mouse C_3 (clone: 11H9) in carbonate buffer and incubated o/n at $4\,°C$ on a shaker (200 rpm). The coating was discarded by flipping the plate into the sink, and the plate was tapped dry. Wells were then blocked

with blocking buffer 01 (Tab. 2.10) and incubated for 1 h at 37 °C. The blocking buffer was discarded in the same manner as before. Next, 1:50 diluted sera in working buffer 01 (Tab. 2.10) were applied and incubated for 1 h at 37 °C. The plate was washed three times with working buffer 01. Subsequently, 1 1000 diluted primary antibody (biotin-chicken α-C_3) in working buffer 01 was applied and incubated for 1 h at 37 °C. The plate was washed three times with working buffer 02 (Tab. 2.10). Following this, 1:64.000 diluted HRP conjugated streptavidin in working buffer 02 was applied for approximately 30 min at RT. After washing three times with working buffer 02, TMB substrate was added and incubated in the dark. The reaction was stopped by adding H_2SO_4. Absorption was measured at 450 nm - 560 nm using an ELISA reader.

3.6.2 Immunofluorescence Tissue Stainings

The following stainings allow verification of the binding of specific (mouse/rabbit) IgG to full-length target protein *in vitro*, as well as determination of the deposition of complement factors due to CP activation. The IgG samples were generated from sera of mCOLVII-immunized mice or rabbits, which consequently develop anti-mCOLVII IgG antibodies, or from recombinantly expressed monoclonal antibodies targeting mCOLVII. An indirect staining is performed after the incubation of IgG with tissue samples *ex vivo*, whereas a direct staining is chosen for tissue samples from mice injected with respective antibodies [167].

Indirect anti-mIgG tissue staining

The tissue slides were thawed, and individual tissue sections were encircled with a hydrophobic barrier pen, creating a physical barrier to prevent spillover between the sections. The slides were dried for 10 min and subsequently re-hydrated in 1 ×PBS for 15 min at RT. Next, 100 µL of 1 ×PBS diluted mAb or serum, along with the corresponding isotype or normal murine/rabbit serum control, were applied per section and incubated o/n at RT in a moisture chamber. Following removal from the moisture chamber, the residual liquid was flicked off the slides, and all slides were placed into a cuvette filled with 1 ×PBS for 5 min at RT, allowing non-bound antibody moieties to be washed away. This washing procedure was repeated two times. Subsequently, all sections were blocked with 100 µL of 4 % BSA in 1 ×PBS for 20 min at RT. After blocking, 100 µL of FITC-conjugated donkey F(ab')2 anti-mouse IgG (H+L) diluted 1:100 in 1 ×PBS + 2 % BSA at 4 °C were applied per tissue section and incubated for 2 h at RT. The slides were further incubated for 10 min at RT. After incubation, the residual liquid was flicked off the

slides again, and all slides were placed into a light-protected cuvette filled with $1\times$PBS for another 5 min at RT to wash away any non-bound antibody moieties; this washing procedure was repeated two times. Subsequently, all sections were dried for 2 min, covered with mounting medium containing DAPI, for DNA counter staining, sealed with a cover slip, and rested at $4\,°$C o/n. Fluorescence was evaluated using a Keyence Keyence BZ-9000E series fluorescence microscope. The DEJ signal was evaluated using mean fluorescence intensity (MFI) assessment in ImageJ.

Direct anti-mIgG tissue staining

The tissue slides were thawed and individual sections were encircled with a hydrophobic barrier pen to create a physical barrier preventing spillover between sections. The slides were then dried for 10 min and subsequently rehydrated in $1\times$PBS for 15 min at RT. For antibody detection, $50\,\mu$L of FITC-conjugated donkey F(ab')2 anti-mouse IgG (H+L), diluted 1:100 in $1\times$PBS + 2 % BSA, was applied to each tissue section and incubated for 45 min at RT. The slides were further incubated for 10 min at RT. Following incubation, the slides were removed from the moisture chamber, excess liquid was flicked off, and they were placed into a light-protected cuvette filled with $1\times$PBS for 5 min at RT. This washing procedure was repeated twice to remove unbound antibodies. Subsequently, all sections were dried for 2 min, covered with mounting medium containing DAPI, for DNA counter staining, sealed with a cover slip, and rested at $4\,°$C o/n. Fluorescence was evaluated using a Keyence BZ-9000E series fluorescence microscope.

Anti-mC_3 tissue staining

The tissue slides were thawed, dried for 2 min and fixated by submergence in cold acetone (100%) for 10 min. Following drying, the individual tissue sections were encircled with a hydrophobic PAP pen, creating a physical barrier to prohibit spillover between the sections. The slides were subsequently rehydrated in 1x PBS for 15 min at RT. All tissue sections were blocked with $200\,\mu$L of 2% BSA in 1x PBS for 30 min at RT in a moisture chamber. For antigen detection, $50\,\mu$L of FITC-conjugated goat anti-mouse C_3 diluted 1:400 in 1x PBS + 2% normal goat serum were applied per tissue section and incubated for 45 min at RT. Following removal from the moisture chamber, the residual liquid was flicked off the slides and all were placed into a light-protected cuvette, filled with 1x PBS for 5 min at RT, allowing for non-bound antibody moieties to be washed away. The washing procedure was repeated twice. Subsequently, all sections were dried for 2 min, covered with mounting medium containing DAPI for DNA counterstaining, sealed with

coverslip and rested at 4 °C o/n. Fluorescence was evaluated using a Keyence BZ-9000E series fluorescence microscope.

3.6.3 Histology: Hematoxylin and Eosin Staining

Hematoxylin and eosin (H&E) staining was performed on paraformaldehyde-fixed skin biopsies to verify the clinical phenotype of EBA and assess the grade of inflammation by evaluating immune cell infiltration and epidermal thickness. Biopsies stored in 4 % paraformaldehyde 3.1.7 were dehydrated by passage through an ascending ethanol series, treated with Histol, a xylene substitute, and embedded in paraffin. 4 µm-thick sections were cut using a microtome, mounted on glass slides, and stained with H&E following the standard protocol of the histopathology routine laboratory of the Department of Dermatology, Allergology and Venerology of the University Hospital Schleswig-Holstein, Lübeck. Sectioning and staining were performed by research assistants Bejtije Naumann and Nikolai L'vov. For analysis, sections were examined using a Keyence BZ-9000E series light microscope at 100 × magnification. Epidermal thickness and extent of inflammatory cell infiltration were evaluated using a semi-quantitative scoring system in a blinded manner by technician Daniela Rick.

3.6.4 Reactive Oxygen Species Release Assay

Reactive oxygen species (ROS) release is one of the major effector functions of mature neutrophils upon activation. In this assay ROS release is triggered by Fcγ activation of isolated neutrophils, using *in vitro* ICs, in the presence of luminol. Lumninol reacts with the released oxygen radicals (superoxide anion) leading to a short whiled exicted state, which releases photons (chemiluminescence) which are measured as an indicator of ROS release.

Generation of immune complexes

Throughout the protocol, all plate-related washing steps were performed with a volume of 200 µL per well. High-binding Lumitrac 96-well plates were coated with 100 µL of a 10 µg mL^{-1} antigen solution (mCOLVII$^{\text{-C}}$, mCOLVII$^{\text{vWFA2}}$) in bicarbonate buffer (Tab. 2.10), covered, and incubated o/n at 4 °C on a rocking platform. The coating solution was discarded, and the plate was washed four times with washing buffer (Tab. 2.10). Following this, the plate was blocked with 200 µL well^{-1} of cold blocking buffer (2.10) for 1 h at RT on a rocking platform. After discarding the blocking buffer, the plate was washed four times with washing buffer. Respective antigen-targeting antibodies were

diluted in blocking buffer, and 1 µg well^{-1} to 4 µg well^{-1} were incubated for 1.5 h at RT on a rocking platform. After antibody incubation, the plate was washed three times with washing buffer and stored in 200 µL well^{-1} of CL medium at 4 °C.

Generation of immune complexes with complement opsonization

Alternatively after the washing procedure of bound antibody, the plate was washed three times with washing buffer, and 100 µL of serially diluted complement-competent serum (Tab 3.1.7) in veronal buffer (2.9) was applied to respective wells and incubated for 30 min at 37 °C for CP activation. Following complement activation, the plate was washed three times with washing buffer and stored in 200 µL well^{-1} of CL medium at 4 °C. Complement presence in the serum was verified by ELISA (Protoc. 3.6.1).

Purification of neutrophils

Non-anesthetized WT mice were euthanized by cervical dislocation (ethics file number 5.1_2025-05-26_Bieber). The tibiae and femora of both hind legs were isolated and stored in 1xPBS on ice. Bone caps were removed, and bone marrow cells were isolated by flushing the tibiae and femora with cold isolation buffer (Tab. 2.10) using a syringe and an appropriate needle. The cells were passed through a pre-wetted 70 µm strainer into a 50 mL Falcon tube. The cells from all four bones per mouse were pooled, and the resulting volume was adjusted to 40 mL for all cell preparations. The cells were processed according to the manufacturer's instructions for the Miltenyi Neutrophil Isolation Kit. An aliquot of each cell preparation was diluted 1:10 in FACS buffer, and cell counts were calculated using a MACSQuant Analyzer 10. The cell count per mL was equalized between samples to a minimum of 1 million cells per mL. The CL medium in the plate was discarded, and 200 µL of a cell suspension containing 1 million cells per mL was added per well. Two mg of luminol were dissolved in 8 µL of 2 M NaOH. The dissolved luminol was then diluted in 1.1 mL of ddH_2O. The injector of the luminescence reader was primed with 600 µL of luminol, and the machine was pre-heated to 37 °C.

Purity measurement

A minimum of 1×10^5 cells per sample was used to determine neutrophil purity using flow cytometry. Cells were pelleted by centrifugation as previously described and stained for 10 min at 4 °C in either 100 µL of 1:1000 diluted ZombieNIR™ or propidium iodide. Cells were pelleted, washed with 200 µL of FACS buffer, and stained with anti-Ly6G PE-Cy7 and anti-Ly6C FITC, both diluted 1:100 in FACS buffer, for 15 min at 4 °C. Following

the previously described washing procedure, cell purity was determined gating on (1) singlets, (2) cell size, (3) viability, (4) $Ly6G^+$ / $Ly6C^-$. A purity of 85% referring to the "live" gate was considered sufficient for including the generated data sets.

3.7 Alpha Fold Modelling of mCOLVII^{vWFA2} Targetings Antibodies

The Fv regions of eight anti-mCOLVII^{vWFA2} antibody clones (C1-C7, C10) were modeled using *AbodyBuilder2*, a computational tool that predicts antibody structures from sequence data while optimizing CDR loop conformations for antigen binding. This approach ensures that the CDR loops are fully exposed to simulate physiologically relevant paratope-antigen interactions.

3.8 Data Analysis and Statistical Significance

Data evaluation, statistical analysis and initial graphing were performed using GraphPad Prism (Tab. 2.13). In figure legends n represents bilogical replicates, while N represents technical replicates. Unless stated differently, data for a certain number of experiments is presented as mean $\pm$ standard error of the mean (SEM). For yes/no experiments e.g. binding or no binding, no statistical analysis was performed. For ROS release assays data were evaluated using a nonparametric approach. Group differences among control and three concentration conditions were assessed with the Kruskal–Wallis test, which compares sample ranks without assuming normally distributed residuals. Following a global significant result, pairwise comparisons were performed using Dunn's multiple comparisons test without multiple comparison correction. For the comparison of avidity across antibody clones, data were analyzed using a mixed-effects two-way ANOVA with NH_4SCN concentrations (repeated measures) and clone type (between-subjects factor) as fixed effects, and random intercepts for individual clones. Where significant main or interaction effects were detected, post hoc Tukey's multiple comparisons tests were performed. The following p-value thresholds were used to indicate statistical significance: $p \leq 0.05$ (*), $p \leq 0.01$ (**), $p \leq 0.001$ (***), and $p \leq 0.0001$ (****). Normality was assessed by QQ plots and homoscedasticity by residual-vs-fitted plots. Analyses were conducted and graphs plotted using GraphPad Prism v10 for all experiments.

3.9 Statement Regarding the Use of Artificial Intelligence

I acknowledge the use of the artificial intelligence (AI) platform Perplexity in the preparation of this dissertation. I take full responsibility for the content, accuracy, and integrity of this thesis. This dissertation was discussed with the artificial intelligence (AI) platform Perplexity. A space within the pro version of the platform was created with the following description.

I am currently writing my PhD thesis in Immunology. I am writing a non cumulative dissertation about antibodies targeting murine collagen Type VII. I am writing in LaTex. I have used immune libraries and phage display to select antibodies myself and acquired antibody clones from other researchers. All clones were expressed as IgG2bs and subsequently tested in vivo for pathogenicity.

To specify the output, the following specifications for the AI were set:

I need feedback on my text passages which I will indicate with "text passage". Always run a general check: First on spelling, then punctuation and grammar. Please check my use of the English language for accuracy - especially in a scientific context and apply rules regarding italic writing in science. Suggest improvements but DO NOT independently change the provided paragraph. Point out if my statements are incorrect, not logic or do not align with previous passages. Always provide feedback - be constructively critical at all times and check my statements first agianst the provided (cite keys), then against all accessible literature. Never use Wikipedia as a source. Only peer reviewed articles or reviews from journals, as well as standard text books, such as Janeways Immunology, Kuby Immunology etc. are acceptable sources. I require intensive scientific discussion of my findings and ideas and statements. Please output correctly formatted LaTex code when asked to correct passages.

All passages were written by the author and then passed to the AI for a thorough language and grammar correction. In addition feedback to the accurary of description was requested and incorporated if deemed needed. Literature searches where performed using Perplexity, where questions regarding specific topics were asked and answers with corresponding literature were generated by the AI. The literature was then verified by the author and in several cases used for this thesis. This dissertation was written in LaTex, a text software, which enables consistent formatting for large documents. TeXStudio, which was used as the editor plattform for LaTex incorporates an AI chat assistent, which was disabled and not used. Table framework code was provided by Perplexity upon description of table dimensions. Tables were then tested for fit and Excel generated data transferred to LaTex code using Perplexity.

Chapter 4

Results

4.1 Successfull Screening and Isolation of mCOLVII Targeting scFvs Using Phage Display Selection

To initiate phage display panning, both of the previously generated immune libraries (Fig. 1.7 S, LN) [162] were propagated. Further, high-titer M13KO7 helper phage preparations were generated, alongside *E. coli* ER2566 lysate. Recombinant mCOLVII^{vWFA2} for the immunization-induced EBA mouse model was produced in *E. coli* ER2566 as described in Protc. 3.1.4.

4.1.1 Immune Library Phage Display Panning

Electrocompetent *E. coli* XL1-Blue were generated as described in Protoc. 3.2.1 for the propagation of antibody immune libraries (Fig. 1.7). Phage-competent *E. coli* TG-1 cells were seeded and infected with M13K07 helper phage, resulting in the formation of virus-induced plaques in the bacterial cell layer (Protoc. 3.2.1). Cultured *E. coli* TG-1 were inoculated with M13K07 from a single plaque for monoclonal phage production, which were precipitated and used for all subsequent phage-related work (Protoc. 3.2.1). S- and LN-derived immune libraries (Fig. 1.7) were propagated (Protoc. 3.2.2) and infected with helper phage to generate scFv phages for phage display selection of antigen-binding scFv phages. The scFv phages were solid-phase-depleted with filtered *E. coli* ER2566 lysate supernatant (Protoc. 3.2.2) three times to prevent the selection of clones raised against residual *E. coli* ER2566 antigen during the immunization of mice. Libraries were then selected against recombinant mCOLVII^{vWFA2} in the presence of *E. coli* ER2566 lysate supernatant. Bound phages were eluted and used to infect *E. coli* XL1-Blue. The resulting

CFU was calculated to assess panning efficacy; *E. coli* XL1-Blue were harvested, and the panning procedure was repeated once. The selection strategy is depicted in Fig. 4.1.

4.1.2 Antigen Specific Selection Results in Library Enrichment After the Second Panning in Both Immune Libraries

To evaluate the efficacy and success of the phage display panning procedure, recovery rates and enrichment factors were calculated. Recovery rates and enrichment factors are critical metrics for assessing the success of phage display selection [202]. The recovery rates quantify the efficiency of phage output relative to the initial input, calculated as the ratio of recovered phages to input phages. Low recovery rates are typically observed in early rounds of panning due to non-specific binding, while higher recovery rates in subsequent rounds indicate enrichment of specific, high-affinity clones. The enrichment factor further assesses selection efficiency by comparing recovery rates between successive rounds of panning, highlighting how effectively antigen-specific clones are enriched. The metrics of both phage display panning rounds are summarized in Tab. 4.1 for spleen- and lymph node-derived libraries.

Table 4.1: Enrichment of immune libraries across phage display panning. Phage display metrics for spleen- and lymph node-derived immune libraries across two rounds of panning. Input phages indicates libray colony forming units (CFU) used for respective panning. Output phages indicates CFU after respective panning. The recovery rate describes the relation between input and output phages. The enrichment factor describes the relation between recovery rates across multiple rounds of panning.

Panning Round	Input Phages	Output Phages	Recovery Rate	Enrichment Factor
		Spleen		
1	5.62×10^{10}	1.24×10^{3}	2.20×10^{-8}	1
2	1.60×10^{12}	2.04×10^{7}	1.28×10^{-5}	5.79×10^{2}
		Lymph Node		
1	2.60×10^{10}	1.98×10^{2}	7.60×10^{-9}	1
2	2.42×10^{12}	1.80×10^{7}	7.44×10^{-6}	9.79×10^{2}

After the first round of panning, both libraries exhibited a drastic drop in phage output (in CFU), as reflected by the recovery rates: 2.20×10^{-8} for (S) and 7.60×10^{-9} for (LN), respectively. After the second round of panning, enhanced recovery rates of 1.28×10^{-5} (S) and 7.44×10^{-6} (LN) indicated the selection of mCOLVII$^{\text{vWFA2}}$-binding scFv phages. This was further confirmed by the respective enrichment factors of 5.79×10^{2} (S) and

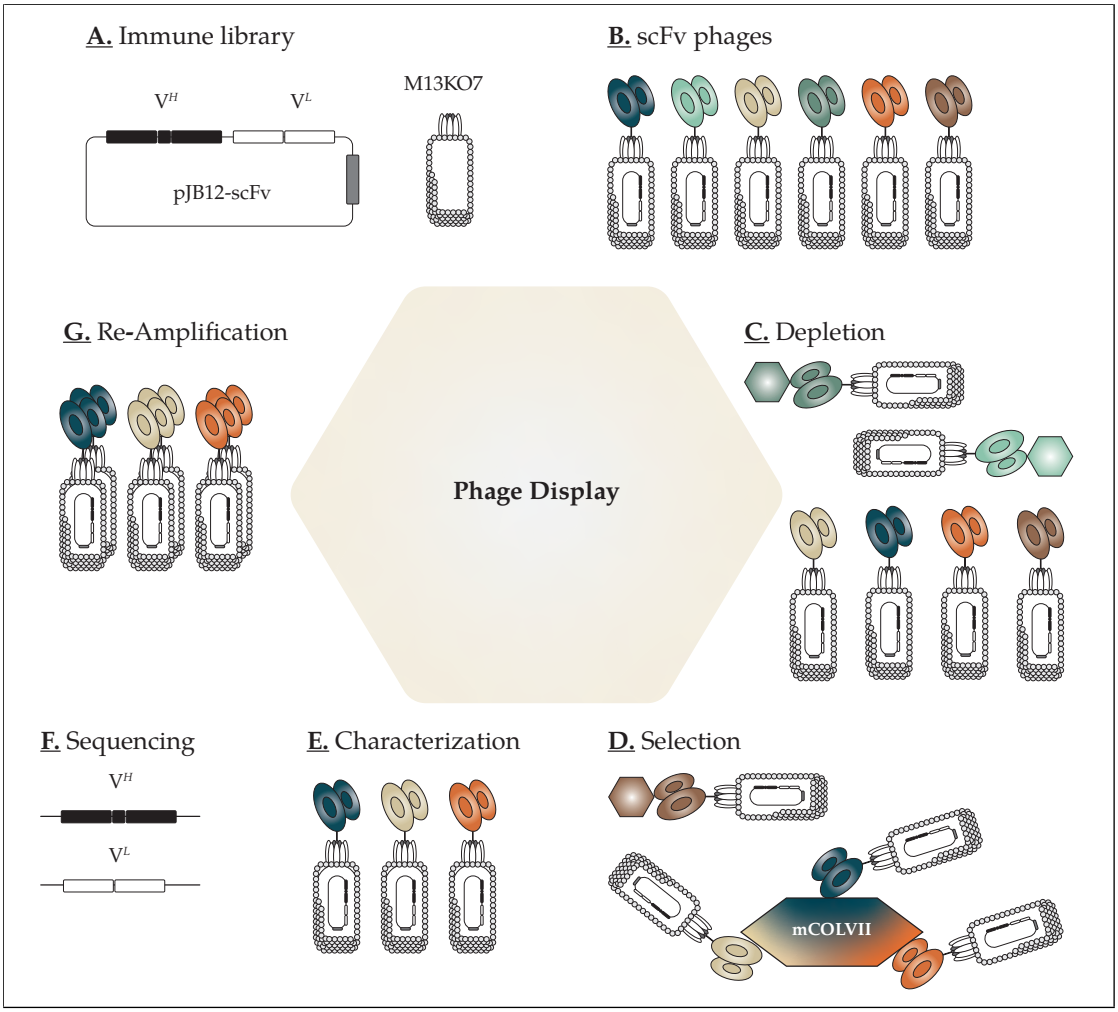

Figure 4.1: Phage display panning strategy to isolate mCOLVII^{vWFA2}-targeting antibodies.
(A.) Phagemid bearing *E. coli* XL1-Blue bacteria were infected with M13K07 helper phages to generate scFv-phage immune libraries. (B.) ScFv phages were precipitated for phage display panning procedure. Phage clonality is represented by varying colors.(C.) ScFv phage libraries were depleted with filtered *E. coli* ER2566 lysate supernatant to remove scFv clones directed against bacterial antigen (sage green shades). (D.) Depleted scFv phage libraries were selected against recombinant mCOLVII^{vWFA2} (multicolor) in the presence of *E. coli* ER2566 lysate supernatant (brown). (E.) Eluted phages were characterized *in vitro* for target binding. (G.) Eluted phages were used to reinfect *E. coli* XL1-Blue, and the panning procedure was repeated. (F.) Validated phages were sequenced for V^H and V^L gene usage.

9.79×10^2 (LN) (Tab. 4.1). The relationship between input and output phages, as well as the enrichment factors and recovery rates, is illustrated in Fig. 4.2. To confirm the selection and enrichment of scFv phages after the first and second rounds of panning, phagemid DNA was isolated from both libraries (Protoc. 3.3.2) and subjected to subsequent next-generation sequencing of V_H (3.4.2), which will be discussed further in Section 4.1.4.

4.1.3 Phage Display-Derived Monoclonal scFv Phages Specifically Target mCOLVII^{vWFA2}

To evaluate whether scFv phages after the second round of panning recognized the target antigen, single colonies were propagated (Protoc.3.2.4) to isolate monoclonal phage supernatant, which was used for phage ELISA (Protoc.3.2.5) without prior titration of monoclonal phages. Monoclonal scFv phage supernatant bound to recombinant *E. coli* ER2566-derived mCOLVII^{vWFA2} but not to *E. coli* ER2566 lysate supernatant, indicating specific target recognition (Fig. 4.3 A). ScFv 4D5 (Trastuzumab) was used as a negative control. 4D5 exhibited a moderate baseline signal, indicating either stickiness of the target or stickiness of the scFv phages. All monoclonal mCOLVII^{vWFA2}-selected scFv phages exceeded the baseline signal of 4D5 (Fig. 4.3 A.). To further evaluate target binding, CHO-derived recombinant mCOLVII^{vWFA2}-fusion protein (Tab. 2.8)was used for coating and detected in a phage ELISA setting using non-titered monoclonal scFv phage antibody supernatants. The mammalian production of this fusion protein ensured post-transcriptional glycosylation, which is absent in recombinant protein derived from bacterial expression. The coating concentration of the fusion protein was adjusted to account for its increased size (approximately threefold) compared to mCOLVII^{vWFA2}, ensuring equimolar coating conditions to the previous experiment. Clone L15 failed to recognize the mCOLVII^{vWFA2}-fusion protein; clones L20 and L14 did not exceed baseline binding provided by the 4D5 control scFv. All other clones recognized the mammalian-derived target protein (Fig. 4.3 B). Since the phage supernatant was not adjusted for phage titer, no definitive conclusion could be drawn regarding the non-reactivity of clones L15, L14, and L20.

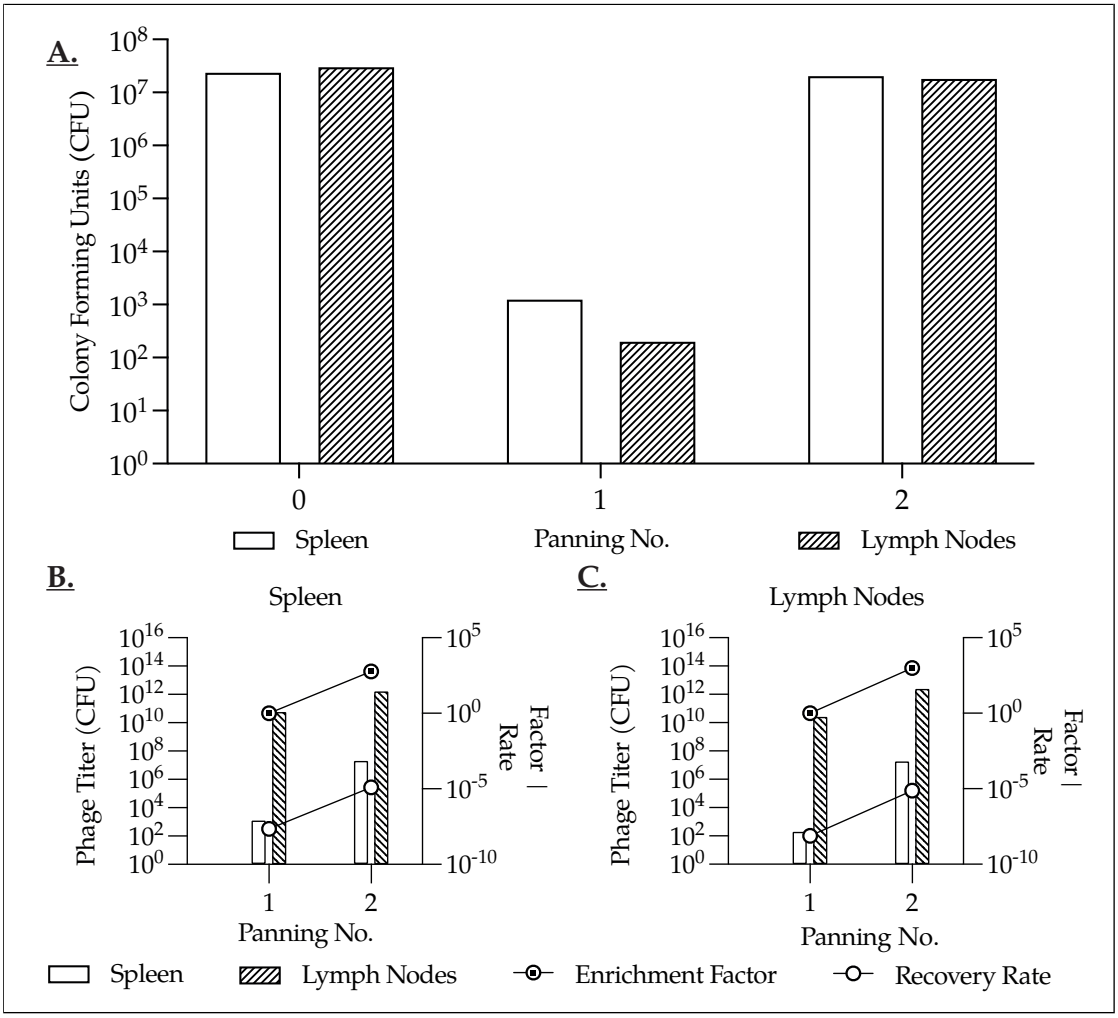

Figure 4.2: Phage display performance metrics: recovery rates and enrichment factors across panning of two immune libraries. (A.) Library CFUs were calculated before (0) and after pannings (1, 2); (B & C)Recovery rates and enrichment factors were calculated based on input phages (M13KO7 helper phage) and output phages (library CFUs), for S and LN immune libraries across pannings. Numerical values can be obtained from Tab. 4.1.

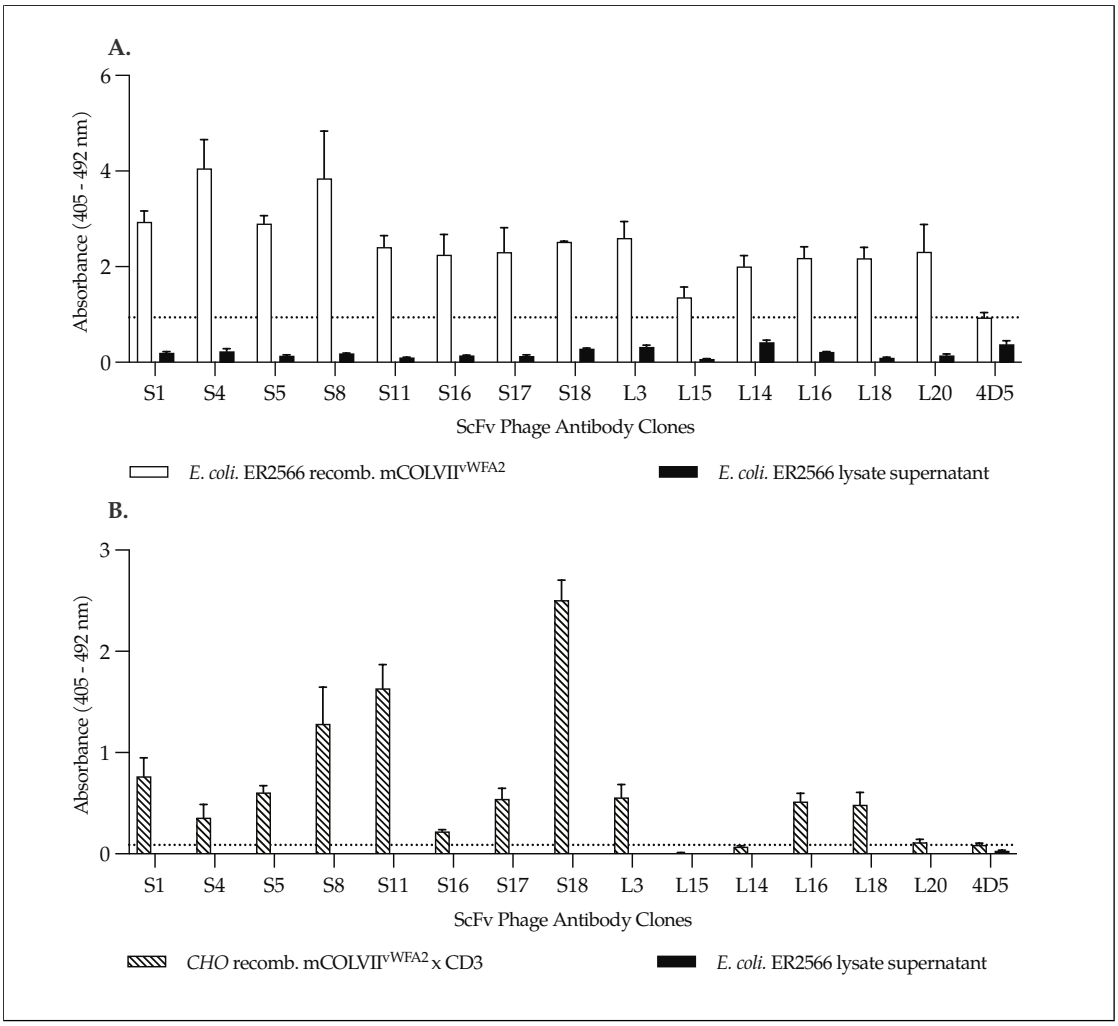

Figure 4.3: Monoclonal scFv-phages bind to recombinant mCOLVII^{vWFA2}. (A.) Non-titered supernatant of monoclonal scFv-phage clones was tested for target recognition against a constant concentration of recombinant mCOLVII^{vWFA2} in a phage ELISA. All clones bound to the target antigen, which was recombinantly produced in *E. coli* ER2566, but not to *E. coli* ER2566 cell lysate supernatant, indicating specificity of binding. The non-mCOLVII-specific scFv-phage clone 4D5 (Trastuzumab) was used as a negative control to provide a baseline background signal. All clones exceeded baseline binding. (B.) all clones were tested for binding against *CHO*-derived mCOLVII^{vWFA2}xCD3, with 4D5 used as a non-specific negative control. Clone L15 did not yield a binding signal, while clones L14 and L20 did not exceed the baseline control signal. All other clones bound to the *CHO*-derived antigen. Mean $\pm$SD of technical replicates (N=3).

4.1.4 V-D-J Clonotyping of V^H and V^L Reveals Distinct Clonotypes Among Isolated ScFv Clones

Due to a drastic reduction in CFU observed after the first round of panning (Tab. 4.1, Fig. 4.2) and successful enrichment and isolation of antigen-specific clones after the second round (Fig. 4.3), no further pannings were performed. Instead, eighteen colonies, representing individual clones, from the S-derived library and fifteen colonies from the LN-derived library were isolated and propagated (Protoc.3.2.4) for vector DNA extraction (Protoc.3.3.2) and Sanger sequencing (Protoc.3.4.1). ScFv size and abundance was assessed using gel-electrophoresis, after SfI digestions of plasmid DNA, prior to sequencing. All isolated colonies contained 650–700 bp sized scFv bands (Fig. 4.4). Sequencing was performed individually for V^H and V^L using sequencing primers, indicated in Tab. 2.5, at the IKMB of the *Christian-Albrechts-Universität zu Kiel*. All chromatograms were quality-controlled, resulting in the exclusion of clone L17 due to sequence corruption.

To compare resulting antibody sequences, a multi-alignment was performed at the codon level using ClustalW with the software MEGA12 (2.13) for both V^H and V^L separately. Phylogenetic analysis of V^H sequences revealed four distinct clusters of sequences, which were annotated as clonotypes (A–D) based on phylogeny tree clustering (Fig. 4.5). Clonotype A [red] was private to lymph node-derived clones, whereas clonotypes B [green] and D [blue] were private to spleen-derived clones. Clonotype C [yellow] was found in clones originating from both spleen- and lymph node-derived libraries. Based on the clustering of clonotypes and the calculated branch distances the herein analyzed clones were most likely derived from three individual B-cell clones, with clonotype D, due to its tree position eventually beeing a derivate of clonotype C. Similarly, phylogenetic analysis of V^L sequences revealed four clonotypes (1–4), which did not correspond to the V^H clonotypes, likely reflecting undirected pairing during immune library generation [203].

Further, the Sanger-derived DNA sequences were annotated for V-D-J gene usage and AA junctions comprising the CDR3 regions (hence termed CDR3) of the V^H and V^L chains using the IMGT/V-QUEST tool (3.4.1) [172, 182, 204]. The cluster-clonotypes identified by phylogenetic tree clustering were independently confirmed by V(D)J gene usage and CDR3 sequence annotation. Mutation counts were extracted from the IMGT/V-QUEST *V-REGION-nt-mutation-statistics* output, which enumerates nucleotide differences from the closest germline V gene and categorizes them as silent (s) or non-silent (Ns) mutations. At the level of V^H, all sequenced clones incorporated *IGHV1-39*01 F* and *IGHJ3*01 F* as

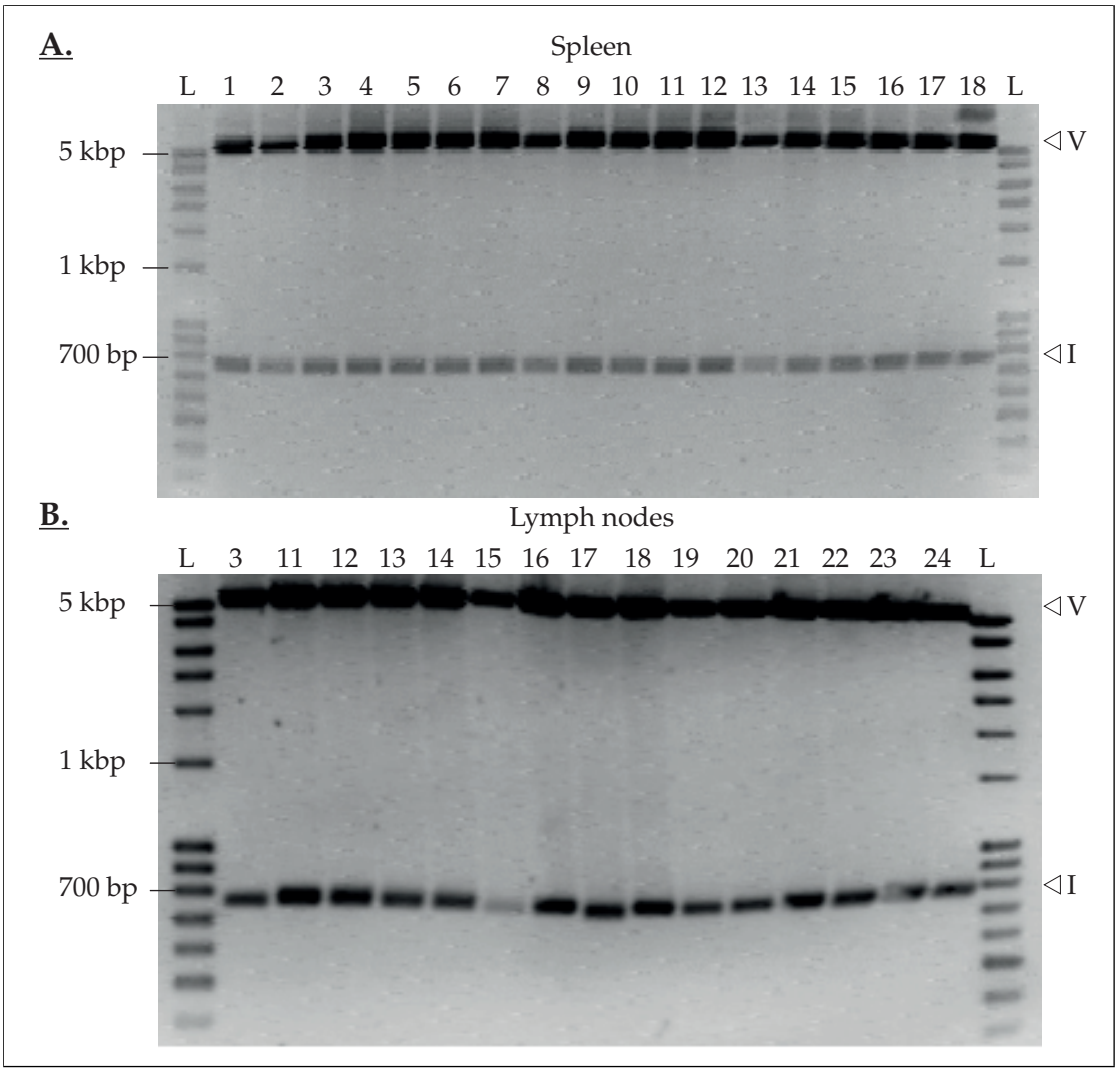

Figure 4.4: Single colony-derived scFv DNA exhibits comparable size across clones. SfiI-restricted plasmid DNA from single colonies, obtained after two rounds of phage display, revealed bands of the expected size for scFvs (600–700 bp)(I) and vector (V) in all isolated plasmids from both (A.) spleen-derived and (B.) lymph node-derived libraries. No stongly apparent differences in scFv DNA size were observed across the different isolated clones.

their respective V- and J-gene alleles. D-gene usage differed between sequenced clones: fourteen clones incorporated *IGHD2-3*01 F*, while eighteen clones incorporated *IGHD6-4*01 F* (Tab. 4.2). Clonotypes were defined based on unique CDR3 AA sequences in combination with V(D)J gene usage. For example, clonotype A (CARSGFDGSYFAW-

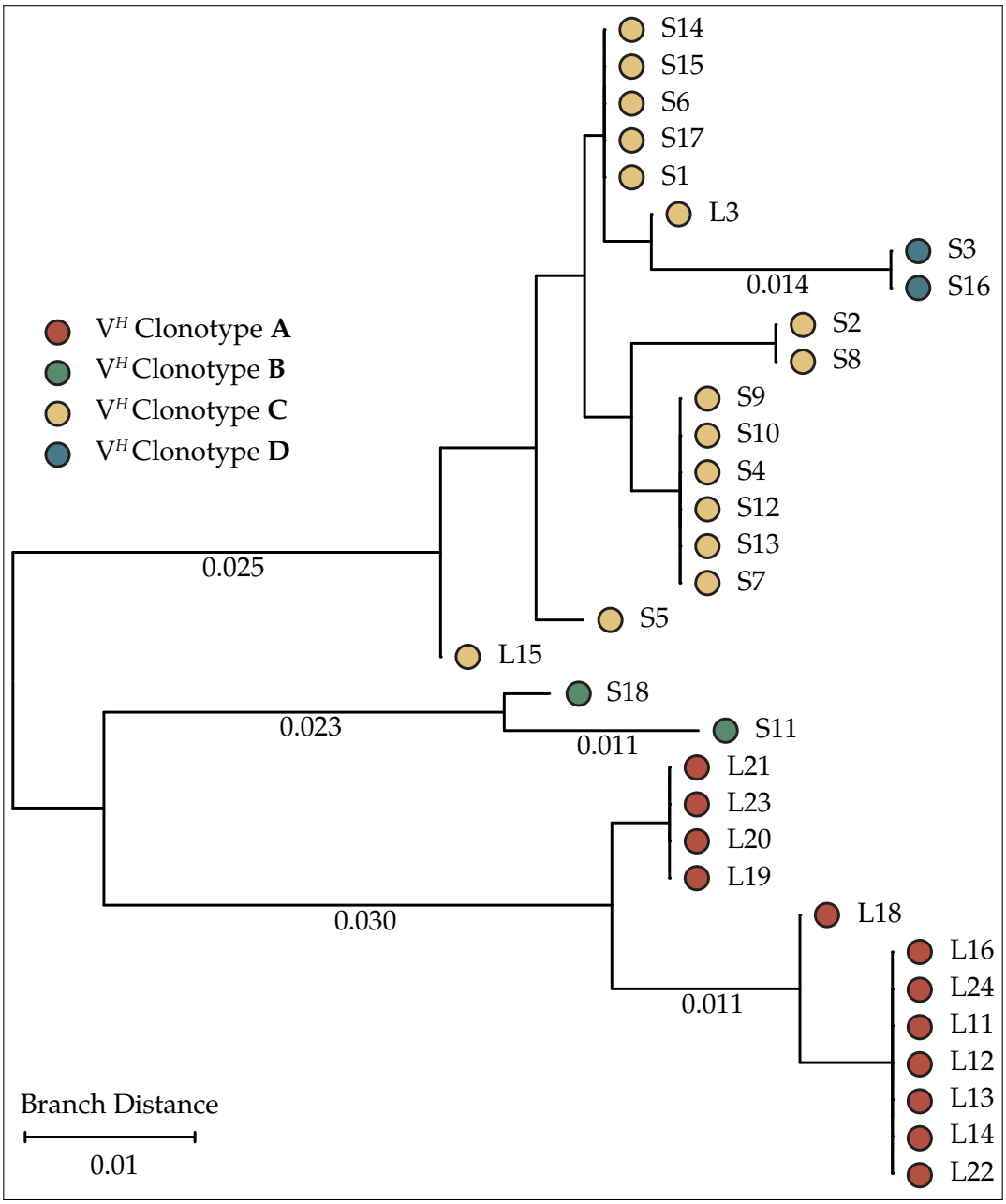

Figure 4.5: V^H phylogeny revealed clustering of phage display-derived clones. Multi-alignment of Sanger sequencing-derived V^H DNA sequences at the codon level were used for the interference of a phylogeny for V^H. V^H clonotypes (A–D) were assigned based on calculated genetic distances. Clonotype A (red) was private to lymph node-derived clones (L). Clonotype B (green) was private to spleen-derived clones (S). Clonotype C (yellow) was shared between both tissues but was more dominant in spleen-derived clones. Clonotype D (blue) was closely neighboring clonotype C and present in only two spleen-derived clones.

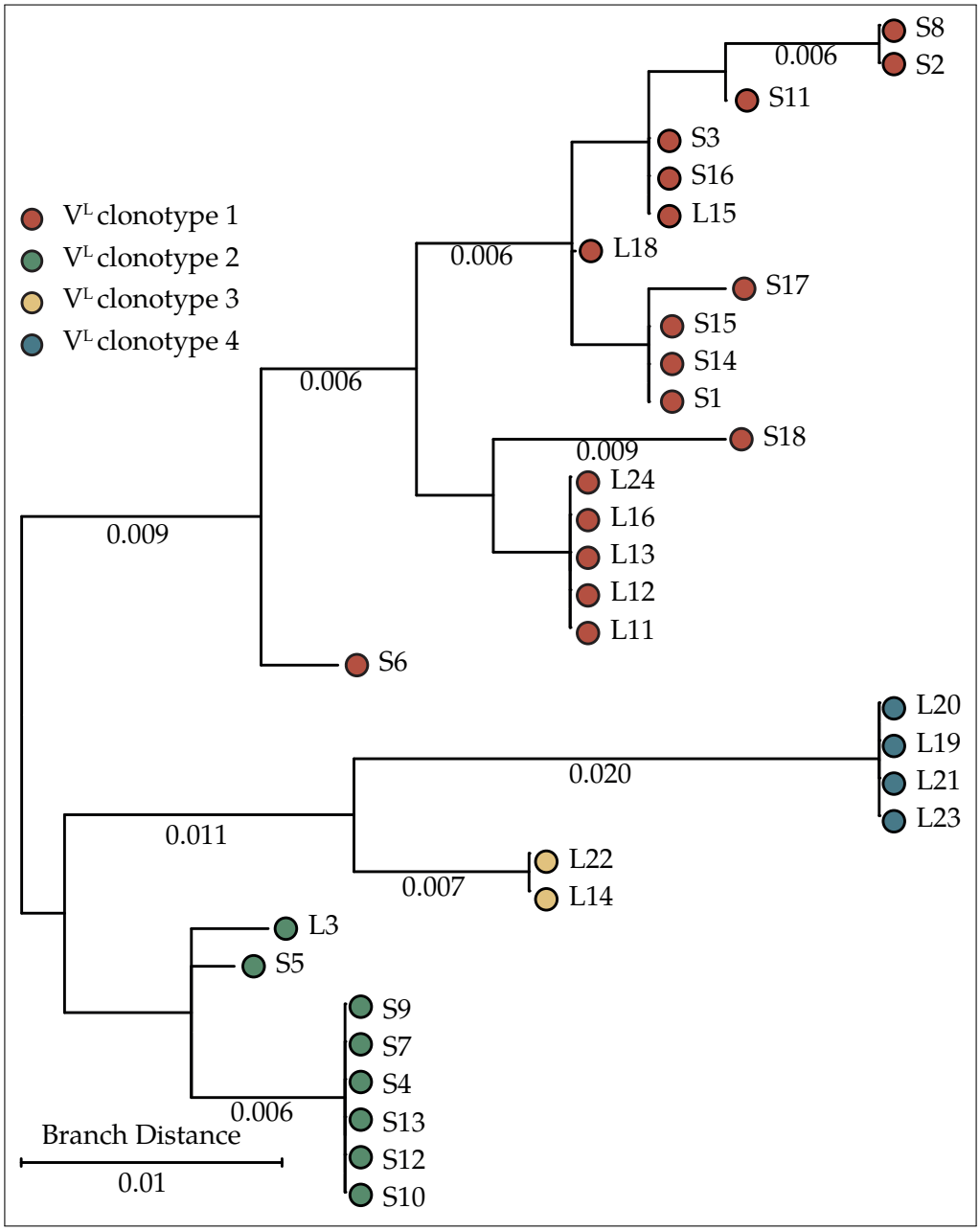

Figure 4.6: V^L phylogeny revealed clustering of phage display-derived clones. Multi-alignment of Sanger sequencing-derived V^L DNA sequences at the codon level allowed inference of a phylogeny for V^L. V^L clonotypes (1-4) were assigned based on calculated genetic distances. Clonotype 1 (red) was present among spleen- (S) and lymph node-derived (L) clones and exhibted the highest frequency. Clonotype 2 (green) was shared between tissues, however more prevalent in spleen-derived clones. Clonotype 3 [yellow] and 4 [blue] were privat to lymph node-derived clones.

FAYW) and clonotype B (CAQSRLGIWFAYW) shared identical V and J genes but differed in their CDR3 sequence, confirming their distinction as separate clonotypes. Within clonotypes, there was variation in the number of V-region mutations, likely reflecting differential patterns of SHM despite conserved CDR3 sequences. Clonotype D differed from clonotype C by a single AA substitution at the second position (CASSRHGLAWFPYW), illustrating how minor CDR3 alterations define phylogenetic subclusters.

Table 4.2: Identified V^H antibody clones from phage display panning. Gene names are abbreviated by omitting the IGH locus prefix. Abbreviations: T (Total mutations), s (Silent mutations), Ns (Non-silent mutations), CT (Clonotype), AA (amino acid). Mutation column refers to mutations within the V-region. Numbers in parentheses in mutation column indicate the number of mutations if the full rearranged V-region is considered (including V-(D)-J junctions), as per IMGT/V-QUEST output. Clonotypes for V^H (A–D) correspond to groupings observed in phylogenetic trees inferred using Maximum Likelihood analysis. Clonotypes are color-coded: A [red], B [green], C [yellow], D [blue].

Clone	V-Gene	D-Gene	J-Gene	CDR3 AA sequence	Mutation			CT
					T	s	Ns	
L11, L12, L13, L14	V1-39*01 F	D2-3*01 F	J3*01 F	CARSGFDGSYFAWFAYW	6	1	5	A
L16	V1-39*01 F	D2-3*01 F	J3*01 F	CARSGFDGSYFAWFAYW	5	1	4	A
L18	V1-39*01 F	D2-3*01 F	J3*01 F	CARSGFDGSYFAWFAYW	5	1	4	A
L19, L20, L21	V1-39*01 F	D2-3*01 F	J3*01 F	CARSGFDGSYFAWFAYW	7	0	7	A
L22, L24	V1-39*01 F	D2-3*01 F	J3*01 F	CARSGFDGSYFAWFAYW	6	1	5	A
L23	V1-39*01 F	D2-3*01 F	J3*01 F	CARSGFDGSYFAWFAYW	7	0	7	A
S11	V1-39*01 F	D2-3*01 F	J3*01 F	CAQSRLGIWFAYW	5 (8)	0 (1)	5 (7)	B
S18	V1-39*01 F	D2-3*01 F	J3*01 F	CAQSRLGIWFAYW	7 (10)	0 (1)	7 (9)	B

Continued on next page

Table 4.2 continued from previous page

Clone	V-Gene	D-Gene	J-Gene	CDR3 AA sequence	Mutation			CT
					T	s	Ns	
L15	V1-39*01 F	D6-4*01 F	J3*01 F	CARSRHGLAWFPYW	11	0	11	C
L3	V1-39*01 F	D6-4*01 F	J3*01 F	CARSRHGLAWFPYW	9	1	8	C
S1, S6	V1-39*01 F	D6-4*01 F	J3*01 F	CARSRHGLAWFPYW	8	0	8	C
S4, S7, S9, S10	V1-39*01 F	D6-4*01 F	J3*01 F	CARSRHGLAWFPYW	10	1	9	C
S12, S13	V1-39*01 F	D6-4*01 F	J3*01 F	CARSRHGLAWFPYW	10	1	9	C
S14, S15, S17	V1-39*01 F	D6-4*01 F	J3*01 F	CARSRHGLAWFPYW	8	0	8	C
S2, S8	V1-39*01 F	D6-4*01 F	J3*01 F	CARSRHGLAWFPYW	9	0	9	C
S5	V1-39*01 F	D6-4*01 F	J3*01 F	CARSRHGLAWFPYW	10	0	10	C
S16, S3	V1-39*01 F	D6-4*01 F	J3*01 F	CASSRHGLAWFPYW	12 (13)	4	8 (9)	D

Analysis of the V^L chain sequences revealed that all clones utilized *IGKV1-117*01 F* as the V-gene allele, in combination with either *IGKJ1*01 F*, *IGKJ2*01 F*, or *IGKJ5*01 F* as the J-gene allele (Tab. 4.3). Clonotype assignment was based on unique CDR3 AA sequence and VJ gene usage. The resulting clonotypes (1–4) corresponded to distinct CDR3 sequences, which exhibited less variability than the V^H clonotypes. All V^L clonotypes were 11 AA in length and incorporated a conserved CFQGSHVPXTF motif, with X being leucine (L, clonotype 1), tyrosine (Y, clonotype 2), tryptophan (W, clonotype 3), or arginine (R, clonotype 4). As observed for the heavy chain, the number of V-region mutations varied within clonotypes (e.g., clonotype 1: 1–4 total mutations), possibly reflecting SHM despite conserved CDR3 sequences.

Table 4.3: Identified V^L antibody clones from phage display panning. Gene names are abbreviated by omitting the IGK locus prefix. Abbreviations: T (Total mutations), s (Silent mutations), Ns (Non-silent mutations), CT (Clonotype), (AA) amino acid. Mutation column refers to mutations within the V-region. Numbers in parentheses in mutation column indicate the number of mutations if the full rearranged V-region is considered (including V-J junctions), as per IMGT/V-QUEST output. Clonotypes for V^L (1–4) correspond to groupings observed in phylogenetic trees inferred using Maximum Likelihood analysis. Clonotypes are color-coded: 1 [red], 2 [green], 3 [yellow], 4 [blue].

Clone	V-Gene	J-Gene	CDR3 AA sequence	Mutation			CT
				T	s	Ns	
L11, L12, L13, L16, L24	V1-117*01 F	J5*01 F	CFQGSHVPLTF	4 (6)	1 (3)	3	1
L15	V1-117*01 F	J5*01 F	CFQGSHVPLTF	3 (5)	1 (3)	2	1
S1, S14, S15	V1-117*01 F	J5*01 F	CFQGSHVPLTF	2 (4)	1 (3)	1	1
S11	V1-117*01 F	J5*01 F	CFQGSHVPLTF	3 (5)	1 (3)	2	1
S17	V1-117*01 F	J5*01 F	CFQGSHVPLTF	1 (3)	1 (3)	0	1
S18	V1-117*01 F	J5*01 F	CFQGSHVPLTF	4 (6)	0 (2)	4	1
S3, S16, L15	V1-117*01 F	J5*01 F	CFQGSHVPLTF	2 (4)	0 (2)	2	1
S6	V1-117*01 F	J2*01 F or J5*01 F	CFQGSHVPLTF	2 (4)	1 (3)	1	1
S7, S2, S8	V1-117*01 F	J5*01 F	CFQGSHVPLTF	4 (6)	2 (4)	2	1
L3, S5	V1-117*01 F	J2*01 F	CFQGSHVPYTF	2 (5)	0 (3)	2	2
S4, S7, S9, S10, S12, S10	V1-117*01 F	J2*01 F	CFQGSHVPYTF	3 (6)	2 (5)	1	2

Continued on next page

Table 4.3 continued from previous page

Clone	V-Gene	J-Gene	CDR3 AA sequence	Mutation			CT
				T	S	NS	
L14, L22	V1-117*01 F	J1*01 F	CFQGSHVPWTF	4 (7)	0 (3)	4	3
L19, L20, L21, L23	V1-117*01 F	J1*01 F	CFQGSHVPRIF	4 (6)	1 (2)	3	4

4.1.5 V^H Clonotyping of Immune Libraries Confirms Enrichment of Isolated scFv Clones

To investigate clonotype frequencies and enrichment within the libraries across pannings, both libraries were subjected to next-generation sequencing of V^H after panning one (PI) and panning two (PII). In contrast to the Sanger-derived sequences, V-D-J annotation was performed using the ARResT platform. V^H clonotypes A-D were also identified in the NGS data, allowing to trace frequencies and thus enrichment of clonotypes across pannings. Enriched clones were cross-checked for clonotype annotation using the IMGT database due to possible annotation differences by the two used plattforms. The annotation format provided by the ARResT platform follows the following structure: VJ:Vh-(Dh)-Jh V1-39 -0/13/-0 J3 CAREDSPAGFAYG, where VJ indicates the rearranged *V*, *D*, and *J* gene segments; -0/13/-0 represents alignment details (e.g., deletions or insertions); and CAREDSPAGFAYG is the resulting CDR3 AA sequence. For better readability, only the gene segments and CDR3 sequences are presented in the following paragraph. From the annotated data, clonotype frequencies (f in %) within the dataset were calculated by relating the number of reads per clonotype to the total read numbers of V^H for the respective dataset. Total read numbers per library sequencing were equated to 100 %. V^H clonotype frequencies were then visualized as part of the total number of reads. In addition, enrichment was calculated by comparing clonotype frequencies across PI and PII. Enrichment refers to the fold change in frequency between panning rounds.

Spleen-derived immune library V^H clonotypes B and C are enriched across pannings

Sequencing of spleen-derived library after PI (Fig. 4.7 A) exhibited low read depth as delineated by 753 individual annotated V^H, compared to an estimated library size

of 1.24×10^3 CFU after PI (Tab. 4.1). Nonetheless, clonotype C [yellow], which had been identified in approximately 78 % of spleen-derived Sanger sequenced clones, was already the second most abundant (4.5 %) clonotype present in the library. The most abundant clonotype (17.5 %), *V*14-4 *J*4 with the resulting CDR3 CTTNYGW, did not exhibit enrichment after PII and was therefore not further investigated. Clonotype B [green], identified in approximately 11 % of Sanger sequences, had a minor abundance of 0.8 % after PI. Approximately 44.5 % of immune library reads were represented by clonotypes with a frequency below 1 %, while 50.2 % were clonotypes with a frequency above 1 % (Fig. 4.7 A). None of these more frequent clones exhibited enrichment or were present at frequencies above 1 % after PII (Fig. 4.7 B) and were therefore excluded from further analysis. Clonotype C exhibited an approximately 18-fold enrichment after PII, representing the majority of sequenced V^H with a frequency of 83.5 %. Clonotype B exhibited an approximately 10-fold enrichment, being present at a frequency of 8.2 % after PII. Clonotype D [blue], absent in V_H sequencing data after PI, possibly due to low read depth, was present at a frequency of 0.10 %. The remaining 8.2 % of V^H clonotypes were those that did not exceed a frequency of 1 % and were not enriched across PI and PII.

Lymph node-derived immune library V^H clonotypes A and C are enriched across pannings

Sequencing of lymph node-derived library after PI (Fig. 4.7 C) exhibited deeper read depth: 7326 individual V^H were annotated, compared to an estimated library size of 1.98×10^2 CFU (Tab. 4.1). Clonotype A [red], annotated as *V*1-39 *J*3 CARSGFDGSY-FAWFAYW by ARResT/Interrogate, was the third most frequent clone after PI, indicated by a frequency of approximately 5.92 % among sequenced V^H. The first and second most abundant V^H clonotypes, *V*1-59 *J*2 CGRVYYSDYLDYW and *V*1-59 *J*2 CARVYYS-DYLDYW, were present at frequencies of approximately 8.5 % and 7.3 %, respectively. Due to their identical gene usage and resulting CDR3 sequences, which differed by only one AA replacement (G to A), it was assumed that these two clonotypes represented derivatives of the same B-cell clone. Similar to the most abundant clonotype in the spleen-derived immune library after panning PI, both identified clonotypes did not exhibit enrichment after PII and were therefore excluded from further analysis.
Clonotype C was present at a frequency of approximately 0.8 % among total annotated V^H clonotypes after PI. Approximately 35.4 % of V^H clonotypes were present at frequencies below 1 %, while approximately 57.9 % exceeded frequencies of 1 %. Except for one

clonotype—*V*1-7 *J*2 CARKDYFGSSYFDYW—none exhibited enrichment after PII and were therefore excluded from further analysis. After PII, clonotype A was present at a frequency of approximately $67.9\,\%$ among total V^H, exhibiting an enrichment factor of approximately 11-fold. Similarly, clonotype C exhibited an enrichment factor of approximately nine-fold. In contrast to the spleen-derived immune library, enrichment was observed for several clones in the lymph node-derived library.
Clonotype *V*1-39 *J*2 CARKDYFGSSYFDYW exhibited an approximately 22-fold enrichment but was present at a minor frequency of only $2.14\,\%$ among total V^H clonotypes after PII. Similarly, clonotypes *V*14-4 *J*4 CTTKAQATGYYAMDYW and *V*1-39 *J*1 CARGYYDRYFDVW exhibited enrichment factors of approximately 14-fold and 13-fold, respectively; however, their frequencies remained low at only approximately $2.08\,\%$ and approximately $1.21\,\%$, respectively, when compared to Sanger-derived clonotypes. Additionally, five other clonotypes exceeded enrichment factors between approximately ten-fold and fifteen-fold but were present at frequencies below $0.5\,\%$. Interestingly, two additional clonotypes—*V*1-55 *J*2 CARAGITGYFDYW and previously mentioned *V*1-7 *J*2 CARKDYFGSSYFDYW—presented with increased enrichment rates (five-fold and four-fold) while also exhibiting frequencies of approximately $3.5\,\%$ and approximately $5\,\%$, respectively.

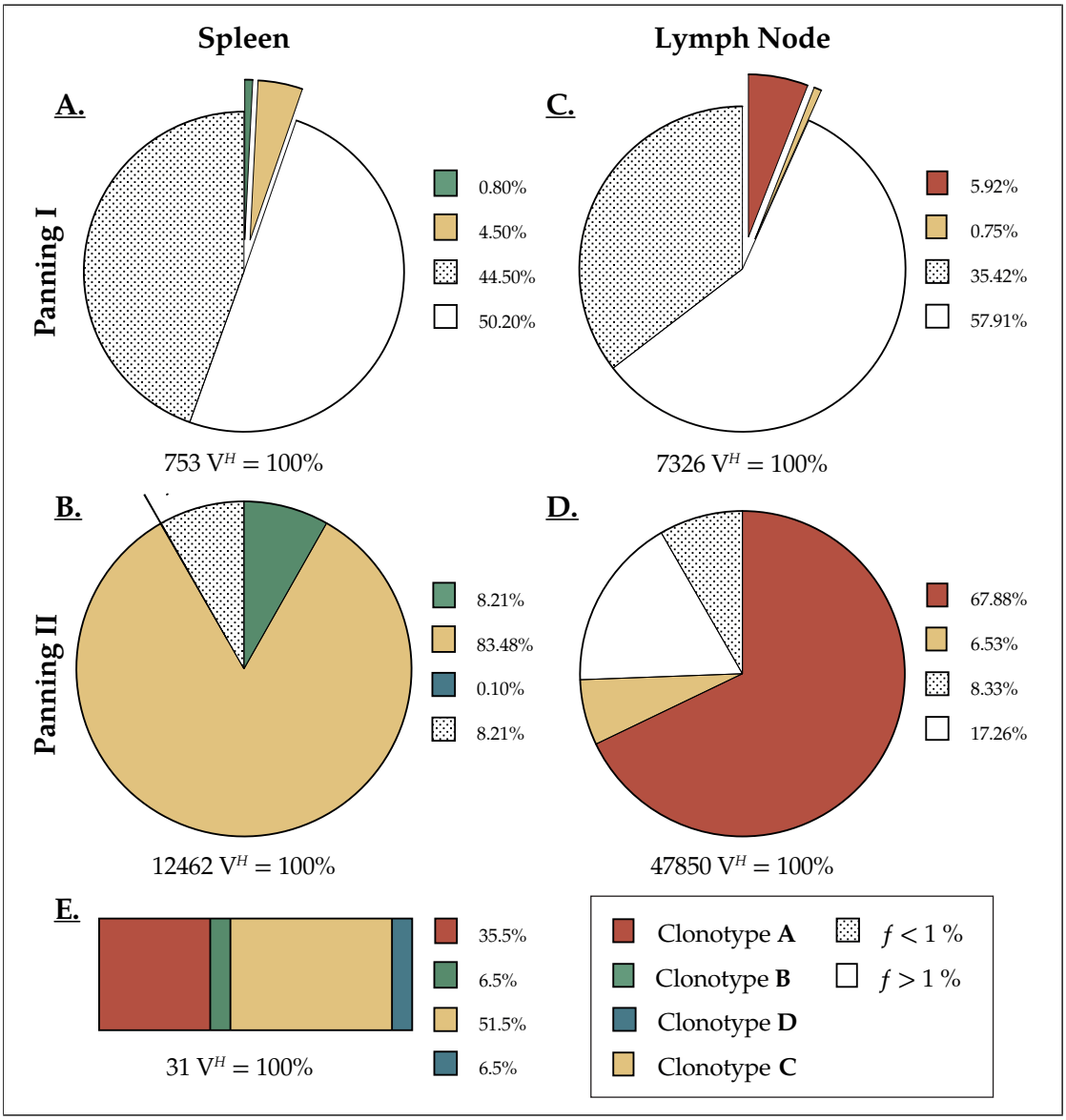

Figure 4.7: NGS sequencing of immune libraries confirms enrichment of V^H clones during phage display. (A-E) NGS V^H sequencing after PI (A, C) and PII (B, D) allowed for tracking of Sanger derived clonotypes (E) across phage display panning. Frequencies of clonotypes A, B, C are enriched with A and C representing the most dominant clonotype within the respective library. Clonotype D is present at a minor abundace after panning II.

4.2 ScFv-Derived and Aquired Antibody Clones Were Successfully Expressed in the mIgG2b Format

From the sequenced scFv panel (Tab. 4.2 and 4.3), six clones were chosen for recombinant expression in the IgG2b format. IgG2b was chosen due to the abundance of this IgG subclass in sera of susceptible mice in the immunization-induced murine model of EBA, as described in Fig. 1.5 [93, 126]. Additionally, previously tested IgG2c clones, such as C7, did not elicit disease in the antibody transfer model of EBA (unpublished data, [205]). While the reported complement fixation capacity of IgG2b and IgG2a/c is comparable [206], their interaction with activating Fcγ receptors ranges from comparable to a higher activation potential for IgG2c [28, 67, 68, 206, 207]. Importantly, both IgG2b and IgG2a/c have been reported to strongly associate with FcγRIV, which has been identified as the most relevant Fcγ receptor for initiating tissue destruction in experimental models of murine EBA [135].
Several sequences of murine IgG2b are available in the IMGT gene database [23]. Of these, the IGH2B*03 allele (accession number BK063712) was chosen, as it originates from C57BL/6J mice (C57BL/6J chromosome 12, GRCm39). The congenic variant of this strain (Tab. 2.1) is most commonly used for the immunization-induced murine model of EBA and is also the strain used to immunize the mouse from which the immune libraries were generated [121, 127, 162].
Prior to full-format IgG expression, the six chosen clones were produced in the scFv-phage format using the previously described procedure (Protoc. 3.2.4). In addition to the previous experiments, resulting monoclonal phages were titered to directly compare antigen-specific binding between the clones. All clones bound to antigen originating from both *E. coli* ER2566 and *CHO* recombinant expression. None of the clones exhibited excessive binding to *E. coli* ER2566 cell lysate supernatant. Notably, all signal rates for phage display-derived clones against *E. coli* ER2566 cell lysate supernatant exceeded the control scFv 4D5 (Fig. 4.8).
Despite the differences in the resulting AA junction regions, different clones could be synthesized by combining V^H and V^L from clones of the same clonotype family. The usage of V^H and V^L for the six chosen clones is indicated in Tab. 4.5. Due to this shared chain usage, phage display-derived antibody clones were assigned with internal IDs (int. ID) to distinguish between scFv's and full IgG2b molecules (Tab. 4.5). Clones S4 (C1), S16 (C4) and L16 (C5) were generated by pairing their respective native $V^H$and V^Lchains. S8 (C2) was generated by combining V^H of S4 with V^L of S16. S11 (C3)

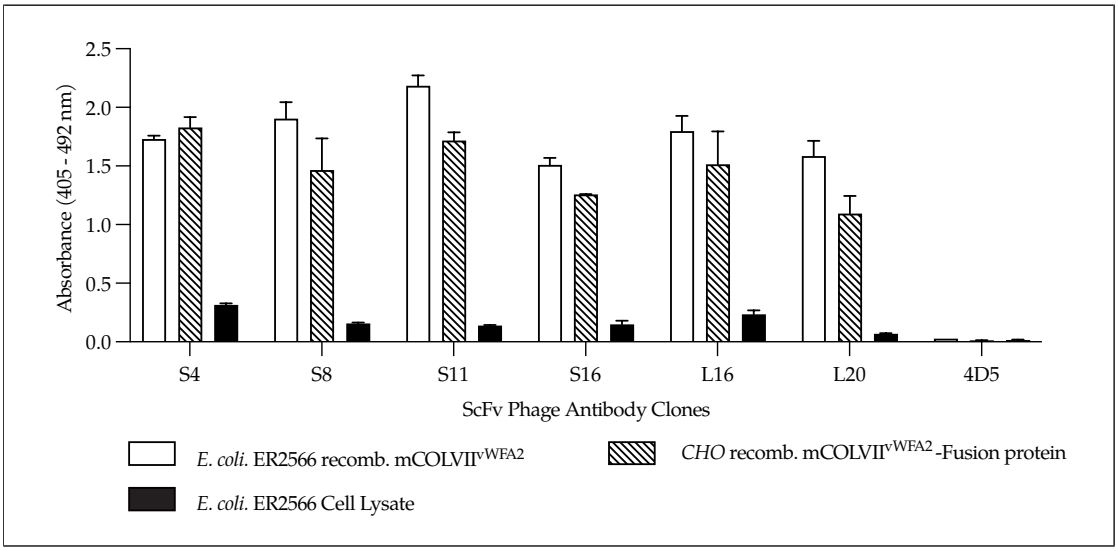

Figure 4.8: Phage ELISA with titered scFv-phages confirms target specificity and comparable binding of different scFvs. Titered scFv-phages were tested for binding to *E. coli* ER2566-produced mCOLVII^{vWFA2}, CHO-produced mCOLVII^{vWFA2}xCD3, and *E. coli* ER2566 cell lysate supernatant in a phage ELISA. All clones specifically recognized recombinant antigens. *E. coli*-derived antigen yielded low signals for all clones, exceeding the baseline signal provided by 4D5. Mean $\pm$SD of technical replicates (N=2).

incorporated it's own V^H and V^L of S16. L20 (C6) was generated by the combination of V^H of L16 and its own V^L. A summary of V^H- and V^L-chain usage as well as the assigned int. IDs is indicated in Tab. 4.5. In addition to the phage display-derived scFv antibody clones, further mCOLVII targeting clones were aquired on cooperation basis and similarily back-cloned and expressed.
Clone 16A1C8, originally an IgG2c antibody, previously generated from the lymph nodes of an mCOLVII^{vWFA2}-immunized S/JL mouse, was acquired from Dr. Anika Kasprick and Prof. Dr. Ralf Ludwig. V^H and V^L of 16A1C8 were backcloned into the IgG2b C^H backbone. Notably, 16A1C8 had previously demonstrated the capacity to block the induction of experimental EBA when co-injected with mCOLVII-targeting rIgG, despite not exhibiting pathogenicity itself [205]. Similarly clone H510, originally an IgG1 antibody, aquired from Prof. Dr. Eva Hadaschik and Dr. Elisabeth Vicari, originating from T-reg deficient scurfy mice was backcloned into the IgG2b backbone.
V^H and V^L pairings, as obtained by phage display (scFv clones) and 16A1C8 and H510 were modelled for the 3D alpha fold structures of the Fv region (Protoc. 3.7), (Fig. S1). V^H CDR3s were highlighted [blue], to demonstrate the differences of the exposed binding pockets of the different clones. The modelling approach revealed distinct (16A1C8, H510) or more similar (S4, S8; L16, L20) structures, which might translate into different or nearing epitope targeting. However V^L CDR3s were not highlighted, which possibly further contributes to epitope specificty.
Sequences of mCOLVII-C-targeting clones were acquired from PD Dr. Andreas Recke at the *Klinik für Dermatologie, Allergologie und Venerologie* (*Hautklinik*), University Medical Center Schleswig-Holstein, Lübeck, Germany. These clones originated from a distinct phage display approach that utilized spleens from SJL/J mice (strain 000686) for immune library generation. The clones target the so-termed C-fragment within the NC-1 domain of mCOLVII, a region within the fibronectin-like domain, spanning AA 757 to 967 (Fig. 1.3) [27], which is located upstream of the vWFA2 domain. Clones C8 and C9 were cloned into the same IgG2b backbone and expressed analogous to the mCOLVII^{vWFA2}-targeting clones. Based on CDR3 sequence similarity, C8 and C9 are predicted to share an epitope, potentially exhibiting cross-blocking properties. On the other side, they may also display binding (cooperativity) or Fc-mediated interaction synergies, thereby facilitating binding of the other or Fcγ activation and subsequent C_{1q} binding [208–210].

Table 4.4: Genetic assessment of acquired antibody clones, chosen for expression. Gene names are abbreviated by omitting the IGH / IGK locus prefix. Abbreviations: T (Total mutations), s (Silent mutations), Ns (Non-silent mutations). Mutation column refers to mutations within the V-region. Numbers in parentheses in mutation columns indicate the number of mutations if the full rearranged V-region is considered (including V-(D)-J junctions), as per IMGT/V-QUEST output. Details for H510 are excluded, due to disclosure agreement with the providers.

Chain	Clone	V-Gene	D-Gene	J-Gene	CDR3 AA sequence	Mutation		
						T	s	Ns
IGH	16A1C8	V1-26*01 F	D4-1*01 F	J3*01 F	CGRGGDAYW	23	4	19
	B8	V5-17*01 F[1]	D2-4*01 F	J2*01 F[2]	CARNYFDY-FYYFDYW	64 (66)	58 (60)	6
	C10	V5-9-1*02 F[3]	D3-1*01 F	J2*01 F[4]	CARGFDY-FYYFDYW	68 (69)	52 (53)	16
	H510					70 (74)	67 (68)	3 (6)
IGK	16A1C8	V1-110*01 F		J5*01 F	CSQSRHWPPTF	11	3	8
	B8	V6-13*01 F[6]		J4*01 F or J5*01 F[7]	CQQYSSYPYTF	69 (71)	67 (69)	2
	C10	V6-17*01 F[8]		J1*01 F or J4*01 F	CQQHYSTPPTF	72	72	0
	H510					75 (79)	75 (76)	0 (3)

V^H and V^L sequences were assembled separately in pcDNA3.1(+) and V^H coupled with

[1] Low V-REGION identity (77.78%)
[2] Other possibilities: IGHJ3*01 (highest number of consecutive identical nucleotides)
[3] Low V-REGION identity (77.08%)
[4] Other possibilities IGHJ3*01 (highest number of consecutive identical nucleotides)
[6] Low V-REGION identity (75.63%))
[7] Other possibilities: IGKJ1*01 (highest number of consecutive identical nucleotides)
[8] Low V-REGION identity (74.55%)

IGHG2B*03. V^H-IGHG2B*03 and V^Lconstructs in pcDNA3.1(+) were ordered from invitrogen. *E. coli* XL1-Blue were transformed with vector DNA as described in Protoc. 3.5.1 to generate vector DNA stocks for transfection. Antibody expression was performed as described in Protoc. 3.5.

Correct assembly and antibody purity were assessed by SDS-page. Reducing SDS-page revealed no contamination of purified antibodies, with $V^H$and V^Lchains present at their expected molecular weights of approximately 50–60 kDa (V^H) and 25 kDa (V^L), respectively. Non-reducing SDS-PAGE confirmed the proper assembly of $V^H$and V^Linto intact antibodies, with a predominant band at 150 kDa, corresponding to the fully assembled IgG2b molecule Fig. 4.9 B. Following SDS-PAGE analysis, recombinant antibodies were further purified using an ÄKTA Pure system to ensure high purity and quality for downstream applications. Size-exclusion chromatography (SEC) was used to remove aggregates and confirm monomeric assembly. UV absorbance at 280 nm was used to monitor antibody elution, and purified fractions were collected for subsequent analyses.

Table 4.5: Chain composition of scFv antibody clones for IgG2b cxpression. IgG2b clones were annotated with internal clone IDs (C) to distinguish between scFv-phage clones and full-length IgG2b. The table lists the V^H and V^L chain usage, their respective clonotypes (A–D / 1–4), and AA junctions of six antibody clones selected for recombinant IgG2b expression.

IgG ID	Clone	V_H			V_L		
		CT	Usage	AA Junction	CT	Usage	AA Junction
C1	S4	C	V_H S4	CARSRHGLAWFPYW	2	V_L S4	CFQGSHVPYTF
C2	S8	C	V_H S4	CARSRHGLAWFPYW	1	V_L S16	CFQGSHVPLTF
C3	S11	B	V_H S11	CAQSRLGIWFAYW	1	V_L S16	CFQGSHVPLTF
C4	S16	D	V_H S16	CASSRHGLAWFPYW	1	V_L S16	CFQGSHVPLTF
C5	L16	A	V_H L16	CASSRHGLAWFPYW	1	V_L L16	CFQGSHVPLTF
C6	L20	A	V_H L16	CASSRHGLAWFPYW	4	V_L L20	CFQGSHVPRTF

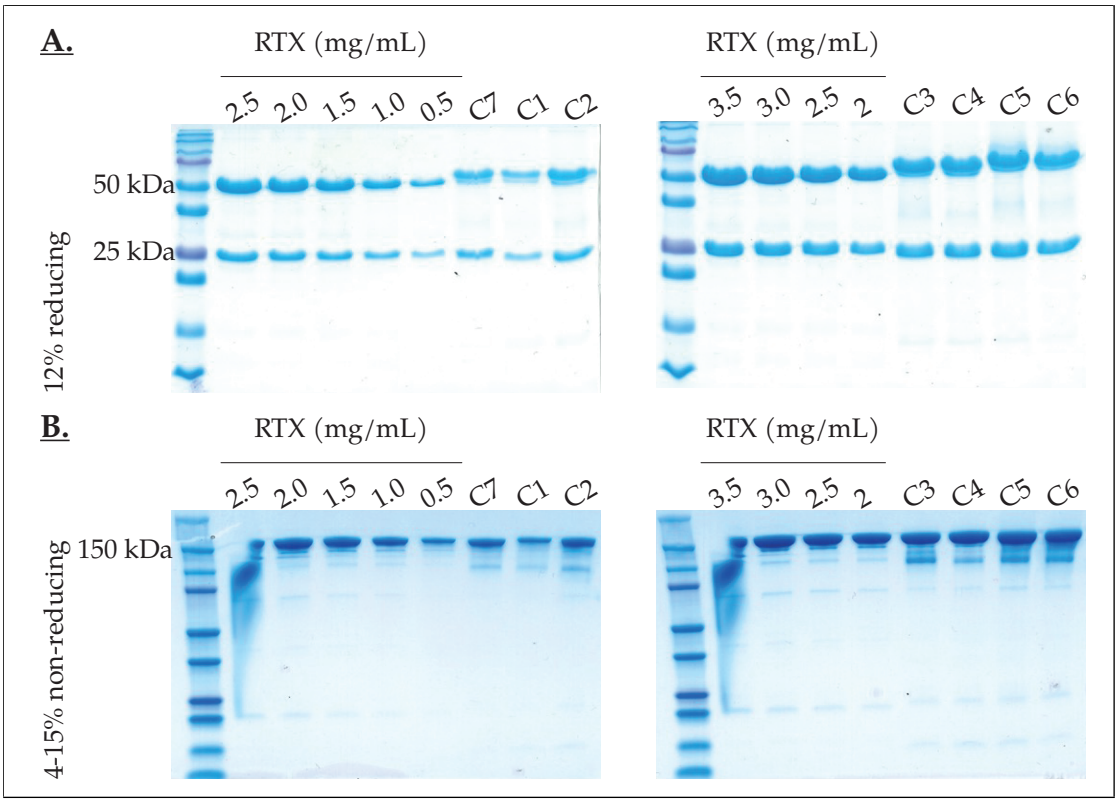

Figure 4.9: Reducing and non-reducing SDS PAGE confirms expression of full length, correctly assembled IgG. (A.) 12% reducing SDS-Page revealed correctly sized V^H (50 kDa) and V^L (25 kDa) bands for C1-C7. Dilutions of rituximab (RTX; hIgG1) were run as a positive control. (B.) Non-reducing electrophoresis, revealed correct assembly of chains with a band at 150 kDa. Expression, characterization and quality control were performed and images kindly provided by Thomas Theocharis.

4.3 Functional Characterization of Recombinant mCOLVII Targeting Antibodies

The previously expressed IgG2b antibodies were subjected to a thorough *in vitro* characterization. Concentration-dependent target binding of all antibody clones was tested in antigen-specific ELISAs (3.6.1). Avidity of binding was assessed by avidity ELISA and compared between clones by calculating of normalized avidity indices (Fig. 4.10). Binding to full-length mCOLVII was tested by quantification of immunofluorescence signal on healthy murine skin sections (3.6.2). Fc functionality in terms of Fcγ-receptor interaction and complement fixation and activation capacity was determined in ROS-release assays using purified neutrophils and serum tested for complement competence (3.6.4). Due to the different targeting domains of C1-C7 (mCOLVII$^{\text{vWFA2}}$) and C8, C9 (mCOLVII$^{\text{-C}}$), the description of the *in vitro* characterization of the clones is split into two parts.

4.3.1 Recombinant IgG2b Clones C1 - C7 Specifically Bind to Recombinant mCOLVII$^{\text{vWFA2}}$ and Elicit Pathogenic Potential *in vitro*

Phage display-derived clones (C1–C6) bound to recombinant mCOLVII$^{\text{vWFA2}}$ but not to mCOLVII$^{\text{-C}}$, as determined by ELISA (Fig. 4.10 A). No striking differences were observed between individual clones at similar concentrations (Fig. 4.10 B). Binding was detectable at a concentration of $1\,\text{ng}\,\text{mL}^{-1}$; no binding was observed at lower concentrations. Clone C7, exhibited comparable binding to clones C1–C6. Despite close sequence similarities (Tab. 4.2), C1–C6 exhibited differences in their avidity of binding, which was determined by antigen-specific ELISA in the presence of increasing concentrations of NH_4SCN to disrupt molecular interactions (Fig. 4.10 C).
From the obtained OD $450\,\text{nm}$ to $560\,\text{nm}$, baseline corrected values, the avidity index was calculated by dividing the maximum binding values (at $0\,\text{M}$ NH_4SCN) by the values in the presence of varying NH_4SCN molarities for each clone, respectively. Non-linear fit curves (exponential decay) were fit for alle clones. Clone C4 exhibited the highest binding across increasing concentrations of NH_4SCN. No binding was detected at a concentration of $6\,\text{M}$ NH_4SCN for all clones. Clones C2 and C3 exhibited comparable avidity indices at similar NH_4SCN molarities. Comparable avidity indices and curves were observed for clones C5 and C7. Clones C1 and C6 presented with the lowest avidity indices and thus demonstrated the lowest avidity of binding. The data highlight the importance of V^H and V^L chain pairing for avidity. For example, clone C1 and clone C2

both incorporate the same V^H, but differ in V^L incorporation (Tab. 4.5).
Antibody clones were tested for concentration-dependent binding to full-length, native mCOLVII, using healthy murine skin sections as a substrate as described in Protoc. 3.6.2. All clones bound to the DEJ, but consistently provided high background in this indirect staining approach, independent of substrate (ear, tail) and concentration, with no clear observed concentration dependency of binding (Fig. 4.11 A). An equimolar composition, constituted by clones C1–C6, exceeded the binding of C1, C2, C3 and C4 alone, suggesting synergistic effects, determined by increased fluorescence intensity (Fig. 4.11 A). Of note, the IgG2b isotype control also provided tissue staining background, but no DEJ deposition was detectable. Despite exhibiting lower avidity of binding (Fig. 4.10 C) C5–C7 exhibited stronger DEJ deposition in high concentrations (10 μg) in this staining.

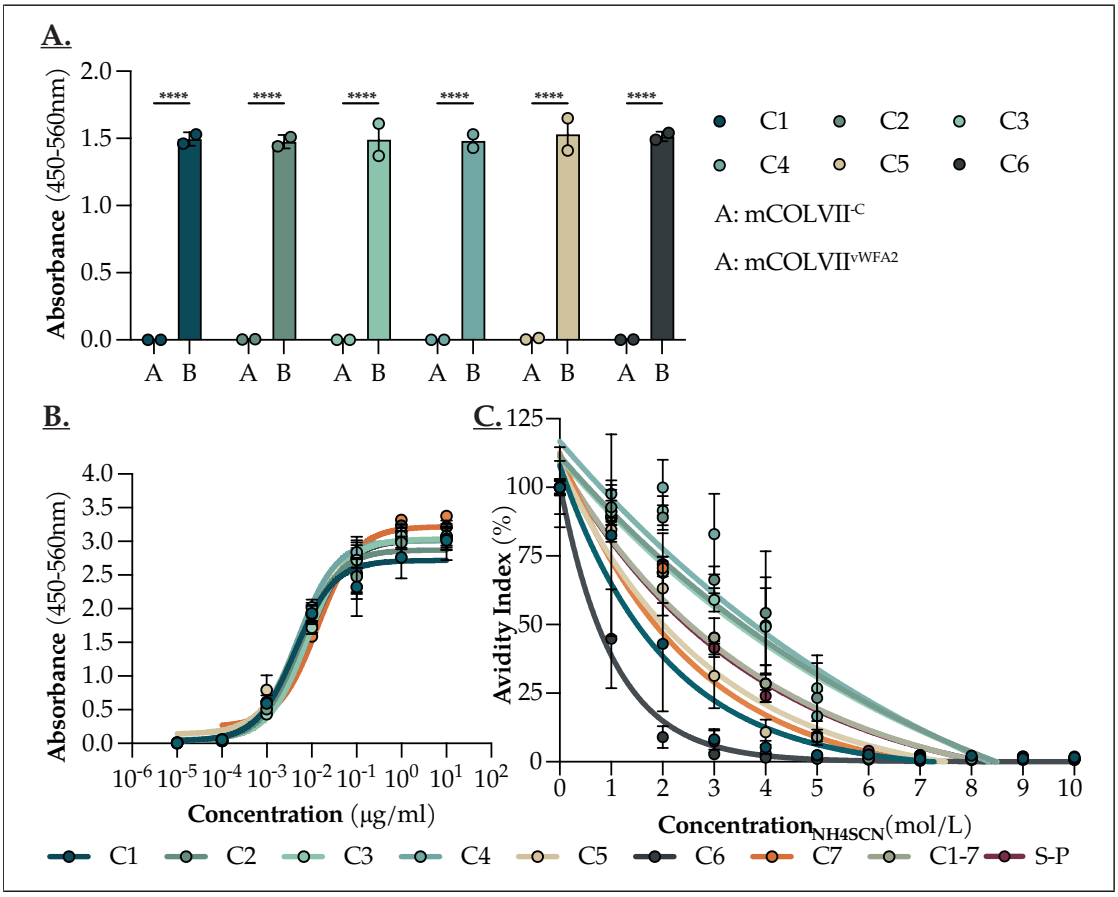

Figure 4.10: Recombinant IgG2b antibody clones (C1–C7) specifically bound to mCOLVII^{vWFA2} in a concentration-dependent manner and exhibited varying avidity. (A.) A constant concentration (1 µg) of IgG2b clones C1–C7 were tested for specific binding to different recombinant fragments of mCOLVII. All clones did exclusively bind to mCOLVII^{vWFA2} but not to mCOLVII^{-C}. (B.) IgG2b clones C1–C7 were tested for specific binding across decreasing concentrations. (C.) At a fixed concentration, clones C1–C7 exhibited different avidities of binding, as determined by the avidity index (% of maximum binding per clone); For mixed-effects statisic analysis referr to Tab. S1; S-P (Pooled serum from mCOLVII^{vWFA2} mice). (A.) n=2, ± SEM, 2wayANOVA with Šídák's test ****p<0.0001; (B.) n=3 ± SEM; (C.) n=3 ±SEM, Mixed-effect analysis with Tukey's test (Tab. S1).

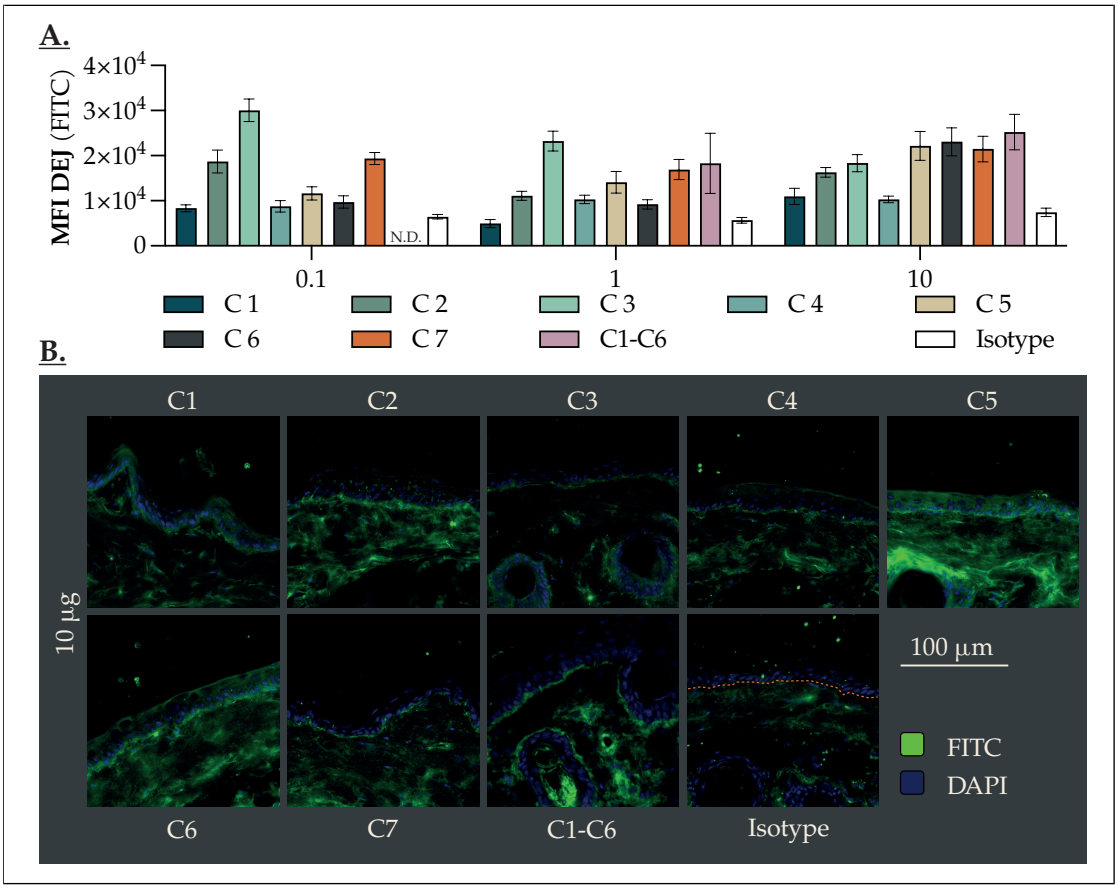

Figure 4.11: Recombinant IgG2b antibody clones (C1–C7) bound to DEJ in healthy murine skin sections. (A.) Three concentrations (0.1, 1, and 10 μg) of C1–C7 were tested for DEJ binding on healthy murine skin sections. Obtained images were quantified using ImageJ. Linear DEJ deposition was observed for all clones, exceeding that of the IgG2b isotype control (A., B.). No clear concentration dependence was observed. (B.) At 10 μg, IgG2b clones showed the best separation of specific clones from the isotype control. An equimolar composition of C1–C6 exceeded the binding of several mAbs. N=6 $\pm$SEM.

Antibody clones C1–C7 were tested for functionality of Fc portion by Fcγ effector functions in ROS-release assays as described in 3.6.4. Three concentrations ($0.4\,\mu g$, $0.2\,\mu g$, $0.1\,\mu g$) of each antibody clone were incubated with a constant concentration of recombinant mCOLVII^{vWFA2} to generate ICs *in vitro*. ROS release from purified bone marrow-derived murine neutrophils (pooled from 4–6 mice, >80% purity, per experiment) was measured by luminescence over time. None of the controls (mAb only, mCOLVII only) exceed baseline signal derived from unstimulated neutrophils over time. Clones 1–6 exhibited comparable capacities to elicit Fcγ-mediated ROS release across the three tested concentrations (Fig 4.12 A-H) with no directly apparent concentration dependency. Normalization of AUC to individual experiment maximum (to account for day to day variation and varying neutrophil cell counts between experiments) and pointed towards trendwise concentration-dependent increase of ROS release for clones C1, C2, C3, and C4 (Fig 4.12 I). C5 and C6, both originating from the same tissue (LN), did not exhibit a concentration dependend trend of induced ROS release at the tested concentrations.
MCOLVII^{vWFA2}-specific polyclonal rIgG exhibited a concentration-dependent trend in ROS-inducing capacities (Fig 4.12 I). Based on the determined CDR3 sequence, C7 targets another epitope than C1–C6. C7 exhibited a trend of elevated potential to induce ROS release in all tested concentrations when compared to both C1–C6 and specific rIgG. Based on these results three different compositions of mAbs were tested for their combined capacity of ROS release and complement fixation. C1–C6, C6–C7 - both originating exclusively from the lymph nodes, and C1–C7 were tested as combinantions (Fig. 4.13). All compositions were tested at a fixed concentration of antibody ($2\,0.2\,\mu g$). Complement opsonization of ICs showed an elevated early ROS response for all clone compositions (Fig. 4.13 A). To assess the effect of opsonization of ICs, AUCs were normalized for the three compositions to their respective non-opsonized control (0) (Fig. 4.13 B). Assessment of AUC and normalization, showed a trend of elevated ROS release upon stimulation with complement opsonized ICs (Fig. 4.13 B).
Similarly individual clones were tested in this modified ROS assay (Fig. 4.13 C). The addition of complement-competent serum and measurement of ROS release showed an increase in the latter for C2, C3, C4, C5, C6, and rIgG, when normalized to their respective non-complement stimulated immune complex controls. This suggests that the chosen IgG2b backbone is not only functional in regard to Fcγ interaction but also able to fix complement and activate CP. The effect was not observed for C7, which leaves room for speculation, since this clone has previously shown an increase in ROS release capacity when compared to C1–C6.

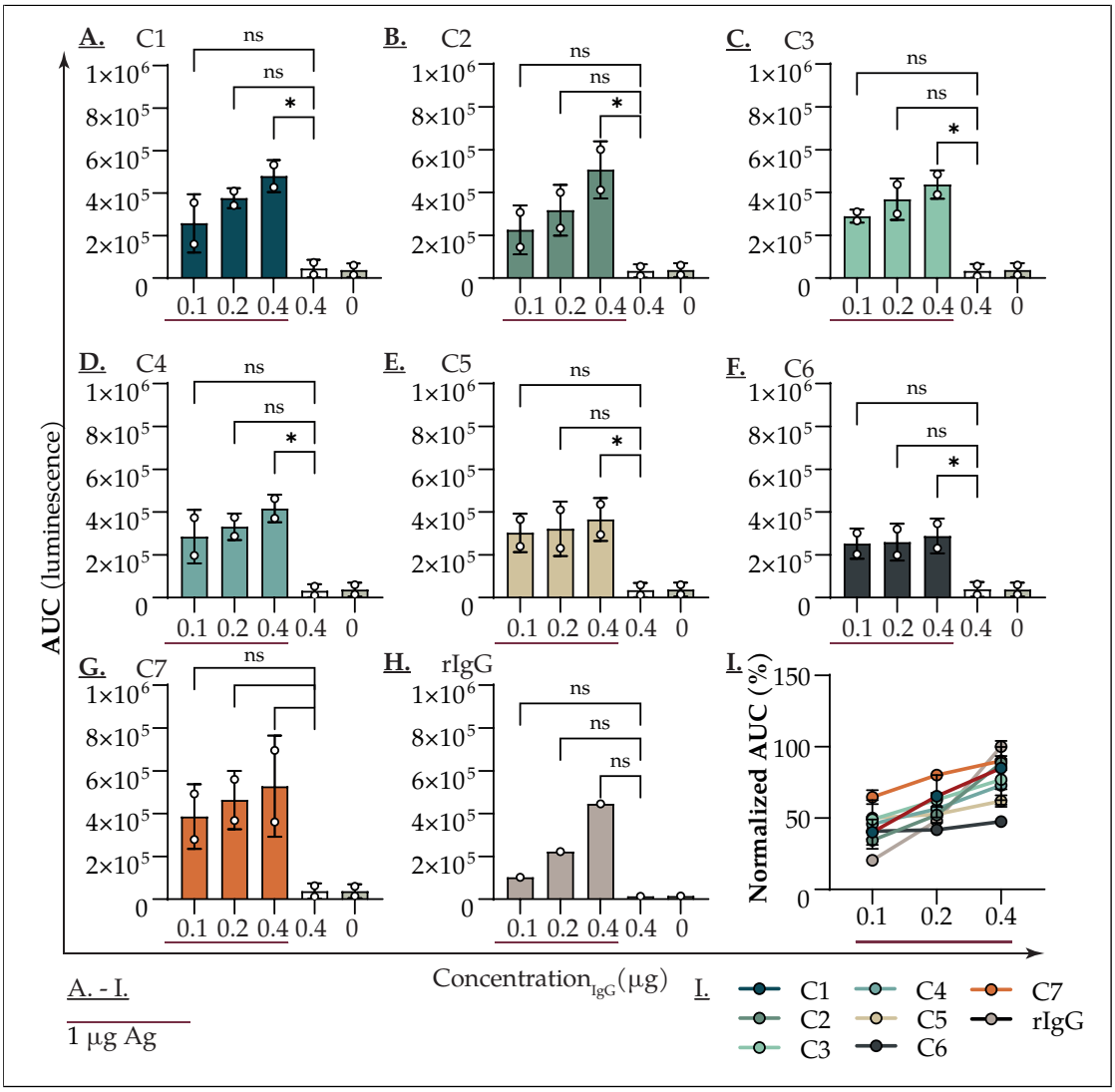

Figure 4.12: Clones C1–C7 induce Fcγ-mediated ROS release. Purified neutrophils released ROS upon stimulation with immune complexes (IC) generated with antibody (Ab) clones C1–C7 or rabbit IgG (rIgG). (A. -G.) Calculated area-under-curve (AUC) of ROS release over time from neutrophils, stimulated with antigen (Ag)-Ab IC (0.1, 0.2, 0.4 µg Ab - red line), Ab alone (0.4 µg) or without Ag and Ab (0 µg). (I.) Log-transformed summary of all clones. Mean ±SD (n=2) with 2 technical replicates per biological replicate, Kruskal-Wallis test with uncorrected Dunn's test, *p<0.05.

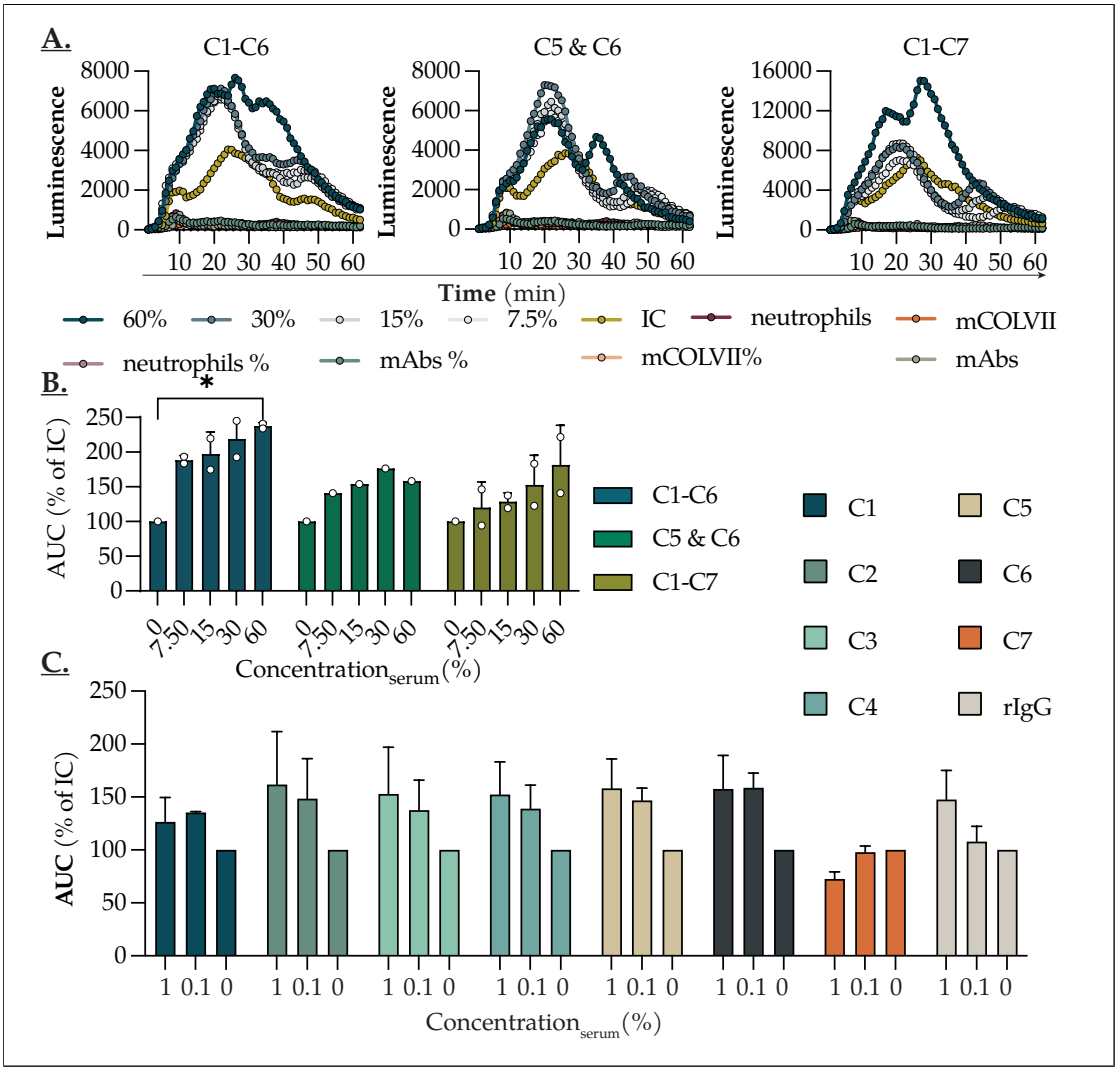

Figure 4.13: ROS release is potentially enhanced by equimolar compositions of several clones and by addition of complement. (A.) Kinetics of ROS release of purified neutrophils upon stimulation with immune complexes (IC) generated with different combinations of clones and addition of complement source. (B.) Area-under-curve (AUC) of ROS release, normalized to IC without complement addition (0), across different clone combinations. (C.) Normalized AUC of opsonized ICs generated from single clones. Mean ±SD (n=2 (n=1 for C5& C6 in B.)) with 2-3 technical replicates per biological replicate. Two-way-ANOVA with Dunn's test, *p<0.05.

4.3.2 Clones C8 and C9: mCOLVII^{-C}

A significant portion of IgG in the mCOLVII^{-C} induced active model of EBA is directed against the GST tag used for protein purification [131]. Pooled EBA sera, 6 weeks p.I. exhibit strong reactivity to both mCOLVII^{-C}-GST and GST alone (Fig. 4.14 A). Since clones C8 and C9 were derived from the mCOLVII^{-C} induced immunization model of EBA, and no information on the depletion strategy during phage display was available, both clones were tested for reactivity against mCOLVII^{-C}-GST, and GST alone (Fig. 4.14 B).

Both antibody clones bound to mCOLVII^{-C}-GST in a concentration-dependent manner ranging from $10\,\mu g\,mL^{-1}$ to $0.1\,\mu g\,mL^{-1}$. Low reactivity was observed for high ($10\,\mu g$) concentrations of C8 towards GST, while C9 reactivity remained marginal (Fig. 4.14 B). Overall target specificity was assumed and clones C8 and C9 were compared regarding their avidity of binding to mCOLVII^{-C} (Fig. 4.14 C). Avidity, as determined by avidity indices, revealed comparability between C9 and serum from aEBA mice at week 6 p.I.. C8 and an equimolar mix of C8 and C9 (Fig. 4.14 C) exhibited a slightly decreased avidity. Both C8 and C9 were assessed for ROS release induction, which was concentration-dependent but revealed an increased maximal capacity for C8 (Fig. 4.14 D-G), despite a diminished avidity index in the previous experiment (Fig. 4.14 C). Interestingly, the equimolar mix exhibited a comparable ROS release capacity to C9.

C8 and C9 bound to healthy murine skin in a concentration-dependent manner as determined by MFI of anti-mIgG (H+L)-FITC (Fig. 4.15 A. B). Both clones strongly bound to murine skin at concentrations of $10\,\mu g$ and $1\,\mu g$. No binding was detected at $0.1\,\mu g$. In high concentrations ($10\,\mu g$) an equimolar mix of both clones exhibited elevated binding when compared to C9. This effect was not observed in lower concentrations ($1\,\mu g$, $0.1\,\mu g$). Side-by-side testing of C8 and C9 with C1–C7 revealed more pronounced binding of the mCOLVII^{-C} targeting clones, as reflected by increased MFI and more distinct DEJ deposition (data not shown).

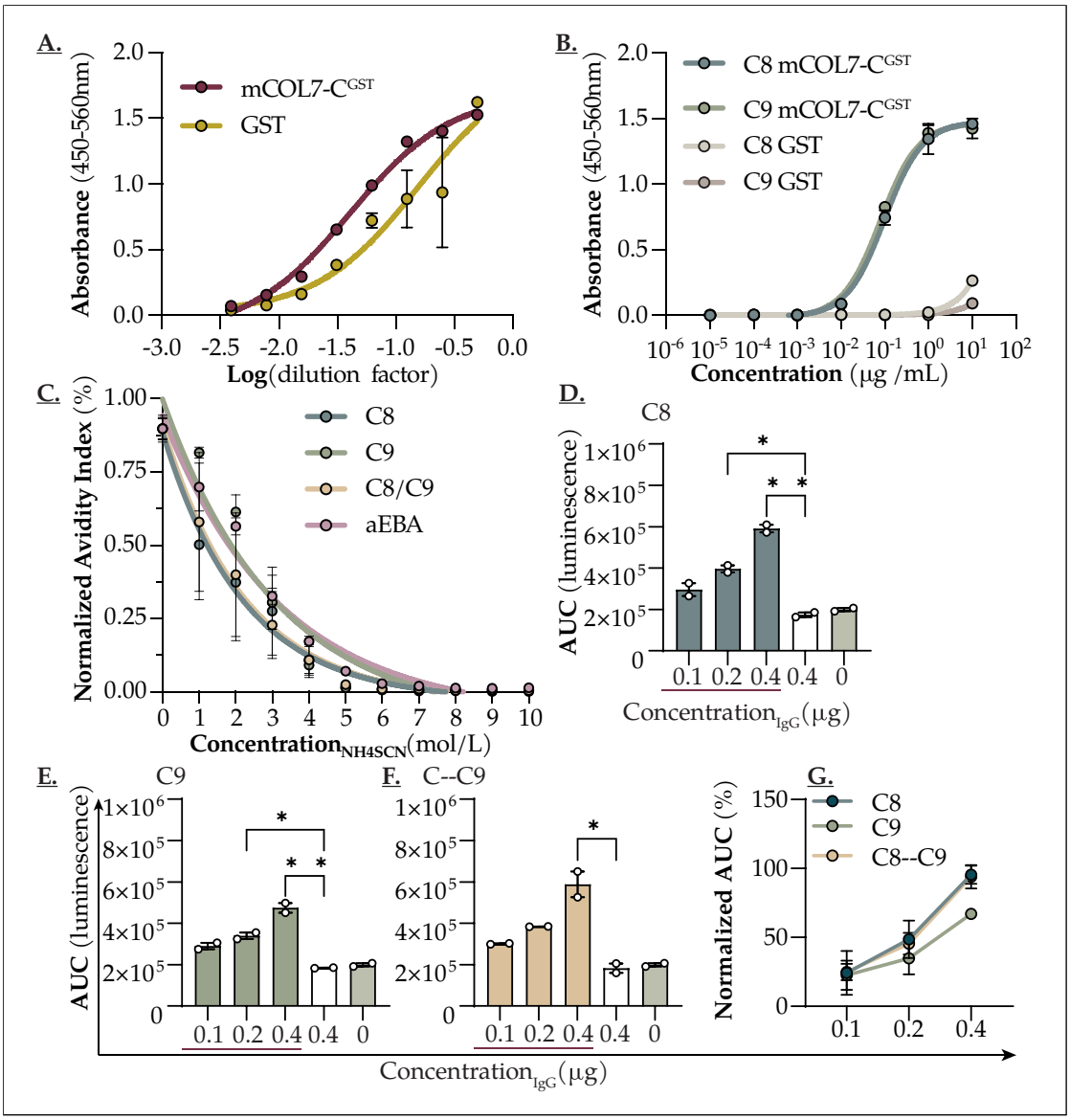

Figure 4.14: Recombinant IgG2b antibody clones C8 and C9 specifically bound to mCOLVII^{-C}. (A.) Pooled EBA sera (6 weeks p.I.) show strong reactivity to both mCOLVII^{-C}-GST and GST alone in ELISA. (B.) Antibody clones C8 and C9 bind to mCOLVII^{-C}-GST in a concentration-dependent manner, with minimal reactivity to GST alone. (C.) Avidity analysis reveals comparable binding strength between C9 and EBA sera, while C8 and the equimolar mix exhibit slightly decreased avidity. (D.-G.) ROS release assay demonstrates concentration-dependent neutrophil activation by both clones, with C8 showing higher maximal capacity despite lower avidity. (G) The equimolar mix of C8 and C9 shows ROS-inducing capacity comparable to C9 alone (normalized data of D-F). A, B Mean ±SEM, (N=2); C-G Mean ±SEM (n=2); D-F Kruskal-Wallis test with uncorrected Dunn's test, *p<0.05, **p<0.01.

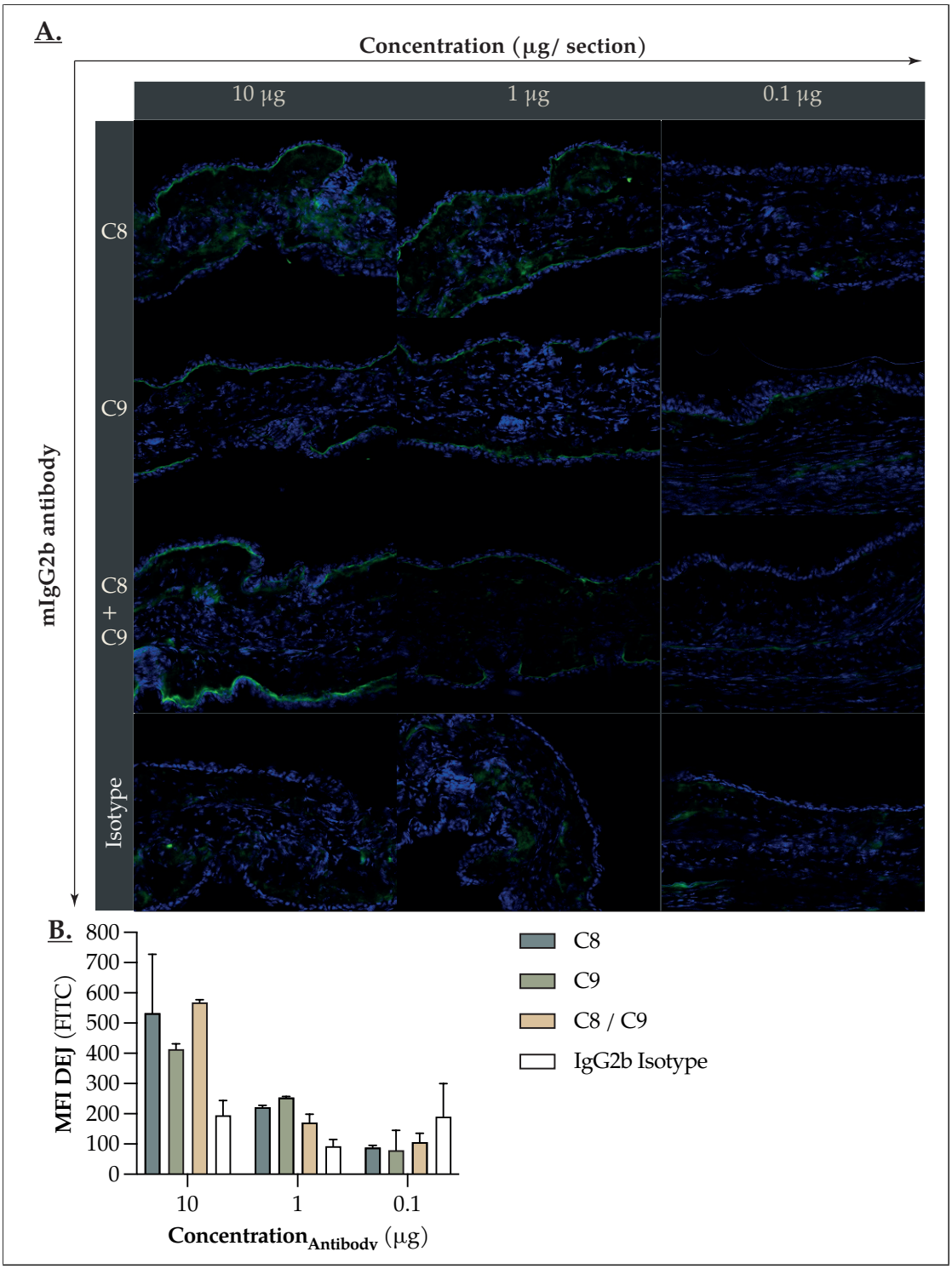
A.
Concentration (µg/ section)
10 µg
1 µg
0.1 µg
mIgG2b antibody
C8
C9
C8 + C9
Isotype
B.
MFI DEJ (FITC)
800
700
600
500
400
300
200
100
0
10
1
0.1
Concentration Antibodv (µg)
C8
C9
C8 / C9
IgG2b Isotype

Figure 4.15: Clones C8 and C9 bind to full length mCOLVII in a concentration dependent manner. (A.) Clones C8 and C9 as well as an equimolar mix, deposit at the DEJ on healthy murine skin sections. Deposition is considered as binding. Three different amounts, 10, 1 and 0.1 µg of antibody were tested for linear deposition. (B.) Anti-mIgG FITC IF intensities at the DEJ were measured from microscope images. 10 and 1 µg of both antibodies exhibted strong to intermediate deposition when compared to isotype control. No signal was obtained for 0.1 ug of antibody. IgG2b isotype did not exhibit specific DEJ IF signal regardless of antibody amount tested. Mean ± SEM; n= 2 independent skin sections per antibody; 3 images per section were obtained and evaluated.

4.4 Pathogenicity Testing *In vivo* of mCOLVII Targeting Clones Does Not Lead to EBA Like Inflammation

4.4.1 An Equimolar Combination of Clones C1-C6 Does Bind *In vivo* But Does not elicit disease

To evaluate, whether the phage display derived clones were able to provoke pathogenicity *in vivo*, clones C1-C6 were subjected to pathogenicity testing in the antibody transfer EBA model. This combination of clones was selected based on three criteria: (1) the observed comparable binding to full-length mCOLVII on healthy murine skin sections (Fig. 4.11), (2) the observed varying avidity profiles (Fig. 4.10), and (3) the observed increased ROS release when using combinations of these mAbs (Fig. 4.13). Clones 1-6 were mixed in equimolar ratios and tested for four days in the local antibody transfer EBA model in increased dosage. The same mice then received i.p. injections of the antibody combination for further 12 days, progressing to the systemic antibody transfer EBA model.

Injection and scoring procedures are summarized in Fig. 3.2. Five healthy B6.J mice (2 males, 3 females) received an initial injection of 50 µg antibody mix into the base of the right ear on day 0. All mice were euthanized on day 16. On day four, two mice (1 female, 1 male) exhibited mild scarring at the right ears, which was attributed to the injection procedure rather than disease activity, as no progressive lesions developed. Male mice developed scarring on the torso starting day 8, which was attributed to fighting behavior rather than disease, as these lesions did not progress. One female mouse exhibited EBA-like scabbing at the snout on day 8 post-injection, but this was not consistently present on subsequent evaluation days.

Upon final evaluation, none of the mice exhibited macroscopic disease affected body surface area that could be clearly attributed to EBA (Fig.4.16 A). Mice were shaved to

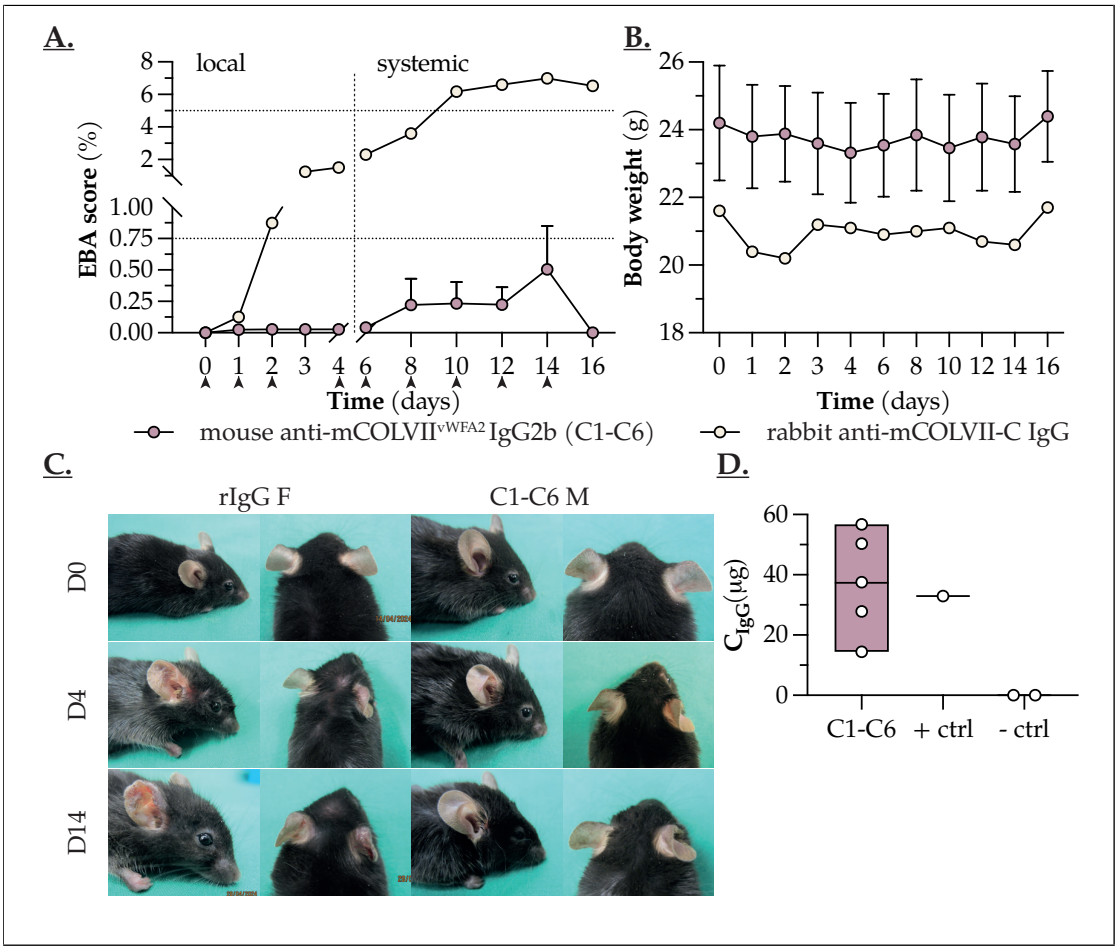

Figure 4.16: An equimolar combination of clones C1-C6 does not elicit pathogenicity *in vivo*. (A.) C1–C6 injected mice did not exhibit an EBA like phenotype. Horizontal lines indicate the score cutt of for assumed pathogenicity for local (0.75%) and systemic (5%) injections. Vertical line indicates the switch from local to systemic injections (day 4). (B.) All mice recovered from initial weight loss by the end of the experiment (D16). (C.) The rabbit IgG (rIgG) injected mouse presented with EBA affected ear surface area, while C1–C6 injected mice did not exhibit signs of EBA-related inflammation. (D.) All injected mice exhibit serum persistence of injected specific IgG / mAbs. Data represent mean ± SEM (A, B); n=5 (C1–C6) n=1 (rIgG) n=2 (non-injected negative control=-ctrl).

permit thorough assessment of the entire body surface. One male mouse exhibited minor lesions and scars with EBA-like phenotype, but these could not be definitively distinguished from fighting-induced injuries.
As a positive control, specific rabbit anti-mCOLVII^{-C} IgG was injected into one control mouse, which exhibited clear disease pathogenicity starting day 2 p.i. The disease continuously progressed until day 16, with the mouse reaching a final EBA score of 6.5% affected body surface area on day 16 (Fig.4.16 A). When comparing images obtained on days 0, 4, and 14 of the experiment from the control mouse and one representative mouse from the experimental group, it became evident that no progressive inflammatory response was induced by antibodies C1-C6 (Fig. 4.16 C). Despite minor macroscopic changes observed on day 4 in the experimental group, these did not progress over time, with ears returning to normal appearance by day 14. In contrast, the control mouse exhibited clear and progressive disease manifestation throughout the observation period. Nearly all (5/6) mice exhibted transient weight loss (up to 2 g) during the local antibody transfer EBA model, which was attributed to the repeated anesthesia procedures (Fig.4.16 B). However, all mice recovered and exceeded their initial pre-experiment weight by the end of the study period (day 16).
To assess antibody persistence, serum samples from the experimental group were tested for reactivity to mCOLVII^{vWFA2}. All serum samples tested positive by ELISA, with approximately 38 µg of antibody remaining in the circulation at day 16 (Fig.4.16 D). To evaluate tissue binding, skin was sampled from each mouse. Cryosections were immunostained for IgG and C_3 deposition at the DEJ, while paraffin-embedded sections were H&E stained to assess split formation, inflammatory cell infiltration, and skin thickening. All mice exhibited IgG deposition in the ears, while none of the mice exhibited C_3 deposition (Fig. 4.16, Tab. 4.6). Epidermal thickening, infiltration and split formation was observed for the positive control mouse, injected with specific rabbit anti-mCOLVII^{-C} IgG, but for none of the mAb injected mice.

4.4.2 Clones C8 and C9 Bind and Lead to Complement C_3 Deposition *In vivo* Without Skin Inflammation

Similarly, the mCOLVII^{-C} targeting clones, C8 and C9, were tested *in vivo* independently (Fig. 4.18 A). While several mice exhibited mild skin irritations at the injected ear sites, none presented with a progressive phenotype. Two male mice per group die or were sacrificed between days 4 to 8. These mice had been involved in fighting and had been separated prior to death. One of these mice presented with significant fluid in the lower

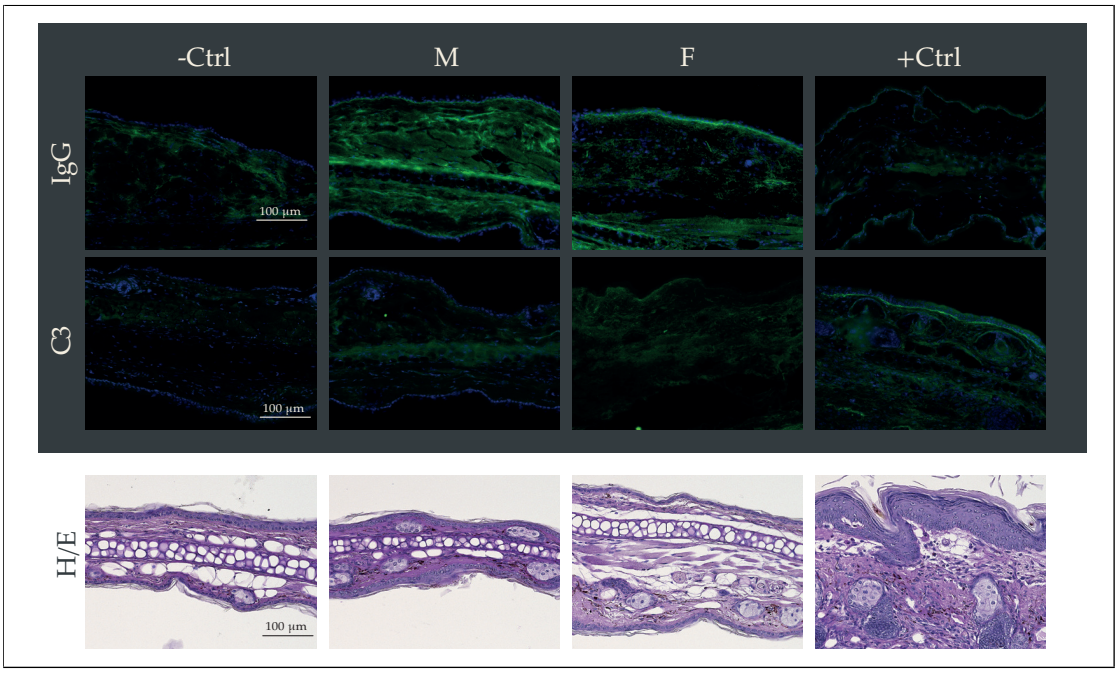

Figure 4.17: An equimolar combination of clones C1–C6 binds to the DEJ *in vivo* but does not mediate complement deposition nor subsequent inflammation. IgG deposition at the DEJ was observed sex independent. Non-injected control mice (-Ctrl) exhibited no IgG deposition. C_3 deposition was absent in -ctrl and C1–C6 injected mice, but present in the mouse injected with specific rabbit anti-mCOLVII^{-C} IgG (+Ctrl). Histology of C1–C6 injected mice remained unchanged when compared to the -Ctrl. +Ctrl exhibited epidermal thickening, cell infiltration and dermal-epidermal split formation.

body cavity, suggesting that on of the applied injections had penetrated internal organs. All other mice exhibited no abnormal internal phenotype that was macroscopically visible. All assessed mice exhibited strong deposition of IgG at the DEJ, while no deposition was observed in non-injected control mice (Fig. 4.19). Further, complement deposition was observed in all available biopsies of C8 and C9 injected mice (Fig. 4.19, Tab. 4.6). Assessment of histology revealed no epidermal thickening or split formation, however mild leukocyte recruitement was observed in two mice Fig. S2.

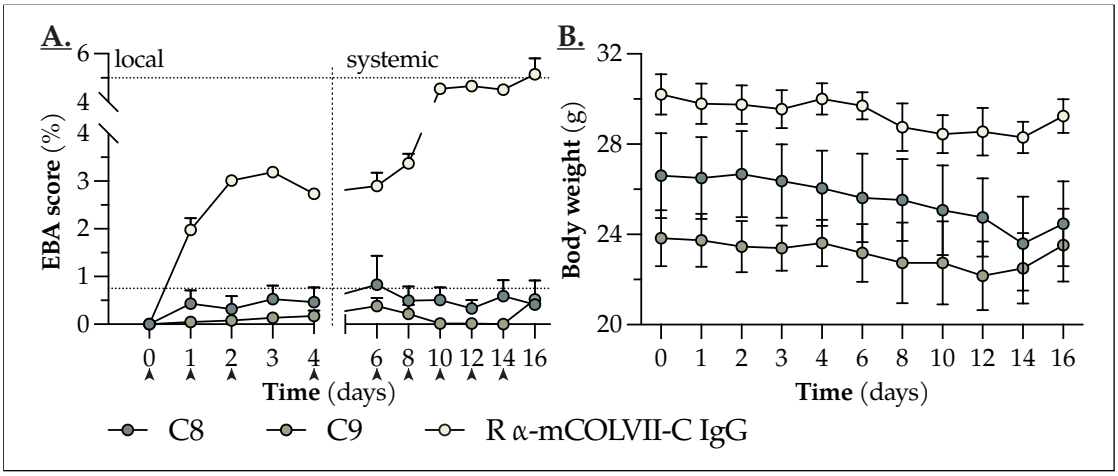

Figure 4.18: Clones C8 and C9 do not elicit pathogenicity *in vivo*. (A.) C8 and C9 did not cause progressive EBA like disease. Horizontal lines indicate the score cutt of for assumed pathogenicity for local (0.75%) and systemic (5%) injections. Vertical line indicates the switch from local to systemic injections (day 4). (B) Several male mice exhibted weightloss during the local antibody transfer model of EBA. Mean ± SEM, n=5 (C8, C9) n=2 (rIgG).

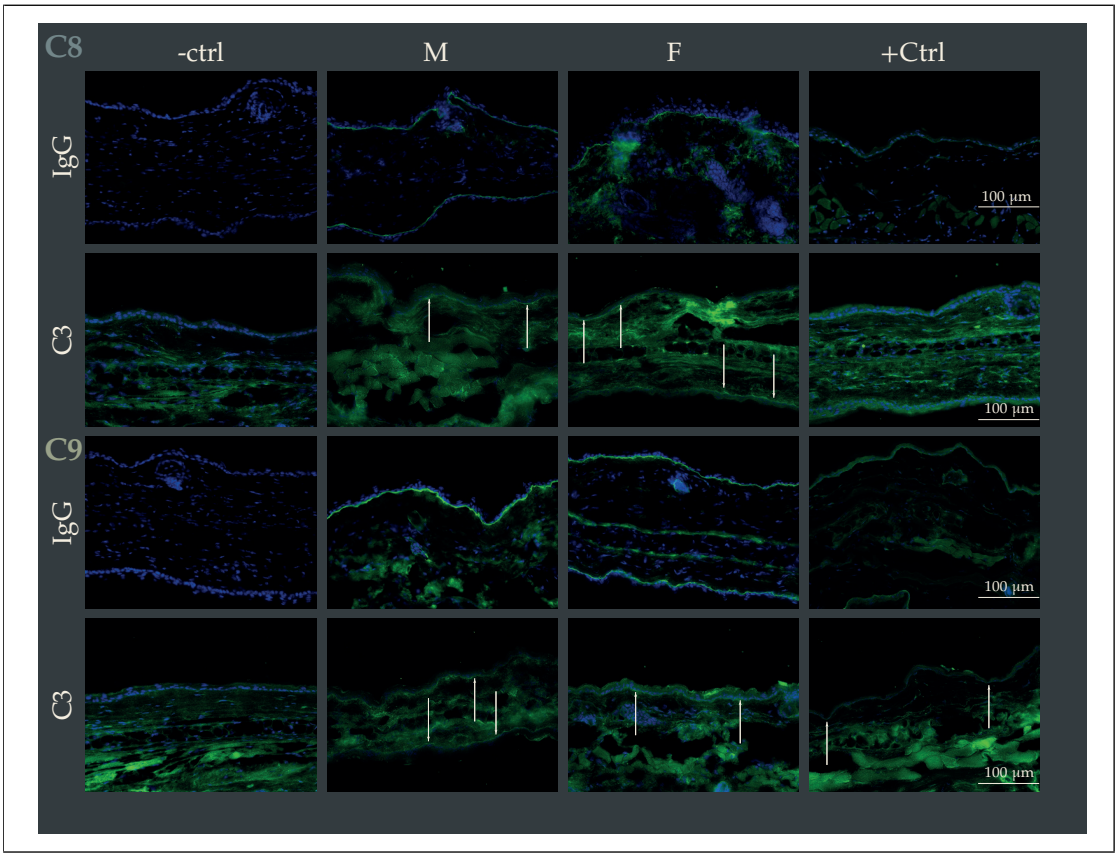

Figure 4.19: Clones C8 and C9 bound to the DEJ *in vivo*, were able to mediate complement deposition but did not lead to immune cell infiltration. IgG deposition at the DEJ was observed sex independent. Non-injected control mice (-ctrl) exhibited no IgG deposition. C_3 deposition was observed in C8, C9 and specific rabbit anti-mCOLVII^{-C} IgG (+ctrl) injected mice, but not in -ctrl mice.

Table 4.6: Immunofluorescence and histology results for *in vivo* tested antibody clones. IgG and C_3 immunofluorescence stainings were not further quantified apart from determination of presence or absence of linear DEJ deposition. Histology was evaluated regarding epithelial thickening, inflammation (score of infiltration 1-3) and split formation (in %). The table summarizes presence or absence of the described parameters.

Clone	Immunofluorescence		Histology		
	IgG	C_3	Epithelial thickening	Inflammation	Split
C1–C6	5/5	0/4	0/5	0/5	0/5
C8	3/3	3/3	0/5	2/5	0/5
C9	4/4	3/4	0/5	0/5	0/5
rIgG	3/3	3/3	3/3	3/3	2/3

4.5 BCR Repertoire Sequencing Reveals Clonal Abundance of Phage Display Derived mCOLVII Specifc V^H and V^L

Due to the observed binding, but no apparent pathogenicity of the phage display derived clones *in vivo*, the RNA samples from spleen and lymph nodes, previously used for immune library preparation, were subjected to BCR-seq as described in Section 3.4.3 by iRepertoire, Inc.. BCR-seq was used to further assess the clonality of the B cell response in the immunization-induced model of EBA and to determine the original isotypes of the phage display derived clones. A custom set of primers was designed to determine C^H constant regions, to assess the natural corresponding isotype of the V^H chains. Costume primer design, BCR seq and primary data analysis was performed by iRepertoire, Inc., based on the provided clonotypes.

BCR repertoire analysis relies on the identification of BCR clonotypes (clonal lineages), translating sequencing reads into clonotypes under the assumption that similar sequences originate from clonal expansion [211]. To annotate BCR clones, sequencing reads are mapped to germline V, D, J genes obtained from the IMGT database using IMGT/V-QUEST, subsequently allowing for CDR3 determination[182, 212]. Post-CDR3 determination, PCR and sequencing errors are corrected using UMIs and clustering algorithms to generate reliable consensus sequences. Repertoire analysis then uses CDR3 sequences to compare repertoire size, clonal diversity, V-D-J gene usage, and inter-sample repertoire similarities [211, 213].

All comparisons to the control provided by the company must be treated with caution, as no further information about this particular mouse is available. Strain, age, sex, and particularly housing conditions have pivotal influences on the adaptive repertoire [211, 214]. Therefore, primarily descriptive comparisons between spleen and lymph node samples will be drawn, with limited reference to the provided control.

4.5.1 BCR Clonality Varies Across Tissues From the Same Mouse

Total receptor counts were increased in both spleen (513,002 $\pm$ 48,480) and lymph node samples (507,236 $\pm$ 12,898) compared to the control sample (358,560 $\pm$ 10,950). The total unique CDR3 (uCDR3) counts revealed an inverse pattern: the control sample exhibited the highest diversity (124,375 $\pm$ 3,406), followed by spleen (58,880 $\pm$ 5,849), with lymph nodes exhibiting the lowest diversity (32,572 $\pm$ 1,231 (Sup-Tab. S2)). When relating total receptor counts to uCDR3 counts (total counts / uCDR3), the lymph node-derived samples exhibited a more restricted repertoire with fewer unique clones but higher expression per clone. The ratio of total receptors to unique CDR3s was 15.6 for lymph nodes, compared to 8.7 for spleen and 2.9 for the control (Fig. 4.20 A). This suggests a more focused, potentially antigen-driven response in the lymph nodes [215].
The distribution of immunoglobulin chains (IGH, IGK, IGL) also differed between tissues. IGH receptor counts were elevated in the lymph node samples (386,311 $\pm$ 9,238), compared to spleen samples (309,672 $\pm$ 43,784) and control (207,044 $\pm$ 6,108) (Sup-Tab. S2). The kappa:lambda ratio was markedly higher in lymph nodes (33:1) compared to spleen (7:1) and control (9:1), exceeding the typical murine ratio of 10-20:1 [44]. This skewed ratio further supports a highly selected B-cell population in the lymph nodes. SHM1 analysis revealed tissue-specific abundancies across isotypes. The overall IGH SHM1 was highest in lymph node samples (0.0228 $\pm$ 0.0006), intermediate in control (0.0154 $\pm$ 0.0000), and lowest in spleen samples (0.0136 $\pm$ 0.0003) (Sup-Tab. S3). Class-switched isotypes showed higher mutation rates than IgM/IgD across all samples, consistent with antigen-driven selection. Notably, IgG1 exhibited the highest SHM1 values in lymph nodes (0.0320 $\pm$ 0.0001), significantly exceeding those in spleen (0.0238 $\pm$ 0.0004) and control (0.0241 $\pm$ 0.0000) (Fig. 4.20 B).

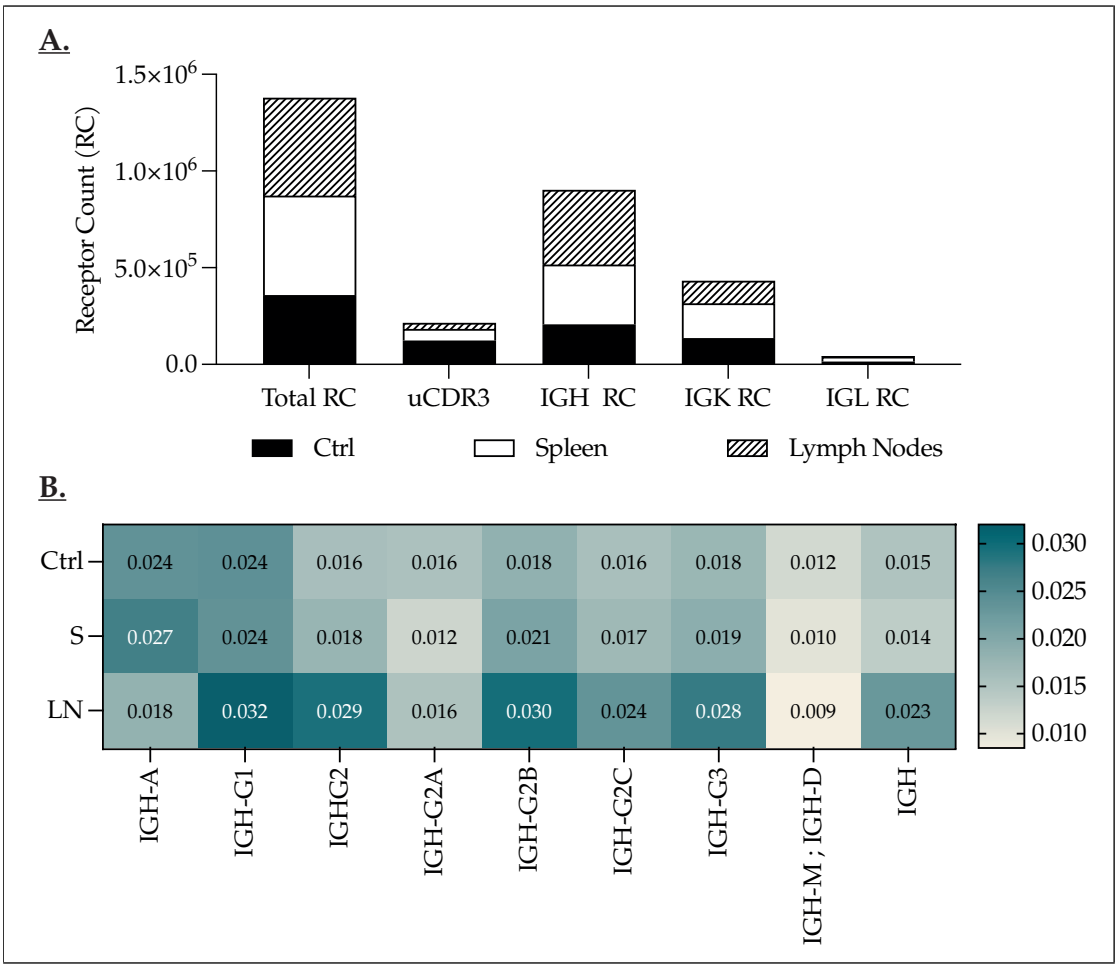

Figure 4.20: BCR repertoire sequencing reveals sample- and tissue-specific differences in chain and isotype composition. (A.) Total receptor counts and IGH counts were increased in spleen- (S) and lymph node-derived (LN) samples, originating from an EBA affected mouse. UDCR3 diversity was diminished in S and LN, when compared to control (Ctrl), originating from spleen. (B.) Mean somatic hypermutation with normalization (SHM1) frequencies showed tissue specific mutation rates of isotypes and subclasses. IGH-G1 and IGH-G2B exhibited the overall highest mutation rates in LN.

4.5.2 Sharing of IGH Chains is More Restricted as Sharing of IGK and IGL Chains Across Samples

The similarity of obtained sequences between samples was assessed using different sharing analysis approaches and visualized in heatmaps (Fig. 4.21, Sup-Fig. S5, S4). Notably, all of the following heatmaps, which compare the sharing of BCR clonotypes (CDR3s) between samples, are asymmetric, where values can differ depending on which sample is searched into the other. Samples were analogously assigned to the previous naming of immune libraries: lymph node-derived sample (LN), spleen-derived sample (S), and control (spleen-derived) sample (Ctrl). The letter "R" in sample names indicates a technical replicate of each sample, which served to confirm technical reproducibility. R^2_{outer} was calculated to assess the statistical correlation between the abundance distributions of CDR3s in two samples. High R^2 values indicate a strong linear correlation in CDR3 distributions, suggesting that the compared datasets are likely to exhibit similar CDR3 profiles. Conversely, low R^2 values indicate that the CDR3 distributions are dissimilar between the compared samples.
Next, a pairwise comparison of uCDR3 sharing was performed,this metric assesses the fraction of unique clonotypes (i.e., presence or absence) shared between two samples, independent of their abundance. High values indicate either high biological similarity or strong technical reproducibility, while low values suggest biological or experimental distinction between samples [189, 215].
Additionally, the shared expression of IGH was calculated, providing a quantitative visualization of the shared abundance of CDR3s between pairs of samples and reflecting clonal expansion dynamics.
Finally, the Sørensen and Morisita-Horn sharing indices were calculated to assess similarity between samples. The Sørensen index provides a normalized, abundance-independent measure of similarity between immune repertoires, based on the incidence of CDR3s. Thus, the Sørensen index complements the uCDR3 sharing analysis by representing normalized repertoire sharing and offering insight into the breadth of sharing and clonal dynamics [189]. The Morisita-Horn index is an abundance-based metric, where similarity is calculated based on both the incidence and abundance of clonotypes. Therefore, the Morisita-Horn index is well-suited to identify public, antigen-driven clonal expansions [189].

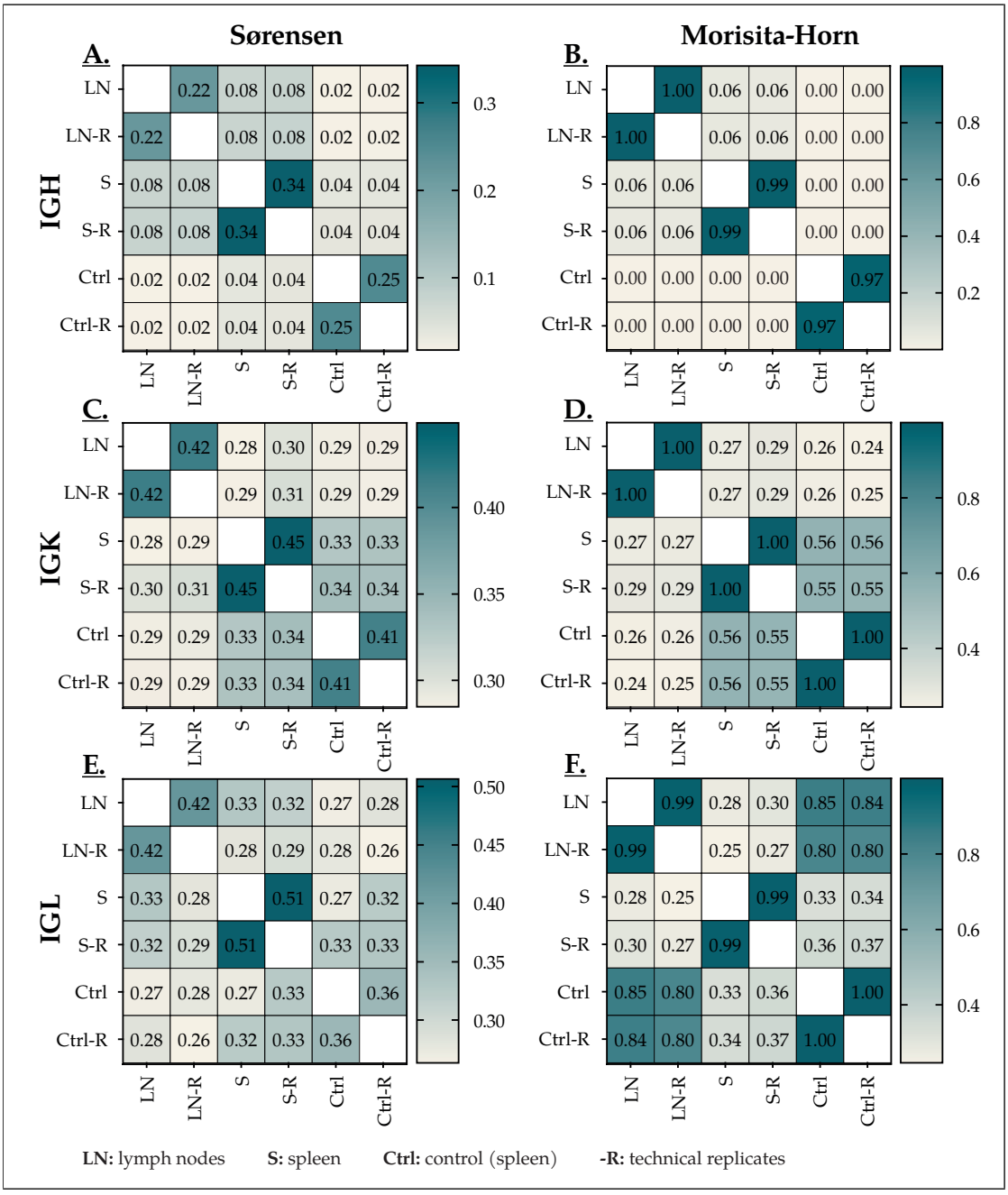

Figure 4.21: Sharing analysis of BCR-clonotypes reveals chain dependent differences in shared clonotypes. Sørensen indicates abundance-independent normalized sharing breadth, while Morisita-Horn incorporates abundance and therefore gives insight on shared expanded clonotypes between samples. IGH (immunoglobulin heavy chain), IGK (immunoglobulin kappa light chain), IGL (immunoglobulin lambda light chain).

Sharing analysis of IGH revealed low partial overlap between spleen and lymph node-derived samples

R^2_{outer} revealed high correlation between samples and their replicates ensuring reproducibility between replicates(Sup-Fig. S4). A 2% correlation between experimental samples LN and S indicated a minor degree of similarity. No correlation was found between the experimental samples and the Ctrl sample.
The uCDR3 comparison revealed that, as expected, the replicates of each sample exhibited the highest clonal overlap with one another(Sup-Fig. S5). Overlap between experimental samples LN and S was in the range of ~6–11%, indicating that there is sharing of unique CDR3s between the samples to a certain degree. Interestingly, when comparing the sharing of the control with the experimental samples, the sharing between S and Ctrl exceeded the sharing with LN, regardless of which sample was searched into the other. Indicating that there is a more naïve repertoire within the spleen-derived samples.
The shared expression analysis of IGH revealed that, despite the non-excessive overlap between samples LN and S (Sup-Fig. S5), shared clonotypes exhibited a high expression in both samples, possibly reflecting an ongoing directed selection process or the nature of the samples (originating from the same mouse, which has encountered environmental antigen). Again, the sharing between S and Ctrl exhibited higher values (~10–12%), indicating closer similarity of these samples than between LN and S, again likely suggesting a more naïve repertoire within the spleen-derived sample overall.
By comparing Sørensen and Morisita-Horn (Fig. 4.21) indices for the three analyzed data sets, conclusions about the repertoire diversity can be drawn in more detail. Sørensen confirmed that sharing between LN and S was elevated (8%) when compared to the sharing with Ctrl (2% / 4%). Again, sharing between S and Ctrl was higher than between LN and S. When comparing to Morisita-Horn, it can be deduced that despite the low sharing observed in Sørensen, there are distinct dominant clones within both repertoires.

Sharing analysis of IGK and IGL revealed overlap between spleen and lymph node-derived samples

R^2_{outer} revealed perfect correlation between samples and replicates (Sup-Fig. S4). IGK correlation between samples LN and S was increased when compared to IGH correlation. Notably the correlation between sample S and Ctrl sample reached up to 35% indicating elevated similarity.
Assesment of uCDR3 sharing revealed elevated sharing between all samples. Directionality of comparison exhibited considerable changes in % of sharing, however overall

sharing between samples S, LN and Ctrl was 20–48%, suggesting high biologic similarity (Sup-Fig. S5). This is interresting, since IGH uCDR3 sharing was quite disimilar, meaning while IGH repertoires underwent drastic changes the IGK repertoire remains less touched across tissues and individual mice. Similarily the expression of the shared CDRs was highly similar across samples, reaching up to 96% when comparing experimental samples, and up to 95% when comparing experimental with control sample. Sorensen and Morisita-Horn indices compiled the previous assesment: Sørensen showed sharing across experimental samples which even was exceeded by sharing between sample S and Ctrl. Morisita-Horn revealed that the clonal overlap extended also on abundance level, with samples S and Ctrl sharing about 55–56% of highly expressed clones. The sharing trend was continued on the IGL chain level, where interrestingly the LN derived sample apparently shared highly abundant clones to up to 85% with the control sample (Fig. 4.21).

4.5.3 Clonal and Isotype Distribution Varies Between Lymphoid Organs

The previously described clonal abundance was visualized using BCR treemaps. Samples are referred to as previously defined: Lymph nodes (LN), Spleen (S), and control (Ctrl) (Fig. 4.22 A-C). Rectangles represent clonotypes, with their respective size indicating abundance by UMI / reads. Each tree is grouped into areas for the IGH-, IGK-, and IGL-chains. Due to the previously described sharing of IGK and IGL between samples, the analysis was focused on IGH. For further reference chain and isotype identification by reads and uCDR3 are shown in Fig. S3.
The already described diminished diversity in the two samples originating from the mCOLVII^{vWFA2} immunized mouse (LN, S) is clearly visible when compared to the Ctrl. Additionally, differences in the extent of individual clonal expansion are apparent when comparing the trees for all three samples. Sample LN is dominated by a group of expanded clones, whereas sample S exhibits a more diverse but less expanded repertoire. No obvious expansion of IGH clones is apparent in the Ctrl sample, which overall exhibited the highest diversity of clonality. The reduced diversity and increased expansion of clonotypes in the LN sample suggest strong participation in a directed immune response. The suggested expansion of clonotypes and decreased diversity compared to the Ctrl is merely suggestive due to the aforementioned reasons regarding the origin of the sample. The isotype distribution between samples provides insight into the origin and ongoing selection within the samples (Fig. 4.22 B). While the Ctrl sample presents with IgG2A isotypes, IgG2A is absent in the experimental samples, reflecting their origin from

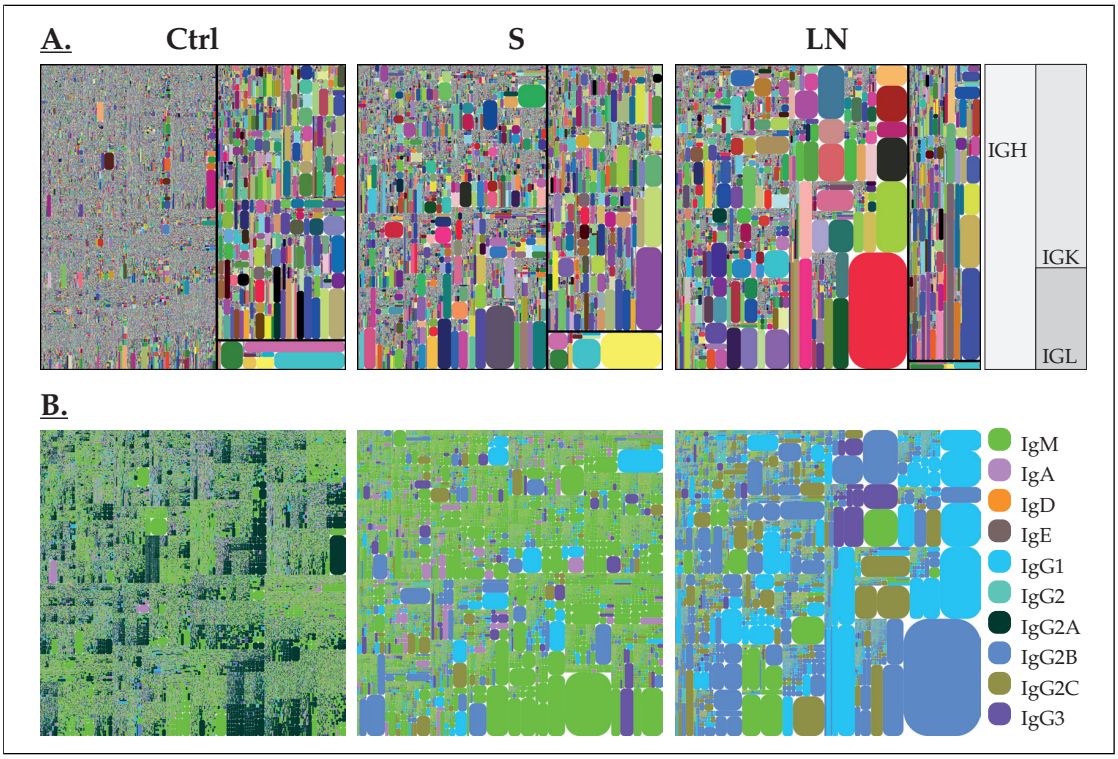

Figure 4.22: Isoytpe trees visualized differing clonality and isotype distribution across samples. (A.) In BCR treemaps unique CDR3 clonotypes are represented by a rectangle. Rectangle sizes indicate the relative frequency (abundance by reads) of an individual clonotype, with varyig square sizes reflecting areas of clonal expansion. IGH, IGK and IGL are displayed according to right figure legend. (B.) IGH isotype trees indicate the identified isotypes of the clonotypes from the IGH panel of A. (C.) Isotype distribution by unique CDR3.

C57BL6S mice. This also confirms the isotype specificity of the custom-designed primers. The LN sample is marked by a striking dominance of expanded IgG clones. Both IgG1 and IgG2 isotypes are strongly represented among expanded clones, followed by a pronounced expression of IgG2C clones. Interestingly, several of the expanded clones exhibit an IgG3 identity. Several expanded clones also exhibit IgM identity. Of note, the majority of non-expanded clones are of the IgM type, suggesting these clones are not participating in an ongoing immune reaction. IgA is almost completely absent from the LN sample. Sample S is characterized by moderately to highly expanded IgM clones. Similar to sample LN, other expanded clones harbored the IgG1 and IgG2B isotype, followed by approximately equal expanded fractions of IgG2C, IgG3, and, interestingly, IgA. The Ctrl sample did not exhibit a striking dominance of expanded clones and was with respect to isotype distribution dominated by IgM and IgG2A. The abundance of IgG2A clones in this sample was not translated into a similar abundance of IgG2C clones in sample S.

4.5.4 Phage Display Derived Clonotypes Do Not Represent The Most Abundant Clonotypes Within the Repertoire

To analyze and visualize the specific V^H and V^L sequences from the IgG2b-expressed phage display clones and 16A1C8 within the BCR repertoire, iRepertoire, Inc. was provided with the respective DNA sequences. CDR3 peptides, V and J genes were identified from the nucleotide sequences using IgBlast and deduplicated. Clonotypes were assigned as previously discussed (Section 4.1.4)– A, B, C, D –based on CDR3s.
Ig treemaps were generated to visualize exact matching (HD-0), and matching with a HD of 2 (HD-2) between CDR3 peptides (Fig. 4.23, 4.24). Clonotypes (IGH: A, B, C, D; IGK: 1, 2, 3, 4) were visualized separately for IGH and IGK in the BCR and isotype treemaps (Fig. 4.22 A, B). For reference to the expressed IgG2b clones, chain usage is detailed in Table 4.5. IGH clonotypes A, B, C, D were absent (Fig. 4.23) in the Ctrl sample, despite its higher overall diversity. This may suggest antigen-driven clonal selection, though differential V/J gene usage in this mouse strain could also explain this observation (Fig. 4.22 B).
In LN and S, phage display-derived IGH clones were not dominant but represented intermediate (A) to smaller (B, C, D) clonotypes (relative frequency indicated by treemap rectangle size). Clonotype A (the most expanded in the LN) was also the most abundant among phage display-identified clonotypes. All clonotypes appeared in both tissues, though frequency differences observed during Sanger- and library sequencing may

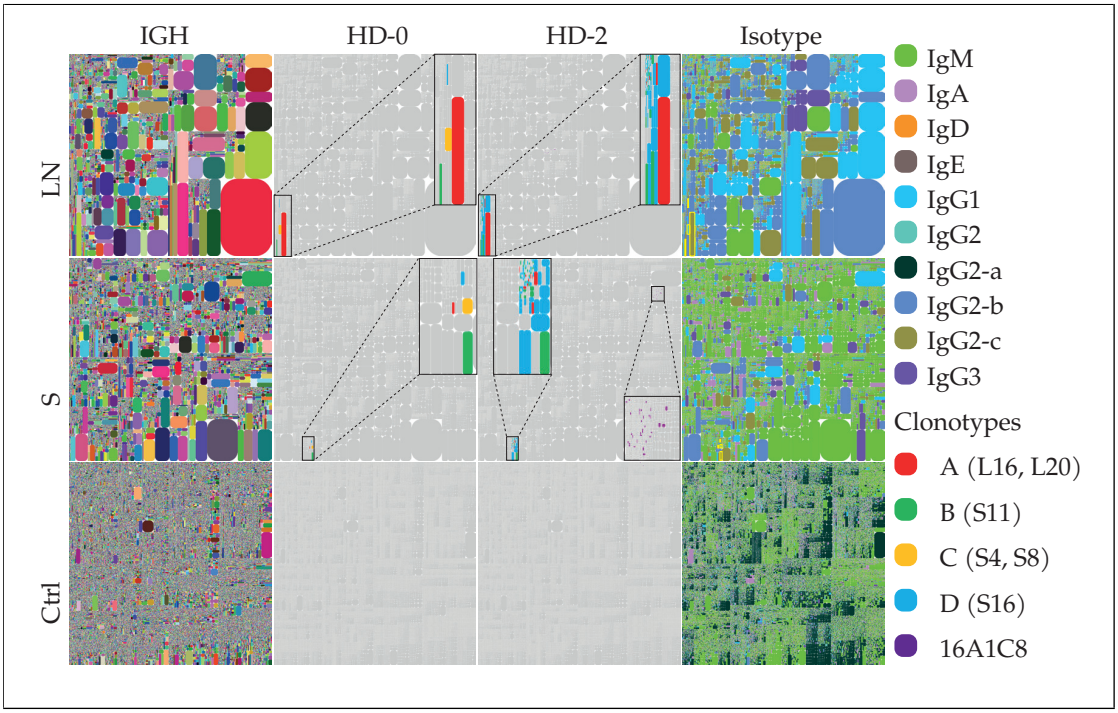

Figure 4.23: Phage display derived IGH clonotypes are not among the most abundant CDR3 clonotypes within the analyzed repertoire. IGH BCR treemaps are displayed for samples lymph nodes (LN), spleen (S) and control (Ctrl) in a horizontal order: IGH clonotype distribution, exact matching (HD-0)) of phage display-derived CDR3s, Hamming distance of 2 (HD-2) between CDR3 peptides, isotype upset plots. IGH clonotypes (A-D), are indicated, with the corresponding expressed IgG2b clone, incorporating the respective chain in parenthesis.

explain phage display enrichment (Fig. 4.7). In sample S, phage-derived clonotype frequencies were lower than in sample LN, consistent with the spleen's comparatively naive state (Fig. 4.21). Frequency rankings were B > C > D > A (vs. C > B in phage display).

HD-2 analysis (Fig. 4.23) revealed clonotypes closely related to D (more dominant in LN) and B in both tissues. Sanger-derived V^H phylogeny positioned D as a derivative of C, with B branching between A and C (Fig. 4.5). This might indicate that clonotype D represents the furthest mutated clone, still involved in SHM at the time the tissues were obtained, supported by: (1) D's prevalence in HD-2 analysis despite lower initial frequencies, higher V-region mutation count in D (Tab. 4.2) and and phylogenetic tree topology (Fig. 4.5). Total specific clonotype frequencies were estimated from HD-2, and were ∼1% (S) to 3% (LN). The 16A1C8 CDR3 appeared in HD-2 maps across all samples, with higher expansion in experimental vs. control tissues. Isotype analysis revealed IgG2C (A, B) and IgG2B (D) in LN, while S clonotypes included IgG2C (B), IgG2B (A, D), and IgG2 (without further classification) (C). Related clonotype D clusters (HD-2) in LN were predominantly IgG2B, with minor IgG2C and IgG1 components.

In contrast to IGH CDR3 clonotypes, IGK clonotypes were present at elevated frequencies across all analyzed samples (Fig. 4.24. Remarkably, IGK clonotypes were shared identically between Ctrl and S, suggesting germline-encoded public clonotypes. The frequency of IGK clonotypes in LN was lower than in spleen-derived samples. Analysis of HD-2 revealed derivatives of the 16A1C8 IGK CDR3—not isolated in these samples—in all tissues, implying low-abundance precursors. Together, these observations suggest IGK CDR3 diversity contributes less to high-affinity clone selection in the immunization-induced mouse model of EBA.

Table 4.7: Relative V^H clonotype frequencies and isotypes for samples LN and S. Relative frequencies (ranked 1–4, 1 = most abundant) and isotype subclass assignments for clonotypes A–D in samples LN and S, derived from the HD-0 map (Fig. 4.23).

Sample	Clonotype	Relative Frequency Rank		Isotype	
		LN	S	LN	S
	A	1	4	IgG2c	IgG2b
	B	3	1	IgG2c	IgG2c
	C	2	2	IgG2	IgG2
	D	4	3	IgG2b	IgG2b

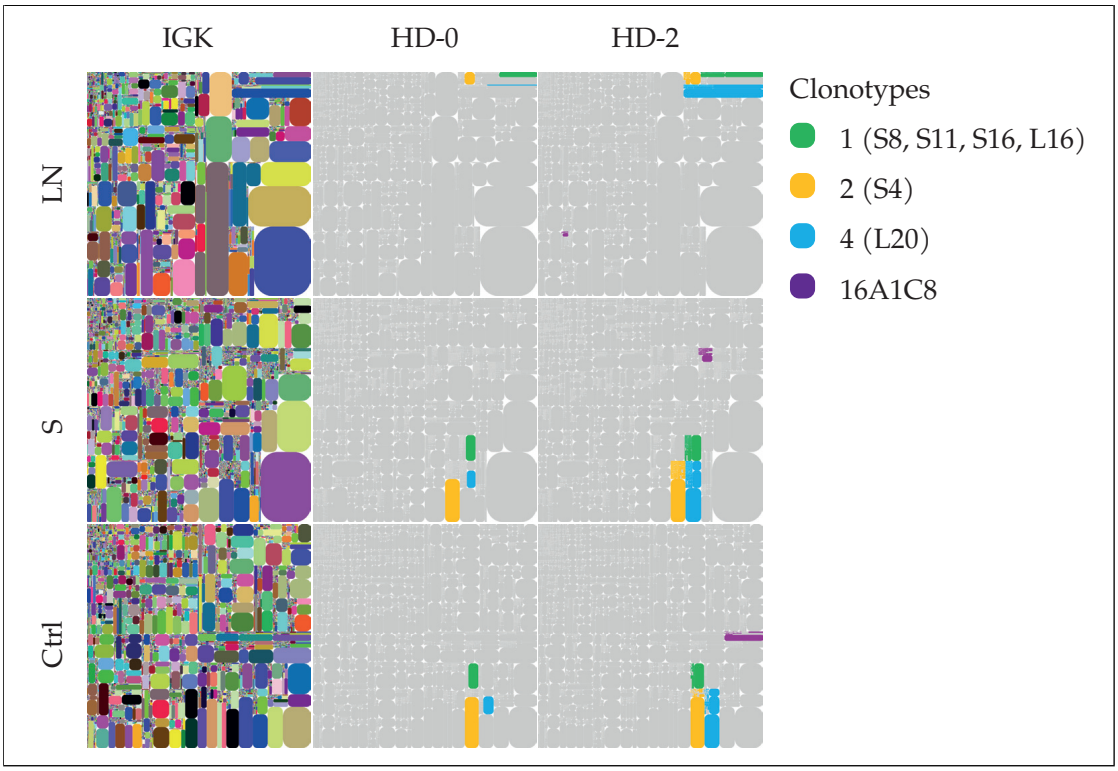

Figure 4.24: Phage display derived IGK clonotypes likely represent public clonality. IGK BCR treemaps are displayed for samples lymph nodes (LN), spleen (S) and control (Ctrl) in a horizontal order: IGH clonotype distribution, exact matching (HD-0) of phage display-derived CDR3s, Hamming distance of 2 (HD-2) between CDR3 peptides.

Chapter 5

Discussion

The primary aim of this work was to isolate mCOLVII^{vWFA2}-specific antibodies from immune libraries, using phage display, perform genetic characterization, and subsequently express autoreactive mAbs for *in vitro* and *in vivo* characterization in the context of experimental murine EBA. The workflow, including key procedures is summarized in 5.1.

5.1 Summary of Experimental Workflow

A set of scFvs was successfully isolated from two antibody immune libraries (Fig 1.7), previously generated from the spleen and lymph node BCR repertoires of an mCOLVII^{vWFA2} immunized mouse. These scFvs were tested for specific target recognition (Fig. 4.1.3), and thoroughly characterized genetically, regarding their rearranged V-(D)-J composition and mutation rates (Tab. 4.2, Tab. 4.3). The phylogeny of V^H and V^L was determined and, based on gene rearrangement and the resulting CDR3s of V^H and V^L, four distinct clonotypes were identified respectively (Fig. 4.5). The efficacy of enrichment of the identified V^H clonotypes across the phage display panning procedure was assessed and verified by NGS V^H sequencing of both libraries (Fig. 4.1.5), demonstrating that the dominant antigen-specific clonotypes were identified using the chosen isolation strategy. Based on cumulative descriptions in the literature [27, 93, 118, 127, 129], that the Aab response in EBA is supposedly associated with a complement-activating subclass composition, a murine IgG2b backbone was chosen for recombinant expression of full-length antibody clones. In addition to the chosen six candidate clones from phage display (Tab. 4.5), other clones, targeting mCOLVII^{vWFA2} (16A1C8 - C7, H510 - C10) or mCOLVII^{-C} (C8, C9), were acquired, genetically characterized (Tab. 4.4), and equally successfully ex-

pressed as IgG2bs (Fig. 4.9). Nine antibodies were thoroughly characterized *in vitro* regarding their antigen specificity, avidity (Fig. 4.10, 4.14), full-length target binding (Fig. 4.11, 4.15), and Fcγ functionality (Fig. 4.12, 4.14). The six phage display-derived candidate clones (C1-C6) together, as well as C8 and C9 separately, were chosen for *in vivo* testing of pathogenicity in a combined, local and systemic antibody-transfer model of EBA (Fig. 3.2). Though all clones exhibited *in vivo* binding, and C8 and C9 were able to induce DEJ C_3 deposition, no leukocyte infiltration was observed in any of the experiments (Tab. 4.6). To assess the complete BCR repertoire and track the identified clonotypes of antigen-specific V^H and V^L, the RNA used for the generation of the S and LN libraries was sequenced (Section 4.5). It was found that both tissues harbored reduced uCDR3 counts (in comparison to the Ctrl) (Fig. 4.20) and that IgG1/IgG2b SHM1 rates were increased in the LN. Sharing between the samples and unrelated Ctrl revealed that both samples are dominated by distinct expanded V^H clonotypes and that S likely represents a more naïve state than LN (Fig. S5, 4.5.2). These initial descriptive findings were confirmed by BCR treemaps, visualizing UMI-based clonotype abundance and isotype distribution (Fig. 4.22). Antigen-specific clonotypes were identified by exact matching, revealing frequencies of approx. 1–3% among the tissue repertoires for V^H (Fig. 4.23), while the identification of antigen-specific V^L clonotypes suggested more public clonotypes, as these were also present in the unrelated Ctrl sample (Fig. 4.24).

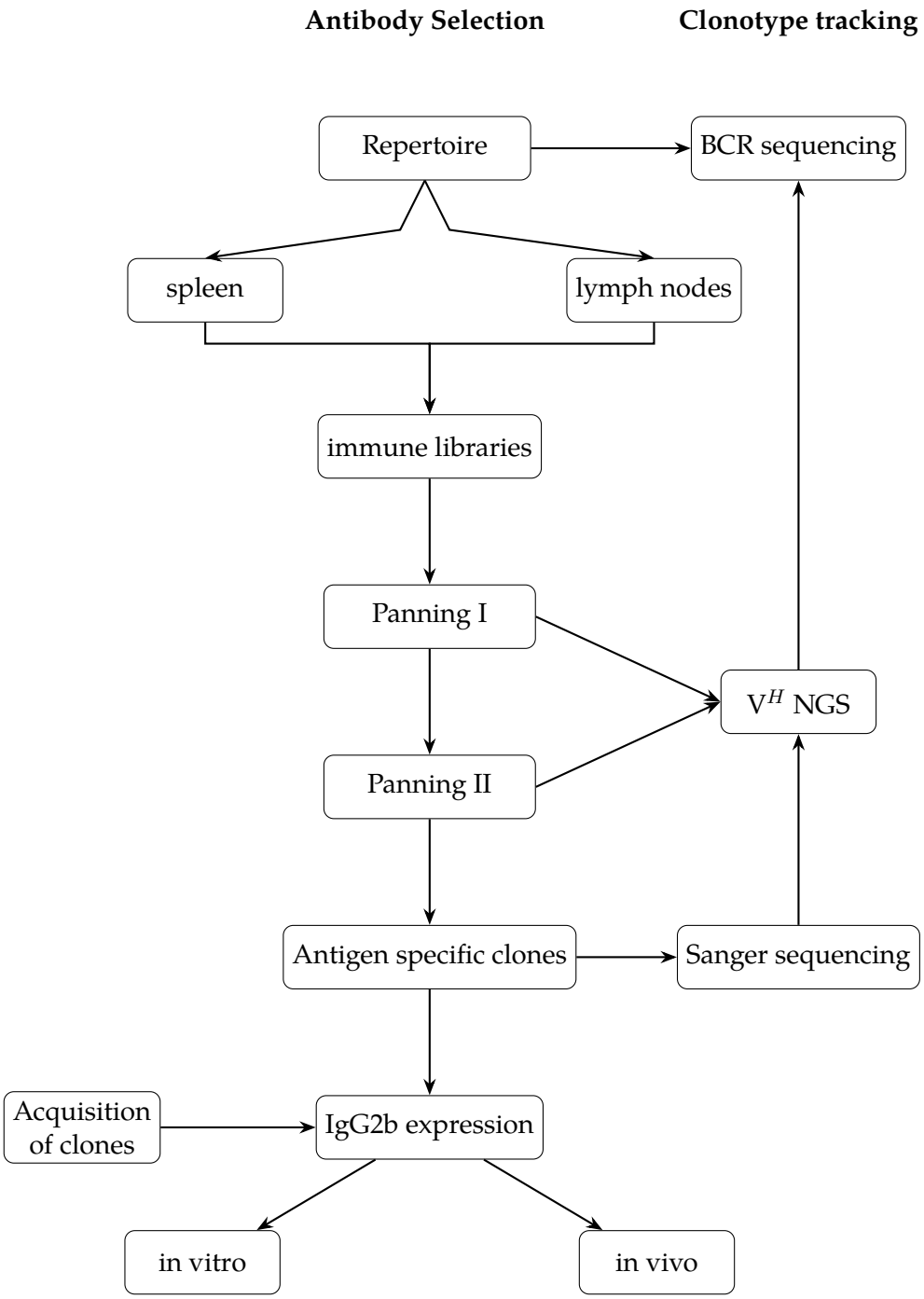

Figure 5.1: Schematic workflow of antibody selection and clonotype tracking. The experimental procedures are split between antibody identification- and characterization-based experiments and genetics-based classification of clonotypes and subsequent tracking across different experimental stages. Arrows indicated the directionality of experimental flow.

5.2 Successful Isolation of High Affinity mCOLVII^{vWFA2} Binding Antibodies

As described in Section 1.6, phage display is a potent approach to thoroughly screen and isolate specific antibodies from broad repertoires through the usage of immune libraries, displaying a repertoire pre-selected against the antigen of interest [150, 161]. Phage display has previously also been used to isolate Aab, mainly employing libraries generated from human patient material in diseases such as systemic lupus erythematosus, rheumatoid arthritis, and importantly pemphigus, another disease from the AIBD spectrum [125, 216–219]. Thereby, phage display has been proven to be a viable platform also to isolate autoreactive antibodies from immune libraries. The selection strategy presented in this work was successfully applied to isolate high-affinity binders to recombinant mCOLVII^{vWFA2}.

Due to the bacterial origin of the recombinant mCOLVII^{vWFA2} (Protoc. 3.1.4) employed for immunization, the immune response in the immunization-induced model of EBA is likely also directed against bacterial contaminants and lipopolysaccharides (LPS), present even after the applied purification strategy (Protoc. 3.1.4) [167]. Bacterial protein and LPS are, due to their foreign entity, highly antigenic and therefore inclined to induce a strong response, potentially exceeding the response directed against self-antigen, as tolerance mechanisms limit autoreactivity and are artificially broken by the use of adjuvant [93]. Whether this holds true in the immunization model of EBA has so far not been addressed. To avoid the isolation of high-affinity antibodies directed against bacterial protein, a subtractive panning strategy was applied, similar to approaches described in the literature, where immune libraries are preabsorbed against irrelevant antigen or already known epitopes on the antigen [161, 220]. The generation and employment of filtrated *E. coli* ER2566 lysate supernatant for both solid phase depletion before the panning and liquid phase depletion during the panning against mCOLVII^{vWFA2} proved to be a vital approach for the successful isolation of scFv phage antibody clones targeting mCOLVII^{vWFA2}.

The success of the subtractive panning was demonstrated by the exclusive binding of phage display-derived clones against mCOLVII^{vWFA2}, but not against *E. coli* ER2566 lysate supernatant, shown in ELISA experiments (Fig. 4.3, Fig. 4.1.3). Human COLVII is known to exhibit N-linked glycosylation [221]. The comparable binding also against mammalian-produced recombinant protein suggested that the binding of the isolated clones was not interfered with by glycosylation sites within the targeted epitopes (Fig. 4.1.3).

5.3 Restricted V-(D)-J Gene Usage of Phage Display-Derived Clones

The possibility for genetic characterization of isolated specific clones is a major advantage of phage display [152, 222]. The sequenced scFv phage antibody clones presented with closely shared to identical gene usage for both V^H and V^L. A similar pattern of shared V^H gene usage of phage display-isolated clones in the context of autoimmune repertoires, employing recombinant protein for selection, has previously been described in Payne *et al.* and Ishii *et al.*, where patient-derived libraries were used to identify desmoglein 1- and 3-targeting antibody clones [218, 219].
The resulting V^H CDR3s and junctional AA sequences, as well as branching phylogeny, suggested the individual development of the obtained clones by at least three individual B cells (clonotypes A, B, C), likely originating independently in spleen and lymph nodes (Fig. 4.5, Tab. 4.2). The similar gene usage in analyzed clones from both tissues (S, LN) indicates that the Aab response against autoantigen, despite the employment of adjuvant, might be limited by the repertoire diversity itself, in line with the previously described germline encoded diversity of mice when compared to humans [42, 223].
The herein identified *IGHV1-39*01* gene has been described as a low-usage gene, accounting for 0.14% of V gene chains in naïve *C57BL/6* mice, whereas highly used genes occur with frequencies ranging from 1–10% [42]. Among the IGH-J genes, *IGHJ1*01* has been reported with a usage frequency of 21.8%. However, as there are only four murine IGH-J genes, frequency differences are less pronounced than among V genes and may provide diminished information about the resulting clone [44, 223]. The herein presented data provides rare but partial insight into the gene usage dynamics in the generation of Aab in mice, whereas the literature so far has focused on determining the dynamics in naïve repertoires [42, 223]. However, as pathogenic clones were not identified, there is a high likelihood that additional clones reside within the repertoire that were not identified due to the limitations of the applied strategy (further discussed in 5.6).

5.3.1 V^H Sequences Exhibit Elevated Mutation Rates Across All Analyzed Clones

The SHM-induced mutation rate within GC-participating B cells is believed to be a fixed rate of 1×10^{-3} per base pair per cell division [224, 225], typically resulting in 3–5 mutations per V^H in mice. In contrast, human mutation counts have been shown to be in the range of 16.5 to 21.8 [42, 226], strongly associated with the corresponding subclass. In

mice, this is rarely observed and associated with strains carrying introduced alterations related to B cell biology and SHM, thereby resulting in hypermutated clones [227].
Prominently, the mutation counts observed in all Sanger-sequenced V^H chain V-regions indicate a strong involvement of SHM in generating these particular clones, as total mutation counts ranged from 5–12, with most mutations considered Ns as determined by IMGT analysis (Tab. 4.2). Even within the annotated clonotypes (A–D) (Fig. 4.5), a range of mutation counts was observed, indicating generation from a single precursor cell and introduction of different mutations during SHM.
In contrast, 16A1C8 exhibited a total count of 23 mutations (19 Ns), exceeding those of the vWFA2-specific phage display-derived clones (Tab. 4.4). This clone originates from another mouse strain (SJL/J)and a hybridoma; however, comparable mutation rates between strains have been described [42]. Importantly, the tissues used to isolate the respective clones were collected at different timepoints. While the GC reaction in mice has been described as shorter-lived and less impactful (regarding repertoire diversification [42]) compared to the human setting, it was shown that antigen deposit formation following adjuvant-mediated immunization may lead to prolonged GC activity and retention [228, 229]. For the immunization-induced model of EBA (mCOLVII$^{\text{-C}}$ immunization), it has been shown that antigen-specific plasma cells are retained for several months and do not egress to the bone marrow [131]. Further, Kovacs *et al.* demonstrated ongoing epitope spreading (weeks 2–6) in the immunization-induced EBA mouse model (mCOLVII$^{\text{vWFA2}}$ immunization) [230]. Taken together, this indicates a high likelihood of ongoing GC reactions driven by antigen-adjuvant immunization. Increased mutation counts at later timepoints may therefore reflect ongoing SHM in GC-participating clones.
Clones B8 (C8) and C10 (C9), originating from another phage display approach in which SLO of mCOLVII$^{\text{-C}}$-immunized mice were used for library assembly. These clones presented unusually high s and elevated Ns mutation counts (Tab. 4.4), attributable to *in situ* codon optimization performed during clone generation (A. Recke, personal communication). Non-optimized sequences had 5–14 mutations. Clone 510 originated from a hybridoma cell line generated from pooled SLOs of T cell–deficient scurfy mice lacking functional Foxp3$^+$ T-regs [139, 168]. H510 exhibited extremely high V-region total mutation counts, likely due to its origin from an environment without T-regs, where their absence permits unsupervised germinal center activity, resulting in highly mutated autoantibodies.
Clonotype D, phylogenetically positioned as a derivative of clonotype C, exhibited the highest total mutation count (12) among phage display-derived clones, supporting

shared ancestry to clonotype C. Repertoire sequencing revealed expanding clusters of clones, when considering HD-2 data (Fig. 4.23), particularly for clonotype D, suggesting ongoing GC participation of this clonotype. In humans subclass switching is considered sequential, linked to germline gene location, the nature of stimulation (cytokine milieu) [129, 231], and further to the number of somatic point mutations in IGHV-genes [232]. In contrast, murine subclass switching may precede SHM [233, 234], with IgG1 consistently exhibiting the highest mutation counts, suggesting affinity-matured antibodies from prolonged GC activity belong to the IgG1 subclass [42, 206, 235]. In line with this, most HD-2–identified clonotype D–related clones in the LN harbor the IgG1 isotype (Fig. 4.23). Further IgG1 exhibited the highest SHM1 rates across all tissues, further strengthening the evidence for increased mutations and thus affinity maturation in IgG1 antibodies (Tab. S3, Fig. 4.20). Of note, Hammers *et al.* have reported an increase in IgG2c titers over time, missaliging with the literature and the herein presented results [129]. However, Hammers *et al.* on the one hand assessed serum ratios of specific IgG, quantified using commercial antibody kits with standard serum, but not antigen specific antibodies resulting in relative, but not quantifiable concentrations. On the other hand the described increased tissue bound ratios, may, as well as the relative serum concentrations not reflect the situation in the dLN, which is described in this study. Interrestingly Hammers *et al.* also describe an early (d21 p.I.) peak of IgG1 deposition (similarly IgG2b and Ig2c are peaking), which does not explain the herein described observation, however in the context of this studies findings leaves room for a speculative role of IgG1 in early tissue deposition and thus pathogenicity.

5.4 V^H Clonotype Enrichment and Privacy is Linked to Tissues of Origin

Combining phage display with NGS sequencing is a meaningful approach to verify clonal enrichment and track single antibody clones [164]. Other Aab-identifying phage display approaches, using recombinant antigen for selection, had employed >2 panning rounds [125, 219]. NGS of V^H in both libraries across pannings revealed that the immune libraries presented here were already heavily dominated by and enriched for clonotypes A, B, and C after two successive rounds of panning (Fig. 4.7 B, D). As clonotypes in subsequent pannings could only arise from those identified in previous rounds, it was assumed that clones dominating the *in vivo* response were already enriched for and identified. However, clonotype D was present in the spleen-derived library only at a fre-

quency of 0.1% after the second panning (Fig. 4.7 B), indicating that low-frequency clones might have been enrichable with further pannings. Further enrichment or isolation of additional clones, such as V1-55 J2 CARAGITGYFDYW and V1-7 J2 CARKDYFGSSYFDYW, which both exhibited intermediate enrichment and frequencies after both pannings, might have been possible; however, the likelihood of these clones being outcompeted by growth or binding competition during library amplification and panning itself is equally high [220].
NGS furthermore indicated that the tissue-specific abundance of antibody clonotypes observed by Sanger sequencing also held valid for the immune libraries, where clonotype A was private to the lymph nodes, whereas clonotypes B and D were private to the spleen, with C being shared by both tissues (Fig. 4.7 A-D). Repertoire sequencing, however, identified all clonotypes in both tissues by exact matching (Fig. 4.23). The frequencies estimated from cluster size indicate why these clones were not found during library NGS. The sequencing depth in the repertoire analysis was deeper (Fig. 4.20, Fig. 4.7 A-D), and the abundance of clonotype A in the lymph nodes was markedly higher than in the spleen. This also held true for clonotype C (second-most abundant in the lymph nodes). In the spleen, clonotype B had the highest abundance, while clonotype A exhibited the lowest abundance. The absence of clonotype D in the lymph node library, despite repertoire sequencing detection, highlights potential technical or biological constraints [236]. When considering the HD-2 data, it is however remarkable that clonotype D was not identified from the lymph node library, suggesting weaker binding, outgrowth by clonotype A, or loss during library construction. As previously discussed, the resulting V^H CDR3s suggested the individual development of the obtained clones by at least three individual B cells (clonotypes A, B, C), most possibly independently in spleen and lymph nodes. It remains unclear whether the clonotype-expressing cells originate from the same precursor lineage and migrate between tissues after antigen encounter, or whether these clonotypes arose independently within both tissues. The current data do not resolve this question. However, comparison of mutation frequencies from the Sanger sequences revealed that, a certain set of counts is genuinely shared by clones originating from the same tissue, thereby indicating separate origins (clonotype C, Tab. 4.2). Clones L20, L19, L21 and L23 all harbored V^L clonotype 4, absent in spleen derived clones, while incorporating V^H clonotype A, equally absent in the spleen. Despite random V^H-V^L pairing during library assembly, this tissue-specific pairing might be suggestive for the independent origin of the clones.

5.5 Germinal Center Dynamics and Antibody Evolution: Implications for Immunization-induced EBA?

Antibody affinity maturation during GC reactions is a dynamic process where a multiplicity of clones, derived from mature precursor cells exhibiting initial target specificity, compete for signaling and thus survival and expansion [237]. Clones within the GC undergo SHM, during which AID introduces random mutations during the G1 phase of the cell cycle. Despite the availability of numerous studies and predictive models, the exact GC dynamics are not resolved [238].

Based on the assumption that AID-mediated mutation during SHM is undirected, the likelihood of decreasing affinity is higher than the respective increase, Merkenschlager *et al.* described that cells exhibiting optimized binding in fact presented with lower mutation rates (via reduced dwelling time in the G0/G1 transition) and that GC reactions include subsets of B cell clones mutating at different rates [224]. The herein presented clones exhibit high total mutation counts, suggesting elevated GC participation (discussed in Section 5.3.1). Considering recent findings on GC dynamics, the question arises whether the most mutated clones are the actual ones to consider when aiming for the highest affinity. However—in contrast to the described study by Merkenschlager *et al.*, which employed species-foreign antigen(4-hydroxy-3-nitrophenylacetyl conjugated to ovalbumin [224])—the EBA model is one of autoimmunity. The GC reaction is limited by the availability of antigen and follicular T cell help [239], of which the former is a non-limiting factor in the immunization-induced mouse model of EBA due to adjuvant-antigen deposit formation at the site of immunization.

Antibody responses in autoimmune GC reactions have been shown to mutate across complex antigens [240, 241]. Whether assumptions about GC dynamics and clonality also apply to the immunization-induced model of EBA remains to be explored. However, the study by Kovacs *et al.* suggests that due to observed epitope spreading over time, a similar reaction might be present [230].

Antibody feedback, in which previously generated epitope-specific antibodies enter the GC and occupy epitopes, may guide the GC response to epitope spreading, as demonstrated by theoretical models [238]. This may serve as an alternative or complementary solution to epitope spreading in EBA and possibly explain why the herein isolated clones did not exhibit pathogenicity. IgG Aabs are first detectable in EBA 1 week p.I. and peak at weeks 3–6, with first signs of disease visible starting at weeks 4–6 p.I.. Spleens and dLN, used for phage display library assembly, were harvested at week 8 p.I.. It can be

speculated that the antibody response, due to the above-described GC dynamics and mechanisms, had evolved away from epitopes relevant for disease induction by this timepoint. Whether this hypothesis holds true must be verified in future studies through further assessment of Aab clonality and GC dynamics in the immunization-induced model of EBA.

5.6 Limitations of Phage Display

Various selection strategies for phage display have been developed [147] [Chapter 12], [242]. The herein-described procedure of using immobilized antigen on immunotubes for phage selection (section 3.2) has been successfully applied before [243]. However, antigen immobilization may result in the loss of epitopes, either due to conformational changes upon immobilization or lack of exposure of functional epitopes [147] [Chapter 12]. Liquid-phase selection and pull-down of bound antigen-phage complex via introduced biotinylation of antigen may solve these drawbacks [244], though the non-directed nature of biotinylation introduces new epitope-masking risks [245]. These technical limitations highlight the importance of alternative selection approaches. Using full-length antigen expressed on cells [161], or even *in vivo* display [246], may solve the aforementioned drawbacks while introducing substantial technical complexity due to the high antigen density on intact cellular surfaces, thereby necessitating advanced depletion strategies or increased selection rounds [147] [Chapter 12], [242].
The technical challenges of phage display selection mirror clinical observations in AIBDs. A pemphigus study demonstrated that regardless of antigen origin (baculovirus-derived/293T HEK) or presentation format (immobilized vs. liquid-phase), selection consistently favored clones utilizing identical V^H germline segments, which proved non-pathogenic *in vivo* [218]. The authors speculated that the pathogenic antibody clones were present in the library but relative to the non-pathogenic clones in low abundance. This paradox between *in vitro* selection outcomes and clinical pathogenicity was resolved through pre-absorption strategies; blocking immunodominant epitopes with the previously identified non-pathogenic clones enabled isolation of disease-relevant clones employing distinct V^H genes.
Despite mechanistic differences between pemphigus (adhesion disruption [75]) and pemphigoid (Fc-mediated inflammation [80]), these findings collectively suggest that low-abundance clones within the antigen-specific fraction drive pathogenesis while a majority of antibodies target non-pathogenic antigen epitopes. The study by Ishii *et al.* further revealed remarkable restriction of pemphigus Aab to five V^H genes, with a single

scFv clone blocking multiple patient sera through shared epitope recognition [218]. This indicates a shared pathogenicity associated epitope among patients, suggesting a possibly restricted response of pathogenic antibodies, which may also hold true for the case of EBA. Further, repertoire based studies are needed, to very this genetic restriction of Aab diversity in the context of EBA, both for patient obtained samples and the murine model system.
All *in vitro* experiments, including the phage display panning, were conducted using monomeric recombinant mCOLVII^{vWFA2}. However, this may not accurately reflect antigen or epitope availability *in vivo*. As described in Section 1.5.2, COLVII forms homotrimeric structures, which can result in the exposure of novel (3D-multistructure related) epitopes or the masking of others *in vivo*. Furthermore, the antibody response in the immunization-induced EBA model (mCOLVII^{vWFA2}) is characterized by epitope spreading [230]. This process may lead to the recognition of epitopes *in vivo* that are absent from the recombinant mCOLVII^{vWFA2} used for phage display, rendering them unavailable for selection of binding antibodies.

5.7 *In vitro* Characterization Demonstrated Target Specificity, Varying Avidity and Fc Functionality of All IgG2b Clones

All expressed IgG2b clones demonstrated target specificity (Fig. 4.10 A, C1–C7; Fig. 4.14 B, C8, C9), strong concentration-dependent target recognition (Fig. 4.10 B, C1–C7; Fig. 4.14, C8, C9) but varying avidity *in vitro* (Fig. 4.14 C, S1 C1–C7; Fig. 4.14 C, C8, C9). While V^H, particularly via the CDR3 region, is considered the primary contributor to antibody binding [7, 247], the isolated V^L chains exhibited less variability (total mutation counts, Tab. 4.3) and closer germline proximity (Fig. 4.22). Despite this, the binding avidity varied prominently among phage display-derived clones (Fig. 4.14 C). Clones C1 and C2, sharing the same V^H (from phage display clone S4, Tab. 4.2), showed drastic avidity differences (Fig. 4.14 C). Similarly, C5 and C6 (both incorporating V^H from L16 4.5) differed in avidity. Conversely, C2, C3, and C4 (sharing S16-derived V^L) exhibited similar avidity despite divergent V^H compositions. Despite the aforementioned lowered diversity and similarity to naïve sequences the V^L does strongly contribute to the strength of target binding. The avidity differences between phage display clones did however not translate to full-length protein binding (Fig.4.11).
The IgG2b isotype was selected for expression, due to its cumulative described association with pathogenicity, in the immunization-induced model of EBA [27, 93, 118, 127, 129].

As shown in Fig. 1.5 and described in section 1.2, IgG subclasses interact differentially with complement and Fcγ receptors. Although IgG2a/c exhibits the highest affinity for activating FcγRIV (4.7-fold > IgG2b [207]), with IgG2c being the strongest activator, monoclonal IgG2c antibodies failed to induce disease *in vivo* [205]. Similar to IgG2a/c, IgG2b potently activates FcγRIV [28, 67, 68] and fixes complement, unlike IgG1 in most contexts [24]. Complement C_3 deposition, observed in multiple studies [93, 127], leads to C5a generation via the CP, which in turn recruits neutrophils to the site of Aab binding [81, 92, 134, 142, 248, 249].
All ICs, consisting of IgG2b clones and antigen, activated neutrophils *in vitro*, further enhanced by IC opsonization with complement (Fig. 4.12, B, C, C1–C7; Fig. 4.14, D, C8, C9), demonstrating the functionality of the chosen IgG2b Fc portion. Clone C7 showed elevated baseline neutrophil activation without complement-driven amplification, suggesting strong intrinsic activation may overshadow complement effects.

5.8 Repetitive FNIII-like Stretch Results in Increased Binding of mCOLVII^{-C} Antibody Clones

Binding to full-length mCOLVII in skin tissue sections was markedly superior for the mCOLVII^{-C}-targeting clones. The mCOLVII^{-C} fragment lies within the FNIII-like stretch of mCOLVII (Fig. 1.3) [93], which has been suggested to present multiple similar epitopes due to its repetitive nature [128]. Thereby, mCOLVII^{-C}-targeting clones may bind to either multiple epitopes or become strongly deposited due to epitope multiplicity. The vWFA2 domain within the NC-1 of mCOLVII is known to serve as a binding partner for other protein members of the DEJ [87, 110], which might explain both the pathogenicity of Aabs targeting this domain and the non-pathogenicity of the herein presented Aabs due to targeting of disease-irrelevant epitopes. Vorobyey *et al.* have immunized rabbits with different human FNIII fragments. Two of the fragments, exhibiting the highest binding to murine skin sections, were also able to induce skin separation and blistering in COLVII-humanized mice. Epitope mapping of C8 and C9 could further elucidate whether these clones target single FNIII fragments, or multiple as observed by Vorobyey *et al.*, and whether the targeted fragments corresponde to those, used in the COLVII-humanized mouse model of antibody transfer.

5.9 The Aab Response in Immunization-Induced EBA is Dominated by IgG2c/b and IgG1 but May Solely Be Defined by Adjuvant

The immunization-induced model of EBA requires adjuvant to overcome self-tolerance and generate Aab targeting type VII collagen [93, 121]. Adjuvant selection critically shapes the immune response profile, including antibody subclass distribution [228, 250, 251]. Immunization routes may further influence immune cell recruitment and determine the anatomical site of adaptive immunity activation.
TiterMax® Classic adjuvant has been described to induce robust IgG1, IgG2a, and IgG2b titers importantly, independent of the employed antigen for immunization [251–254]. This aligns with the observed IgG2a/b and IgG1 predominance in the BCR lymph node repertoire (Fig. 4.20 B, 4.22 B, S3 C, D) , antigen-specific clones (Fig. 4.23) and the consistently reported serum abundance and issue deposition of Aab in EBA [93, 121, 127, 129]. Together, these data suggest adjuvant-driven Th1 polarization (also experimental dertermined in Hammers *et al.*) rather than antigen-specific mechanisms govern subclass distribution in the immunization-induced model of EBA. This study provides the first genetic-level confirmation of the observed serum IgG subclass patterns, further enabling precise quantification of specific IgG2b Aabs in murine EBA sera via the generated mAbs. The dLN serve as the primary site for mCOLVII-specific plasmablast generation in the mCOLVII^{-C} immunization-induced model of EBA [131]. BCR repertoire analysis confirms dLN dominance, showing expanded class-switched clonotypes versus the spleen's more naïve repertoire (Fig. 4.22 A, B). The proportion of antigen-specific IGH clone enrichment in dLNs (Fig. 4.23) further implicates these structures as hubs for Aab production.

5.10 Antibody Binding and Complement Fixation *in vivo* Does Not Elicit Disease

Despite strong (C8–C9) to intermediate (C1–C6) binding to the DEJ *in vivo* (Fig. 4.19), none of the injected clones elicited dermal-epidermal separation or pathogenicity (Fig. 4.16, 4.18). C8 and C9 activated the complement system, evidenced by C_3 deposition at the DEJ, which confirmed Fc-portion functionality *in vivo*. In contrast, C1–C6 induced only marginal to no C_3 deposition.
All clones harbor the same IgG2b-Fc, suggesting epitope specificity within mCOLVII

drives differential complement activation, as previously discussed in section 5.8. CP activation depends on C_{1q} binding to Ig(G)-Fc fragments, which varies by subclass [24]. Enhanced C_{1q} binding occurs through Fc density and hexameric Fc structures formed by neighboring IgGs [210], a process requiring hinge flexibility for optimal hexamer assembly [255]. Importantly, murine IgG1 has been shown to effectively disrupt hexamerization of other IgG subclasses [256], confronting the previous observations, that in murine EBA, IgG1 antibodies are supposedly the most affinity maturated subclass and possibly pivotal to pathogenicity.
The dense deposition of C8/C9, combined with IgG2b's intermediate hinge flexibility [33], likely facilitates C_{1q} pentamer binding and subsequent C_3 deposition. In contrast, C1–C6 may target spatially clustered epitopes, as suggested by trend-wise marginally increased ROS release *in vitro* when testing clone combinations (Fig. 4.13). Such epitope proximity could sterically hinder Fc-Fc cooperativity, limiting hexamer formation and C_{1q} binding. This aligns with observations that antigen density and epitope spacing critically regulate IgG hexamerization in human systems [210].
Despite complement activation, no neutrophil - or other leukocyte infiltration was observed. Polyclonal rabbit anti-mCOLVII^{-C} IgG, purified non-sterilely, may introduce residual LPS during column purification. Combined with the described reactivity to non-murine rIgG [257], this provides PAMPs/DAMPs that may result in an overall increase immune excited state (LPS) and enhance neutrophil recruitment (xenogeneic reactivity). Models like collagen antibody-induced arthritis intentionally spike mAbs with LPS to amplify inflammation [258, 259]. In contrast, the herein sterilely produced mCOLVII^{-C} clones possibly lack such adjuvants, potentially explaining absent neutrophil recruitment. Determination of the current endotoxin activity in purified rIgG and mAbs, followed by equalizing endotoxin activity by LPS coadministration could test this hypothesis.
Complement activation alone may insufficiently recruit neutrophils. The AP is pivotal in the antibody-mediated EBA model [118]. While AP could amplify CP activation here, it remains unclear whether CP-generated C5a alone may reach thresholds required for leukocyte chemotaxis.

5.11 Lessons to Learn From Antibody Transfer Arthritis Models: The K/BxN Serum Transfer Arthritis Mouse Model.

Arthritis is another Aab-mediated disease that is used to study inflammation following Aab binding to self-antigen. The K/BxN model represents a robust and paradigmatic

example of Aab-induced inflammation [259]. Similar to the situation in EBA, the autoantigen is known (glucose-6-phosphate isomerase (GPI) [260]), and an active model of disease is available, which, notably, is not immunization-induced but develops spontaneously due to the introduction of a transgene (KRN T cell receptor, MHCII Ag7) into mice [261]. Again, similar to EBA, the transfer of Aab from diseased mice into healthy mice results in inflammation and disease in the latter [262]. In addition to other factors, both Fcy receptors and complement have been identified as promoters of inflammation in the K/BxN model, with neutrophils acting as first-line early responders [263, 264], again exhibiting similarity to the EBA mouse model system. Interestingly, the AP of complement activation has been identified as disease-driving [263], whereas the CP has been attributed with less impact, which is again a striking similarity to the Aab transfer model of EBA [118, 265]. The source of Aab has been delineated as the spleen [266]—unlike EBA, which is driven by Aab-producing plasma cells in the dLN [131], likely reflecting the difference between spontaneous disease development and an immunization-induced response.

While the autoantigens are completely unrelated—one being a structural protein (EBA), the other an active enzyme (K/BxN)—the transfer of monoclonal Aab in the K/BxN model has similarly failed to reproduce disease *in vivo* [266]. However, the transfer of pairs or larger pools of monoclonal Aab was highly effective in eliciting arthritis-related inflammation [266]. This requirement for multiple antibodies targeting different epitopes was reflected in the improved formation of ICs, which were able to stimulate effector cells, such as neutrophils, with enhanced efficacy. Interestingly, IgG1 was found to be the predominant subclass required to induce disease by transfer, which contrasts with other arthritis models, where IgG2a antibodies were predominant. Also, IgG1 titers increased with age, with IgG2b and IgG2a present in younger mice [266].

The non-intuitive role of IgG1 in an inflammatory response was attributed to its affinity for FcyRIII (Fig. 1.5), an Fc receptor so far scarcely in the context of EBA, and its capacity, through covalent binding of C_{3b}, to stabilize the AP of complement activation by preventing factor H-mediated inactivation [25]. The identification in this work of IgG1 as an expanded clonotype in the lymph node repertoire gives rise to the speculation that, indeed, IgG1 may, similar to the K/BxN arthritis model, be a relevant candidate for testing in the antibody-transfer model of EBA. Though transfer of rabbit anti-mCOLVII^{-C} IgG into FcyRIII did not affect the extend of disease [135], a fully murine system may confer a different outcome, as rabbits do not express IgG subclasses [267].

5.12 Antibody Glycosylation Patterns Pivotally Impacts Antibody Effector Functions

In the context of murine EBA, IgG1 has mainly been addressed regarding its glycosylation [134], [138], [133] and thereby attributed with an anti-inflammatory role within the involved pathogenicity mechanisms. Numerous studies have shown that N-linked glycosylation of IgG heavily influences downstream effector mechanisms [38], while the choice of adjuvant in turn regulates Fc sialylation during GC reaction [268]. A-fucosylation of antibodies is considered pathogenic, with patient antibodies presenting with a-fucosylated N-glycosylation [269]. Similarly, a-galactosylated antibodies have been associated with pathogenicity [134], [30], while sialylation has been associated with anti-inflammatory effects during IVIG treatment [30]. Importantly Clauder *et al.* demonstrated that IgG1 in disease-permitting H2s haplotype mice shows elevated agalactosylated Fc glycans and reduced sialylation, correlating with enhanced neutrophil ROS release [138], which again points towards a more nuanced role of IgG1 in the pathogenicity of EBA. The exact glycosylation pattern of the herein generated antibodies is unknown. However, expression in CHO cells without specific glycolysation-modifying expression should lead to glycosylated antibodies, presenting core fucosylation, variable galactosylation and low sialylation [270]. To provoke pathogenicity modification of glycosylation is an attractive strategy, also for the presented antibodies.

Chapter 6

Conclusion and Outlook

Aab generation, target binding, and subsequent Aab-mediated inflammation represent the disease-driving factors in EBA. Despite increased knowledge about Aab-mediated effector mechanisms through murine model systems, monoclonal Aab capable of eliciting inflammation upon transfer remain enigmatic in the murine EBA model. This study successfully employed phage display for Aab identification from murine repertoires, combined with NGS to track antigen-specific clonotypes. The subtractive phage display panning strategy proved effective in ensuring isolation of antigen-specific clones; however, usage of the herein generated clones in a modified subtractive panning strategy may prove valuable to isolate clones targeting different epitopes. Based on the herein identified clonotypes, future studies should prioritize isolating distinct clonotypes through modified selection strategies, including epitope blocking with the herein presented antibodies and modified antigen presentation approaches.

This work represents the first approach for a genetic-level analysis of the murine BCR repertoire in EBA research. The genetic characterization of antigen-specific clones verified that the Aab response in murine EBA is driven by class-switched B cells in the draining lymph nodes, with autoreactive B cells participating extensively in GC reactions as evidenced by elevated mutation rates. The restricted V^H V-D-J gene usage and independent emergence of similar clonotypes in spleen and lymph nodes indicate genetic constraints during Aab formation. However, the failure of the generated clones to elicit disease suggests that additional, potentially low-abundance Aab clonotypes with pathogenic potential reside within the repertoire.

The striking shift towards IgG1 in highly mutated clones revealed by NGS challenges the conventional understanding of IgG1 as solely anti-inflammatory in EBA. Evidence from arthritis models demonstrates IgG1 as the disease-driving subclass through AP

complement activation and enhanced FcγRIII engagement. This paradigm shift warrants systematic evaluation of IgG1 versions of the isolated antibodies. Further, the untested clones, based on their CDR3—most likely targeting different epitopes within mCOLVII^{vWFA2}—require systematic investigation. Due to the advantage of knowing the sequences of the isolated clones, all can be recombinantly expressed in various forms, providing a valuable toolbox for EBA research. Antibody- and glycoengineering offer powerful approaches to modulate effector functions through subclass switching, glycan structure modification, and enhanced Fcγ receptor and C_{1q} affinity. Given the complex role of glycosylation in determining pathogenic potential, systematic modification of these parameters may reveal critical determinants of Aab pathogenicity in EBA.

Beyond mechanistic insights, this work provides valuable research tools and potential for therapeutic platforms. The monoclonal antigen-specific antibodies enable quantitative Aab measurement in immunized mouse sera, advancing beyond previous semi-quantitative approaches. These antibodies may serve as targeting vehicles for tissue-specific therapeutic strategies, with several clones already employed for C_5 inhibitor delivery in experimental fusion constructs.

The finding that complement activation alone proved insufficient for leukocyte recruitment and progressive inflammation challenges prevailing paradigms in EBA pathogenesis. These results contradict assumptions that complement-fixing Aab deposition sufficiently induces disease. The data suggest that additional factors—potentially including AP amplification, specific neutrophil Fc receptor engagement patterns, or synergistic antibody combinations—are required for effective inflammatory cell recruitment and tissue injury. This aligns with arthritis model evidence where individual monoclonal antibodies fail to induce disease, while antibody combinations targeting different epitopes prove highly pathogenic.

To determine the temporal evolution of the BCR clonotype composition during disease development, antigen-specific B cell identification coupled with single-cell RNA sequencing could prove valuable. Such an approach would provide further insight into clonal dynamics of mCOLVII^{vWFA2}-reactive B cells throughout the immunization-induced EBA model. This approach would enable tracking of Aab clonality and individual B cell lineages not only across tissues but also across timepoints. In addition, this strategy would enable systematic characterization of Aab-producing B cells, enabling direct comparisons between disease-susceptible versus non-susceptible mice to clarify whether susceptibility stems from epitope specificity or antibody characteristics.

References

1. Martins, Y. C., Ribeiro-Gomes, F. L. & Daniel-Ribeiro, C. T. A Short History of Innate Immunity. *Memorias Do Instituto Oswaldo Cruz* **118,** e230023. ISSN: 1678-8060. pmid: 37162063 (2023).
2. Janeway, C. Approaching the Asymptote? Evolution and Revolution in Immunology. *Cold Spring Harbor Symposia on Quantitative Biology* **54,** 1–13. ISSN: 0091-7451, 1943-4456. http://symposium.cshlp.org/cgi/doi/10.1101/SQB.1989.054.01.003 (2025) (Jan. 1, 1989).
3. Caroll, M. C. & Prodeus, A. P. Linkages of Innate and Adaptive Immunity. *Current Opinion in Immunology* **10,** 36–40. ISSN: 09527915. https://linkinghub.elsevier.com/retrieve/pii/S0952791598800289 (2025) (Feb. 1998).
4. Fuchs, E. J. & Matzinger, P. Is Cancer Dangerous to the Immune System? *Seminars in Immunology* **8,** 271–280. ISSN: 10445323. https://linkinghub.elsevier.com/retrieve/pii/S1044532396900354 (2025) (Oct. 1996).
5. O'Neill, L. A. J., Golenbock, D. & Bowie, A. G. The History of Toll-like Receptors — Redefining Innate Immunity. *Nature Reviews Immunology* **13,** 453–460. ISSN: 1474-1733, 1474-1741. https://www.nature.com/articles/nri3446 (2025) (June 2013).
6. Janeway, C. A. The Immune System Evolved to Discriminate Infectious Nonself from Noninfectious Self. *Immunology Today* **13,** 11–16. ISSN: 01675699. https://linkinghub.elsevier.com/retrieve/pii/016756999290198G (2025) (Jan. 1992).
7. Murphy, K. M. & Weaver, C. *Janeway's Immunobiology* 9th edition. 1 p. ISBN: 978-0-8153-4505-3 (GS, Garland Science, Taylor & Francis Group, New York London, 2017).

8. Chambers, D. A. & Norton, W. E. The Adaptome. *American Journal of Preventive Medicine* **51,** S124–S131. ISSN: 07493797. https://linkinghub.elsevier.com/retrieve/pii/S0749379716301817 (2025) (Oct. 2016).

9. Han, J. & Lotze, M. T. in *Biomarkers for Immunotherapy of Cancer* (eds Thurin, M., Cesano, A. & Marincola, F. M.) 369–397 (Springer New York, New York, NY, 2020). ISBN: 978-1-4939-9772-5. https://link.springer.com/10.1007/978-1-4939-9773-2_17 (2025).

10. Chi, H., Pepper, M. & Thomas, P. G. Principles and Therapeutic Applications of Adaptive Immunity. *Cell* **187,** 2052–2078. ISSN: 1097-4172. pmid: 38670065 (Apr. 25, 2024).

11. Rossjohn, J. *et al.* T Cell Antigen Receptor Recognition of Antigen-Presenting Molecules. *Annual Review of Immunology* **33,** 169–200. ISSN: 0732-0582, 1545-3278. https://www.annualreviews.org/doi/10.1146/annurev-immunol-032414-112334 (2025) (Mar. 21, 2015).

12. Dong, Y. *et al.* Structural Principles of B Cell Antigen Receptor Assembly. *Nature* **612,** 156–161. ISSN: 1476-4687. pmid: 36228656 (Dec. 2022).

13. Pandey, S. *et al.* Antigen and Immunogen: An Investigation into the Heterogeneity of Immunology Terminology in Learning Resources. *ImmunoHorizons* **6,** 312–323. ISSN: 2573-7732. https://academic.oup.com/immunohorizons/article/6/5/312/7816771 (2025) (May 1, 2022).

14. Cooper, M. D. The Early History of B Cells. *Nature Reviews Immunology* **15,** 191–197. ISSN: 1474-1733, 1474-1741. https://www.nature.com/articles/nri3801 (2025) (Mar. 2015).

15. Alt, F. Synthesis of Secreted and Membrane-Bound Immunoglobulin Mu Heavy Chains Is Directed by mRNAs That Differ at Their 3′ Ends. *Cell* **20,** 293–301. ISSN: 00928674. https://linkinghub.elsevier.com/retrieve/pii/0092867480906157 (2025) (June 1980).

16. Cushley, W., Coupar, B. E. H., Mickelson, C. A. & Williamson, A. R. A Common Mechanism for the Synthesis of Membrane and Secreted Immunoglobulin α, γ and μ Chains. *Nature* **298,** 77–79. ISSN: 0028-0836, 1476-4687. https://www.nature.com/articles/298077a0 (2025) (July 1982).

17. Pennell, M., Rodriguez, O. L., Watson, C. T. & Greiff, V. The Evolutionary and Functional Significance of Germline Immunoglobulin Gene Variation. *Trends in Immunology* **44,** 7–21. ISSN: 14714906. https://linkinghub.elsevier.com/retrieve/pii/S1471490622002368 (2025) (Jan. 2023).

18. Hozumi, N. & Tonegawa, S. Evidence for Somatic Rearrangement of Immunoglobulin Genes Coding for Variable and Constant Regions. *Proceedings of the National Academy of Sciences* **73,** 3628–3632. ISSN: 0027-8424, 1091-6490. https://pnas.org/doi/full/10.1073/pnas.73.10.3628 (2025) (Oct. 1976).

19. Tonegawa, S. Somatic Generation of Antibody Diversity. *Nature* **302,** 575–581. ISSN: 0028-0836, 1476-4687. https://www.nature.com/articles/302575a0 (2025) (Apr. 1983).

20. Rajewsky, K. Clonal Selection and Learning in the Antibody System. *Nature* **381,** 751–758. ISSN: 0028-0836, 1476-4687. https://www.nature.com/articles/381751a0 (2025) (June 27, 1996).

21. Mhanna, V. *et al.* Adaptive Immune Receptor Repertoire Analysis. *Nature Reviews Methods Primers* **4,** 6. ISSN: 2662-8449. https://www.nature.com/articles/s43586-023-00284-1 (2025) (Jan. 25, 2024).

22. Schroeder, H. W. & Cavacini, L. Structure and Function of Immunoglobulins. *Journal of Allergy and Clinical Immunology* **125,** S41–S52. ISSN: 00916749. https://linkinghub.elsevier.com/retrieve/pii/S0091674909014651 (2025) (Feb. 2010).

23. Giudicelli, V., Chaume, D. & Lefranc, M.-P. IMGT/GENE-DB: A Comprehensive Database for Human and Mouse Immunoglobulin and T Cell Receptor Genes. *Nucleic Acids Research* **33,** D256–261. ISSN: 1362-4962. pmid: 15608191 (Database issue Jan. 1, 2005).

24. Neuberger, M. S. & Rajewsky, K. Activation of Mouse Complement by Monoclonal Mouse Antibodies. *European Journal of Immunology* **11,** 1012–1016. ISSN: 00142980, 15214141. https://onlinelibrary.wiley.com/doi/10.1002/eji.1830111212 (2023) (1981).

25. Klaus, G. G., Pepys, M. B., Kitajima, K. & Askonas, B. A. Activation of Mouse Complement by Different Classes of Mouse Antibody. *Immunology* **38,** 687–695. ISSN: 0019-2805. pmid: 521057 (Dec. 1979).

26. Cho, H. J., Lee, I. J. & Kim, S. C. Complement-Fixing Abilities and IgG Subclasses of Autoantibodies in Epidermolysis Bullosa Acquisita. *Yonsei Medical Journal* **39,** 339. ISSN: 0513-5796. https://eymj.org/DOIx.php?id=10.3349/ymj.1998.39.4.339 (2024) (1998).

27. Sitaru, C., Mihai, S. & Zillikens, D. The Relevance of the IgG Subclass of Autoantibodies for Blister Induction in Autoimmune Bullous Skin Diseases. *Archives of Dermatological Research* **299,** 1–8. ISSN: 0340-3696, 1432-069X. https://link.springer.com/10.1007/s00403-007-0734-0 (2024) (Apr. 2007).

28. Nimmerjahn, F. *et al.* FcγRIV Deletion Reveals Its Central Role for IgG2a and IgG2b Activity in Vivo. *Proceedings of the National Academy of Sciences* **107,** 19396–19401. ISSN: 0027-8424, 1091-6490. https://pnas.org/doi/full/10.1073/pnas.1014515107 (2025) (Nov. 9, 2010).

29. Vidarsson, G., Dekkers, G. & Rispens, T. IgG Subclasses and Allotypes: From Structure to Effector Functions. *Frontiers in Immunology* **5.** ISSN: 1664-3224. http://www.frontiersin.org/Immunotherapies_and_Vaccines/10.3389/fimmu.2014.00520/abstract (2025) (Oct. 20, 2014).

30. Collin, M. & Ehlers, M. The Carbohydrate Switch between Pathogenic and Immunosuppressive Antigen-specific Antibodies. *Experimental Dermatology* **22,** 511–514. ISSN: 0906-6705, 1600-0625. https://onlinelibrary.wiley.com/doi/10.1111/exd.12171 (2024) (Aug. 2013).

31. Mishell, R. I. & Fahey, J. L. MOLECULAR AND SUBMOLECULAR LOCALIZATION OF TWO ISOANTIGENS OF MOUSE IMMUNOGLOBULINS. *Science (New York, N.Y.)* **143,** 1440–1442. ISSN: 0036-8075. pmid: 14112710 (Mar. 27, 1964).

32. Fahey, J. L., Wunderlich, J. & Mishell, R. THE IMMUNOGLOBULINS OF MICE. II. TWO SUBCLASSES OF MOUSE 7S GAMMA-2-GLOBULINS: GAMMA-2A- AND GAMMA-2B-GLOBULINS. *The Journal of Experimental Medicine* **120,** 243–251. ISSN: 0022-1007. pmid: 14206439 (Aug. 1, 1964).

33. Kolenko, P. *et al.* New Insights into Intra- and Intermolecular Interactions of Immunoglobulins: Crystal Structure of Mouse IgG2b-Fc at 2·1-Å Resolution. *Immunology* **126,** 378–385. ISSN: 0019-2805, 1365-2567. https://onlinelibrary.wiley.com/doi/10.1111/j.1365-2567.2008.02904.x (2025) (Mar. 2009).

34. Lefranc, M.-P. & Lefranc, G. *The Immunoglobulin FactsBook* 676 pp. ISBN: 978-0-08-057447-9 (Elsevier Science, Burlington, 2001).

35. Volkov, M. *et al.* Comprehensive Overview of Autoantibody Isotype and Subclass Distribution. *Journal of Allergy and Clinical Immunology* **150,** 999–1010. ISSN: 00916749. https://linkinghub.elsevier.com/retrieve/pii/S0091674922008454 (2025) (Nov. 2022).

36. Kim, H., Matsunaga, C., Yoshino, A., Kato, K. & Arata, Y. Dynamical Structure of the Hinge Region of Immunoglobulin G as Studied by 13C Nuclear Magnetic Resonance Spectroscopy. *Journal of Molecular Biology* **236,** 300–309. ISSN: 00222836. https://linkinghub.elsevier.com/retrieve/pii/S0022283684711363 (2025) (Feb. 1994).

37. Kim, H. *et al.* O-Glycosylation in Hinge Region of Mouse Immunoglobulin G2b. *The Journal of Biological Chemistry* **269,** 12345–12350. ISSN: 0021-9258. pmid: 7512967 (Apr. 22, 1994).

38. Damelang, T. *et al.* Impact of Structural Modifications of IgG Antibodies on Effector Functions. *Frontiers in Immunology* **14,** 1304365. ISSN: 1664-3224. https://www.frontiersin.org/articles/10.3389/fimmu.2023.1304365/full (2025) (Jan. 8, 2024).

39. Albert, H., Collin, M., Dudziak, D., Ravetch, J. V. & Nimmerjahn, F. *In Vivo* Enzymatic Modulation of IgG Glycosylation Inhibits Autoimmune Disease in an IgG Subclass-Dependent Manner. *Proceedings of the National Academy of Sciences* **105,** 15005–15009. ISSN: 0027-8424, 1091-6490. https://pnas.org/doi/full/10.1073/pnas.0808248105 (2025) (Sept. 30, 2008).

40. Kao, D. *et al.* A Monosaccharide Residue Is Sufficient to Maintain Mouse and Human IgG Subclass Activity and Directs IgG Effector Functions to Cellular Fc Receptors. *Cell Reports* **13,** 2376–2385. ISSN: 22111247. https://linkinghub.elsevier.com/retrieve/pii/S2211124715013273 (2024) (Dec. 2015).

41. Dekkers, G., Rispens, T. & Vidarsson, G. Novel Concepts of Altered Immunoglobulin G Galactosylation in Autoimmune Diseases. *Frontiers in Immunology* **9,** 553. ISSN: 1664-3224. http://journal.frontiersin.org/article/10.3389/fimmu.2018.00553/full (2024) (Mar. 19, 2018).

42. Collins, A. M., Wang, Y., Roskin, K. M., Marquis, C. P. & Jackson, K. J. L. The Mouse Antibody Heavy Chain Repertoire Is Germline-Focused and Highly Variable between Inbred Strains. *Philosophical Transactions of the Royal Society of London. Series B, Biological Sciences* **370,** 20140236. ISSN: 1471-2970. pmid: 26194750 (Sept. 5, 2015).

43. Lefranc, M.-P. IMGT, the International ImMunoGeneTics Database. *Nucleic Acids Research* **29,** 207–209. ISSN: 13624962. https://academic.oup.com/nar/article-lookup/doi/10.1093/nar/29.1.207 (2025) (Jan. 1, 2001).

44. Aoki-Ota, M., Torkamani, A., Ota, T., Schork, N. & Nemazee, D. Skewed Primary Igκ Repertoire and V–J Joining in C57BL/6 Mice: Implications for Recombination Accessibility and Receptor Editing. *The Journal of Immunology* **188,** 2305–2315. ISSN: 0022-1767, 1550-6606. https://academic.oup.com/jimmunol/article/188/5/2305/7981448 (2025) (Mar. 1, 2012).

45. Jackson, K. J. L. *et al.* A BALB/c IGHV Reference Set, Defined by Haplotype Analysis of Long-Read VDJ-C Sequences From F1 (BALB/c x C57BL/6) Mice. *Frontiers in Immunology* **13,** 888555. ISSN: 1664-3224. https://www.frontiersin.org/articles/10.3389/fimmu.2022.888555/full (2025) (June 3, 2022).

46. Nemazee, D. Mechanisms of Central Tolerance for B Cells. *Nature Reviews Immunology* **17,** 281–294. ISSN: 1474-1733, 1474-1741. https://www.nature.com/articles/nri.2017.19 (2025) (May 2017).

47. Mattos, M. S., Vandendriessche, S., Waisman, A. & Marques, P. E. The Immunology of B-1 Cells: From Development to Aging. *Immunity & Ageing* **21,** 54. ISSN: 1742-4933. https://immunityageing.biomedcentral.com/articles/10.1186/s12979-024-00455-y (2024) (Aug. 2, 2024).

48. Petersone, L. *et al.* T Cell/B Cell Collaboration and Autoimmunity: An Intimate Relationship. *Frontiers in Immunology* **9,** 1941. ISSN: 1664-3224. pmid: 30210496 (2018).

49. Crotty, S. A Brief History of T Cell Help to B Cells. *Nature Reviews Immunology* **15,** 185–189. ISSN: 1474-1733, 1474-1741. https://www.nature.com/articles/nri3803 (2025) (Mar. 2015).

50. Hershberg, U. & Luning Prak, E. T. The Analysis of Clonal Expansions in Normal and Autoimmune B Cell Repertoires. *Philosophical Transactions of the Royal Society of London. Series B, Biological Sciences* **370,** 20140239. ISSN: 1471-2970. pmid: 26194753 (Sept. 5, 2015).

51. Theofilopoulos, A. N., Kono, D. H. & Baccala, R. The Multiple Pathways to Autoimmunity. *Nature Immunology* **18,** 716–724. ISSN: 1529-2908, 1529-2916. https://www.nature.com/articles/ni.3731 (2024) (July 2017).

52. Burnet, F. M. *The Clonal Selection Theory of Acquired Immunity* https://www.biodiversitylibrary.org/bibliography/8281 (2025) (Vanderbilt University Press, Nashville, 1959).

53. Nemazee, D. Antigen Receptor 'capacity' and the Sensitivity of Self-Tolerance. *Immunology Today* **17,** 25–29. ISSN: 0167-5699. pmid: 8652047 (Jan. 1996).

54. Goodnow, C. C. *et al.* Altered Immunoglobulin Expression and Functional Silencing of Self-Reactive B Lymphocytes in Transgenic Mice. *Nature* **334,** 676–682. ISSN: 0028-0836, 1476-4687. nee (2025) (Aug. 1988).

55. Duong, B. H. *et al.* Decoration of T-independent Antigen with Ligands for CD22 and Siglec-G Can Suppress Immunity and Induce B Cell Tolerance in Vivo. *The Journal of Experimental Medicine* **207,** 173–187. ISSN: 1540-9538. pmid: 20038598 (Jan. 18, 2010).

56. Nemazee, D. Receptor Editing in Lymphocyte Development and Central Tolerance. *Nature Reviews Immunology* **6,** 728–740. ISSN: 1474-1733, 1474-1741. https://www.nature.com/articles/nri1939 (2025) (Oct. 1, 2006).

57. Hampe, C. S. B Cells in Autoimmune Diseases. *Scientifica* **2012,** 1–18. ISSN: 2090-908X. http://www.hindawi.com/journals/scientifica/2012/215308/ (2025) (2012).

58. Linterman, M. A. *et al.* Follicular Helper T Cells Are Required for Systemic Autoimmunity. *Journal of Experimental Medicine* **206,** 561–576. ISSN: 1540-9538, 0022-1007. https://rupress.org/jem/article/206/3/561/40461/Follicular-helper-T-cells-are-required-for (2025) (Mar. 16, 2009).

59. Lee, D. S. W., Rojas, O. L. & Gommerman, J. L. B Cell Depletion Therapies in Autoimmune Disease: Advances and Mechanistic Insights. *Nature Reviews Drug Discovery* **20,** 179–199. ISSN: 1474-1776, 1474-1784. https://www.nature.com/articles/s41573-020-00092-2 (2025) (Mar. 2021).

60. Rawlings, D. J., Metzler, G., Wray-Dutra, M. & Jackson, S. W. Altered B Cell Signalling in Autoimmunity. *Nature Reviews Immunology* **17,** 421–436. ISSN: 1474-1733, 1474-1741. https://www.nature.com/articles/nri.2017.24 (2024) (July 2017).

61. Cooper, G. S. & Stroehla, B. C. The Epidemiology of Autoimmune Diseases. *Autoimmunity Reviews* **2,** 119–125. ISSN: 15689972. https://linkinghub.elsevier.com/retrieve/pii/S1568997203000065 (2025) (May 2003).

62. Xu, X. *et al.* Inhibition of Increased Circulating Tfh Cell by Anti-CD20 Monoclonal Antibody in Patients with Type 1 Diabetes. *PLoS ONE* **8** (ed Xu, A.) e79858. ISSN: 1932-6203. https://dx.plos.org/10.1371/journal.pone.0079858 (2025) (Nov. 20, 2013).

63. Tabrizi, M., Bornstein, G. G. & Suria, H. Biodistribution Mechanisms of Therapeutic Monoclonal Antibodies in Health and Disease. *The AAPS journal* **12,** 33–43. ISSN: 1550-7416. pmid: 19924542 (Mar. 2010).

64. Meyer-Hermann, M. Injection of Antibodies against Immunodominant Epitopes Tunes Germinal Centers to Generate Broadly Neutralizing Antibodies. *Cell Reports* **29,** 1066–1073.e5. ISSN: 22111247. https://linkinghub.elsevier.com/retrieve/pii/S2211124719312550 (2024) (Oct. 2019).

65. Barrington, R., Zhang, M., Fischer, M. & Carroll, M. C. The Role of Complement in Inflammation and Adaptive Immunity. *Immunological Reviews* **180,** 5–15. ISSN: 0105-2896, 1600-065X. https://onlinelibrary.wiley.com/doi/10.1034/j.1600-065X.2001.1800101.x (2024) (Apr. 2001).

66. Dunkelberger, J. R. & Song, W.-C. Complement and Its Role in Innate and Adaptive Immune Responses. *Cell Research* **20,** 34–50. ISSN: 1001-0602, 1748-7838. https://www.nature.com/articles/cr2009139 (2024) (Jan. 2010).

67. Nimmerjahn, F. & Ravetch, J. V. Divergent Immunoglobulin G Subclass Activity Through Selective Fc Receptor Binding. *Science* **310,** 1510–1512. ISSN: 0036-8075, 1095-9203. https://www.science.org/doi/10.1126/science.1118948 (2024) (Dec. 2, 2005).

68. Bruhns, P. Properties of Mouse and Human IgG Receptors and Their Contribution to Disease Models. *Blood* **119,** 5640–5649. ISSN: 0006-4971, 1528-0020. https://ashpublications.org/blood/article/119/24/5640/30328/Properties-of-mouse-and-human-IgG-receptors-and (2023) (June 14, 2012).

69. Hematianlarki, M. & Nimmerjahn, F. Immunomodulatory and Anti-inflammatory Properties of Immunoglobulin G Antibodies. *Immunological Reviews* **328,** 372–386. ISSN: 0105-2896, 1600-065X. https://onlinelibrary.wiley.com/doi/10.1111/imr.13404 (2025) (Nov. 2024).

70. Siloşi, I. *et al.* The Role of Autoantibodies in Health and Disease. *Romanian Journal of Morphology and Embryology = Revue Roumaine De Morphologie Et Embryologie* **57,** 633–638. ISSN: 2066-8279. pmid: 27833954 (2 Suppl 2016).

71. Ludwig, R. J. *et al.* Mechanisms of Autoantibody-Induced Pathology. *Frontiers in Immunology* **8,** 603. ISSN: 1664-3224. http://journal.frontiersin.org/article/10.3389/fimmu.2017.00603/full (2025) (May 31, 2017).

72. Haller-Kikkatalo, K. *et al.* Demographic Associations for Autoantibodies in Disease-Free Individuals of a European Population. *Scientific Reports* **7,** 44846. ISSN: 2045-2322. https://www.nature.com/articles/srep44846 (2025) (Mar. 28, 2017).

73. Ma, H., Murphy, C., Loscher, C. E. & O'Kennedy, R. Autoantibodies - Enemies, and/or Potential Allies? *Frontiers in Immunology* **13,** 953726. ISSN: 1664-3224. https://www.frontiersin.org/articles/10.3389/fimmu.2022.953726/full (2025) (Oct. 19, 2022).

74. Stevens, N. E., Cowin, A. J. & Kopecki, Z. Skin Barrier and Autoimmunity—Mechanisms and Novel Therapeutic Approaches for Autoimmune Blistering Diseases of the Skin. *Frontiers in Immunology* **10,** 1089. ISSN: 1664-3224. https://www.frontiersin.org/article/10.3389/fimmu.2019.01089/full (2025) (May 14, 2019).

75. Schmidt, E., Kasperkiewicz, M. & Joly, P. Pemphigus. *The Lancet* **394,** 882–894. ISSN: 01406736. https://linkinghub.elsevier.com/retrieve/pii/S0140673619317787 (2025) (Sept. 2019).

76. Van Beek, N. *et al.* State-of-the-Art Diagnosis of Autoimmune Blistering Diseases. *Frontiers in Immunology* **15,** 1363032. ISSN: 1664-3224. https://www.frontiersin.org/articles/10.3389/fimmu.2024.1363032/full (2025) (June 6, 2024).

77. Akbarialiabad, H. *et al.* Bullous Pemphigoid. *Nature Reviews Disease Primers* **11,** 12. ISSN: 2056-676X. https://www.nature.com/articles/s41572-025-00595-5 (2025) (Feb. 20, 2025).

78. Tigges, M. *et al.* Pemphigoid Disease Model Systems for Clinical Translation. *Frontiers in Immunology* **16,** 1537428. ISSN: 1664-3224. pmid: 40165962 (2025).

79. Koga, H. *et al.* Epidermolysis Bullosa Acquisita: The 2019 Update. *Frontiers in Medicine* **5.** ISSN: 2296-858X. https://www.frontiersin.org/articles/10.3389/fmed.2018.00362 (2019).

80. Bieber, K., Koga, H. & Nishie, W. In Vitro and in Vivo Models to Investigate the Pathomechanisms and Novel Treatments for Pemphigoid Diseases. *Experimental Dermatology* **26,** 1163–1170. ISSN: 09066705. https://onlinelibrary.wiley.com/doi/10.1111/exd.13415 (2023) (Dec. 2017).

81. Kasperkiewicz, M. *et al.* Epidermolysis Bullosa Acquisita: From Pathophysiology to Novel Therapeutic Options. *Journal of Investigative Dermatology* **136,** 24–33. ISSN: 0022202X. http://linkinghub.elsevier.com/retrieve/pii/S0022202X15000068 (2023) (Jan. 2016).

82. Tešanović Perković, D., Bukvić Mokos, Z. & Marinović, B. Epidermolysis Bullosa Acquisita—Current and Emerging Treatments. *Journal of Clinical Medicine* **12,** 1139. ISSN: 2077-0383. https://www.mdpi.com/2077-0383/12/3/1139 (2025) (Feb. 1, 2023).

83. Gammon, W. R. *et al.* Autoantibodies to Type VII Collagen Recognize Epitopes in a Fibronectin-Like Region of the Noncollagenous (NC1) Domain. *Journal of Investigative Dermatology* **100,** 618–622. ISSN: 0022202X. https://linkinghub.elsevier.com/retrieve/pii/S0022202X9390003Z (2023) (May 1993).

84. Müller, R. *et al.* T and B Cells Target Identical Regions of the Non-Collagenous Domain 1 of Type VII Collagen in Epidermolysis Bullosa Acquisita. *Clinical Immunology* **135,** 99–107. ISSN: 15216616. https://linkinghub.elsevier.com/retrieve/pii/S1521661609009188 (2025) (Apr. 2010).

85. Lapiere, J. C. *et al.* Epitope Mapping of Type VII Collagen. Identification of Discrete Peptide Sequences Recognized by Sera from Patients with Acquired Epidermolysis Bullosa. *The Journal of Clinical Investigation* **92,** 1831–1839. ISSN: 0021-9738. pmid: 7691888 (Oct. 1993).

86. Wegener, H., Leineweber, S. & Seeger, K. The vWFA2 Domain of Type VII Collagen Is Responsible for Collagen Binding. *Biochemical and Biophysical Research Communications* **430,** 449–453. ISSN: 0006291X. https://linkinghub.elsevier.com/retrieve/pii/S0006291X12023534 (2025) (Jan. 2013).

87. Gebauer, J. M. *et al.* Structural and Biophysical Characterization of the Type VII Collagen vWFA2 Subdomain Leads to Identification of Two Binding Sites. *FEBS Open Bio* **10,** 580–592. ISSN: 2211-5463, 2211-5463. https://febs.onlinelibrary.wiley.com/doi/10.1002/2211-5463.12807 (2024) (Apr. 2020).

88. Prost-Squarcioni, C. *et al.* International Bullous Diseases Group: Consensus on Diagnostic Criteria for Epidermolysis Bullosa Acquisita. *British Journal of Dermatology* **179,** 30–41. ISSN: 00070963. https://academic.oup.com/bjd/article/179/1/30/6732306 (2025) (July 2018).

89. Woodley, D. T., Briggaman, R. A., Gammon, W. & O'Keefe, E. J. Epidermolysis Bullosa Acquisita Antigen Is Synthesized by Human Keratinocytes Cultured in Serum-Free Medium. *Biochemical and Biophysical Research Communications* **130,** 1267–1272. ISSN: 0006291X. https://linkinghub.elsevier.com/retrieve/pii/0006291X85917516 (2023) (Aug. 1985).

90. Woodley, D. T. *et al.* Epidermolysis Bullosa Acquisita Antigen, a New Major Component of Cutaneous Basement Membrane, Is a Glycoprotein with Collagenous Domains. *Journal of Investigative Dermatology* **86,** 668–672. ISSN: 0022202X. https://linkinghub.elsevier.com/retrieve/pii/S0022202X86900461 (2023) (June 1986).

91. Woodley, D. T. *et al.* Epidermolysis Bullosa Acquisita Antigen Is the Globular Carboxyl Terminus of Type VII Procollagen. *Journal of Clinical Investigation* **81,** 683–687. ISSN: 0021-9738. http://www.jci.org/articles/view/113373 (2023) (Mar. 1, 1988).

92. Sitaru, C. *et al.* Induction of Dermal-Epidermal Separation in Mice by Passive Transfer of Antibodies Specific to Type VII Collagen. *Journal of Clinical Investigation* **115,** 870–878. ISSN: 0021-9738. http://www.jci.org/articles/view/21386 (2023) (Apr. 1, 2005).

93. Sitaru, C. *et al.* Induction of Complement-Fixing Autoantibodies against Type VII Collagen Results in Subepidermal Blistering in Mice. *The Journal of Immunology* **177,** 3461–3468. ISSN: 0022-1767, 1550-6606. https://journals.aai.org/jimmunol/article/177/5/3461/37942/Induction-of-Complement-Fixing-Autoantibodies (2023) (Sept. 1, 2006).

94. Sasai, Y. & Fujiyama, T. Histochemical Study on the Pathogenesis of *Epidermolysis Bullosa Acquisita*. *The Tohoku Journal of Experimental Medicine* **99,** 9–17. ISSN: 0040-8727, 1349-3329. http://www.jstage.jst.go.jp/article/tjem1920/99/1/99_1_9/_article (2023) (1969).

95. Roenigk, H. H. Epidermolysis Bullosa Acquisita: Report of Three Cases and Review of All Published Cases. *Archives of Dermatology* **103,** 1. ISSN: 0003-987X. http://archderm.jamanetwork.com/article.aspx?doi=10.1001/archderm.1971.04000130003001 (2025) (Jan. 1, 1971).

96. Kushniruk, W. The Immunopathology of Epidermolysis Bullosa Acquisita. *Canadian Medical Association Journal* **108,** 1143–1146. ISSN: 0008-4409. pmid: 4574408 (May 5, 1973).

97. Paller, A. S. *et al.* A Mouse Monoclonal Antibody Against a Newly Discovered Basement Membrane Component, the Epidermolysis Bullosa Acquisita Antigen. *Journal of Investigative Dermatology* **84,** 215–217. ISSN: 0022202X. https://linkinghub.elsevier.com/retrieve/pii/S0022202X15436279 (2023) (Mar. 1985).

98. Ray Gammon, W., Inman, A. O. & Wheeler, C. E. Differences in Complement-Dependent Chemotactic Activity Generated by Bullous Pemphigoid and Epidermolysis Bullosa Acquisita Immune Complexes: Demonstration by Leukocytic Attachment and Organ Culture Methods. *Journal of Investigative Dermatology* **83,** 57–61. ISSN: 0022202X. https://linkinghub.elsevier.com/retrieve/pii/S0022202X15434396 (2023) (July 1984).

99. Gammon, W. R. & Briggaman, R. A. Functional Heterogeneity of Immune Complexes in Epidermolysis Bullosa Acquisita. *Journal of Investigative Dermatology* **89,** 478–483. ISSN: 0022202X. https://linkinghub.elsevier.com/retrieve/pii/S0022202X87900674 (2023) (Nov. 1987).

100. Leigh, I. M., Purkis, P. E. & Bruckner-Tuderman, L. LH7.2 Monoclonal Antibody Detects Type VII Collagen in the Sublamina Densa Zone of Ectodermally-Derived Epithelia, Including Skin. *Epithelia* **1,** 17–29 (1987).

101. Shigemoto, T., Nashiro, K., Tsuchida, T., Seki, Y. & Tamaki, K. Administration of IgG Fraction of Epidermolysis Bullosa Acquisita (EBA) Serum into Mice. *The Journal of Dermatology* **15,** 123–127. ISSN: 03852407. https://onlinelibrary.wiley.com/doi/10.1111/j.1346-8138.1988.tb03663.x (2023) (Apr. 1988).

102. Mestas, J. & Hughes, C. C. W. Of Mice and Not Men: Differences between Mouse and Human Immunology. *The Journal of Immunology* **172,** 2731–2738. ISSN: 0022-1767, 1550-6606. https://journals.aai.org/jimmunol/article/172/5/2731/82520/Of-Mice-and-Not-Men-Differences-between-Mouse-and (2023) (Mar. 1, 2004).

103. Lux, A. & Nimmerjahn, F. Of Mice and Men: The Need for Humanized Mouse Models to Study Human IgG Activity in Vivo. *Journal of Clinical Immunology* **33,** 4–8. ISSN: 0271-9142, 1573-2592. http://link.springer.com/10.1007/s10875-012-9782-0 (2023) (Jan. 2013).

104. Sadeghi, H. *et al.* The Retinoid-Related Orphan Receptor Alpha Is Essential for the End-Stage Effector Phase of Experimental Epidermolysis Bullosa Acquisita: RORα in EBA. *The Journal of Pathology* **237,** 111–122. ISSN: 00223417. https://onlinelibrary.wiley.com/doi/10.1002/path.4556 (2023) (Sept. 2015).

105. Uitto, J., Chung-Honet, L. C. & Christiano, A. M. Molecular Biology and Pathology of Type VII Collagen*. *Experimental Dermatology* **1,** 2–11. ISSN: 0906-6705, 1600-0625. https://onlinelibrary.wiley.com/doi/10.1111/j.1600-0625.1992.tb00065.x (2025) (Feb. 1992).

106. Parente, M. G. *et al.* Human Type VII Collagen: cDNA Cloning and Chromosomal Mapping of the Gene. *Proceedings of the National Academy of Sciences* **88,** 6931–6935. ISSN: 0027-8424, 1091-6490. https://pnas.org/doi/full/10.1073/pnas.88.16.6931 (2025) (Aug. 15, 1991).

107. Tanaka, T., Takahashi, K., Furukawa, F. & Imamura, S. Molecular Cloning and Characterization of Type VII Collagen cDNA. *Biochemical and Biophysical Research Communications* **183,** 958–963. ISSN: 0006291X. https://linkinghub.elsevier.com/retrieve/pii/S0006291X05802839 (2023) (Mar. 1992).

108. Villone, D. *et al.* Supramolecular Interactions in the Dermo-epidermal Junction Zone. *Journal of Biological Chemistry* **283,** 24506–24513. ISSN: 00219258. https://linkinghub.elsevier.com/retrieve/pii/S0021925819491965 (2025) (Sept. 2008).

109. Woodley, D. T., Hou, Y., Martin, S., Li, W. & Chen, M. Characterization of Molecular Mechanisms Underlying Mutations in Dystrophic Epidermolysis Bullosa Using Site-Directed Mutagenesis. *The Journal of Biological Chemistry* **283,** 17838–17845. ISSN: 0021-9258. pmid: 18450758 (June 27, 2008).

110. Leineweber, S., Schönig, S. & Seeger, K. Insight into Interactions of the Von-Willebrand-factor-A-like Domain 2 with the FNIII-like Domain 9 of Collagen VII by NMR and SPR. *FEBS Letters* **585,** 1748–1752. ISSN: 00145793. http://doi.wiley.com/10.1016/j.febslet.2011.04.071 (2024) (June 23, 2011).

111. Colombo, M. *et al.* Procollagen VII Self-Assembly Depends on Site-Specific Interactions and Is Promoted by Cleavage of the NC2 Domain with Procollagen C-proteinase. *Biochemistry* **42,** 11434–11442. ISSN: 0006-2960. pmid: 14516194 (Oct. 7, 2003).

112. Chung, H. J. & Uitto, J. Type VII Collagen: The Anchoring Fibril Protein at Fault in Dystrophic Epidermolysis Bullosa. *Dermatologic Clinics* **28,** 93–105. ISSN: 1558-0520. pmid: 19945621 (Jan. 2010).

113. Lapiere, J.-C. *et al.* Type VII Collagen Specifically Binds Fibronectin via a Unique Subdomain Within the Collagenous Triple Helix. *Journal of Investigative Dermatology*

103, 637–641. ISSN: 0022202X. https://linkinghub.elsevier.com/retrieve/pii/S0022202X94904294 (2025) (Nov. 1994).

114. Ludwig, R. J. Clinical Presentation, Pathogenesis, Diagnosis, and Treatment of Epidermolysis Bullosa Acquisita. *ISRN dermatology* **2013,** 812029. ISSN: 2090-4592. pmid: 23956869 (2013).

115. Yoshiike, T., Woodley, D. T. & Briggaman, R. A. Epidermolysis Bullosa Acquisita Antigen: Relationship between the Collagenase-Sensitive and -Insensitive Domains. *The Journal of Investigative Dermatology* **90,** 127–133. ISSN: 0022-202X. pmid: 2828479 (Feb. 1988).

116. Sitaru, C., Kromminga, A., Hashimoto, T., Bröcker, E. B. & Zillikens, D. Autoantibodies to Type VII Collagen Mediate Fcγ-Dependent Neutrophil Activation and Induce Dermal-Epidermal Separation in Cryosections of Human Skin. *The American Journal of Pathology* **161,** 301–311. ISSN: 00029440. https://linkinghub.elsevier.com/retrieve/pii/S000294401064182X (2025) (July 2002).

117. Woodley, D. T. *et al.* Induction of Epidermolysis Bullosa Acquisita in Mice by Passive Transfer of Autoantibodies from Patients. *Journal of Investigative Dermatology* **126,** 1323–1330. ISSN: 0022202X. https://linkinghub.elsevier.com/retrieve/pii/S0022202X15329213 (2023) (June 2006).

118. Mihai, S. *et al.* The Alternative Pathway of Complement Activation Is Critical for Blister Induction in Experimental Epidermolysis Bullosa Acquisita. *The Journal of Immunology* **178,** 6514–6521. ISSN: 0022-1767, 1550-6606. https://journals.aai.org/jimmunol/article/178/10/6514/74089/The-Alternative-Pathway-of-Complement-Activation (2023) (May 15, 2007).

119. Sesarman, A. *et al.* Binding of Avian IgY to Type VII Collagen Does Not Activate Complement and Leucocytes and Fails to Induce Subepidermal Blistering in Mice: Binding of Avian IgY to Type VII Collagen. *British Journal of Dermatology* **158,** 463–471. ISSN: 00070963, 13652133. https://academic.oup.com/bjd/article/158/3/463/6643789 (2024) (Jan. 17, 2008).

120. Sesarman, A., Sitaru, A. G., Olaru, F., Zillikens, D. & Sitaru, C. Neonatal Fc Receptor Deficiency Protects from Tissue Injury in Experimental Epidermolysis Bullosa Acquisita. *Journal of Molecular Medicine* **86,** 951–959. ISSN: 0946-2716, 1432-1440. http://link.springer.com/10.1007/s00109-008-0366-7 (2024) (Aug. 2008).

121. Iwata, H. *et al.* B Cells, Dendritic Cells, and Macrophages Are Required To Induce an Autoreactive CD4 Helper T Cell Response in Experimental Epidermolysis Bullosa Acquisita. *The Journal of Immunology* **191,** 2978–2988. ISSN: 0022-1767, 1550-6606. https://journals.aai.org/jimmunol/article/191/6/2978/40902/B-Cells-Dendritic-Cells-and-Macrophages-Are (2023) (Sept. 15, 2013).

122. Bieber, K. *et al.* Animal Models for Autoimmune Bullous Dermatoses: Animal Models for Autoimmune Skin Blistering Diseases. *Experimental Dermatology* **19,** 2–11. ISSN: 09066705, 16000625. https://onlinelibrary.wiley.com/doi/10.1111/j.1600-0625.2009.00948.x (2023) (Jan. 2010).

123. Csorba, K. *et al.* Cross-Reactivity of Autoantibodies from Patients with Epidermolysis Bullosa Acquisita with Murine Collagen VII. *Cellular and Molecular Life Sciences* **67,** 1343–1351. ISSN: 1420-682X, 1420-9071. http://link.springer.com/10.1007/s00018-009-0256-3 (2025) (Apr. 2010).

124. Csorba, K. *et al.* Blister-inducing Antibodies Target Multiple Epitopes on Collagen VII in Mice. *Journal of Cellular and Molecular Medicine* **18,** 1727–1739. ISSN: 1582-1838, 1582-4934. https://onlinelibrary.wiley.com/doi/10.1111/jcmm.12338 (2024) (Sept. 2014).

125. Recke, A. *et al.* Pathogenicity of IgG Subclass Autoantibodies to Type VII Collagen: Induction of Dermal–Epidermal Separation. *Journal of Autoimmunity* **34,** 435–444. ISSN: 08968411. https://linkinghub.elsevier.com/retrieve/pii/S0896841109001437 (2023) (June 2010).

126. Sitaru, A. G. *et al.* T Cells Are Required for the Production of Blister-Inducing Autoantibodies in Experimental Epidermolysis Bullosa Acquisita. *The Journal of Immunology* **184,** 1596–1603. ISSN: 0022-1767, 1550-6606. https://journals.aai.org/jimmunol/article/184/3/1596/82373/T-Cells-Are-Required-for-the-Production-of-Blister (2023) (Feb. 1, 2010).

127. Ludwig, R. J. *et al.* Generation of Antibodies of Distinct Subclasses and Specificity Is Linked to H2s in an Active Mouse Model of Epidermolysis Bullosa Acquisita. *Journal of Investigative Dermatology* **131,** 167–176. ISSN: 0022202X. https://linkinghub.elsevier.com/retrieve/pii/S0022202X15350144 (2025) (Jan. 2011).

128. Vorobyev, A. *et al.* Autoantibodies to Multiple Epitopes on the Non-Collagenous-1 Domain of Type VII Collagen Induce Blisters. *Journal of Investigative Dermatology*

135, 1565–1573. ISSN: 0022202X. https://linkinghub.elsevier.com/retrieve/pii/S0022202X15372985 (2025) (June 2015).

129. Hammers, C. M. *et al.* Complement-Fixing Anti-Type VII Collagen Antibodies Are Induced in Th1-Polarized Lymph Nodes of Epidermolysis Bullosa Acquisita-Susceptible Mice. *The Journal of Immunology* **187,** 5043–5050. ISSN: 0022-1767, 1550-6606. https://journals.aai.org/jimmunol/article/187/10/5043/85076/Complement-Fixing-Anti-Type-VII-Collagen (2023) (Nov. 15, 2011).

130. Manz, R. A., Hauser, A. E., Hiepe, F. & Radbruch, A. MAINTENANCE OF SERUM ANTIBODY LEVELS. *Annual Review of Immunology* **23,** 367–386. ISSN: 0732-0582, 1545-3278. https://www.annualreviews.org/doi/10.1146/annurev.immunol.23.021704.115723 (2025) (Apr. 1, 2005).

131. Tiburzy, B. *et al.* Persistent Autoantibody-Production by Intermediates between Short-and Long-Lived Plasma Cells in Inflamed Lymph Nodes of Experimental Epidermolysis Bullosa Acquisita. *PLoS ONE* **8** (ed Frey, O.) e83631. ISSN: 1932-6203. https://dx.plos.org/10.1371/journal.pone.0083631 (2024) (Dec. 26, 2013).

132. Kasperkiewicz, M. *et al.* Clearance Rates of Circulating and Tissue-Bound Autoantibodies to Type VII Collagen in Experimental Epidermolysis Bullosa Acquisita: Clearance of Autoantibodies to Type VII Collagen in EBA. *British Journal of Dermatology* **162,** 1064–1070. ISSN: 0007-0963. https://academic.oup.com/bjd/article/162/5/1064/6642607 (2025) (May 2010).

133. Hirose, M. *et al.* Enzymatic Autoantibody Glycan Hydrolysis Alleviates Autoimmunity against Type VII Collagen. *Journal of Autoimmunity* **39,** 304–314. ISSN: 08968411. https://linkinghub.elsevier.com/retrieve/pii/S0896841112000455 (2025) (Dec. 2012).

134. Karsten, C. M. *et al.* Anti-Inflammatory Activity of IgG1 Mediated by Fc Galactosylation and Association of FcγRIIB and Dectin-1. *Nature Medicine* **18,** 1401–1406. ISSN: 1078-8956, 1546-170X. https://www.nature.com/articles/nm.2862 (2023) (Sept. 2012).

135. Kasperkiewicz, M. *et al.* Genetic Identification and Functional Validation of FcγRIV as Key Molecule in Autoantibody-induced Tissue Injury. *The Journal of Pathology* **228,** 8–19. ISSN: 0022-3417, 1096-9896. https://pathsocjournals.onlinelibrary.wiley.com/doi/10.1002/path.4023 (2025) (Sept. 2012).

136. Ludwig, R. J. Signalling and Targeted Therapy of Inflammatory Cells in Epidermolysis Bullosa Acquisita. *Experimental Dermatology* **26,** 1179–1186. ISSN: 0906-6705, 1600-0625. https://onlinelibrary.wiley.com/doi/10.1111/exd.13335 (2025) (Dec. 2017).

137. Bieber, K. *et al.* Regulatory T Cells Suppress Inflammation and Blistering in Pemphigoid Diseases. *Frontiers in Immunology* **8,** 1628. ISSN: 1664-3224. http://journal.frontiersin.org/article/10.3389/fimmu.2017.01628/full (2025) (Nov. 24, 2017).

138. Clauder, A.-K. *et al.* IgG Fc N-Glycosylation Translates MHCII Haplotype into Autoimmune Skin Disease. *Journal of Investigative Dermatology* **141,** 285–294. ISSN: 0022202X. https://linkinghub.elsevier.com/retrieve/pii/S0022202X20318327 (2025) (Feb. 2021).

139. Vicari, E. *et al.* Pathogenic Autoantibody Derived from Regulatory T Cell−Deficient Scurfy Mice Targets Type VII Collagen and Leads to Epidermolysis Bullosa Acquisita−Like Blistering Disease. *Journal of Investigative Dermatology* **142,** 980–984.e4. ISSN: 0022202X. https://linkinghub.elsevier.com/retrieve/pii/S0022202X21023125 (2023) (Mar. 2022).

140. Haeger, S. C. *et al.* Therapeutic Effects of Fc Gamma RIV Inhibition Are Mediated by Selectively Blocking Immune Complex-Induced Neutrophil Activation in Epidermolysis Bullosa Acquisita. *Frontiers in Immunology* **13,** 938306. ISSN: 1664-3224. https://www.frontiersin.org/articles/10.3389/fimmu.2022.938306/full (2025) (Oct. 13, 2022).

141. Manthey, H. D., Woodruff, T. M., Taylor, S. M. & Monk, P. N. Complement Component 5a (C5a). *The International Journal of Biochemistry & Cell Biology* **41,** 2114–2117. ISSN: 13572725. https://linkinghub.elsevier.com/retrieve/pii/S1357272509001253 (2024) (Nov. 2009).

142. Sadik, C. D., Miyabe, Y., Sezin, T. & Luster, A. D. The Critical Role of C5a as an Initiator of Neutrophil-Mediated Autoimmune Inflammation of the Joint and Skin. *Seminars in Immunology* **37,** 21–29. ISSN: 10445323. https://linkinghub.elsevier.com/retrieve/pii/S1044532317301380 (2024) (June 2018).

143. Papara, C. *et al.* The Relevance of Complement in Pemphigoid Diseases: A Critical Appraisal. *Frontiers in Immunology* **13,** 973702. ISSN: 1664-3224. https://www.frontiersin.org/articles/10.3389/fimmu.2022.973702/full (2025) (Aug. 16, 2022).

144. Köhler, G. & Milstein, C. Continuous Cultures of Fused Cells Secreting Antibody of Predefined Specificity. *Nature* **256,** 495–497. ISSN: 0028-0836, 1476-4687. https://www.nature.com/articles/256495a0 (2025) (Aug. 1975).

145. Moraes, J. Z. *et al.* Hybridoma Technology: Is It Still Useful? *Current Research in Immunology* **2,** 32–40. ISSN: 2590-2555. pmid: 35492397 (2021).

146. Yu, X., McGraw, P. A., House, F. S. & Crowe, J. E. An Optimized Electrofusion-Based Protocol for Generating Virus-Specific Human Monoclonal Antibodies. *Journal of Immunological Methods* **336,** 142–151. ISSN: 00221759. https://linkinghub.elsevier.com/retrieve/pii/S0022175908001397 (2025) (July 2008).

147. *Antibody Engineering* (eds Kontermann, R. & Dübel, S.) ISBN: 978-3-642-01143-6. http://link.springer.com/10.1007/978-3-642-01144-3 (2024) (Springer Berlin Heidelberg, Berlin, Heidelberg, 2010).

148. Kütemeier, G., Harloff, C. & Mocikat, R. Rapid Isolation of Immunoglobulin Variable Genes from Cell Lysates of Rat Hybridomas by Polymerase Chain Reaction. *Hybridoma* **11,** 23–32. ISSN: 0272-457X, 0272-457X. http://www.liebertpub.com/doi/10.1089/hyb.1992.11.23 (2023) (Feb. 1992).

149. Krebber, A. *et al.* Reliable Cloning of Functional Antibody Variable Domains from Hybridomas and Spleen Cell Repertoires Employing a Reengineered Phage Display System. *Journal of Immunological Methods* **201,** 35–55. ISSN: 00221759. https://linkinghub.elsevier.com/retrieve/pii/S0022175996002086 (2023) (Feb. 1997).

150. Hoogenboom, H. R. Selecting and Screening Recombinant Antibody Libraries. *Nature Biotechnology* **23,** 1105–1116. ISSN: 1087-0156, 1546-1696. https://www.nature.com/articles/nbt1126 (2025) (Sept. 1, 2005).

151. Smith, G. P. Filamentous Fusion Phage: Novel Expression Vectors That Display Cloned Antigens on the Virion Surface. *Science* **228,** 1315–1317. ISSN: 0036-8075, 1095-9203. https://www.science.org/doi/10.1126/science.4001944 (2023) (June 14, 1985).

152. Clackson, T., Hoogenboom, H. R., Griffiths, A. D. & Winter, G. Making Antibody Fragments Using Phage Display Libraries. *Nature* **352,** 624–628. ISSN: 0028-0836, 1476-4687. https://www.nature.com/articles/352624a0 (2023) (Aug. 1991).

153. Plückthun, A. Antibodies from Escherichia Coli. *Nature* **347,** 497–498. ISSN: 0028-0836, 1476-4687. https://www.nature.com/articles/347497a0 (2025) (Oct. 1990).

154. Shim, H. Synthetic Approach to the Generation of Antibody Diversity. *BMB Reports* **48,** 489–494. ISSN: 1976-6696. http://koreascience.or.kr/journal/view.jsp?kj=E1MBB7&py=2015&vnc=v48n9&sp=489 (2025) (Sept. 30, 2015).

155. Frenzel, A. *et al.* Designing Human Antibodies by Phage Display. *Transfusion Medicine and Hemotherapy* **44,** 312–318. ISSN: 1660-3796, 1660-3818. https://karger.com/article/doi/10.1159/000479633 (2025) (2017).

156. Glockshuber, R., Malia, M., Pfitzinger, I. & Plueckthun, A. A Comparison of Strategies to Stabilize Immunoglobulin Fv-fragments. *Biochemistry* **29,** 1362–1367. ISSN: 0006-2960, 1520-4995. https://pubs.acs.org/doi/abs/10.1021/bi00458a002 (2025) (Feb. 13, 1990).

157. McCafferty, J., Griffiths, A. D., Winter, G. & Chiswell, D. J. Phage Antibodies: Filamentous Phage Displaying Antibody Variable Domains. *Nature* **348,** 552–554. ISSN: 0028-0836, 1476-4687. https://www.nature.com/articles/348552a0 (2025) (Dec. 1990).

158. Dübel, S. *et al.* A Family of Vectors for Surface Display and Production of Antibodies. *Gene* **128,** 97–101. ISSN: 03781119. https://linkinghub.elsevier.com/retrieve/pii/037811199390159Z (2025) (June 1993).

159. Parmley, S. F. & Smith, G. P. Antibody-Selectable Filamentous Fd Phage Vectors: Affinity Purification of Target Genes. *Gene* **73,** 305–318. ISSN: 03781119. https://linkinghub.elsevier.com/retrieve/pii/0378111988904957 (2025) (Dec. 1988).

160. Peipp, M. *et al.* An Improved Procedure for the Generation of Recombinant Single-Chain Fv Antibody Fragments Reacting with Human CD13 on Intact Cells. *Journal of Immunological Methods* **251,** 161–176. ISSN: 00221759. https://linkinghub.elsevier.com/retrieve/pii/S0022175901002988 (2024) (May 2001).

161. Krohn, S. *et al.* Combining Cellular Immunization and Phage Display Screening Results in Novel, FcγRI-Specific Antibodies. *Viruses* **16,** 596. ISSN: 1999-4915. https://www.mdpi.com/1999-4915/16/4/596 (2024) (Apr. 12, 2024).

162. Schmidt-Jiménez, L. F. *Generation of Selfreactive Murine COL7vWFA Antibodies in Context of an Active Epidermolysis Bullosa Acquisita Mouse Model* Thesis (Universität zu Lübeck, Lübeck, June 12, 2020). 82 pp.

163. Krohn, S. *Identifizierung neuer Antikörper durch die Kombination von Phagen-Display und Next-Generation-Sequencing* PhD thesis (Christian-Albrechts-Universität zu Kiel, Kiel, July 1, 2021). 110 pp. https://macau.uni-kiel.de/receive/macau_mods_00001646?lang=de (2025).

164. Krohn, S. *et al.* Identification of New Antibodies Targeting Malignant Plasma Cells for Immunotherapy by Next-Generation Sequencing-Assisted Phage Display. *Frontiers in Immunology* **13,** 908093. ISSN: 1664-3224. pmid: 35784366 (2022).

165. Ravn, U. *et al.* By-Passing in Vitro Screening—next Generation Sequencing Technologies Applied to Antibody Display and in Silico Candidate Selection. *Nucleic Acids Research* **38,** e193–e193. ISSN: 1362-4962, 0305-1048. https://academic.oup.com/nar/article-lookup/doi/10.1093/nar/gkq789 (2025) (Nov. 2010).

166. Rouet, R., Jackson, K. J. L., Langley, D. B. & Christ, D. Next-Generation Sequencing of Antibody Display Repertoires. *Frontiers in Immunology* **9,** 118. ISSN: 1664-3224. http://journal.frontiersin.org/article/10.3389/fimmu.2018.00118/full (2025) (Feb. 2, 2018).

167. Kasprick, A., Bieber, K. & Ludwig, R. J. Drug Discovery for Pemphigoid Diseases. *Current Protocols in Pharmacology* **84,** e55. ISSN: 19348282. https://onlinelibrary.wiley.com/doi/10.1002/cpph.55 (2023) (Mar. 2019).

168. Haeberle, S. *et al.* Regulatory T-cell Deficiency Leads to Pathogenic Bullous Pemphigoid Antigen 230 Autoantibody and Autoimmune Bullous Disease. *Journal of Allergy and Clinical Immunology* **142,** 1831–1842.e7. ISSN: 00916749. https://linkinghub.elsevier.com/retrieve/pii/S0091674918306146 (2025) (Dec. 2018).

169. Abanades, B. *et al.* ImmuneBuilder: Deep-Learning Models for Predicting the Structures of Immune Proteins. *Communications Biology* **6,** 575. ISSN: 2399-3642. https://www.nature.com/articles/s42003-023-04927-7 (2025) (May 29, 2023).

170. Dunbar, J. *et al.* SAbPred: A Structure-Based Antibody Prediction Server. *Nucleic Acids Research* **44,** W474–W478. ISSN: 0305-1048, 1362-4962. https://academic.oup.com/nar/article-lookup/doi/10.1093/nar/gkw361 (2025) (July 8, 2016).

171. Brochet, X., Lefranc, M.-P. & Giudicelli, V. IMGT/V-QUEST: The Highly Customized and Integrated System for IG and TR Standardized V-J and V-D-J Sequence Analysis. *Nucleic Acids Research* **36,** W503–508. ISSN: 1362-4962. pmid: 18503082 (Web Server issue July 1, 2008).

172. Giudicelli, V., Brochet, X. & Lefranc, M.-P. IMGT/V-QUEST: IMGT Standardized Analysis of the Immunoglobulin (IG) and T Cell Receptor (TR) Nucleotide Sequences. *Cold Spring Harbor Protocols* **2011,** 695–715. ISSN: 1559-6095. pmid: 21632778 (June 1, 2011).

173. Kumar, S. *et al.* MEGA12: Molecular Evolutionary Genetic Analysis Version 12 for Adaptive and Green Computing. *Molecular Biology and Evolution* **41** (ed Battistuzzi, F. U.) msae263. ISSN: 0737-4038, 1537-1719. https://academic.oup.com/mbe/article/doi/10.1093/molbev/msae263/7930299 (2025) (Dec. 6, 2024).

174. *TeX Studio* version 4.8.6. Open-source LaTeX Editor (organized by Benito van der Zander). https://www.texstudio.org.

175. Kasprick, A. *et al.* Conditional Depletion of Mast Cells Has No Impact on the Severity of Experimental Epidermolysis Bullosa Acquisita. *European Journal of Immunology* **45,** 1462–1470. ISSN: 0014-2980, 1521-4141. https://onlinelibrary.wiley.com/doi/10.1002/eji.201444769 (2025) (May 2015).

176. Gross, N. *et al.* Inhibition of Interferon Gamma Impairs Induction of Experimental Epidermolysis Bullosa Acquisita. *Frontiers in Immunology* **15,** 1343299. ISSN: 1664-3224. https://www.frontiersin.org/articles/10.3389/fimmu.2024.1343299/full (2025) (May 10, 2024).

177. Sambrook, J. & Russell, D. W. *Molecular Cloning: A Laboratory Manual* 3rd ed. 3 pp. ISBN: 978-0-87969-577-4 (Cold Spring Harbor Laboratory Press, Cold Spring Harbor, N.Y, 2001).

178. Winter, G., Griffiths, A. D., Hawkins, R. E. & Hoogenboom, H. R. Making Antibodies by Phage Display Technology. *Annual Review of Immunology* **12,** 433–455. ISSN: 0732-0582, 1545-3278. https://www.annualreviews.org/doi/10.1146/annurev.iy.12.040194.002245 (2025) (Apr. 1994).

179. *MACHEREY-NAGEL User Manual Nucleo Spin Plasmid* https://www.mn-net.com/media/pdf/45/51/02/Instruction-NucleoSpin-Plasmid.pdf.

180. *MACHEREY-NAGEL User Manual Endotoxin-free Plasmid DNA Purification NucleoBond PC 2000 EF* https://www.mn-net.com/media/pdf/ab/f0/1b/Instruction-NucleoBond-PC-EF.pdf (2025).

181. Sanger, F., Nicklen, S. & Coulson, A. R. DNA Sequencing with Chain-Terminating Inhibitors. *Proceedings of the National Academy of Sciences of the United States of America* **74,** 5463–5467. ISSN: 0027-8424. pmid: 271968 (Dec. 1977).

182. Giudicelli, V. *et al.* in *Immunogenetics* (ed Langerak, A. W.) 477–531 (Springer US, New York, NY, 2022). ISBN: 978-1-07-162114-1. https://link.springer.com/10.1007/978-1-0716-2115-8_24 (2025).

183. Nei, M. & Kumar, S. *Molecular Evolution and Phylogenetics* 333 pp. ISBN: 978-0-19-513584-8 (Oxford University Press, Oxford ; New York, 2000).

184. Estimation of the Number of Nucleotide Substitutions in the Control Region of Mitochondrial DNA in Humans and Chimpanzees. *Molecular Biology and Evolution.* ISSN: 1537-1719. https://academic.oup.com/mbe/article/10/3/512/1016366/Estimation-of-the-number-of-nucleotide (2025) (May 1993).

185. Darzentas, N. in *Immunogenetics* (ed Langerak, A. W.) 571–584 (Springer US, New York, NY, 2022). ISBN: 978-1-07-162114-1. https://link.springer.com/10.1007/978-1-0716-2115-8_26 (2025).

186. Bashford-Rogers, R. J. M. *et al.* Analysis of the B Cell Receptor Repertoire in Six Immune-Mediated Diseases. *Nature* **574,** 122–126. ISSN: 0028-0836, 1476-4687. https://www.nature.com/articles/s41586-019-1595-3 (2025) (Oct. 3, 2019).

187. Hou, D. *et al.* Immune Repertoire Diversity Correlated with Mortality in Avian Influenza A (H7N9) Virus Infected Patients. *Scientific Reports* **6,** 33843. ISSN: 2045-2322. https://www.nature.com/articles/srep33843 (2025) (Sept. 27, 2016).

188. Miho, E. *et al.* Computational Strategies for Dissecting the High-Dimensional Complexity of Adaptive Immune Repertoires. *Frontiers in Immunology* **9,** 224. ISSN: 1664-3224. http://journal.frontiersin.org/article/10.3389/fimmu.2018.00224/full (2025) (Feb. 21, 2018).

189. Chiffelle, J. *et al.* T-Cell Repertoire Analysis and Metrics of Diversity and Clonality. *Current Opinion in Biotechnology* **65,** 284–295. ISSN: 09581669. https://linkinghub.elsevier.com/retrieve/pii/S0958166920301051 (2025) (Oct. 2020).

190. Li, F., Vijayasankaran, N., Shen, A. (, Kiss, R. & Amanullah, A. Cell Culture Processes for Monoclonal Antibody Production. *mAbs* **2,** 466–479. ISSN: 1942-0862, 1942-0870. http://www.tandfonline.com/doi/abs/10.4161/mabs.2.5.12720 (2025) (Sept. 2010).

191. Harding, F. A., Stickler, M. M., Razo, J. & DuBridge, R. B. The Immunogenicity of Humanized and Fully Human Antibodies: Residual Immunogenicity Resides in the CDR Regions. *mAbs* **2,** 256–265. ISSN: 1942-0870. pmid: 20400861 (2010).

192. Jefferis, R. Recombinant Antibody Therapeutics: The Impact of Glycosylation on Mechanisms of Action. *Trends in Pharmacological Sciences* **30,** 356–362. ISSN: 01656147. https://linkinghub.elsevier.com/retrieve/pii/S0165614709000911 (2025) (July 2009).

193. Frenzel, A., Hust, M. & Schirrmann, T. Expression of Recombinant Antibodies. *Frontiers in Immunology* **4.** ISSN: 1664-3224. http://journal.frontiersin.org/article/10.3389/fimmu.2013.00217/abstract (2025) (2013).

194. Croset, A. *et al.* Differences in the Glycosylation of Recombinant Proteins Expressed in HEK and CHO Cells. *Journal of Biotechnology* **161,** 336–348. ISSN: 01681656. https://linkinghub.elsevier.com/retrieve/pii/S0168165612003768 (2025) (Oct. 2012).

195. Wurm, F. M. Production of Recombinant Protein Therapeutics in Cultivated Mammalian Cells. *Nature Biotechnology* **22,** 1393–1398. ISSN: 1087-0156, 1546-1696. https://www.nature.com/articles/nbt1026 (2025) (Nov. 2004).

196. Steger, K. *et al.* CHO-S Antibody Titers >1 Gram/Liter Using Flow Electroporation-Mediated Transient Gene Expression Followed by Rapid Migration to High-Yield Stable Cell Lines. *SLAS Discovery* **20,** 545–551. ISSN: 24725552. https://linkinghub.elsevier.com/retrieve/pii/S2472555222072197 (2025) (Apr. 2015).

197. Jiang, Z. & Sharfstein, S. T. Sodium Butyrate Stimulates Monoclonal Antibody Over-expression in CHO Cells by Improving Gene Accessibility. *Biotechnology and Bioengineering* **100,** 189–194. ISSN: 0006-3592, 1097-0290. https://onlinelibrary.wiley.com/doi/10.1002/bit.21726 (2025) (May 2008).

198. Aydin, S. *et al.* An Overview of ELISA: A Review and Update on Best Laboratory Practices for Quantifying Peptides and Proteins in Biological Fluids. *Journal of International Medical Research* **53,** 03000605251315913. ISSN: 0300-0605, 1473-2300. https://journals.sagepub.com/doi/10.1177/03000605251315913 (2025) (Feb. 2025).

199. Oostindie, S. C., Lazar, G. A., Schuurman, J. & Parren, P. W. H. I. Avidity in Antibody Effector Functions and Biotherapeutic Drug Design. *Nature Reviews. Drug Discovery* **21,** 715–735. ISSN: 1474-1784. pmid: 35790857 (Oct. 2022).

200. Correa, V. A., Rodrigues, T. S., Portilho, A. I., Trzewikoswki De Lima, G. & De Gaspari, E. Modified ELISA for Antibody Avidity Evaluation: The Need for Standardization. *Biomedical Journal* **44,** 433–438. ISSN: 23194170. https://linkinghub.elsevier.com/retrieve/pii/S2319417020301803 (2025) (Aug. 2021).

201. MacDonald, R. A., Hosking, C. S. & Jones, C. L. The Measurement of Relative Antibody Affinity by ELISA Using Thiocyanate Elution. *Journal of Immunological Methods* **106,** 191–194. ISSN: 00221759. https://linkinghub.elsevier.com/retrieve/pii/0022175988901962 (2025) (Feb. 1988).

202. Jaroszewicz, W., Morcinek-Orłowska, J., Pierzynowska, K., Gaffke, L. & Węgrzyn, G. Phage Display and Other Peptide Display Technologies. *FEMS Microbiology Reviews* **46,** fuab052. ISSN: 1574-6976. https://academic.oup.com/femsre/article/doi/10.1093/femsre/fuab052/6407522 (2025) (Mar. 3, 2022).

203. Cai, X. & Garen, A. Comparison of Fusion Phage Libraries Displaying V_H or Single-Chain Fv Antibody Fragments Derived from the Antibody Repertoire of a Vaccinated Melanoma Patient as a Source of Melanoma-Specific Targeting Molecules. *Proceedings of the National Academy of Sciences* **94,** 9261–9266. ISSN: 0027-8424, 1091-6490. https://pnas.org/doi/full/10.1073/pnas.94.17.9261 (2025) (Aug. 19, 1997).

204. Lefranc, M.-P. *et al.* IMGT Unique Numbering for Immunoglobulin and T Cell Receptor Variable Domains and Ig Superfamily V-like Domains. *Developmental & Comparative Immunology* **27,** 55–77. ISSN: 0145305X. https://linkinghub.elsevier.com/retrieve/pii/S0145305X02000393 (2024) (Jan. 2003).

205. Finkelman, F. *et al. pat.* WO2021050978A1 (United States of America). https://patentscope.wipo.int/search/de/detail.jsf?docId=WO2021050978(2021).

206. Collins, A. M. IgG Subclass Co-expression Brings Harmony to the Quartet Model of Murine IgG Function. *Immunology & Cell Biology* **94,** 949–954. ISSN: 0818-9641, 1440-1711. https://onlinelibrary.wiley.com/doi/abs/10.1038/icb.2016.65 (2023) (Nov. 2016).

207. Falconer, D. J. & Barb, A. W. Mouse IgG2c Fc Loop Residues Promote Greater Receptor-Binding Affinity than Mouse IgG2b or Human IgG1. *PloS One* **13,** e0192123. ISSN: 1932-6203. pmid: 29408873 (2018).

208. Einav, T. & Bloom, J. D. When Two Are Better than One: Modeling the Mechanisms of Antibody Mixtures. *PLOS Computational Biology* **16** (ed Antia, R.) e1007830. ISSN: 1553-7358. https://dx.plos.org/10.1371/journal.pcbi.1007830 (2025) (May 4, 2020).

209. Van Osch, T. L. J. *et al.* Fc Galactosylation Promotes Hexamerization of Human IgG1, Leading to Enhanced Classical Complement Activation. *Journal of Immunology*

(*Baltimore, Md.: 1950*) **207,** 1545–1554. ISSN: 1550-6606. pmid: 34408013 (Sept. 15, 2021).

210. Diebolder, C. A. *et al.* Complement Is Activated by IgG Hexamers Assembled at the Cell Surface. *Science* **343,** 1260–1263. ISSN: 0036-8075, 1095-9203. https://www.science.org/doi/10.1126/science.1248943 (2025) (Mar. 14, 2014).

211. Benichou, J., Ben-Hamo, R., Louzoun, Y. & Efroni, S. Rep-Seq: Uncovering the Immunological Repertoire through Next-generation Sequencing. *Immunology* **135,** 183–191. ISSN: 0019-2805, 1365-2567. https://onlinelibrary.wiley.com/doi/10.1111/j.1365-2567.2011.03527.x (2025) (Mar. 2012).

212. Lefranc, M.-P. *et al.* IMGT®, the International ImMunoGeneTics Information System® 25 Years On. *Nucleic Acids Research* **43,** D413–D422. ISSN: 1362-4962, 0305-1048. http://academic.oup.com/nar/article/43/D1/D413/2436677/IMGT-the-international-ImMunoGeneTics-information (2025) (Jan. 28, 2015).

213. Mandric, I. *et al.* Profiling Immunoglobulin Repertoires across Multiple Human Tissues Using RNA Sequencing. *Nature Communications* **11,** 3126. ISSN: 2041-1723. pmid: 32561710 (June 19, 2020).

214. Greiff, V. *et al.* Systems Analysis Reveals High Genetic and Antigen-Driven Predetermination of Antibody Repertoires throughout B Cell Development. *Cell Reports* **19,** 1467–1478. ISSN: 22111247. https://linkinghub.elsevier.com/retrieve/pii/S221112471730565X (2025) (May 2017).

215. Greiff, V. *et al.* Quantitative Assessment of the Robustness of Next-Generation Sequencing of Antibody Variable Gene Repertoires from Immunized Mice. *BMC Immunology* **15,** 40. ISSN: 1471-2172. https://bmcimmunol.biomedcentral.com/articles/10.1186/s12865-014-0040-5 (2025) (Dec. 2014).

216. Hammers, C. M. & Stanley, J. R. Antibody Phage Display: Technique and Applications. *Journal of Investigative Dermatology* **134,** 1–5. ISSN: 0022202X. https://linkinghub.elsevier.com/retrieve/pii/S0022202X15366288 (2024) (Feb. 2014).

217. Hammers, C. M. *et al.* Persistence of Anti-Desmoglein 3 IgG+ B-Cell Clones in Pemphigus Patients over Years. *Journal of Investigative Dermatology* **135,** 742–749. ISSN: 0022202X. https://linkinghub.elsevier.com/retrieve/pii/S0022202X15371396 (2025) (Mar. 2015).

218. Ishii, K., Lin, C., Siegel, D. L. & Stanley, J. R. Isolation of Pathogenic Monoclonal Anti-Desmoglein 1 Human Antibodies by Phage Display of Pemphigus Foliaceus Autoantibodies. *Journal of Investigative Dermatology* **128,** 939–948. ISSN: 0022-202X. https://linkinghub.elsevier.com/retrieve/pii/S0022202X15338112 (2025) (Apr. 2008).

219. Payne, A. S. *et al.* Genetic and Functional Characterization of Human Pemphigus Vulgaris Monoclonal Autoantibodies Isolated by Phage Display. *Journal of Clinical Investigation* **115,** 888–899. ISSN: 0021-9738. http://www.jci.org/articles/view/24185 (2025) (Apr. 1, 2005).

220. Ledsgaard, L. *et al.* Advances in Antibody Phage Display Technology. *Drug Discovery Today* **27,** 2151–2169. ISSN: 13596446. https://linkinghub.elsevier.com/retrieve/pii/S1359644622001738 (2025) (Aug. 2022).

221. Chen, M. *et al.* Interactions of the Amino-terminal Noncollagenous (NC1) Domain of Type VII Collagen with Extracellular Matrix Components. *Journal of Biological Chemistry* **272,** 14516–14522. ISSN: 0021-9258. https://linkinghub.elsevier.com/retrieve/pii/S0021925819624233 (2025) (June 1997).

222. Sidhu, S. S., Lowman, H. B., Cunningham, B. C. & Wells, J. A. in *Methods in Enzymology* 333–IN5 (Elsevier, 2000). ISBN: 978-0-12-182229-3. https://linkinghub.elsevier.com/retrieve/pii/S0076687900284061 (2024).

223. Rettig, T. A., Ward, C., Bye, B. A., Pecaut, M. J. & Chapes, S. K. Characterization of the Naive Murine Antibody Repertoire Using Unamplified High-Throughput Sequencing. *PLOS ONE* **13** (ed Melcher, U.) e0190982. ISSN: 1932-6203. https://dx.plos.org/10.1371/journal.pone.0190982 (2025) (Jan. 10, 2018).

224. Merkenschlager, J. *et al.* Regulated Somatic Hypermutation Enhances Antibody Affinity Maturation. *Nature* **641,** 495–502. ISSN: 0028-0836, 1476-4687. https://www.nature.com/articles/s41586-025-08728-2 (2025) (May 8, 2025).

225. Di Noia, J. M. & Neuberger, M. S. Molecular Mechanisms of Antibody Somatic Hypermutation. *Annual Review of Biochemistry* **76,** 1–22. ISSN: 0066-4154, 1545-4509. https://www.annualreviews.org/doi/10.1146/annurev.biochem.76.061705.090740 (2025) (June 7, 2007).

226. Jackson, K. J. L., Wang, Y. & Collins, A. M. Human Immunoglobulin Classes and Subclasses Show Variability in VDJ Gene Mutation Levels. *Immunology & Cell Biology* **92,** 729–733. ISSN: 0818-9641, 1440-1711. https://onlinelibrary.wiley.com/doi/10.1038/icb.2014.44 (2025) (Sept. 2014).

227. Daly, J. *et al.* Altered Ig Hypermutation Pattern and Frequency in Complementary Mouse Models of DNA Polymerase ζ Activity. *Journal of Immunology (Baltimore, Md.: 1950)* **188,** 5528–5537. ISSN: 1550-6606. pmid: 22547703 (June 1, 2012).

228. Olafsdottir, T. A. *et al.* Comparative Systems Analyses Reveal Molecular Signatures of Clinically Tested Vaccine Adjuvants. *Scientific Reports* **6,** 39097. ISSN: 2045-2322. https://www.nature.com/articles/srep39097 (2025) (Dec. 13, 2016).

229. Matz, H. C., McIntire, K. M. & Ellebedy, A. H. 'Persistent Germinal Center Responses: Slow-Growing Trees Bear the Best Fruits'. *Current Opinion in Immunology* **83,** 102332. ISSN: 1879-0372. pmid: 37150126 (Aug. 2023).

230. Kovacs, B. *et al.* Fcγ Receptor IIB Controls Skin Inflammation in an Active Model of Epidermolysis Bullosa Acquisita. *Frontiers in Immunology* **10,** 3012. ISSN: 1664-3224. https://www.frontiersin.org/article/10.3389/fimmu.2019.03012/full (2023) (Jan. 14, 2020).

231. Deenick, E. K., Hasbold, J. & Hodgkin, P. D. Switching to IgG3, IgG2b, and IgA Is Division Linked and Independent, Revealing a Stochastic Framework for Describing Differentiation. *Journal of Immunology (Baltimore, Md.: 1950)* **163,** 4707–4714. ISSN: 0022-1767. pmid: 10528168 (Nov. 1, 1999).

232. De Jong, B. G. *et al.* Human IgG2- and IgG4-expressing Memory B Cells Display Enhanced Molecular and Phenotypic Signs of Maturity and Accumulate with Age. *Immunology & Cell Biology* **95,** 744–752. ISSN: 0818-9641, 1440-1711. https://onlinelibrary.wiley.com/doi/10.1038/icb.2017.43 (2025) (Oct. 2017).

233. Hara, Y. *et al.* High Affinity IgM+ Memory B Cells Are Generated through a Germinal Center-Dependent Pathway. *Molecular Immunology* **68,** 617–627. ISSN: 01615890. https://linkinghub.elsevier.com/retrieve/pii/S0161589015300936 (2025) (Dec. 2015).

234. Jacob, J., Kelsoe, G., Rajewsky, K. & Weiss, U. Intraclonal Generation of Antibody Mutants in Germinal Centres. *Nature* **354,** 389–392. ISSN: 0028-0836, 1476-4687. https://www.nature.com/articles/354389a0 (2025) (Dec. 1991).

235. Sarvas, H., Seppälä, I., Tähtinen, T., Péterfy, F. & Mäkelä, O. Mouse IgG Antibodies Have Subclass Associated Affinity Differences. *Molecular Immunology* **20,** 239–246. ISSN: 01615890. https://linkinghub.elsevier.com/retrieve/pii/0161589083900627 (2025) (Mar. 1983).

236. Nannini, F. *et al.* Combining Phage Display with SMRTbell Next-Generation Sequencing for the Rapid Discovery of Functional scFv Fragments. *mAbs* **13,** 1864084. ISSN: 1942-0862, 1942-0870. https://www.tandfonline.com/doi/full/10.1080/19420862.2020.1864084 (2025) (Jan. 1, 2021).

237. Victora, G. D. & Nussenzweig, M. C. Germinal Centers. *Annual Review of Immunology* **30,** 429–457. ISSN: 0732-0582, 1545-3278. https://www.annualreviews.org/doi/10.1146/annurev-immunol-020711-075032 (2025) (Apr. 23, 2012).

238. Meyer-Hermann, M. A Molecular Theory of Germinal Center B Cell Selection and Division. *Cell Reports* **36,** 109552. ISSN: 22111247. https://linkinghub.elsevier.com/retrieve/pii/S2211124721009864 (2025) (Aug. 2021).

239. Garg, A. K., Mitra, T., Schips, M., Bandyopadhyay, A. & Meyer-Hermann, M. Amount of Antigen, T Follicular Helper Cells and Affinity of Founder Cells Shape the Diversity of Germinal Center B Cells: A Computational Study. *Frontiers in Immunology* **14,** 1080853. ISSN: 1664-3224. pmid: 36993964 (2023).

240. Degn, S. E. *et al.* Clonal Evolution of Autoreactive Germinal Centers. *Cell* **170,** 913–926.e19. ISSN: 00928674. https://linkinghub.elsevier.com/retrieve/pii/S0092867417308334 (2024) (Aug. 2017).

241. Kuraoka, M. *et al.* Complex Antigens Drive Permissive Clonal Selection in Germinal Centers. *Immunity* **44,** 542–552. ISSN: 1074-7613. https://linkinghub.elsevier.com/retrieve/pii/S1074761316300486 (2025) (Mar. 2016).

242. Hoogenboom, H. R. & Chames, P. Natural and Designer Binding Sites Made by Phage Display Technology. *Immunology Today* **21,** 371–378. ISSN: 01675699. https://linkinghub.elsevier.com/retrieve/pii/S0167569900016674 (2025) (Aug. 2000).

243. Hust, M., Maiss, E., Jacobsen, H.-J. & Reinard, T. The Production of a Genus-Specific Recombinant Antibody (scFv) Using a Recombinant Potyvirus Protease. *Journal of Virological Methods* **106,** 225–233. ISSN: 01660934. https://linkinghub.elsevier.com/retrieve/pii/S0166093402001660 (2025) (Dec. 2002).

244. Schier, R. *et al.* Isolation of High-affinity Monomeric Human Anti-c-erbB-2 Single Chain Fv Using Affinity-driven Selection. *Journal of Molecular Biology* **255,** 28–43. ISSN: 00222836. https://linkinghub.elsevier.com/retrieve/pii/S0022283696900042 (2025) (Jan. 1996).

245. Panyutich, A. V., Baturevich, E. A., Kolesnikova, T. S. & Ganz, T. The Effect of Biotinylation on the Antigenic Specificity of Anti-Defensin Monoclonal Antibodies. *Journal of Immunological Methods* **158,** 237–242. ISSN: 00221759. https://linkinghub.elsevier.com/retrieve/pii/002217599390219W (2025) (Feb. 1993).

246. Robert, R. *et al.* Identification of Human scFvs Targeting Atherosclerotic Lesions. *Journal of Biological Chemistry* **281,** 40135–40143. ISSN: 00219258. https://linkinghub.elsevier.com/retrieve/pii/S0021925820768493 (2025) (Dec. 2006).

247. Scheffer, L. *et al.* Predictability of Antigen Binding Based on Short Motifs in the Antibody CDRH3. *Briefings in Bioinformatics* **25,** bbae537. ISSN: 1477-4054. pmid: 39438077 (Sept. 23, 2024).

248. Seiler, D. L. *et al.* C5aR2 Deficiency Ameliorates Inflammation in Murine Epidermolysis Bullosa Acquisita by Regulating Fcγ Receptor Expression on Neutrophils. *The Journal of Investigative Dermatology* **142,** 2715–2723.e2. ISSN: 1523-1747. pmid: 35007559 (Oct. 2022).

249. Sezin, T. *et al.* The Leukotriene B4 and Its Receptor BLT1 Act as Critical Drivers of Neutrophil Recruitment in Murine Bullous Pemphigoid-Like Epidermolysis Bullosa Acquisita. *Journal of Investigative Dermatology* **137,** 1104–1113. ISSN: 0022202X. https://linkinghub.elsevier.com/retrieve/pii/S0022202X17300180 (2025) (May 2017).

250. Awate, S., Babiuk, L. A. & Mutwiri, G. Mechanisms of Action of Adjuvants. *Frontiers in Immunology* **4.** ISSN: 1664-3224. http://journal.frontiersin.org/article/10.3389/fimmu.2013.00114/abstract (2024) (2013).

251. Leenaars, M., Koedam, M. A., Hendriksen, C. F. & Claassen, E. Immune Responses and Side Effects of Five Different Oil-Based Adjuvants in Mice. *Veterinary Immunology and Immunopathology* **61,** 291–304. ISSN: 01652427. https://linkinghub.elsevier.com/retrieve/pii/S0165242797001335 (2025) (Feb. 1998).

252. Bennett, B., Check, I. J., Olsen, M. R. & Hunter, R. L. A Comparison of Commercially Available Adjuvants for Use in Research. *Journal of Immunological Methods* **153,** 31–40. ISSN: 00221759. https://linkinghub.elsevier.com/retrieve/pii/002217599290302A (2025) (Aug. 1992).

253. Sjölander, A., Lövgren Bengtsson, K., Johansson, M. & Morein, B. Kinetics, Localization and Isotype Profile of Antibody Responses to Immune Stimulating Complexes (Iscoms) Containing Human Influenza Virus Envelope Glycoproteins.

Scandinavian Journal of Immunology **43,** 164–172. ISSN: 0300-9475, 1365-3083. https://onlinelibrary.wiley.com/doi/10.1046/j.1365-3083.1996.d01-29.x (2025) (Feb. 1996).

254. Fontes, J. A. *et al.* Complete Freund's Adjuvant Induces Experimental Autoimmune Myocarditis by Enhancing IL-6 Production during Initiation of the Immune Response. *Immunity, Inflammation and Disease* **5,** 163–176. ISSN: 2050-4527. pmid: 28474508 (June 2017).

255. De Jong, R. N. *et al.* A Novel Platform for the Potentiation of Therapeutic Antibodies Based on Antigen-Dependent Formation of IgG Hexamers at the Cell Surface. *PLOS Biology* **14** (ed Nemazee, D.) e1002344. ISSN: 1545-7885. https://dx.plos.org/10.1371/journal.pbio.1002344 (2025) (Jan. 6, 2016).

256. Lilienthal, G.-M. *et al.* Potential of Murine IgG1 and Human IgG4 to Inhibit the Classical Complement and Fcγ Receptor Activation Pathways. *Frontiers in Immunology* **9,** 958. ISSN: 1664-3224. http://journal.frontiersin.org/article/10.3389/fimmu.2018.00958/full (2025) (May 9, 2018).

257. Niebuhr, M. *et al.* Evidence for a Contributory Role of a Xenogeneic Immune Response in Experimental Epidermolysis Bullosa Acquisita. *Experimental Dermatology* **26,** 1207–1213. ISSN: 09066705. https://onlinelibrary.wiley.com/doi/10.1111/exd.13439 (2023) (Dec. 2017).

258. Nandakumar, K. S. & Holmdahl, R. Antibody-Induced Arthritis: Disease Mechanisms and Genes Involved at the Effector Phase of Arthritis. *Arthritis Research & Therapy* **8,** 223. ISSN: 1478-6362. pmid: 17254316 (2006).

259. Christensen, A. D., Haase, C., Cook, A. D. & Hamilton, J. A. K/BxN Serum-Transfer Arthritis as a Model for Human Inflammatory Arthritis. *Frontiers in Immunology* **7.** ISSN: 1664-3224. http://journal.frontiersin.org/Article/10.3389/fimmu.2016.00213/abstract (2025) (June 2, 2016).

260. Matsumoto, I., Staub, A., Benoist, C. & Mathis, D. Arthritis Provoked by Linked T and B Cell Recognition of a Glycolytic Enzyme. *Science* **286,** 1732–1735. ISSN: 0036-8075, 1095-9203. https://www.science.org/doi/10.1126/science.286.5445.1732 (2025) (Nov. 26, 1999).

261. Kouskoff, V. *et al.* Organ-Specific Disease Provoked by Systemic Autoimmunity. *Cell* **87,** 811–822. ISSN: 00928674. https://linkinghub.elsevier.com/retrieve/pii/S0092867400819893 (2025) (Nov. 1996).

262. Ji, H. *et al.* Genetic Influences on the End-Stage Effector Phase of Arthritis. *The Journal of Experimental Medicine* **194,** 321–330. ISSN: 0022-1007, 1540-9538. https://rupress.org/jem/article/194/3/321/26037/Genetic-Influences-on-the-End-Stage-Effector-Phase (2025) (Aug. 6, 2001).

263. Ji, H. *et al.* Arthritis Critically Dependent on Innate Immune System Players. *Immunity* **16,** 157–168. ISSN: 10747613. https://linkinghub.elsevier.com/retrieve/pii/S1074761302002753 (2025) (Feb. 2002).

264. Wipke, B. T. & Allen, P. M. Essential Role of Neutrophils in the Initiation and Progression of a Murine Model of Rheumatoid Arthritis. *The Journal of Immunology* **167,** 1601–1608. ISSN: 0022-1767, 1550-6606. https://journals.aai.org/jimmunol/article/167/3/1601/35041/Essential-Role-of-Neutrophils-in-the-Initiation (2025) (Aug. 1, 2001).

265. Solomon, S. *et al.* Transmission of Antibody-Induced Arthritis Is Independent of Complement Component 4 (C4) and the Complement Receptors 1 and 2 (CD21/35). *European Journal of Immunology* **32,** 644. ISSN: 00142980, 15214141. https://onlinelibrary.wiley.com/doi/10.1002/1521-4141(200203)32:3%3C644::AID-IMMU644%3E3.0.CO;2-5 (2025) (Mar. 2002).

266. Maccioni, M. *et al.* Arthritogenic Monoclonal Antibodies from K/BxN Mice. *The Journal of Experimental Medicine* **195,** 1071–1077. ISSN: 0022-1007. pmid: 11956298 (Apr. 15, 2002).

267. Weber, J., Peng, H. & Rader, C. From Rabbit Antibody Repertoires to Rabbit Monoclonal Antibodies. *Experimental & Molecular Medicine* **49,** e305. ISSN: 2092-6413. pmid: 28336958 (Mar. 24, 2017).

268. Bartsch, Y. C. *et al.* IgG Fc Sialylation Is Regulated during the Germinal Center Reaction Following Immunization with Different Adjuvants. *Journal of Allergy and Clinical Immunology* **146,** 652–666.e11. ISSN: 00916749. https://linkinghub.elsevier.com/retrieve/pii/S0091674920307284 (2025) (Sept. 2020).

269. Wuhrer, M. *et al.* Regulated Glycosylation Patterns of IgG during Alloimmune Responses against Human Platelet Antigens. *Journal of Proteome Research* **8,** 450–456. ISSN: 1535-3893, 1535-3907. https://pubs.acs.org/doi/10.1021/pr800651j (2025) (Feb. 6, 2009).

270. Krambeck, F. J., Bennun, S. V., Andersen, M. R. & Betenbaugh, M. J. Model-Based Analysis of N-glycosylation in Chinese Hamster Ovary Cells. *PLOS ONE* **12** (ed

Lisacek, F.) e0175376. ISSN: 1932-6203. https://dx.plos.org/10.1371/journal.pone.0175376 (2025) (May 9, 2017).

Supplementary Material

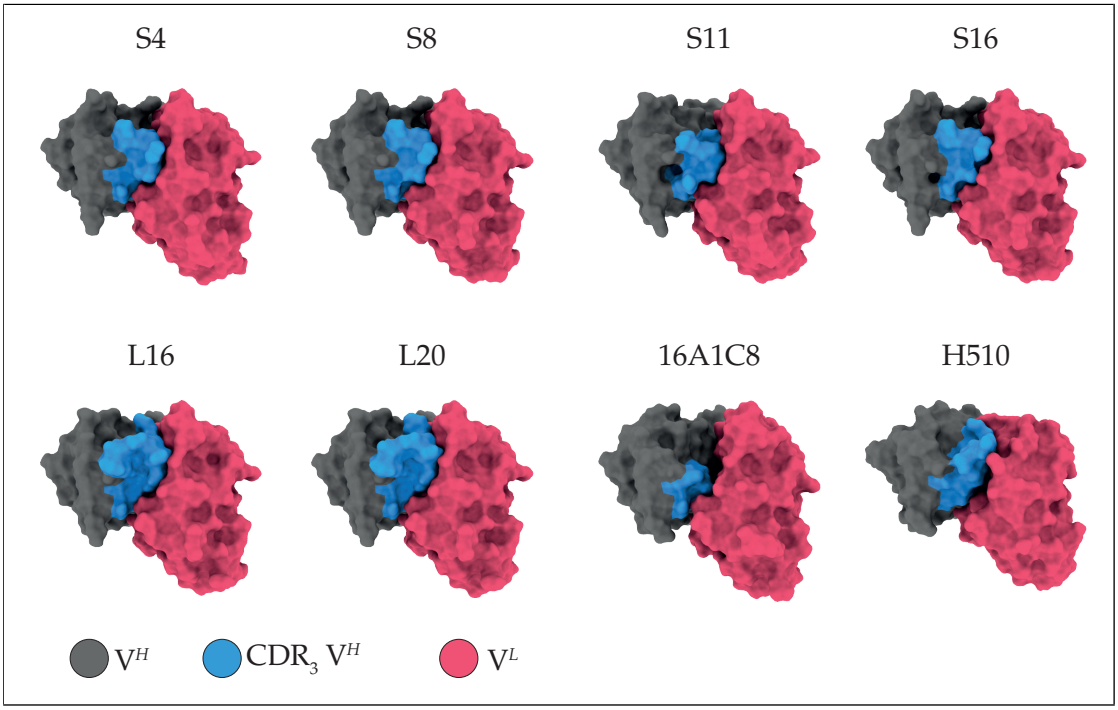

Supplementary Figure S1: Alphafold derived structures of scFv's. AlphaFold models of V^H-V^L pairings present in the indicated scFv's. V^H with highlighted CDR3 (blue) is shown in charcoal, V^L in pink.

Table S1: Mixed-effects analysis (Fig. 4.10) for antibody avidity. Tukey's multiple comparisons for NH_4SCN concentrations (mol/L) across groups, showing summary significance and adjusted p values.

NH_4SCN (mol/L)	**Tukey's multiple comparisons test**	**Summary**	**Adjusted p Value**
2	C2 vs. C6	****	<0.0001
2	C2 vs. C1-C7	**	0.0101
2	C2 vs. EBA Serum	**	0.0012
2	C3 vs. C6	****	<0.0001
2	C3 vs. C1-C7	**	0.004
2	C3 vs. EBA Serum	*	0.0215
2	C4 vs. C6	**	0.0012
2	C5 vs. C6	**	0.0033
2	C6 vs. C7	**	0.0045
2	C6 vs. C1-C7	**	0.0099
2	C6 vs. EBA Serum	**	0.0023
3	C1 vs. C3	****	<0.0001
3	C1 vs. C4	*	0.0115
3	C1 vs. C1-C7	**	0.0145
3	C1 vs. EBA Serum	****	<0.0001
3	C2 vs. C3	****	<0.0001
3	C2 vs. C6	****	<0.0001
3	C2 vs. C7	****	<0.0001
3	C2 vs. C1-C7	**	0.0116
3	C2 vs. EBA Serum	**	0.0018
3	C3 vs. C7	****	<0.0001
3	C3 vs. C1-C7	*	0.0164
3	C3 vs. EBA Serum	*	0.0178
3	C4 vs. C5	***	0.0005
3	C4 vs. C6	**	0.0259
3	C4 vs. C7	**	0.0110
3	C6 vs. C1-C7	****	<0.0001
3	C6 vs. EBA Serum	**	0.0028

Continued on next page

Table S1 – continued from previous page

NH_4SCN (mol/L)	Tukey's multiple comparisons test	Summary	Adjusted p Value
3	C7 vs. C1-C7	*	0.0234
3	C7 vs. EBA Serum	***	0.0002
4	C1 vs. EBA Serum	**	0.0028
4	C5 vs. EBA Serum	**	0.0034
4	C6 vs. C1-C7	***	0.0009
4	C6 vs. EBA Serum	*	0.0294
4	C7 vs. EBA Serum	**	0.0085
5	C1 vs. EBA Serum	*	0.0171
5	C5 vs. EBA Serum	*	0.0162
5	C6 vs. EBA Serum	*	0.0357
6	C4 vs. EBA Serum	*	0.0437
7	C1 vs. EBA Serum	**	0.0072
7	C4 vs. EBA Serum	*	0.0186
8	C5 vs. EBA Serum	*	0.0367

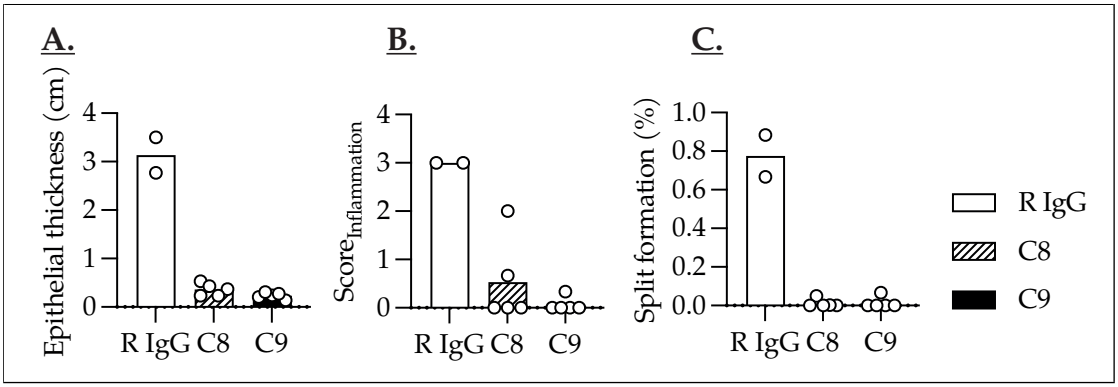

Supplementary Figure S2: Assessment of epithelial thickness, inflammation and split formation of histology samples, obtained from *in vivo* testing of C8 and C9 A. Epithelial thickness in cm. B. Score of inflammation (leukocyte infiltrate) (1-4). C. Split formation in %. n=2-5.

Table Description: Table S2 presents B cell receptor quantification metrics, showing elevated IGH dominance in LN compared to S and Ctrl. Table S3 details somatic hypermutation patterns, with lymph node samples exhibiting higher SHM1 rates in class-switched

Table S2: B cell receptor distribution metrics across control and experimental samples. Shown are total receptor counts, unique CDR3 (CDR3) counts, and immunoglobulin heavy/light chain distributions. Abbreviations: Ctrl (control - spleen), S (spleen), LN (lymph nodes), R (technical replicate).

Sample	Total Receptor Count	Total uCDR3	IGH Count	IGK Count	IGL Count
Ctrl-R	356,290	126,781	211,356	140,362	14,581
Ctrl	350,821	121,969	202,732	136,621	14,468
S-R	437,922	53,742	270,743	176,070	23,909
S	548,282	63,017	340,601	181,460	26,221
LN-R	516,358	33,441	392,842	119,950	3,566
LN	498,114	31,702	379,780	114,788	3,546

Table S3: Somatic hypermutation rates (SHM1) across immunoglobulin isotypes. Values represent normalized mutation frequencies relative to germline sequences. Ctrl (control - spleen), S (spleen), LN (lymph nodes), R (technical replicate).

Sample	IGHA	IGG1	IGG2	IGG3	IGG2A	IGG2B	IGG2C	IGHM/D	Total IGH
Ctrl-R	0.0298	0.0241	0.0163	0.0176	0.0156	0.0159	0.0151	0.0118	0.0154
Ctrl	0.0299	0.0242	0.0160	0.0174	0.0156	0.0186	0.0158	0.0118	0.0154
S-R	0.0267	0.0235	0.0175	0.0187	0.0087	0.0206	0.0171	0.0108	0.0134
S	0.0268	0.0241	0.0189	0.0198	0.0157	0.0212	0.0171	0.0109	0.0138
LN-R	0.0178	0.0321	0.0292	0.0268	0.0167	0.0294	0.0230	0.0082	0.0229
LN	0.0187	0.0320	0.0294	0.0285	0.0143	0.0298	0.0240	0.0088	0.0227

isotypes (particularly IgG1 and IgG2 subtypes), consistent with antigen-driven selection. The normalized SHM1 values reveal compartment-specific differences in affinity maturation processes.

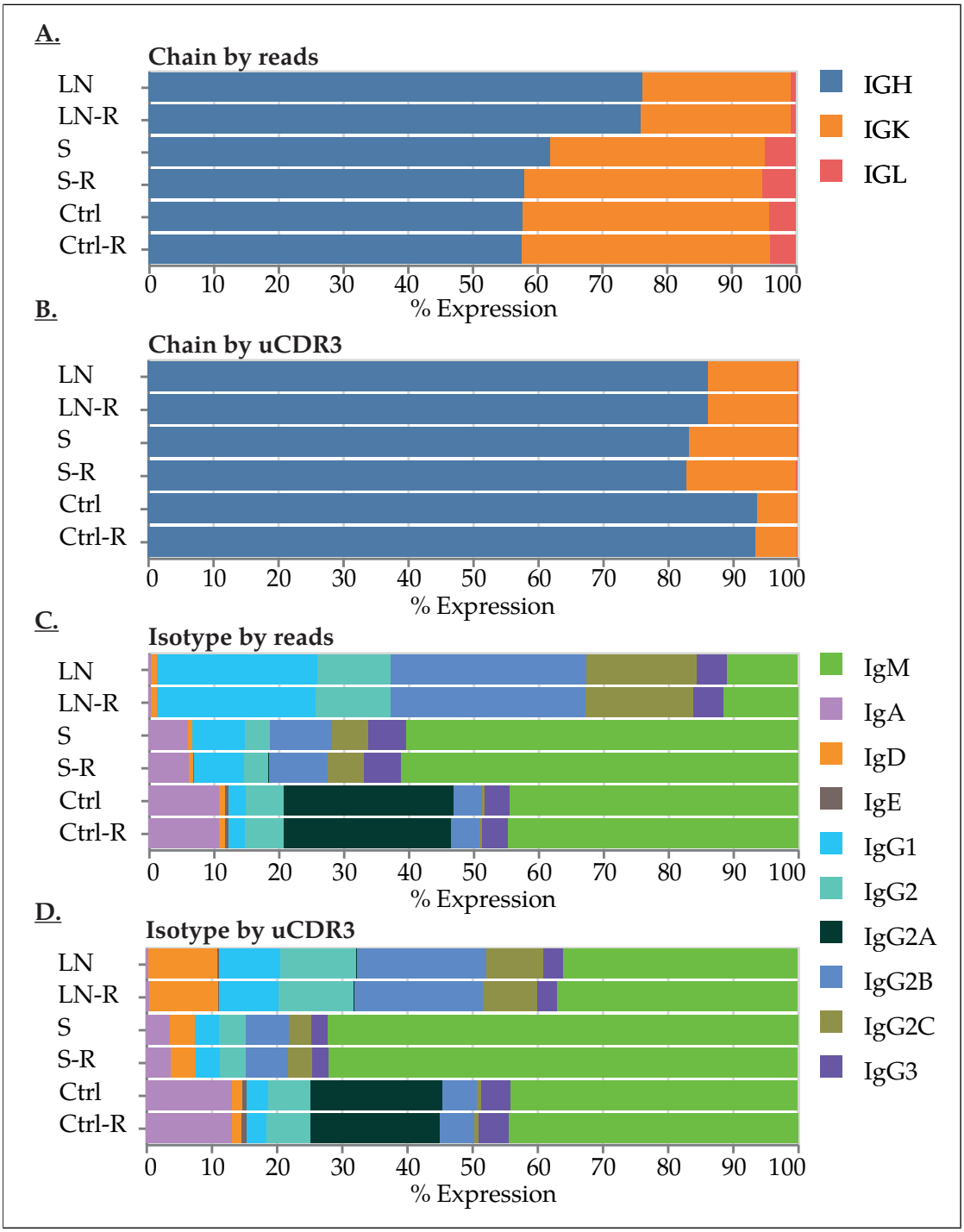

Supplementary Figure S3: Chain and isotype destribution in spleen and lymphnode BCR repertoire. A. Chain (IGH, IGK, IGL) expression annotated by reads. B. Chain expression annotated by unique CDR3s (uCDR3). C. Isotype expression annotated by reads. D. Isotype expression annotated by uCDR3. Sample annotation: LN - lymph nodes; spleen - S; control - ctrl (spleen); replicate - -R.

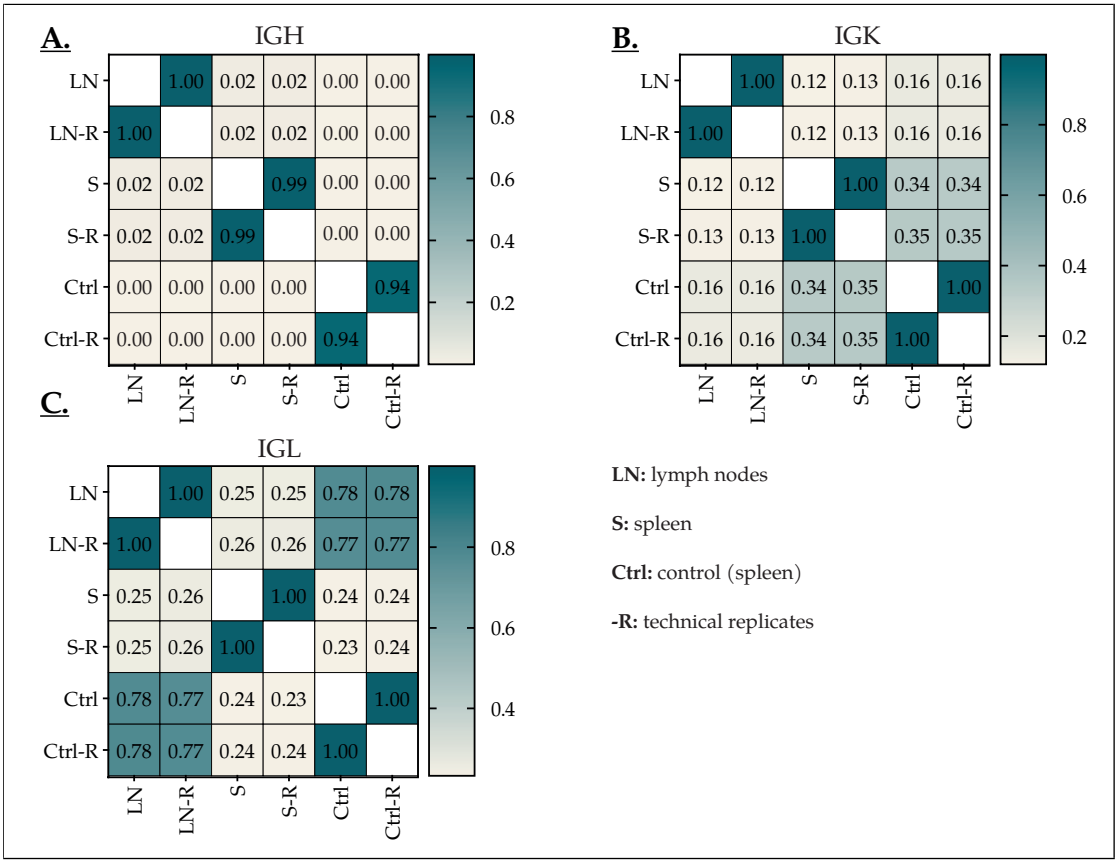

Supplementary Figure S4: R^2_{outer} sharing analysis of sequenced BCR repertoires. IGH (A.) IGK (B.) and IGL (B.) R^2_{outer} sharing analysis between samples lmyph nodes (LN), spleen (S) and control (Ctrl) and their respective technical replicates (-R). High R^2 values indicate a strong linear correlation in CDR3 distributions, suggesting that the compared datasets are likely to exhibit similar CDR3 profiles. Conversely, low R^2 values indicate that the CDR3 distributions are dissimilar between the compared samples

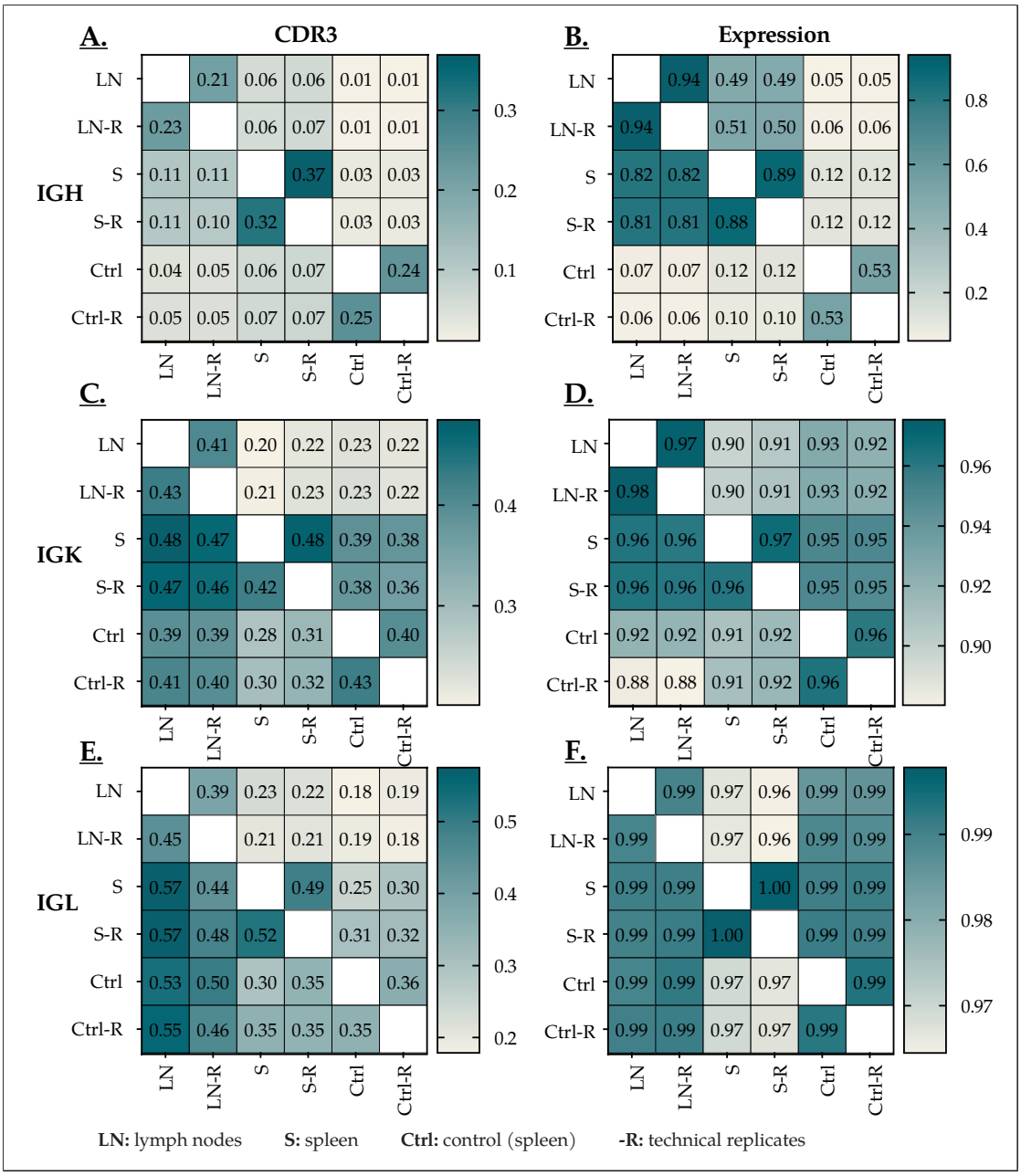

Supplementary Figure S5: CDR3 and expression sharing analysis of sequenced BCR repertoires. IGH (A., B.) IGK (C., D.) and IGL (E., F.) sharing analysis between samples lmyph nodes (LN), spleen (S) and control (Ctrl) and their respective technical replicates (-R). uCDR3 describes the fraction of unique CDR3 clonotypes shared between samples, independent of abundance. Expression sharing analysis provides a quantitative visualization of the shared abundance of CDR3s between pairs of samples, reflecting clonal expansion dynamics.

Table S4: Prediction error values for antibody regions as output by ABBuilder2 for AlphaFold models of V_H-V_L pairings. Error values are reported for frameworks and CDRs of both heavy and light chains across all modeled antibodies.

Antibody region	**S4**	**S8**	**S11**	**S16**	**L16**	**L20**	**16A1C8**	**H510**
Framework H-chain	0.41	0.41	0.29	0.43	0.41	0.41	0.33	0.33
CDR-H1	0.24	0.23	0.19	0.18	0.25	0.28	0.24	0.27
CDR-H2	0.20	0.20	0.18	0.20	0.20	0.20	0.17	0.18
CDR-H3	0.24	0.25	0.15	0.24	0.35	0.37	0.14	0.22
Framework L-chain	0.20	0.19	0.16	0.20	0.19	0.19	0.23	0.25
CDR-L1	0.33	0.34	0.21	0.42	0.32	0.30	0.23	0.25
CDR-L2	0.18	0.17	0.17	0.18	0.18	0.18	0.18	0.34
CDR-L3	0.16	0.15	0.20	0.15	0.18	0.23	0.39	0.25

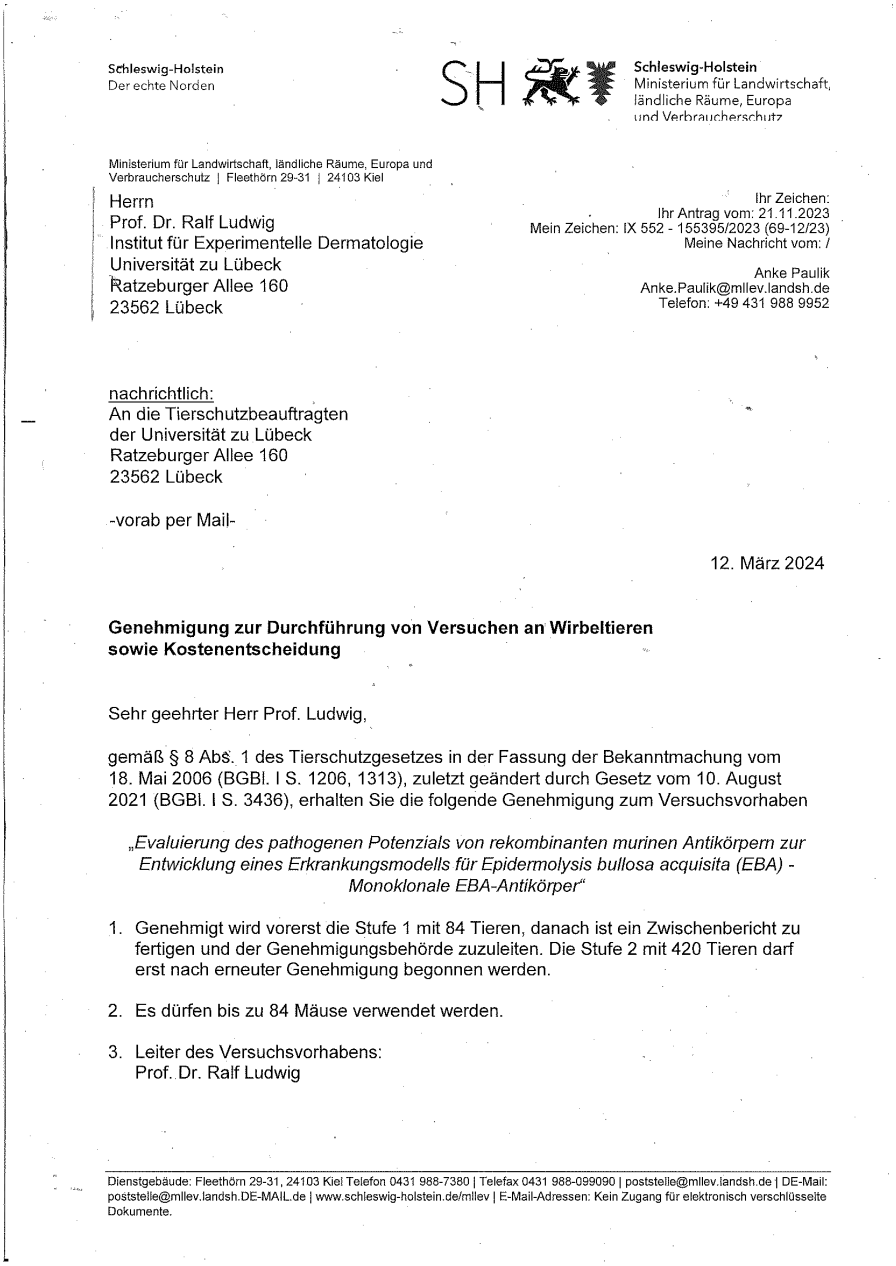

Schleswig-Holstein
Der echte Norden

Schleswig-Holstein
Ministerium für Landwirtschaft, ländliche Räume, Europa und Verbraucherschutz

Ministerium für Landwirtschaft, ländliche Räume, Europa und Verbraucherschutz | Fleethörn 29-31 | 24103 Kiel

Herrn
Prof. Dr. Ralf Ludwig
Institut für Experimentelle Dermatologie
Universität zu Lübeck
Ratzeburger Allee 160
23562 Lübeck

Ihr Zeichen:
Ihr Antrag vom: 21.11.2023
Mein Zeichen: IX 552 - 155395/2023 (69-12/23)
Meine Nachricht vom: /

Anke Paulik
Anke.Paulik@mllev.landsh.de
Telefon: +49 431 988 9952

nachrichtlich:
An die Tierschutzbeauftragten
der Universität zu Lübeck
Ratzeburger Allee 160
23562 Lübeck

-vorab per Mail-

12. März 2024

Genehmigung zur Durchführung von Versuchen an Wirbeltieren sowie Kostenentscheidung

Sehr geehrter Herr Prof. Ludwig,

gemäß § 8 Abs. 1 des Tierschutzgesetzes in der Fassung der Bekanntmachung vom 18. Mai 2006 (BGBl. I S. 1206, 1313), zuletzt geändert durch Gesetz vom 10. August 2021 (BGBl. I S. 3436), erhalten Sie die folgende Genehmigung zum Versuchsvorhaben

„Evaluierung des pathogenen Potenzials von rekombinanten murinen Antikörpern zur Entwicklung eines Erkrankungsmodells für Epidermolysis bullosa acquisita (EBA) - Monoklonale EBA-Antikörper“

1. Genehmigt wird vorerst die Stufe 1 mit 84 Tieren, danach ist ein Zwischenbericht zu fertigen und der Genehmigungsbehörde zuzuleiten. Die Stufe 2 mit 420 Tieren darf erst nach erneuter Genehmigung begonnen werden.

2. Es dürfen bis zu 84 Mäuse verwendet werden.

3. Leiter des Versuchsvorhabens:
   Prof. Dr. Ralf Ludwig

Dienstgebäude: Fleethörn 29-31, 24103 Kiel Telefon 0431 988-7380 | Telefax 0431 988-099090 | poststelle@mllev.landsh.de | DE-Mail: poststelle@mllev.landsh.DE-MAIL.de | www.schleswig-holstein.de/mllev | E-Mail-Adressen: Kein Zugang für elektronisch verschlüsselte Dokumente.

(**a**) Page-1

Supplementary Figure S6: Approval of animal proposal 5.1 (69-12/23)_Ludwig

4. Stellvertreter:
   PD Dr. Katja Bieber

5. Wechselt die Leitung des Versuchsvorhabens oder die Stellvertretung, so ist diese Änderung unverzüglich anzuzeigen; die Genehmigung gilt weiter, wenn sie nicht innerhalb eines Monats widerrufen wird.

6. Ort der Durchführung: Universität Lübeck Gemeinsame Tierhaltung, Haus 63, Räume der Kernzucht und Vermehrungszucht, Ratzeburger Allee 160, 23538 Lübeck

7. Das Versuchsvorhaben ist gem. § 35 Tierschutz-Versuchstierverordnung nicht rückblickend zu bewerten.

8. Die im Antrag gemachten Angaben sind im übrigen Bestandteil dieser Genehmigung.

Die Genehmigung ist mit folgenden Nebenbestimmungen verbunden:

9. Die Genehmigung ist bis zum 11. März 2029 befristet.

10. Dieser Bescheid ist mit folgenden Auflagen gemäß § 107 Abs. 1 Alternative 1 Landesverwaltungsgesetz (LVwG) in Verbindung mit § 33 Abs. 1 Nr. 4 Tierschutz-Versuchstierverordnung (TierSchVersV) verbunden:

10.1 Jede weitere beabsichtigte Abweichung vom Antrag ist der Genehmigungsbehörde zuvor -über die Tierschutzbeauftragten- mitzuteilen.

10.2 Nach jedem Versuchsteil (je nach Umfang) ist unaufgefordert und vor Weiterführung der Versuche ein kurzer Zwischenbericht zu den bei den Tieren aufgetretenen Schmerzen, Leiden und Schäden einzureichen.

10.3 Spätestens 12 Wochen nach Abschluss der Versuche ist die Beendigung des Vorhabens mitzuteilen. Dabei ist ein kurzer Abschlussbericht über die im Versuch aufgetretenen Schmerzen, Leiden und Schäden vorzulegen.

10.4 Bei unvorhersehbaren Zwischenfällen (z. B. erhöhte Mortalität, Erhöhung der Belastung, besondere Vorkommnisse) ist die Behörde unverzüglich -über die Tierschutzbeauftragten- zu informieren.

Zur Genehmigung ergeht folgende Kostenentscheidung:

Es werden keine Kosten erhoben.

Begründung:

Zur Hauptsache:
Mit Wirkung vom 26. Juni 2021 ist das Tierschutzgesetz im Bereich der Tierversuche geändert worden. Die Voraussetzungen für die Genehmigung nach § 8 Abs. 1 TierSchG in der Fassung der Bekanntmachung vom 18. Mai 2006 (BGBl. I S. 1206, 1313), zuletzt geändert durch Gesetz vom 10. August 2021 (BGBl. I S. 3436) sind für dieses Vorhaben

(**b**) Page-2

weiterhin erfüllt. Dazu wurde das entsprechende Ergänzungsformular mit den erweiterten Angaben ausgefüllt und der Genehmigungsbehörde vorgelegt.

Zu den Nebenbestimmungen:
Zu 9) Vom beantragten Zeitraum wurde nicht abgewichen.

Zu 10.1) Änderungen unterliegen grundsätzlich der Genehmigungspflicht gemäß § 8 Absatz 1 TierSchG in Verbindung mit § 34 TierSchVersV. Sie bedürfen nur dann keiner Genehmigung, wenn der Zweck des Versuchsvorhabens beibehalten wird, den Versuchstieren keine stärkeren Schmerzen, Leiden oder Schäden entstehen, die Versuchstierzahl nicht wesentlich erhöht wird und die Änderung der zuständigen Behörde angezeigt wurde.

Zu 10.2 und 10.3) Gemäß § 29 TierSchVersV sind zu jedem Versuchsvorhaben Aufzeichnungen zu führen, welche auf Verlangen der Behörde vorzulegen. Es müssen Angaben zu Art und Durchführung der Tierversuche gemacht werden, aber auch Eingriffe und Behandlungen sowie die dadurch ausgelösten Schmerzen, Leiden, Ängste und Schäden nach Ausmaß, zeitlicher Dauer und Zahl der Wiederholungen angegeben werden. Das Ergebnis ist verständlich zu dokumentieren.

Zu 10.4) Gemäß § 16a TierSchG trifft die zuständige Behörde zur Verhütung künftiger Verstöße notwendigen Anordnungen. Die Auflage dient dem Zweck, zu überprüfen, ob tierschutzrechtliche Anforderungen umgesetzt werden bzw. etwaige tierschutzrechtliche Versäumnisse oder Verstöße frühzeitig entdeckt und unterbunden werden. Mit dieser Auflage ist der Behörde ein frühzeitiges Einschreiten ermöglicht.

Zur Kostenentscheidung:
Ihre Einrichtung ist gem. § 8 Abs. 1 Nr. 6 Verwaltungskostengesetz des Landes Schleswig-Holstein als rechtsfähige Körperschaft des öffentlichen Rechts / öffentlich-rechtliche Stiftung, die gemeinnützigen Zwecken dient, von Verwaltungsgebühren befreit, da die der Kostenentscheidung zugrundeliegende Angelegenheit nicht einen steuerpflichtigen wirtschaftlichen Geschäftsbetrieb betrifft.

Rechtsbehelfsbelehrung
Gegen diesen Bescheid kann innerhalb eines Monats nach Bekanntgabe Klage bei dem Schleswig-Holsteinischen Verwaltungsgericht, Brockdorff-Rantzau-Straße 13, 24837 Schleswig erhoben werden.

Mit freundlichen Grüßen

Dr. Christiane von Münchhausen

(**c**) Page-3

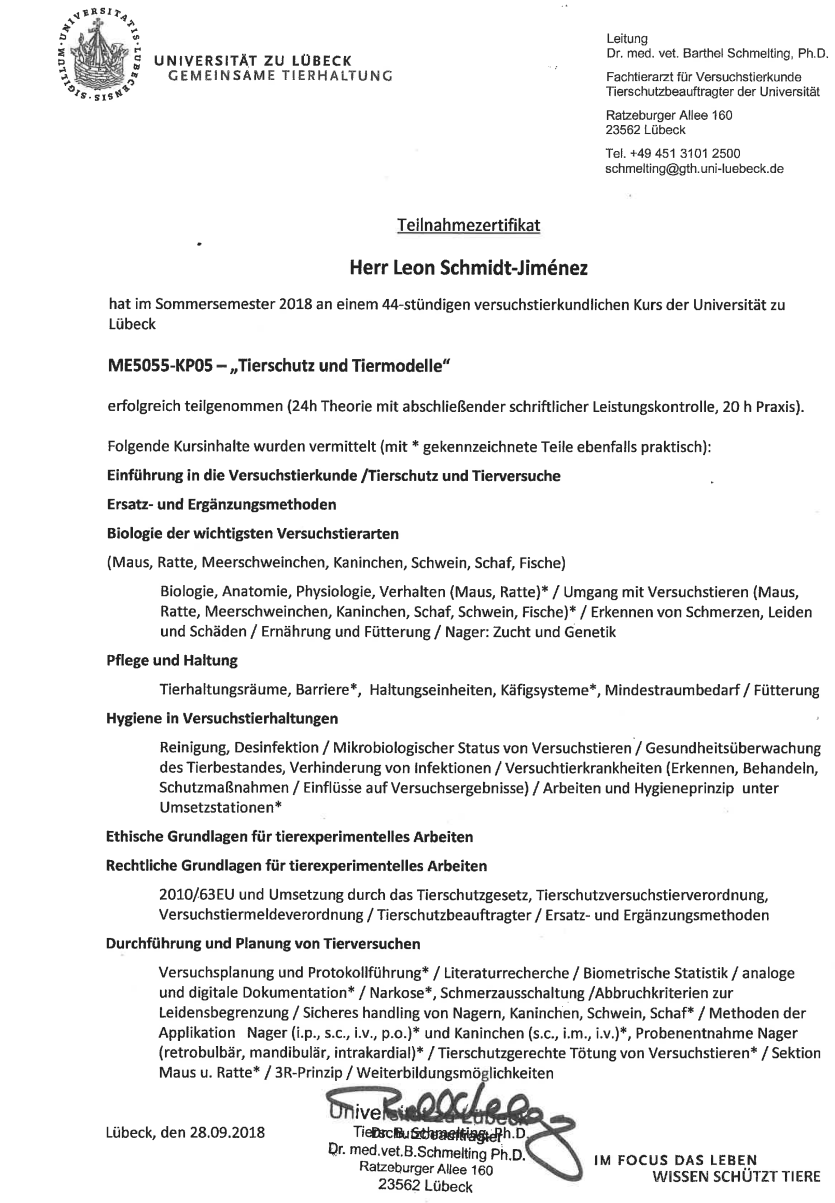

UNIVERSITÄT ZU LÜBECK
GEMEINSAME TIERHALTUNG

Leitung
Dr. med. vet. Barthel Schmelting, Ph.D.
Fachtierarzt für Versuchstierkunde
Tierschutzbeauftragter der Universität
Ratzeburger Allee 160
23562 Lübeck
Tel. +49 451 3101 2500
schmelting@gth.uni-luebeck.de

Teilnahmezertifikat

Herr Leon Schmidt-Jiménez

hat im Sommersemester 2018 an einem 44-stündigen versuchstierkundlichen Kurs der Universität zu Lübeck

ME5055-KP05 – „Tierschutz und Tiermodelle"

erfolgreich teilgenommen (24h Theorie mit abschließender schriftlicher Leistungskontrolle, 20 h Praxis).

Folgende Kursinhalte wurden vermittelt (mit * gekennzeichnete Teile ebenfalls praktisch):

Einführung in die Versuchstierkunde /Tierschutz und Tierversuche

Ersatz- und Ergänzungsmethoden

Biologie der wichtigsten Versuchstierarten

(Maus, Ratte, Meerschweinchen, Kaninchen, Schwein, Schaf, Fische)

Biologie, Anatomie, Physiologie, Verhalten (Maus, Ratte)* / Umgang mit Versuchstieren (Maus, Ratte, Meerschweinchen, Kaninchen, Schaf, Schwein, Fische)* / Erkennen von Schmerzen, Leiden und Schäden / Ernährung und Fütterung / Nager: Zucht und Genetik

Pflege und Haltung

Tierhaltungsräume, Barriere*, Haltungseinheiten, Käfigsysteme*, Mindestraumbedarf / Fütterung

Hygiene in Versuchstierhaltungen

Reinigung, Desinfektion / Mikrobiologischer Status von Versuchstieren / Gesundheitsüberwachung des Tierbestandes, Verhinderung von Infektionen / Versuchtierkrankheiten (Erkennen, Behandeln, Schutzmaßnahmen / Einflüsse auf Versuchsergebnisse) / Arbeiten und Hygieneprinzip unter Umsetzstationen*

Ethische Grundlagen für tierexperimentelles Arbeiten

Rechtliche Grundlagen für tierexperimentelles Arbeiten

2010/63EU und Umsetzung durch das Tierschutzgesetz, Tierschutzversuchstierverordnung, Versuchstiermeldeverordnung / Tierschutzbeauftragter / Ersatz- und Ergänzungsmethoden

Durchführung und Planung von Tierversuchen

Versuchsplanung und Protokollführung* / Literaturrecherche / Biometrische Statistik / analoge und digitale Dokumentation* / Narkose*, Schmerzausschaltung /Abbruchkriterien zur Leidensbegrenzung / Sicheres handling von Nagern, Kaninchen, Schwein, Schaf* / Methoden der Applikation Nager (i.p., s.c., i.v., p.o.)* und Kaninchen (s.c., i.m., i.v.)*, Probenentnahme Nager (retrobulbär, mandibulär, intrakardial)* / Tierschutzgerechte Tötung von Versuchstieren* / Sektion Maus u. Ratte* / 3R-Prinzip / Weiterbildungsmöglichkeiten

Lübeck, den 28.09.2018

Universität zu Lübeck
Tierschutzbeauftragter
Dr. med.vet.B.Schmelting Ph.D.
Ratzeburger Allee 160
23562 Lübeck

IM FOCUS DAS LEBEN
WISSEN SCHÜTZT TIERE

Supplementary Figure S5: Animal experimentation certificate Leon F. Schmidt-Jiménez

Acknowledgements

Looking back, there are so many people—both in and out of the lab—who made this whole PhD journey (or mountaineering, depending on the day) possible and I just want to say thanks to all of you for the continuous support.

Special thanks go to my (official and unofficial) supervisory team: PD Dr. Katja Bieber, Prof. Dr. Admar Verschoor, Prof. Dr. Ralf Ludwig, and Prof. Dr. Matthias Peipp, who together gave me the opportunity to work on this project. I found the supervision to be absolutely outstanding and am grateful to have had such an excellent team of experienced scientists around me. Each of you, in your own unique aspect, made this project possible and taught me valuable personal lessons along the way, for which I am deeply thankful. Ralf and Matthias—for your unwavering optimism and constant support; Admar—for your passion for controls and for sharp critical thinking; Katja—for your attention to detail, pragmatism, and for giving me a push when I needed it (and sometimes even when I didn't).

I'm especially grateful to my mentor, Dr. Steffen Krohn, who not only introduced me to the wild world of phage display but also offered intensive guidance, crucial support, and advice—plus plenty of memorable scientific (and not-so-scientific) conversations that made my time in Kiel both productive and a lot of fun.

My sincere thanks to Thomas Theocharis, without whose outstanding work in antibody expression this study would not have been possible—and for all the fruitful discussions and long evenings together, whether in the lab or at conferences.

I would like to thank Dr. Natalie Gross, Claudia Kauderer, Alexandra Wobig, Daniela Rick, Bejtije Naumann, and Nikolai L'vov for their outstanding scientific and technical support in protein production and testing, as well as in the preparation and evaluation

of tissue sections.

A special thanks to my students, Wendy Hwang and Sophia Jarrar, who, like true Minions to my Gru, worked inseparably together as a truly symbiotic team.

Big thanks to Dr. Sören Dräger for all the great (and failed) experiments and the even better company—truly: "THE ONLY THING MISSING HERE IS A CUP OF COFFEE ON THE BENCH!"

Overall, I'd like to thank everyone in the Ludwig and Peipp groups for the great atmosphere, all the support, and many memorable (mostly marginally science-related) moments with both such great teams. Shout out to Nancy— just for all the laughs. It was (and still is) a real pleasure to be part of each group.

I would also like to thank PD Dr. Andreas Recke, Dr. Anika Kasprick, Prof. Dr. Eva Hadaschik, and Dr. Elisabeth Vicari for providing the antibody clones used in my research.

To the "Eels" – Dr. Max Hahn, Dr. Fabio Nickels, and (soon to be Dr.) Ramin Shakiba – thanks for all the laughs, unwavering mentaal support, and real friendship through all these years of science and beyond.

Last but not least, I thank my family, especially my mother Edith, for years of support during my studies, for always being there when needed, and for her constant encouragement (and for always asking when I'd finally be finished). I'm also grateful to my godmother Ingeborg and my uncle Ulrich for their continuous support.

Statement of Authenticity

I hereby declare that I, Leon F. Schmidt-Jiménez, have written the herein presented dissertation independently and without unauthorized assistance from external parties. I have used no other sources or aids than those indicated in the manuscript. All ideas, concepts, intellectual property, and quotations from other sources are clearly attributed to their respective authors with proper citation.

This dissertation has not been submitted in the same, similar, or partial form to any other institution for grading or degree purposes. I have not previously or simultaneously submitted an application for admission to a doctoral program elsewhere, nor have I presented this dissertation to any other examining body. I declare that I have not previously undergone another doctoral procedure.

Lübeck, 18.06.2025 _____

Signature: _____
Leon F. Schmidt-Jiménez

List of Tables

List of Figures

List of Abbreviations

Table S5: List of Abbreviations

Abbreviation	Definition
AA	Amino acid
Aab	Autoantibody
AI	Artificial intelligence
AIBD	Autoimmune blistering disease
AIRR	Adaptive immune receptor repertoire
AP	Alternative pathway
BCR	B cell receptor
BCR-seq	B cell receptor sequencing
BP	Bullous pemphigoid
C_3	Complement factor 3
C_5	Complement factor 5
C_{1q}	Complement factor C1q
CDRs	Complementarity-determining regions
CFU	Colony forming units
CH	Constant heavy
CHO	Chinese hamster ovary
CL	Constant light
COL I	Type I collagen
COLVII	Type VII collagen
CP	Classical pathway
D	Diversity gene
DAMP	Danger associated molecular patterns

Continued on next page

Table S5 – continued from previous page

Abbreviation	Definition
DC	Dendritic cell
DEJ	Dermal-epidermal junction
dLN	Draining lymph nodes
EBA	Epidermolysis bullosa acquisita
ECM	Extracellular matrix
ELISA	Enzyme-linked immunosorbent assay
Fc	Fragment crystallizable
FcRn	Neonatal Fc receptor
FNIII	Fibronectin type III-like
FR	Framework
Fv	Fragment variable
GC	Germinal center
H	Heavy
H&E	Hematoxylin and eosin
HD	Hamming distance (0, 1, 2)
HRP	Horseradish peroxidase
i.p.	Intraperitoneal
IC	Immune complex
IG	Immunoglobulin gene (loci)
Ig	Immunoglobulin
IGH	Heavy chain locus
IGK	Kappa light chain locus
IGL	Lambda light chain locus
IKMB	Institute of Clinical Molecular Biology
IMGT	The International ImMunoGeneTics Information System
int. ID	Internal ID
J	Joining gene
L	Light
L332	Laminin 332
LN	Lymph nodes (sample)
LPS	Lipopolysaccharides
mAb	Monoclonal antibody

Continued on next page

Table S5 – continued from previous page

Abbreviation	Definition
mCOLVII^{vWFA2}	Murine type VII collagen Von Willebrand factor A
mCOLVII^{-C}	Murine type VII collagen fragment C
MFI	Mean fluorescence intensity
MHC	Major histocompatibility complex
MHCII	MHC class II receptor
MOI	Multiplicity of infection
MSC	Multiple cloning site
N	Non-templated
NC	Non-collagenous
NGS	Next generation sequencing
NJ	Neighbor joining
Ns	Non-silent
P	Palindromic
p.i.	Post injection
p.I.	Post immunization
PAMP	Pathogen associated molecular patterns
PD	Pemphigoid diseases
PFU	Plaque forming units
PI	Panning 1
PII	Panning 2
PRR	Pattern recognition receptor
rIgG	Rabbit IgG
ROS	Reactive oxygen species
S	Spleen (sample)
s	silent
s.c.	Subcutaneous
scFv	Single-chain fragment variable
SHM	Somatic hypermutation
SHM1	Somatic hypermutation with normalization
SLO	Secondary lymphoid organ
T-reg	T regulatory cell
TCR	T cell receptor

Continued on next page

Table S5 – continued from previous page

Abbreviation	Definition
TdT	Terminal deoxynucleotidyl transferase
Th1	T helper cell 1
UMI	Unique molecular identifiers
UV	Ultraviolet
V	Variable gene
V^H	Variable heavy
V^L	Variable light
VWA	Von Willebrand factor A domain
VWFA2	Von Willebrand factor A-like domain 2
WT	Wild type

Table S6: Common units and abbreviations used in this study. The table provides abbreviations for scientific units and their meanings.

Abbreviation	**Definition**
mg	milligram
µg	microgram
ng	nanogram
L	liter
mL	milliliter
µL	microliter
°C	degrees Celsius
h	hour
min	minute
mol	mole (amount of substance)
g	gram
rpm	revolutions per minute
mM	millimolar
m	meter
M	molar (mol/L)
n	biological replicate
N	technical replicate
OD	optical density
w/v	weight/volume
bp	base pair(s)
kDa	kilo Dalton
nm	nanometer
Mb	megabase pair
o/n	overnight
R^2	coefficient of determination
pH	measure of acidity/basicity
%	percent (per hundred)

Table S7: Laboratory practice related abbreviations. The table provides commonly used abbreviations and their meanings.

Abbreviation	Definition
DNA	Deoxyribonucleic acid
cDNA	Complementary DNA
RNA	Ribonucleic acid
mRNA	Messenger RNA
ELISA	Enzyme-linked immunosorbent assay
PCR	Polymerase chain reaction
AA	Amino acid
Gly	Glycine

Table S8: Abbreviated chemical compounds used in this study. The table lists the abbreviations alongside their corresponding full chemical names.

Abbreviation	Chemical Name
β-mercaptoethanol	2-Sulfanylethan-1-ol
MOPS	(Morpholino)propanesulfonic acid
bromophenol blue	3′,3″,5′,5″ Tetrabromophenolsulphonphthalein
DAPI	4′,6-Diamidino-2-phenylindole
Luminol	5-Amino-2,3-dihydrophthalazine 1,4-dione
ABTS	2,2′-Azino-bis(3-ethylbenzothiazoline-6-sulfonic acid)
Antisedan	Atipamezole hydrochloride
DMSO	Dimethylsulfoxide
EDTA	Ethylenediaminetetraacetic acid disodium salt dihydrate
Domitor	Medetomidine hydrochloride
FCS	Fetal Bovine Serum
BSA	Faction V, bovine serum albumin
IPTG	β-D-1-thiogalactopyranoside
TRIS	Tris(hydroxymethyl)aminomethane
TMB	3′,3″,5′,5″-Tetramethylbenzidine
FITC	Fluorescein isothiocyanate
TAE	Tris-acetate-EDTA buffer